UNIVERSITÉ DU LUXEMBOURG

PhD-FSTM-2025-106
The Faculty of Science, Technology and Medicine

DISSERTATION

Defence held on 22/10/2025 in Esch-sur-Alzette

to obtain the degree of

DOCTEUR DE L'UNIVERSITÉ DU LUXEMBOURG

EN BIOLOGIE

by

Elisa Zuccoli
Born on 16 June 1996 in city of Luxembourg, (Luxembourg)

MODELLING ENDOGENOUS PARKINSON'S DISEASE PATHOLOGY USING PATIENT-SPECIFIC MIDBRAIN ASSEMBLOIDS.

Dissertation defence committee

Dr Jens C. Schwamborn, dissertation supervisor
Professor, Université du Luxembourg

Dr Alexander Skupin, Chairman
Associate Professor, Université du Luxembourg

Dr Soyon Hong
Group Leader, University College London

Dr Silvia Bolognin
Assistant Professor, Maastricht University

Dr Wilma van de Berg
Professor, Amsterdam UMC

UNIVERSITY OF LUXEMBOURG

DOCTORAL THESIS

MODELLING ENDOGENOUS PARKINSON'S DISEASE PATHOLOGY USING PATIENT-SPECIFIC MIDBRAIN ASSEMBLOIDS.

by

Elisa Zuccoli

Developmental and Cellular Biology Group

Luxembourg Centre for Systems Biomedicine

Dissertation defence committee

Dr Jens C. Schwamborn, dissertation supervisor

Dr Alexander Skupin

Dr Soyon Hong

Dr Silvia Bolognin

Dr Wilma van de Berg

October 22, 2025

Affidavit

I declare that this thesis:

- is the result of my own work. Any contribution from any other party, and any use of generative artificial intelligence technologies have been duly cited and acknowledged;
- is not substantially the same as any other that I have submitted, and;
- is not being concurrently submitted for a degree, diploma or other qualification at the University of Luxembourg or any other University or similar institution except as specified in the text.

With my approval I furthermore confirm the following:

- I have adhered to the rules set out in the University of Luxembourg's Code of Conduct and the Doctoral Education Agreement (DEA), in particular with regard to Research Integrity.
- I have documented all methods, data, and processes truthfully and fully.
- I have mentioned all the significant contributors to the work.
- I am aware that the work may be screened electronically for originality.

I acknowledge that if any issues are raised regarding good research practices based on the review of the thesis, the examination may be postponed pending the outcome of any investigation of such issues. If a degree was conferred, any such subsequently discovered issues may result in the cancellation of the degree.

Approved on 8th of August 2025 Elisa Zuccoli

Acknowledgments

My PhD journey began in November 2021, and over the past years I have been fortunate to work with an inspiring group of people who supported and guided me every step of the way. I am deeply grateful to everyone who made this journey possible.

First, I would like to thank my thesis supervisor Prof. Jens Schwamborn, for giving me the opportunity to work in his group. His guidance, trust, and support have been invaluable, allowing me to explore new approaches, think critically, and grow as a scientist. Under his supervision, I also learned the importance of patience, hard work, and resilience.

I sincerely thank my CET committee members Dr. Soyon Hong and Dr. Knut Biber for following my progress and providing valuable advice throughout my PhD. I would also like to express my gratitude to Prof. Silvia Bolognin, Prof. Wilma van de Berg, and Prof. Alexander Skupin for being part of my thesis committee and taking the time to evaluate my work.

I would like to thank the wonderful DVB group and alumni for making my PhD experience so enjoyable and memorable. I was lucky to be part of a team of caring, respected and highly skilled scientists who were always willing to help and offer advice. I am very grateful to Dr. Henry Kurniawan, my Postdoc supervisor, for his insightful guidance, which greatly helped me shape my project.

A special thanks goes to my fellow “Powerpipettes”, who made my PhD journey so much fun and unforgettable. Isabel, I will never forget our heated discussions and endless laughter over 4 pm waffles! Sònia, your energy and charming clumsiness always brightened my days, and I loved our gossip sessions! Alise, my Step Dance friend and Reproducibility buddy, your support, efficiency, and brilliant scientific ideas kept me motivated! Gemma, your calming personality made every moment easier, and I will always treasure our shared Harry Potter obsession! Anna-Sophie, I deeply appreciate how we motivated and supported each other throughout the PhD, and how our epic complaining sessions always turned stressful days into laughter-filled therapy! Catarina, my chicken nugget, your fantastic sense of humour made lab life pure joy, and I will never forget the moments that had us crying with laughter! Kiki, your unstoppable energy and resilience inspired me every day, and I will fondly remember our passion for movies! Girls, I loved every weekend trip, vacation, and conference we shared!

Special thanks to Matthieu, who revised my thesis, provided really helpful feedback, and patiently endured me as desk neighbour, always asking questions. I am also grateful to all current and past members of the DVB group: Mona, Daniela, Cláudia, Nathasia, Michele, Sarah, Javi, Silvia, Raquel, Marco, David, Haya, Giulia and Noemi. Thank you for all the help, advice, and laughter along the way; it truly made my PhD years unforgettable. I will fondly remember our intense lunch debates about science and food, our coffee breaks and snacks from our usual spot, and all the fun we had together in the lab.

I would also like to thank my colleagues from LCSB, in particular Jón and Carmen, for their support and enjoyable coffee breaks. From my PhD, I am grateful to Candy, Vanessa, and Kim for their friendship and their outsider input. I also want to acknowledge my i2TRON DTU colleagues for their advice, and inspiring discussions during the retreats and courses.

Finally, I would like to thank my family and friends for their unwavering love and support throughout my PhD journey. My parents have always believed in me, encouraged me, and helped me pursue my dreams with confidence. My sister has always pushed me to grow, cared for me, and reminded me to enjoy life. I am also grateful to her husband for his constant support and availability. Being an aunt has been a true joy, and I look forward to introducing my niece gently to the fascinating world of science. To all my friends, thank you for cheering me on, sharing laughs, partying, dancing, and patiently listening to my endless stories and scientific speeches. You have made this journey brighter and more memorable than I could have imagined.

Abbreviations

2D	Two-dimensional
2-DG	2-deoxy-D-glucose
3-BP	3-bromopyruvate
3D	Three-dimensional
3xSNCA	SNCA triplication
53BP1	p53-binding protein 1
6-OHDA	6-hydroxydopamine
AS160	Akt substrate of 160 kDa
ASB	Assembloid
ATP	Adenosine triphosphate
BDNF	Brain-derived neurotrophic factor
BMP	Bone morphogenic protein
BSA	Bovine serum albumin
CBE	Conduritol B epoxide
CCR6	C-C Chemokine receptor type 6
CDs	Cluster of differentiations
cDNA	complementary DNA
CHIR	CHIR-99021
CNS	Central nervous system
CSF	Cerebrospinal fluid
CX3CR1	CX3C motif chemokine receptor 1
cAMP	Cyclic adenosine monophosphate
DEGs	Differentially expressed genes
DJ-1	Parkinsonism-associated deglycase
DNA	Deoxyribonucleic acid
DMEM	Dulbecco’s Modified Eagle Medium
EBs	Embryoid bodies
ECAR	Extracellular Acidification Rate
ECM	Extracellular matrix
FACS	Fluorescence-activated cell sorting
FDR	False-discovery rate
FGF8	Fibroblast growth factor 8

GBA	Glucosylceramidase beta
GCase	Glucocerebrosidase
GDNF	Glial cell-derived neurotrophic factor
GFAP	Glial fibrillary acidic protein
GLUT4	Glucose transporter type 4
GM-CSF	Granulocyte-macrophage colony-stimulating factor
GO	Gene ontology
GWAS	Genome-wide association study
IBA1	Ionized calcium binding adaptor molecule 1
IBD	Inflammatory bowel disease
IFN-γ	Interferon γ
ILs	Interleukins
iPSC	Induced pluripotent stem cell
KEGG	Kyoto Encyclopedia of Genes and Genomes
LBD	Lewy body dementia
LPS	Lipopolysaccharide
LRRK2	Leucine-rich repeat kinase 2
MAP2	Microtubule-associated protein 2
M-CSF	Macrophage colony-stimulating factor
MHC-II	Major histocompatibility complex II
Miro1	Mitochondrial Rho GTPase 1
MPTP	1-methyl-4-phenyl-1,2,3,6-tetrahydropyridine
mTOR	Mammalian target of rapamycin
NAC	Non-amyloid-β component
NADPH	Nicotinamide adenine dinucleotide phosphate
NESC	Neuroepithelial stem cell
NO	Nitric oxide
OCR	Oxygen consumption rate
P2RY12	Purinergic receptor P2Y12
PBS	Phosphate-buffered saline
PCA	Principal Component Analysis
PD	Parkinson’s disease
PDD	Parkinson’s disease dementia
PFF	Preformed α-synuclein fibril

PHGDH	Phosphoglycerate dehydrogenase
PINK1	PTEN-induced kinase 1
PMA	Purmorphamine
pMacPre	Macrophage precurosors
PRKN	Parkin RBR E3 Ubiquitin Protein Ligase
pS129	Phosphorylated α-synuclein at Serine 129
PSAT1	Phosphoserine Aminotransferase 1
PVCA	Principal Variance Component Analysis
REM	Rapid Eye Movement
RIPA	Radioimmunoprecipitation
RNA	Ribonucleic acid
ROS	Reactive oxygen species
RPTOR	Regulatory associated protein of MTOR complex 1
RT	Room temperature
S100β	S100 calcium binding protein B
SCF	Stem cell factor
SHH	Sonic hedgehog
SNCA	α-synuclein (gene)
SNpc	Substantia nigra pars compacta
TCA	Tricarboxylic acid cycle
TGF-β	Transforming growth factor beta
TH	Tyrosine hydroxylase
TLRs	Toll-like receptors
TMEM119	Transmembrane protein 119
TNF-α	Tumor necrosis factor α
TSPO	Translocator protein
VEGF-165	Vascular endothelial growth factor 165
VSP35	Vacuolar protein sorting-associated protein 35
VTA	Ventral tegmental area
WNT	Wingless-related integration site
WT	Wild type

List of publications

The work conducted during my PhD resulted in two first-author manuscripts, one joint first-author publication, and three contributing author manuscripts, collectively reflecting the scientific objectives of my PhD. Three of the manuscripts are included in this thesis.

Published

Zuccoli E, Al Sawaf H, Tuzza M, Nickels SL, Zagare A, Schwamborn JC. Reproducibility of PD patient-specific midbrain organoid data for *in vitro* disease modeling. *iScience*. 2025;28(10):113541. Published 2025 Sep 10. doi:10.1016/j.isci.2025.113541; PMID: 41050933

Kurniawan H, Nickels SL, Zagare A, **Zuccoli E**, Rosety I, Gomez-Giro G, Glaab E, Schwamborn JC. The Parkinson's disease-associated LRRK2-G2019S variant restricts serine metabolism, leading to microglial inflammation and dopaminergic neuron degeneration. *J Neuroinflammation*. 2025;22(1):244. Published 2025 Oct 27. doi:10.1186/s12974-025-03577-2; PMID: 41146185

In revision

Elisa Zuccoli, Henry Kurniawan, Isabel Rosety, Alise Zagare, Sonia Sabate-Soler, Anna-Sophie Zimmermann, Jens C. Schwamborn (Sept 2025). “Parkinson’s disease microglia induce endogenous α-synuclein pathology in patient-specific midbrain organoids.” *Under revision in Nature Communications.*

Sarah L. Nickels, Claudia Saraiva, Michele Bassis, Alise Zagare, Gemma Gomez-Giro, Sylvie Delcambre, Gianfranco Frigerio, Javier Jarazo, **Elisa Zuccoli**, Semra Smajic, Isabel Rosety, Henry Kurniawan, Mohamed Soudy, Raquel Forte Marques, Mona Tuzza, Mudiwa Nathasia Muwanigwa, Lucie Remark, Pauline Lambert, Andreas Keller, Paul M. Anthony, Olga Kofanova, Silvia Bolognin, Lukas Pavelka, Emma L. Schymanski, Thomas Gasser, Enrico Glaab, Anne Grünewald, Rejko Krüger, Jens C. Schwamborn (Sept 2025). “Parkinson’s disease blood biomarkers correspond to a selectively vulnerable group of dopaminergic neurons.”, *Under revision in Science Translational Medicine.*

Catarina Serra-Almeida, Javier Jarazo, Gemma Gomez-Giro, Isabel Rosety, Alise Zagare, Daniele Ferrante, Cláudia Saraiva, Daniela Frangenberg, **Elisa Zuccoli**, Ana Clara Cristóvão, Liliana Bernardino, Jens C. Schwamborn. “Autophagy Dysfunction in iPSC-

Derived Neurons and Midbrain Organoids Carrying a *SNCA* Triplication (Sept 2025)." *Under revision in npj Parkinson's Disease.*

In preparation

Elisa Zuccoli, Daniela M. Vega Gutiérrez, Aelyn Chong Castro, Lina M. Amaya Mejía, José I. Delgado-Centeno, Miguel A. Olivares Mendez, Carol Martinez Luna, Jens C. Schwamborn (2025). "Microgravity enhances the viability of midbrain organoids on the International Space Station."

Abstract

Parkinson's disease (PD) is a multifactorial neurodegenerative disorder characterized by the progressive loss of dopaminergic neurons in the midbrain, the accumulation of misfolded α-synuclein, and chronic neuroinflammation. Despite its prevalence, the mechanisms driving PD onset and progression remain incompletely understood, partly due to limitations of conventional animal and 2D cellular models. In this thesis, we employed advanced human midbrain organoid and assembloid models derived from patient-specific induced pluripotent stem cells (iPSCs) to investigate key pathological features of PD. Midbrain organoids, enriched in dopaminergic neurons and multicellular architectures, provide a physiologically relevant platform to study disease mechanisms. We demonstrated that organoids derived from PD patients carrying GBA-N370S mutation consistently reproduced disease-relevant transcriptomic, metabolic, and proteomic signatures across independently generated batches and time points. These findings validate midbrain organoids as robust and reproducible models of genetic forms of PD. To address the neuroimmune contribution to PD, we established the assembloid model where we incorporated iPSC-derived microglia into midbrain organoids. Microglia carrying the LRKK2-G2019S mutation exhibited heightened activation, increased phagocytic capacity, and elevated pro-inflammatory cytokine secretion. These phenotypes are accompanied by metabolic reprogramming, including enhanced glycolysis and impaired serine biosynthesis. Crucially, overactivated microglia induced dopaminergic neuron degeneration within the organoid environment, a phenotype reversible by restoring metabolic balance. This highlights the interplay between microglial metabolism and neurotoxicity. Finally, to explore α-synuclein pathology, we generated patient-specific assembloids carrying the SNCA triplication (3xSNCA). Remarkably, these assembloids developed early endogenous formation of phosphorylated α-synuclein (pS129) pathology by day 50 of culture, in the absence of exogenous fibril seeding. This pathology was absent in healthy control assembloids, underscoring the critical role of patient-derived microglia in driving early synucleinopathy. This model thus provides a unique platform for studying initial neuroimmune interactions underlying α-synuclein aggregation. Together, the studies presented in this thesis highlight the utility of organoid and assembloid technologies for modelling distinct aspects of PD pathogenesis. We established robust, human-relevant systems for investigating the genetic, inflammatory, and metabolic contributors to neurodegeneration and for identifying strategies that may guide future therapeutic development.

Motivation and Aims

Parkinson's disease (PD) is the fastest-growing neurodegenerative disorder and represents a major medical and societal challenge due to its prevalence and lack of disease-modifying therapies. Its clinical course is shaped by both motor and non-motor symptoms, which arise from hallmark pathological processes including the selective degeneration of dopaminergic neurons, accumulation of misfolded α-synuclein, and chronic neuroinflammation. The interplay of genetic mutations (e.g. LRRK2, GBA, SNCA) with environmental risk factors creates substantial variability in disease onset and progression, complicating efforts to pinpoint early pathogenic mechanisms and develop effective therapeutic treatments.

To address this complexity, physiologically relevant human-based *in vitro* models are essential. While conventional 2D neuronal cultures provide valuable mechanistic insights, they lack the spatial and cellular complexity of the midbrain. Animal models, on the other hand, provide whole-organism context but fail to recapitulate human-specific neurodegenerative processes. Patient-derived midbrain organoids have emerged as promising tools for PD modelling, as they recapitulate aspects of human midbrain development and harbour functional dopaminergic neurons. These organoids also include neural progenitors, astrocytes, and oligodendrocytes, which interact through synaptic activity and neurotransmitter signalling. Despite their complexity, midbrain organoids lack certain cell populations, most notably microglia, which are central players in immune surveillance, neuroinflammation, and α-synuclein pathology.

Incorporating patient-derived microglia into midbrain organoids allows the investigation of mutation-specific immune responses and their interactions with neurons in a physiologically relevant context. This approach allows insights into how genetic variants such as LRRK2-G2019S and SNCA triplication shape microglial behaviour, influence neuronal health, and contribute to PD heterogeneity. Additionally, this model provides a platform to test therapeutic strategies targeting microglial states, such as modulation of metabolic pathways to reduce inflammation and protect neurons from degeneration.

The overall aim of this thesis is to enhance the physiological relevance and predictive power of *in vitro* PD models by integrating microglia into midbrain organoids. This approach will offer a deeper exploration of patient-specific mechanisms of PD pathogenesis and test new strategies that could restore neuronal health and slow disease progression.

The distinct aims of the thesis are:

- Validate the reproducibility of midbrain organoids for PD modelling by analysing independently generated batches of healthy and GBA-PD organoids using transcriptomics, metabolomics, and high-content imaging.
- Identify technical and biological variables that influence reproducibility in midbrain organoids.
- Characterize patient-derived microglia carrying the LRRK2-G2019S or SNCA triplication mutations, focusing on their immune, metabolic, and lysosomal phenotypes.
- Integrate microglia into midbrain organoids to investigate hallmarks and mutation-specific microglial mechanisms driving neuroinflammation, dopaminergic neuron degeneration, and α-synuclein aggregation.
- Evaluate glycolysis inhibition with oxamic acid as a therapeutic strategy to modulate pro-inflammatory microglial states and protect dopaminergic neurons.

Table of Contents

Chapter 1: Synopsis

1. Introduction

1.1 Parkinson's disease

Parkinson's disease (PD) is a progressive neurodegenerative disorder that was first described in 1817 by James Parkinson in "An Essay on the Shaking Palsy" (Parkinson 2002). Today, PD is considered the second most common neurodegenerative disorder after Alzheimer's disease (Dorsey et al., 2007; Kalia & Lang, 2015; Gadhave et al., 2024), affecting approximately 1-2% of the population over the age of 65 (Dorsey et al., 2018). The global burden of Parkinson's disease has risen dramatically in recent decades, more than doubling between 1990 and 2019 to an estimated 8.5 million worldwide. This upward trend makes PD one of the fastest-growing neurological conditions in terms of prevalence, disability, and mortality (Ou et a., 2021). Despite two centuries of research, PD remains incurable, with available treatments providing only symptomatic relief. Although remarkable progress has been made in understanding the underlying biology of PD, the exact mechanisms driving disease initiation and progression remain incompletely defined (Tenchov et al., 2025).

1.1.1 Clinical manifestation

The clinical presentation of PD is heterogenous and comprises both motor and non-motor features. The cardinal motor symptoms, including bradykinesia, rigidity, resting tremor, and postural instability, form the basis for clinical diagnosis (Jankovic 2008; Tolosa et al., 2021). However, these motor deficits typically manifest only after more than 50-80% of dopaminergic neurons in the substantia nigra pars compacta (SNpc) of the midbrain have been lost (DeMaagd & Philip., 2015; Gadhave et al., 2024). Increasing evidence highlights that PD pathology begins long before motor symptom onset, during a prodromal phase characterized by non-motor symptoms. These may precede motor dysfunction by decades and include olfactory deficits, sleep disturbances (such as REM sleep behaviour disorder, insomnia, and excessive daytime sleepiness), constipation, urinary dysfunction, depression, anxiety, pain, fatigue, hallucinations, and mild cognitive impairment (Chaudhuri et al., 2006; Poewe et al., 2017; Peña-Zelayeta et al., 2025). Non-motor features often persist and worsen alongside motor decline, greatly impairing quality of life (Jankovic & Tan, 2020). The heterogeneity in symptom profile, disease progression, and severity represents a major challenge for early diagnosis and individual treatment strategies.

1.1.2 Etiology and risk factors

PD is a multifactorial disorder resulting from the interaction of genetic predisposition, aging, and environmental exposures. Monogenic causes explain only a small proportion of Parkinson's disease, estimated at ~3-5% of sporadic cases and a larger share of familial cases. Overall detection rates can reach up to ~10-15% depending on ancestry and cohort (Klein & Westenberger, 2012; Westenberger et al., 2025). These monogenic forms are primarily due to rare, high-penetrance mutations, such as SNCA duplications, LRRK2 p.G2019S (with incomplete, age-dependent penetrance), and biallelic mutations in PRKN, PINK1, or DJ-1. In contrast, most PD cases (~ 90%) are idiopathic, driven by polygenic risk and environmental factors. Genome-wide association studies (GWAS) have identified numerous common variants with small effect sizes that collectively contribute to PD susceptibility. The genetic landscape of Parkinson's disease therefore encompasses both rare, high-penetrance mutations identified through linkage studies and common low-risk variants found in large population cohorts (Figure 1) (Chandler et al., 2021).

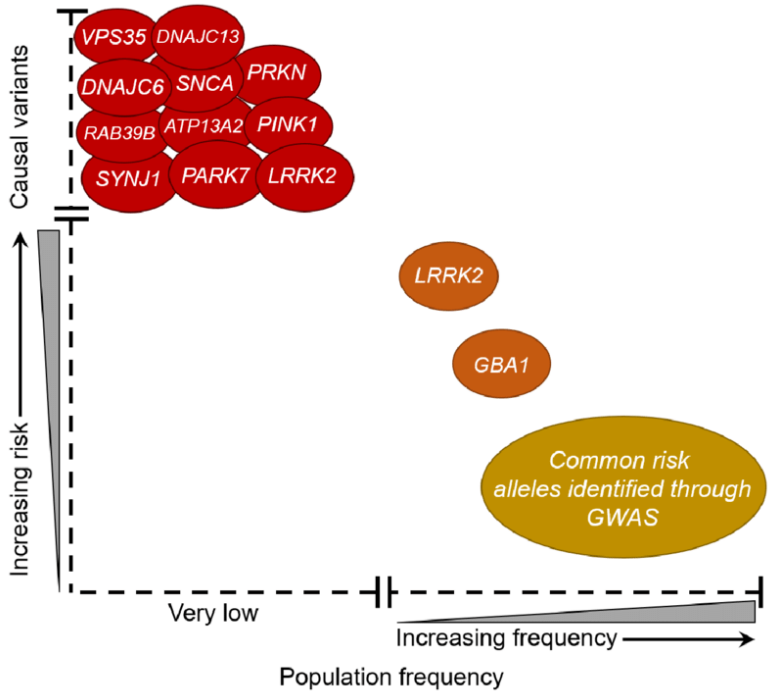

Figure 1. Genetic architecture of Parkinson's disease. *Genes in red represent rare, high-penetrance mutations identified through linkage studies and known to cause familial PD. Orange indicates genes with moderate to high risk, often discovered via exome sequencing or GWAS. Yellow highlights common low-risk variants identified in large-scale GWAS* (Chandler et al., 2021).

Familial forms follow autosomal dominant inheritance patterns (e.g., SNCA, LRRK2, VPS35) or autosomal recessive inheritance patterns (e.g., PRKN, PINK1, DJ-1, ATP13A2). Research on these genes has revealed diverse pathogenic mechanisms: SNCA mutations

highlight the central role of α-synuclein aggregation (Nuytemans et al., 2010; Spillantini et al., 1997), PRKN and PINK1 variants emphasize deficits in mitochondrial quality control and mitophagy (Youle & Narendra, 2011; Pickrell & Youle, 2015), and LRRK2 mutations implicate kinase signalling pathways and lysosomal homeostasis in neuronal vulnerability (Bentley-DeSousa et al., 2025; Madureira et al., 2020). GWAS have also identified common risk variants in LRRK2 and GBA. Several mutation variants in the GBA gene, namely p.N370S and p.L444P, are strongly associated with PD, while others (e.g., p.T369M, p.E326K) act more as risk modifiers with lower effect sizes. These variants increase risk but show incomplete penetrance, underscoring the role of additional genetic and environmental modifiers (Jankovic & Tan, 2020; Day & Mullin, 2021).

Age is the strongest risk factor in PD, with incidence rising sharply after the age of 50 (Pang et al., 2019; Bloem et al., 2021). Aging itself promotes vulnerability to neurodegeneration, since mitochondrial dysfunction, impaired protein clearance, accumulated DNA damage, and chronic low-grade inflammation progressively weaken neuronal resilience (López-Otín et al., 2023). These age-related processes overlap with the key pathological features of Parkinson's disease and help explain why most cases occur sporadically in old age and are not attributable to monogenic causes (Kalia & Lang, 2015). Sex differences also exist, with men being more frequently affected than women (Taylor et al., 2007; Russillo et al., 2022; Cattaneo & Pagonabarraga, 2025).

Environmental exposures including pesticides (e.g. paraquat, rotenone), heavy metals (e.g., iron, manganese, copper, mercury, lead), and industrial toxicants are consistently associated with a higher risk (Hatcher et al., 2008; Baldi et al., 2003; Caudle et al., 2012; Zhao et al., 2023). Lifestyle factors such as traumatic brain injury, obesity, and physical inactivity also appear to contribute (Delic et al., 2020; Chen et al., 2005; Chen et al., 2004). Importantly, several of these risk factors are modifiable, and thus offer potential opportunities for prevention or delay of disease onset (Li et al., 2025). For example, type 2 diabetes has been identified as a comorbid condition and potentially causative factor, with evidence of overlapping pathophysiological pathways (Athauda et al., 2022). Interestingly, inverse associations have been observed between PD risk and lifestyle factors such as nicotine and caffeine consumption, suggesting potential protective mechanisms that remain poorly understood (Kalia & Lang, 2015).

Beyond these environmental lifestyle risks, epigenetic mechanisms, including alterations in DNA methylation and histone modifications, are increasingly recognized as factors contributing to Parkinson's disease susceptibility. Importantly, evidence from both *in vitro* and *in vivo* models suggest that environmental exposures can shape the epigenetic

landscape, thereby linking external risk factors with disease-relevant molecular changes (Jankovic & Tan, 2020; Tsalenchuk et al., 2023).

1.2 Neuropathology

The neuropathological hallmarks of PD include the progressive degeneration of dopaminergic neurons in the SNpc and the accumulation of abnormal protein inclusions collectively referred to as Lewy pathology. These inclusions, primarily composed of misfolded α-synuclein, appear as Lewy bodies within neuronal somata and Lewy neurites in axonal and dendritic processes (Spillantini et al., 1998; Kouli et al., 2018). Together, selective neuronal vulnerability and α-synuclein aggregation define the central pathological framework of Parkinson's disease. However, multiple interconnected mechanisms, including mitochondrial dysfunction, impaired protein clearance, and immune activation, contribute to disease progression and shape the broader neuropathological landscape (Poewe et al., 2017; Morris et al., 2024).

1.2.1 Selective loss of dopaminergic neurons

The progressive degeneration of neuromelanin-containing dopaminergic neurons in the SNpc is the most characteristic neuropathological feature of PD and underlies its cardinal motor symptoms. Although PD involves widespread neurodegeneration, including subtle atrophy in the hippocampus, thalamus, brainstem, and other subcortical structures (Zeighami et al., 2015; Tremblay et al., 2021; Oltra et al., 2022), the selective vulnerability of SNpc neurons, particularly those in the ventrolateral tier, remains a defining feature (Fearnley & Lees, 1991; Damier et al., 1999).

The neurons from the nigrostriatal pathway project densely to the putamen, where they modulate motor control through dopaminergic signalling (Menegas et al., 2015). Their degeneration leads to severe striatal dopamine depletion, disrupting basal ganglia circuits and causing the characteristic motor symptoms of PD, including bradykinesia, rigidity, and resting tremor. By the time of clinical diagnosis, it is estimated that more than 50-80% of SNpc dopaminergic neurons have already been lost, underscoring the need for early biomarkers and neuroprotective strategies (DeMaagd & Philip, 2015).

A striking feature of SNpc neurons is their extensive axonal arborization. Each dopaminergic neuron forms up to 1 - 2.5 million synaptic contacts in the striatum, which far exceeds the connectivity of neighbouring neurons in the ventral tegmental area (VTA) or striatal interneurons (Bolam & Pissadeki, 2012). This vast synaptic network imposes extraordinary bioenergetic demands on these neurons and makes them particularly susceptible to metabolic stress (Pissadeki & Bolam, 2013).

Functionally, SNpc neurons exhibit autonomous pacemaker activity driven by sustained calcium influx through L-type Cav1.3 channels. This continuous activity, combined with a reliance on oxidative phosphorylation for ATP production, renders them vulnerable to mitochondrial dysfunction and oxidative stress (Pissadeki & Bolam, 2013; Ni & Ernst, 2022). Disruptions in calcium homeostasis, ATP synthesis, or mitochondrial quality control, whether due to genetic mutations (e.g. in PINK1, PRKN) or environmental toxins, can disproportionately affect these neurons and contribute to their selective degeneration (Zhang et al., 2022).

Moreover, the presence of neuromelanin, a pigment that accumulates with age and binds potentially toxic metals and compounds, can further exacerbate susceptibility. While neuromelanin may serve a protective role under physiological conditions, its degradation during neuronal death can trigger microglial activation and neuroinflammation, thereby amplifying local damage (Kouli et al., 2018; Poewe et al., 2017).

1.2.2 Lewy pathology and α-synuclein aggregation

Lewy pathology, consisting of Lewy bodies and Lewy neurites, is the second fundamental neuropathological feature of Parkinson's disease. Lewy bodies are spherical intracytoplasmic inclusions characterized by a dense core surrounded by radiating fibrils, while Lewy neurites are dystrophic axonal and dendritic processes that contain filamentous α-synuclein (Spillantini et al., 1998; Braak et al., 1999, Shahmoradian et al., 2019). These pathological structures were once considered inert byproducts of neurodegeneration. However, growing evidence suggests that Lewy pathology reflects a dynamic and toxic process that directly contributes to neuronal dysfunction and neurodegeneration (Mahul-Mellier et al., 2020).

The protein α-synuclein, encoded by the *SNCA* gene, is a small 140 amino acids protein with a molecular weight of approximately 14 kDa. It is predominantly expressed in neurons, especially at presynaptic terminals, and is also found in the nucleus and mitochondria under certain conditions. Structurally, α-synuclein consists of three different domains: an N-terminal amphipathic region that mediates lipid binding and membrane association, a central non-amyloid-β component (NAC) domain that is prone to aggregation, and a C-terminal acidic tail that regulates protein-protein interactions and modulates aggregation dynamics (Figure 2A) (Bisaglia et al., 2006; Cox et al., 2014).

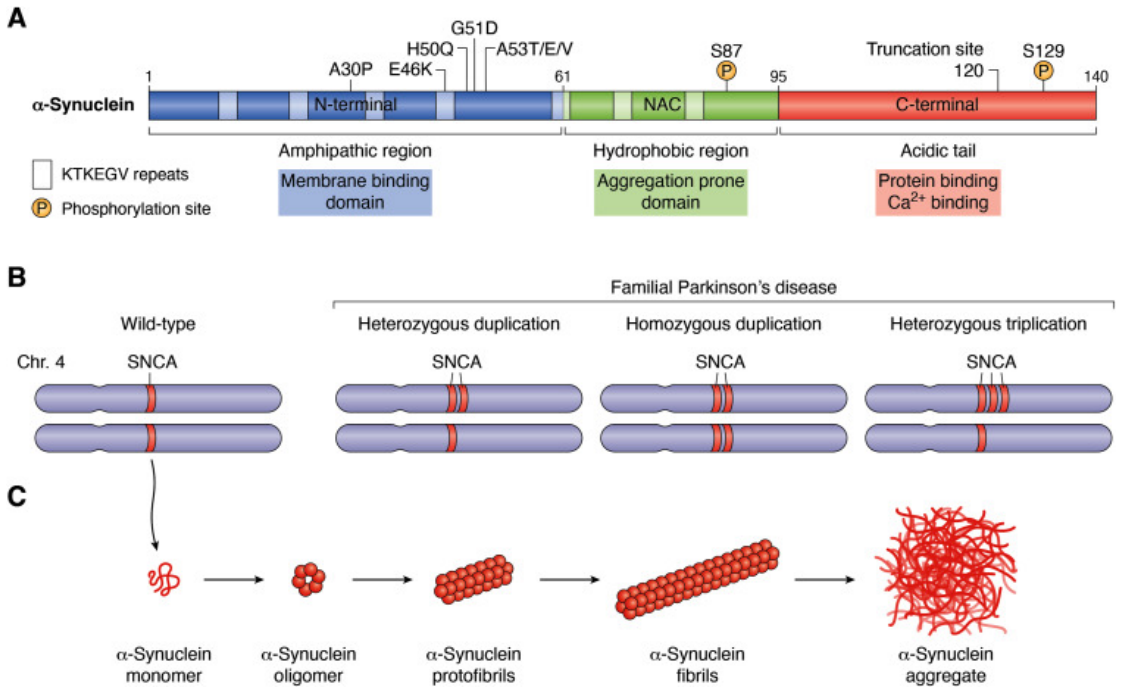

Figure 2. α-synuclein structure, gene-dosage effect, and aggregation in PD. *(A) α-synuclein is a 140-amino acid protein with three functional domains: an N-terminal membrane-binding region with KTKEGV repeats, a central NAC domain critical for aggregation, and a c-terminal region involved in protein interactions and phosphorylation. Familial PD mutations cluster in the membrane-binding domain. (B) SNCA gene multiplications (duplication and triplication) lead to increased α-synuclein expression with gene dosage influencing disease onset and severity. (C) α-synuclein monomers aggregate into oligomers and fibrils, which leads to Lewy body formation* (Bayati & McPherson, 2024).

Under physiological conditions, α-synuclein plays several important roles. It regulates synaptic vesicle trafficking, facilitates neurotransmitter release, and contributes to membrane curvature sensing. When bound to lipid membranes, α-synuclein adopts an α-helical conformation, which is essential for its function in vesicle clustering and fusion. Beyond its synaptic role, α-synuclein is involved in mitochondrial homeostasis, where it influences mitochondrial dynamics and bioenergetics, as well as nuclear processes, including DNA repair and transcriptional regulation (Rosborough et al., 2017; Wong & Krainc, 2017; Bayati & McPherson, 2024). Under pathological conditions, α-synuclein undergoes misfolding and aggregation driven by various post-translational modifications such as phosphorylation (notably at serine 129), ubiquitination, nitration, and truncation. These modifications destabilize its native conformation and promote the formation of β-sheet-rich oligomers, protofibrils, and fibrils. The central NAC domain is particularly critical in this process, as it facilitates the self-assembly of α-synuclein into toxic aggregates (Du et al., 2020). While mature Lewy bodies contain fibrillar α-synuclein, increasing evidence suggests that soluble oligomeric and protofibrillar intermediates are the most neurotoxic

species. These intermediates can disrupt cellular membranes, leading to calcium dysregulation, impaired mitochondrial function, disruption of autophagy and proteasomal degradation, and triggering neuroinflammatory responses (Figure 2C) (Yi et al., 2022; Dong-Chen et al., 2023; Wong & Krainc, 2017). Notably, Lewy bodies do not consist exclusively of α-synuclein fibrils. Proteomic analyses have revealed that they also contain lipids, fragmented organelles, ubiquitin, and components of the autophagy-lysosomal system. This complex composition suggests that Lewy bodies are formed through an active cellular sequestration response aimed at isolating toxic materials, rather than by passive simple protein accumulation (Gai et al., 2000; Mahul-Mellier et al., 2020). Thus, Lewy bodies may be both a marker of proteostasis failure and a factor contributing to further neuronal dysfunction.

The spread of Lewy pathology follows a stereotypical progression described by Braak staging. This progression begins in the olfactory bulb and dorsal motor nucleus of the vagus nerve, then spreads across the brainstem and midbrain structures, and ultimately affects the cortical regions (Braak et al., 2003; Braak et al., 2004). This anatomical spread of Lewy pathology aligns with the clinical evolution of PD, which typically begins with non-motor symptoms and progresses to motor dysfunction and cognitive decline (Morris et al., 2024). Mechanistically, α-synuclein aggregates appear to propagate in a prion-like manner, involving cell-to-cell transmission of misfolded α-synuclein, which in turn can lead to misfolding of native α-synuclein in recipient neurons and glial cells. This propagation can occur via exosomes, tunnelling nanotubes, or direct synaptic connections, and is thought to underlie the progressive nature of Lewy pathology (Wong & Krainc, 2017; Bayati & McPherson, 2024). Although Braak staging describes a typical sequence of Lewy pathology, exceptions exist. Notably, some genetic forms, particularly certain LRRK2 cases, show limited or absent Lewy pathology despite clinical parkinsonism (Healy et al., 2008; Kalia & Lang, 2015; Kouli et al., 2018).

Genetic studies have provided compelling evidence for the central role of α-synuclein in PD. Mutations in the SNCA gene are associated with familial forms of Parkinson's disease and affect both the expression levels and aggregation properties of the protein. Point mutations such as A53T, A30P, and E46K, alter the protein's structures and increase its tendency to form toxic aggregates. These mutations are linked to early-onset PD and are often accompanied by a more aggressive disease progression. Moreover, SNCA gene multiplications, including duplications and triplications, cause autosomal dominant forms of PD. These mutations lead to increased α-synuclein expression, which correlates with disease severity. Patients with SNCA duplications typically exhibit classic PD symptoms with slower progression, while patients with triplications often develop PD at a younger age

and experience more rapid motor and cognitive decline (Figure 2B) (Zafar et a., 2018; Magistrelli et al., 2021). This gene-dosage effect underscores the importance of α-synuclein levels in disease pathogenesis of the disease and supports its role as a therapeutic target.

In PD-related neurodegenerative disorders, including Parkinson's disease dementia (PDD) and Lewy body dementia (LBD), α-synuclein aggregates frequently coexist with other misfolded proteins, including tau neurofibrillary tangles and amyloid-β plaques. This molecular interaction suggests converging mechanisms of proteinopathy and may enhance neurotoxicity. It also helps explain the overlapping clinical features observed across synucleinopathies and Alzheimer's spectrum disorders (Irwin et al., 2023).

1.2.3 Neuroinflammation

In Parkinson's disease, neuroinflammation has emerged as a key contributor to disease progression, complementing the effects of dopaminergic neuron loss and α-synuclein pathology. While acute inflammation can have a neuroprotective effect in response to injury or infection, chronic inflammation is increasingly associated with the development and exacerbation of neurodegeneration (Kwon & Koh, 2020).

Multiple factors, including aging, protein aggregation, chronic infections, and genetic predisposition, can initiate and sustain neuroinflammatory responses. The central players in this process are microglia and astrocytes, which respond to pathological stimuli by releasing cytokines, chemokines, and reactive oxygen and nitrogen species. Although these responses are initially aimed at restoring homeostasis, their persistence leads to oxidative stress, mitochondrial dysfunction, and synaptic damage, thereby promoting neuronal degeneration (Isik et al., 2023; Pajares et al., 2020). Microglia, the resident immune cells of the brain, are consistently found in an activated state in the substantia nigra and other affected brain regions in PD patients (McGeer et al., 1988; Zhang et al., 2023). Upon activation, microglia secrete pro-inflammatory cytokines such as tumor necrosis factor-α (TNF-α), interleukin-1β (IL-1β), and interleukin-6 (IL-6), which contribute to a cytotoxic microenvironment. Moreover, post-mortem studies have shown increased expression of major histocompatibility complex II (MHC-II) molecules in microglia within the substantia nigra, suggesting their involvement in antigen presentation and potential engagement of the adaptive immune system (McGeer et al., 1988, Pajares et al., 2020).

Astrocytes, which normally support neuronal function through metabolic regulation, neurotransmitter recycling, and maintenance of the blood-brain barrier, also undergo changes in PD. Reactive astrocytes can lose their neuroprotective properties and begin to secrete pro-inflammatory mediators, further amplifying microglial activation and neuronal stress (Yi et al., 2022). Notably, several genes implicated in monogenic PD, such as DJ-1

and LRRK2, are highly expressed in astrocytes, and mutations in these genes have been shown to alter astrocytic inflammatory responses (Booth et al., 2018; Streubel-Gallasch et al., 2021). Moreover, the crosstalk between activated microglia and reactive astrocytes intensifies inflammatory signalling and promotes a hostile microenvironment that accelerates neuronal loss (Yi et al., 2022).

Recent research has also highlighted the role of glial senescence in PD. Senescent microglia and astrocytes exhibit a senescence-associated secretory phenotype (SASP), characterized by the release of pro-inflammatory cytokines and chemokines that can be toxic to surrounding neurons, including dopaminergic neurons (Russo & Riessland, 2022; Ma et al., 2025). This loss of immune competence and gain of toxic functions further contribute to the chronic inflammatory state observed in PD.

A key link between neuroinflammation and PD pathology is α-synuclein aggregation. Misfolded and aggregated α-synuclein can directly activate microglia through pattern recognition receptors such as TLR2 and TLR4, thereby triggering inflammatory cascades. In turn, the inflammatory environment promotes further α-synuclein misfolding and propagation of α-synuclein, creating a bidirectional relationship between protein aggregation and immune activation. This cycle involves microglial release of pro-inflammatory mediators, oxidative stress, and neuronal damage, which in turn facilitates the spread of α-synuclein pathology across brain regions (Figure 3) (Zhang et al., 2023; Pajares et al., 2020; Eo et al., 2024; Tansey et al., 2022).

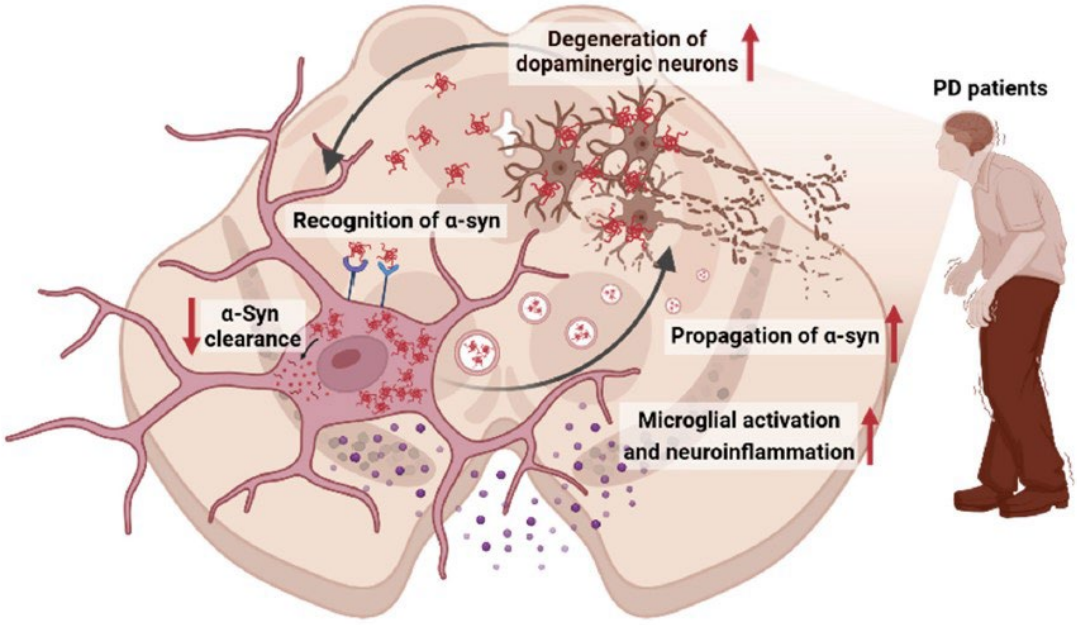

Figure 3. Bidirectional interaction between α-synuclein and microglia in PD. *Microglia recognize α-synuclein aggregates via surface receptors and internalize them. Impaired clearance leads to intracellular accumulation and release of α-synuclein, promoting its spread. This process activates microglia, triggering the release of pro-inflammatory cytokines and contributing to neuroinflammation and dopaminergic neuron degeneration* (Eo et al., 2024).

1.3 Microglia, the resident immune cells of the brain

Microglia are the resident immune cells of the central nervous system (CNS) and play a vital role in maintaining brain homeostasis. Originating from yolk sac progenitors during early embryogenesis, microglia populate the brain independently of peripheral immune cells and are uniquely adapted to the neural environment (Lacaud & Kouskoff, 2017; Ginhoux et al., 2013; Ormel et al., 2018). In the CNS, they make up to 12% of all cells and their density varies depending on the brain region (Hickman et al., 2018). In their physiological state, microglia continuously survey the brain parenchyma and respond to subtle changes in neuronal activity, synaptic remodelling, and tissue integrity. As resident macrophages of the brain parenchyma, microglia contribute to synaptic pruning, phagocytosis of apoptotic cells, clearance of debris, and modulation of neurogenesis, thereby supporting neural circuit development and plasticity (Nimmerjahn et al., 2005; Paolicelli et al., 2011; 2022; Butler et al., 2020; Fu et al., 2014).

Microglia also play a role in regulating immune tolerance within the CNS. Under healthy conditions, they maintain a balance between surveillance and restraint, avoiding unnecessary inflammatory responses. However, this balance is disrupted in neurodegenerative disorders such as Parkinson's disease, where microglia adopt a chronically activated phenotype that contributes to persistent neuroinflammation and neuronal damage (Badjanak et al., 2021; Gao et al., 2023). In PD, microglia are implicated in several key pathological processes. One of their primary roles is the recognition and clearance of misfolded α-synuclein aggregates which accumulate into Lewy bodies and neurites. Microglia detect these aggregates via pattern recognition receptors such as toll-like receptors (TLRs), initiating inflammatory signalling cascades. While this response is initially protective, chronic exposure to α-synuclein leads to overactivation, resulting in the release of pro-inflammatory cytokines, reactive oxygen species (ROS), and nitric oxide (NO), which exacerbate oxidative stress and contribute to dopaminergic neuron loss (Kim & Joh, 2006; Lv et al., 2023; Eo et al., 2024).

Moreover, microglia influence synaptic function through their interactions with neurons and astrocytes. In PD, dysregulated microglial activity can impair synaptic plasticity and neurotransmission, further contributing to motor and cognitive symptoms. Recent studies

have also highlighted the role of microglial autophagy and phagocytosis in modulating the inflammatory response. Deficits in these processes can lead to impaired clearance of α-synuclein and cellular debris, perpetuating inflammation and neurotoxicity (Choi et al., 2020; Lv et al., 2023). Importantly, microglia are increasingly recognized as context-dependent regulators of neurodegeneration. Their phenotype and function are shaped by environmental cues, genetic background, and disease stage. For instance, microglia in the prodromal and early stages of PD may exhibit a primed state that predisposes them to exaggerated responses upon encountering pathological stimuli, reflecting a dynamic that evolves across disease stages (Figure 4) (Zhang et al., 2005; Lind-Holm Mogensen et al., 2025). Genetic studies have identified variants associated with PD risk that are preferentially expressed in microglia, suggesting that microglial dysfunction may be a primary driver of disease in certain individuals (Nalls, et al., 2019; Langston et al., 2022).

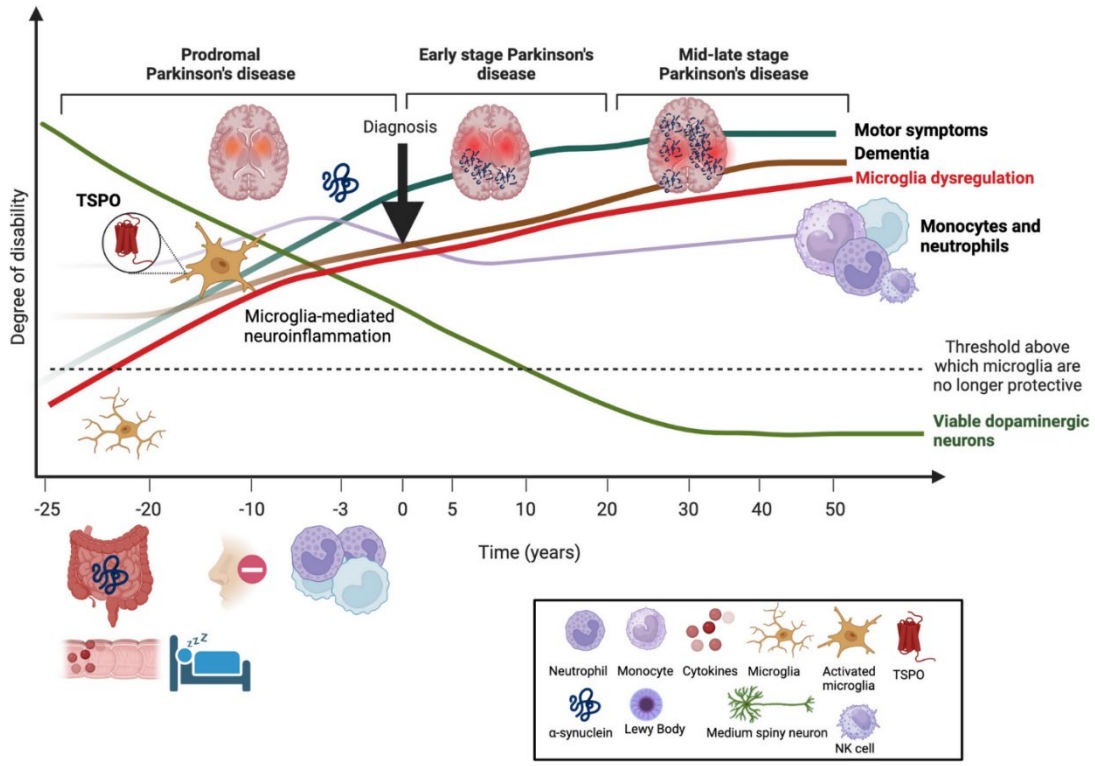

Figure 4. Immune dysregulation and clinical changes along the PD trajectory. *Degree of disability (y-axis) is plotted against the relative time to diagnosis (x-axis). Prodromal symptoms such as constipation, hyposmia, and REM sleep behaviour disorder emerge up to two decades before diagnosis. At diagnosis (black arrow), ~50-80% of dopaminergic neurons are dead, and α-synuclein pathology is present. Microglial dysregulation (red) and peripheral immune cell involvement (purple) increase with disease progression. Motor symptoms (green) and dementia (brown) worsen over time, while dopaminergic neurons (dark green) steadily decline. A threshold Is crossed where microglia shift from protective to detrimental. TSPO marks microglial activation* (Lind-Holm Mogensen et al., 2025).

Given their central role in both neuroprotection and neurodegeneration, microglia represent a promising target for therapeutic intervention. Strategies aimed at modulating microglial activation, enhancing phagocytic clearance, or restoring homeostatic function may offer new avenues for slowing or halting disease progression (Lind-Holm Mogensen et al., 2025; Trainor et al., 2024).

1.4 Models of Parkinson's disease

Understanding Parkinson's disease requires experimental systems that allow researchers to replicate key pathological features, test hypotheses about disease mechanisms, and evaluate potential therapeutic strategies. A variety of models have been developed, ranging from animal and cellular systems to advanced 3D brain organoids. Experimental models are indispensable for studying PD pathogenesis and testing therapeutic strategies. No single model fully recapitulates the human disease, but together they provide complementary insights into the molecular and cellular mechanisms underlying PD.

1.4.1 Animal models

Animal models have historically provided the foundation for PD research. Rodents, non-human primates, and non-mammalian species such as zebrafish and *Drosophila* have been used to investigate the effects of PD-related genetic mutations, environmental toxins, or their combination. Neurotoxin-based models commonly employ 6-hydroxydopamine (6-OHDA), which selectively destroys dopaminergic neurons in the nigrostriatal pathway, and MPTP, which induces mitochondrial dysfunction and dopaminergic neuron loss (Langston et al., 1983; Ungerstedt, 1968; Schober, 2004). Environmental toxins such as rotenone and paraquat have been used to model mitochondrial impairment and oxidative stress, mimicking environmental risk factors for PD (Vaccari et al., 2019; McCormack et al., 2002; Richardson et al., 2005). Genetic models involve transgenic or viral vector-mediated overexpression of human PD-associated genes, including SNCA, LRRK2, PINK1 and DJ-1. Additionally, injection of α-synuclein preformed fibrils (PFFs) into animal brains induces progressive propagation of α-synuclein pathology, recapitulating prion-like spreading observed in human PD (Konnova & Swanberg, 2018).

While animal models provide insights into dopaminergic neuron loss, motor dysfunction, and some aspects of PD pathology, they are limited by species-specific differences in brain structure, transcriptomics, metabolism, and immune responses, which constrain translation to the human disease context (Potashkin et al., 2010; Pembroke et al., 2021). Notably, rodents do not produce neuromelanin in their dopaminergic neurons, a hallmark of human substantia nigra neurons (Marsden, 1961; Vila, 2019). Endogenous α-synuclein pathology does not develop spontaneously in these rodent models and typically requires external

seeding with preformed fibrils to initiate aggregation, limiting the model's ability to model full spectrum PD pathology. However, more robust and progressive pathology can be achieved by combining fibril seeding with α-synuclein overexpression or viral vector-mediated delivery (Jackson-Lewis et al., 2012; Polinski et al., 2018; Thakur et al., 2017; Negrini et al., 2022). Microglia also differ between rodents and humans in their transcriptional signatures and regional distribution, underscoring the need for human-based models (Geirsdottir et al., 2019). Nonetheless, rodent models remain indispensable in preclinical drug development, as they allow *in vivo* testing of novel therapeutics prior to clinical trials (Srivastava et al., 2024; Cenci & Björklund, 2020). Additionally, ethical considerations restrict experimental design and long-term studies.

1.4.2 Postmortem brain samples

Human postmortem brain tissue is essential for validating PD pathology, confirming dopaminergic neuron loss, Lewy body deposition, and neuroinflammatory changes (Signaevsky et al., 2022). Such studies provide definitive evidence of end-stage disease and enable correlation of molecular alterations with neuropathology. However, postmortem tissue only represents the terminal stage of disease and cannot resolve whether observed cellular changes are causes or consequences of neuronal health (Hartmann, 2004). Access to high-quality tissue is further limited by donor recruitment, collection protocols, and preservation methods, which vary across institutions and reduce standardization and reproducibility (Sheperd et al., 2019).

1.4.3 2D cell culture systems

Two-dimensional (2D) cell culture systems offer accessible and controllable models to investigate PD at the cellular level. Primary neurons derived from rodent brains better reflect *in vivo* and can capture aspects of dopaminergic neuron biology, although they are technically demanding and limited in scalability (Falkenburger et al., 2016). Human primary fibroblasts are easily obtained from patients, allowing the study of patient-specific cellular dysfunction, but they lack neuronal characteristic and fail to capture dopaminergic neuron-specific pathology (Auburger et al. 2012). Immortalized cell lines such as SH-SY5Y neuroblastoma and PC12 pheochromocytoma can be differentiated into neuron-like phenotypes and are well suited for genetic manipulation (Biedler et al., 1978). Although these cell lines do not fully recapitulate mature dopaminergic neurons, they remain useful for studying general cellular processes relevant to PD, including α-synuclein dysfunction, oxidative stress and mitochondrial impairment (Xicoy et al., 2017).

The discovery of induced pluripotent stem cells (iPSC) has revolutionised PD modelling by enabling reprogramming of human somatic cells into stem cells that can be differentiated

into virtually any cell types (Takahashi & Yamanaka, 2006; Cerneckis et al., 2024). iPSC-derived dopaminergic neurons are generated based on midbrain developmental principles during embryogenesis (Arenas et al., 2015; Hegarty et al., 2013). Differentiation first involves guiding iPSCs to the neuroectoderm fate through inhibition of SMAD signalling, which includes members of the transforming growth factor β (TGF-β) protein family and the bone morphogenetic protein (BMP) (Chambers et al., 2009). Midbrain dopaminergic lineage is subesquently specified by activation of sonic hedgehog (SHH), WNT, and fibroblast growth factor 8 (FGF8) signalling (Arenas, 2014). Further maturation is achieved using neurotrophic factors including brain-derived neurotrophic factor (BDNF) and glia cell line-derived neurotrophic factor (GDNF) (Galet et al., 2020). Neuronal models derived from stem cells have therefore become a powerful platform to investigate human disease *in vitro* (Sterneckert et al., 2014).

Although these 2D models allow the study of specific neuronal populations, they do not fully capture interactions between different cell types. Therefore, co-culture systems have been developed to better understand cellular crosstalk in PD. For example, co-cultures of iPSC-derived neurons and astrocytes enable researchers to investigate how neurons are affected by healthy or diseased astrocytes (di Domenico et al., 2019). Similarly, co-culturing dopaminergic neurons with microglia has revealed that microglial cells play a crucial role in the maturation, synaptic function, and survival of dopaminergic neurons (Schmidt et al., 2021). Tri-culture systems that include neurons, astrocytes and microglia have been used to study neuroinflammatory mechanisms and the contribution of glial-neuronal interactions to neurodegeneration (Ryan et al., 2020). Despite these advancements, 2D culture models still lack the complexity of cellular interactions and brain architecture in a physiologically relevant context (Ferrari et al., 2020; Avazzadeh et al., 2021).

1.4.4 3D models and midbrain-specific organoids

Three-dimensional (3D) organoids are self-organizing structures derived from pluripotent stem cells that recapitulate aspects of human brain development and architecture (Yin et al., 2016; Setia & Muotri, 2019). Derived from patient-specific iPSCs, they also enable personalized medicine approaches by linking disease modelling directly to patient care. The first cerebral organoids were generated using unguided differentiation, producing varying proportions of cell types across different brain regions, but this variability limited reproducibility and spatial organization (Lancaster et al., 2013). Guided differentiation protocols have since enabled the generation of brain region-specific organoids, including cortical, cerebellar, hippocampal, and midbrain (Qian et al., 2020; Mugurama et al., 2015; Sakaguchi et al., 2015; Jo et al., 2016; Lee et al., 2017). Organoids offer a unique balance between physiological relevance and experimental control, bridging the gap between 2D

cultures and *in vivo* models in terms of cellular complexity and tissue architecture (Figure 5) (Aguilar et al., 2021).

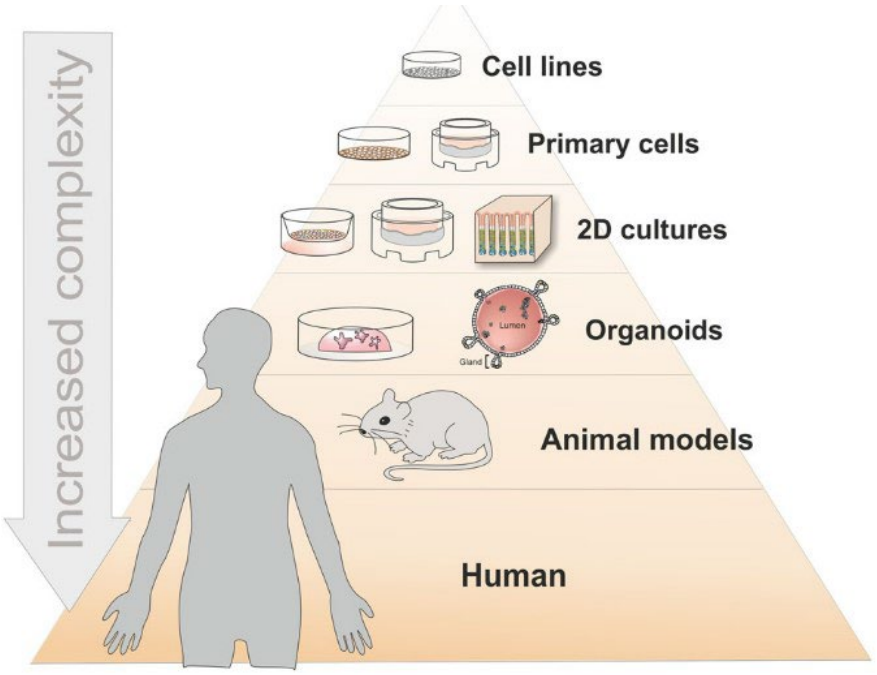

Figure 5. Increasing complexity in cell culture and organoid models. *Organoids offer enhanced physiological relevance compared to traditional 2D cell and primary cultures, enabling the study of 3D tissue architecture and cellular diversity. These models bridge the gap between simplified 2D cultures and whole-organism systems, supporting more accurate investigation of human biology* (Aguilar et al., 2021).

Midbrain organoids are particularly relevant to PD research because they contain dopaminergic neurons, astrocytes, and oligodendrocytes, exhibit electrophysiological activity, and form functional synaptic networks, thus mimicking key features of the human brain (Monzel et al., 2017; Smits et al., 2020; Zagare et al., 2021). Protocols using neuroepithelial stem cells (NESCs) derived from iPSCs enable efficient and reproducible midbrain organoid formation through SHH and WNT pathway activation (Reinhardt et al., 2013; Monzel et al., 2017; Nickels et al., 2020; Smits et al., 2019). Electrophysiological assays demonstrate that neurons within these organoid form active neuronal networks, making them suitable for studying synaptic function, dopaminergic vulnerability, and early pathogenic events. Interestingly, midbrain organoids at day 35 resemble human embryonic midbrain development at around week 9, while organoids at day 70 correspond to week 10, highlighting their ability to recapitulate early developmental stages (Zagare et al., 2022). Importantly, midbrain organoids carrying PD-related mutations, including LRRK2, SNCA, GBA, and PINK1, recapitulate disease-relevant phenotypes such as dopaminergic neuron loss, synaptic disturbances, protein aggregation, and altered neuronal development (Jarazo

et al., 2021; Rosety et al., 2023; Zagare et al., 2022; Muwanigwa et al., 2024). These organoids provide a platform for studying patient-specific genetic contributions and early disease mechanisms.

Recent work has introduced the concept of ‘chimeroids’, generated by fusing organoids derived from genetically distinct individuals. This strategy enables the study of inter-individual susceptibility to neurotoxic triggers in a controlled environment (Antón-Bolaños et al., 2024). By combining cells from genetically distinct individuals, chimeroids provide direct comparison of patient-specific responses and gene-environment interactions, providing a platform to model the heterogenous vulnerability, disease progression, and treatment response observed in PD.

However, since midbrain organoids are derived from neuroectodermal lineages, they lack cell types originating from other lineages, such as mesoderm-derived immune cells and pericytes (Urrestizala-Arenaza et al., 2024). Consequently, they cannot fully recapitulate the dynamic intercellular interactions present in the human brain, despite containing a variety of neuronal and glial cell types.

1.4.5. Advanced 3D brain organoid models - assembloids

Recent advances have extended organoid technology into assembloids, which combine distinct brain region-specific organoids or integrate non-ectodermal cell types to mimic cellular interactions, connectivity, and the immune environment (Paşca et al, 2022; Sabate-Soler, Bernini et al., 2022; Sabate-Soler, Kurniawan et al., 2024; Makrygianni & Chrousos, 2021; Paşca, 2018). A key advancement in PD research is the incorporation of microglia into midbrain organoids. Human iPSC-derived macrophage precursors are generated following the protocol described by Haenseler et al (2017), in which iPSCs are differentiated into MYB-independent macrophage/microglial progenitors through a series of mesodermal and hematopoietic intermediates. In Sabate-Soler et al (2022), these iPSC-derived macrophage precursors are co-cultured with developing midbrain organoids, where they migrate, integrate, and acquire ramified morphologies resembling resident brain microglia. Their presence enhances neuronal maturation, increases synaptic density, and promotes functional electrophysiological activity, providing a more physiologically relevant environment for PD modelling. Integration of microglia allows the study of microglia-neuron interactions, including their roles in synaptic pruning, neuroinflammation, and neurodegeneration, which are central to PD pathophysiology. This approach creates a patient-relevant, three-dimensional platform to investigate genetic risk factors, patient-specific cellular responses, and therapeutic interventions in a controlled *in vitro* human

system (Abud et al., 2017; Song et al., 2019; Xu et al., 2021; Zhang et al., 2023; Hong et al., 2023; Fiorenzano et al., 2025).

Another important model is the midbrain-striatal assembloid, which allows the study of connectivity between dopaminergic neurons and their striatal projection targets, a key interaction underlying motor circuit dysfunction in PD (Barmpa et al., 2024; Miura et al., 2020). Advanced 3D models can also include vascular-like structures to improve nutrient delivery and further mimic brain microenvironments (Cakir et al., 2019; Zimmermann et al., 2025). While these models improve physiological relevance, challenges remain in standardization, reproducibility, and long-term maintenance. Additionally, they reflect early-stage PD because organoids are largely embryonic in nature, which highlights the need for incorporating aging characteristic to study disease progression (Fiorenzano et al., 2025; Tho et al., 2023; Babu et al., 2024; Setia & Muotri, 2019; Barmpa et al., 2024). Despite these limitations, assembloids represent a powerful platform for modelling cellular, regional and immune interactions in PD.

2. Summary and Discussion of the results

This section presents key findings from three interconnected manuscripts (see Chapter 3) demonstrating the reproducibility of midbrain organoids for Parkinson's disease modelling, and how the integration of patient-specific microglia enhances their physiological relevance. This assembloid system enables the investigation of neuroinflammation, dopaminergic neuron degeneration, and Lewy body-associated α-synuclein pathology.

2.1 A reproducible midbrain organoid model for Parkinson's disease.

A major challenge in disease modelling using human pluripotent stem cell-derived organoids is ensuring reproducibility across experiments, particularly when complex 3D differentiation protocols are used (Ludwig et al., 2023; Sandoval et al., 2024). In **Manuscript I**, we focused on the generation and characterization of patient-derived midbrain organoids carrying the GBA-N370S mutation, a known genetic risk factor for Parkinson's disease, with particular attention to the assessment of technical reproducibility and biological variability. Our findings highlight two key aspects. First, the midbrain organoid model is highly reproducible across independently generated batches and sensitive to technical variables such as NESC passage number. Second, the patient-derived organoids carrying the GBA-N370S mutation consistently display disease-associated phenotypes that are in line with previous studies.

Using multiple independently generated midbrain organoid batches derived from GBA-N370S patient lines (**Manuscript I, Figure 1**), we observed that batch-to-batch variability was relatively low (**Manuscript I, Figure 2B-D**). Instead, the passage number of the neuroepithelial stem cells (NESCs) used to initiate organoid formation emerged as a more influential technical variable that contributed to transcriptomic shifts (**Manuscript I, Figure 2B-D**). Both early- and late-passage cultures exhibited disease-relevant features, but early-passage organoids consistently yielded a stronger and more stable transcriptomic signature, particularly related to dopaminergic loss and cellular senescence (**Manuscript I, Figure 3A-C, Figure S2**). These observations emphasize the importance of tracking and controlling the passage number, a factor that can easily be overlooked in experimental design but has a significant impact on data reproducibility.

Principal variance component analysis (PVCA) further demonstrated that biological variables such as donor identity, disease status, and sex were the primary drivers of transcriptional variance across samples (**Manuscript I, Figure 2A-B**). Nonetheless, technical variables, particularly passage, must be accounted for when designing organoid experiments. This is especially important for longitudinal or multi-omics studies, where small

transcriptional shifts can affect biological interpretation. In addition, we performed sample size and power analyses for our bulk RNA sequencing, high-content imaging, and metabolomics datasets, as also recommended by the International Society for Stem Cell Research (ISSCR) (Ludwig et al., 2023; Sandoval et al., 2024). These analyses confirmed that the predefined number of biological replicates and independent batches in our experimental design was sufficient to detect statistically meaningful differences across all modalities. While including multiple batches increased the robustness of our findings (**Manuscript I, Figure 6**), we emphasize that batches should not be treated as additional biological replicates for the purpose of inflating statistical power. Instead, they should be used as technical replicates to evaluate consistency across independent differentiations.

It is important to emphasize that the midbrain organoids in this study were generated using a guided differentiation protocol which reduces variability by directing cells toward a defined midbrain identity. The high reproducibility we observed likely reflects the controlled nature of this approach. In contrast, unguided brain organoid systems rely on spontaneous self-pattering and often exhibit greater heterogeneity in cell type composition and regional identity (Lancaster et al., 2017; Qian et al., 2019). As a result, such models generally require larger sample sizes and more rigorous standardization to detect robust, biologically meaningful effects. Our results thus provide a strong foundation for the use of guided midbrain organoids as a reliable and reproducible model system for studying PD.

Having established the technical reproducibility of the model, we next evaluated whether GBA-N370S patient-derived organoids recapitulate characteristic molecular and cellular features of GBA-associated Parkinson’s disease. The GBA gene encodes the lysosomal enzyme glucocerebrosidase (GCase), which is critical for the breakdown of glycolipids within lysosomes. Heterozygous mutations such as the common missense variant c.1226A>G (p.N370S) are among the most prevalent genetic risk factors for PD. This variant leads to reduced GCase enzymatic activity, disrupting lysosomal function and promoting the accumulation of substrates such as glucosylceramide and α-synuclein, two key features implicated in PD pathogenesis. Although GBA-N370S does not cause Parkinson’s disease in all individuals who carry it, it is one of the most common genetic risk factors and is associated with an increased likelihood of developing the disease, as well as earlier onset and faster progression in diagnosed individuals. Similar to variants such as LRRK2-G2019S, the pathogenic impact of GBA-N370S is thought to depend on interactions with additional molecular and environmental factors to drive neurodegeneration (Sidransky et al., 2009; Schapira & Gegg, 2013; Smith & Schapira 2022).

In our study, we aimed to validate and further explore known features of GBA-associated PD using highly reproducible midbrain organoid datasets. Across multiple independently generated batches, we consistently observed hallmarks of GBA-PD pathology, including decrease in TH-positive dopaminergic neurons (**Manuscript I, Figure 4A-C, Figure S3**), increased expression of senescence-associated genes (**Manuscript I, Figure 3, Figure 4D-F, Figure S2, Figure S4**), and distinct metabolic alterations (**Manuscript I, Figure 5, Figure S5**). These phenotypes align closely with previously published work (Rosety et al., 2023; Zagare et al., 2024) and were validated across transcriptomic (**Manuscript I, Figure 3, Figures S2-4**), proteomic (**Manuscript I, Figure 4**), and metabolomic levels (**Manuscript I, Figure 5, Figure S5**). The consistency of these findings across batches and timepoints supports the biological robustness of the model and underscores its value in recapitulating disease-relevant mechanisms.

Altogether, our study demonstrates that midbrain organoids derived from GBA-N370S patient cells are a reproducible and phenotypically faithful *in vitro* model for Parkinson's disease. By identifying and controlling key sources of variability, particularly passage number, and validating disease phenotypes across multiple experimental levels, this work contributes to the standardization and scalability of organoid-based disease modelling. These findings provide a practical framework for improving reproducibility in future organoid studies and for advancing the use of patient-derived models in translational PD research.

2.2 Human patient-specific microglia drive Parkinson's disease pathology in midbrain organoids.

While conventional midbrain organoids recapitulate dopaminergic neuron vulnerability (**Manuscript** I), they lack a neuroimmune component. To address this, we incorporated iPSC-derived microglia into midbrain organoids, following an optimized approach described by Sabate-Soler et al. (2022). This assembloid model allows the investigation of microglia-driven mechanisms in PD and provides a foundation for studying patient-specific neuroimmune responses.

Manuscript II focuses on the LRRK2-G2019S mutation, the most prevalent variant associated with both familial and sporadic forms of Parkinson's disease. Although the mutation substantially increases the risk of developing PD, not all carriers are affected, indicating that additional genetic, molecular, or environmental factors likely contribute to disease onset and progression (Day & Mullin, 2021). LRRK2 is highly expressed during early brain development, particularly in neuronal progenitors, and also plays a central role in microglial function by regulating vesicle trafficking, cytokine release, and lysosomal activity (Zechel et al., 2010; Milosevic et al., 2009). The G2019S mutation has been shown

to enhance microglial inflammatory responses and contribute to a chronic pro-inflammatory environment in the brain (Russo et al., 2014; Moehle et al., 2012). This neuroinflammatory state may exacerbate dopaminergic neuron vulnerability, especially in the substantia nigra where microglia are densely concentrated. These dual roles of LRRK2, in both neurons and microglia, support a model in which the G2019S mutation contributes to PD pathogenesis through a combination of intrinsic neuronal dysfunction and microglia-mediated neuroinflammation, ultimately increasing the susceptibility of dopaminergic neurons to cellular stress and degeneration.

To further decipher the contribution of LRRK2-G2019S to microglial dysfunction, we investigated its effects in iPSC-derived human microglia. While the mutant microglia retained typical identity markers and differentiation capacity (**Manuscript II, Figure 1**), they exhibited a distinctly altered immune profile, characterized by increased phagocytic capacity (**Manuscript II, Figure 2C-D**). This phenotype aligns with previous studies showing that LRRK2 mutations, particularly p.G2019S, enhance phagocytosis in myeloid cells through dysregulation of vesicle trafficking and cytoskeletal dynamics (Russo et al., 2014; Bonet-Ponce & Cookson, 2022). Furthermore, LRRK2-G2019S microglia showed selective upregulation of TNF-α (**Manuscript II, Figure 2E-F**), a pro-inflammatory cytokine implicated in both apoptotic and necroptotic mechanisms of neuronal death, suggesting a potential pathway through which mutant microglia contribute to neurotoxicity (Brenner et al., 2015; Ohtonen et al., 2023). At the metabolic level, we observed a shift towards a pro-inflammatory immunometabolic state characterized by increased mTOR signalling and elevated glycolytic flux (**Manuscript II, Figure 3E-F, Figure 4A-E, Figure S3C, Figure S4A-C**). Metabolomic profiling and isotope tracing further revealed a disruption in serine biosynthesis, specifically reduced expression of PHGDH and PSAT1, accompanied by lower incorporation of glucose-derived carbon into the serine pool (**Manuscript II, Figure 4D-J)**. Although ROS levels remained unchanged, the transcriptional enrichment of oxidative stress-related pathways suggests the presence of compensatory antioxidant responses to the elevated metabolic demands (**Manuscript II, Figure 3C-E, Figure S3C**). Collectively, these findings point to a metabolically driven pro-inflammatory microglial state induced by the LRRK2-G2019S mutation, which may lower the threshold for neuroinflammatory damage and contribute to disease-relevant pathology in Parkinson's disease.

To better capture the multicellular dynamics underlying Parkinson's disease pathogenesis, we integrated LRRK2-G2019S microglia into healthy control (WT) midbrain organoids. This co-culture system allowed us to investigate neuroimmune crosstalk in a physiologically relevant human model. In this context, LRRK2-G2019S microglia exerted a neurotoxic

influence, leading to a selective loss of dopaminergic neurons compared to organoids containing WT microglia (**Manuscript II, Figure 5B-D**). This neuronal vulnerability was accompanied by elevated CD86 expression, increased phagocytic activity, and higher TNF-α levels (**Manuscript II, Figure 6C-E**). These findings suggest that microglial dysfunction in PD may act as a primary driver of disease-relevant pathology when predisposing mutations are present, since mutant microglia alone are sufficient to trigger dopaminergic neuron degeneration in an otherwise healthy neuronal environment.

Given our previous findings that LRRK2-G2019S iPSC-derived microglia exhibit a metabolically primed, pro-inflammatory state, characterized by increased glycolysis, mTOR activation, and TNF-α secretion, we hypothesized that this immune-metabolic dysregulation contributes directly to neurotoxicity. To explore whether targeting this imbalance could mitigate microglia-induced neuronal damage, we treated the assembloids with oxamic acid, a lactate dehydrogenase inhibitor known to suppress glycolysis and mTOR signalling (Fiume et al., 2011; Zhao et al., 2015). Oxamic acid treatment restored key metabolic parameters in LRRK2-G2019S microglia (**Manuscript II, Figure 6A-B**), reduced CD86 expression, and lowered TNF-α secretion, without impairing phagocytic capacity (**Manuscript II, Figure 6A-E**). Importantly, oxamic acid prevented dopaminergic neuron loss (**Manuscript II, Figure 6F**) supporting a TNF-α-dependent mechanism of microglial neurotoxicity.

Overall, the data described in **Manuscript II** demonstrates that the LRRK2-G2019S mutation reprograms human microglia into a metabolically primed, pro-inflammatory state that promotes dopaminergic neuron degeneration. This supports a model in which microglial dysfunction acts as a primary driver of neurodegeneration in PD, even in the absence of intrinsic neuronal pathology. Our findings align with previous reports of LRRK2-mediated immune dysregulation, including enhanced cytokine release and phagocytic activity (Russo et al., 2014; Ho et al., 2019; Bonet-Ponce & Cookson, 2022), but extend them by showing that metabolic reprogramming, specifically increased glycolysis and mTOR activation, may be a critical upstream event in microglia-induced neurotoxicity. This metabolic shift reflects a broader theme in PD pathogenesis, where immune cell metabolism is increasingly recognized as a key regulator of inflammatory responses and neuronal vulnerability (Mark & Tansey, 2025). Targeting altered metabolic states, specifically through glycolysis inhibition, reduced TNF-α driven neurotoxicity while preserving beneficial phagocytic function, highlighting microglial metabolism as a promising therapeutic entry point. These findings are further supported by Blasco-Agell et al., (2025), showing that LRRK2-mutant microglia are sufficient to induce dopaminergic neuron loss in iPSC-derived models, confirming the concept that microglial dysfunction alone can drive PD-relevant pathology.

Our results raise important questions about the temporal dynamics of microglial activation and metabolic shifts during PD progression. For instance, it remains unclear whether metabolic priming precedes inflammatory signalling or emerges as a consequence of chronic activation. Moreover, whether similar immune-metabolic mechanisms are present in other PD-associated mutations warrants further investigation. Future studies could explore combinatorial interventions targeting both immune and metabolic pathways, and leverage patient-derived assembloids to dissect genotype-specific responses and therapeutic sensitivities. Importantly, our assembloid system provides a scalable and physiologically relevant platform for testing such interventions, bridging the gap between mechanistic insights and translational applications.

Using the assembloid model, we next investigated how microglia carrying the SNCA triplication (3xSNCA) affect PD pathology within midbrain organoids. This mutation is a well-characterized genetic cause of PD, in which individuals carry three instead of two copies of the SNCA gene. This dosage increase leads to elevated α-synuclein expression and is associated with early-onset, rapidly progressing PD with widespread Lewy-pathology (Singleton et al., 2003; Devine et al., 2011).

In vitro studies using midbrain organoids derived from 3xSNCA patient lines have consistently demonstrated increased total α-synuclein levels and, with prolonged culture showing the progressive appearance of α-synuclein accumulation (Cui et al., 2024). For example, Oliveira et al. (2015) reported that dopaminergic neurons from 3xSNCA iPSCs display elevated total α-synuclein and mitochondrial abnormalities. Jo et al. (2021) showed that when 3xSNCA midbrain organoids were exposed to conduritol B epoxide (CBE), a lysosomal inhibitor, Lewy body-like inclusions formed by day 90, suggesting that disruption of proteostasis is required to trigger visible pathology. Long term culture studies have described progressive accumulation of phosphorylated α-synuclein (pS129), particularly between days 100 and 180 of cultures (Mohamed et al., 2021; Becerra-Calixto et al., 2023; Muwanigwa et al., 2024). These findings are consistent with a model in which SNCA overexpression induces slow, cumulative pathological changes that eventually reach a disease-relevant threshold. Notably, Lashuel et al. (2022) emphasized the need to distinguish between diffuse phosphorylated α-synuclein and more structured, filamentous aggregates with biochemical and morphological features of Lewy pathology. Nevertheless, most *in vitro* models are unable to produce these mature pathological α-synuclein structures, likely due to limitations in culture duration and cellular maturity.

In this context, **Manuscript III** presents a significant advance by demonstrating that co-culture of 3xSNCA microglia with midbrain organoids accelerates α-synuclein pathology,

resulting in robust formation of pS129-positive aggregates at day 50, notably earlier than previously reported. Phosphorylation at serine 129, located in the C-terminal region of α-synuclein, is a key post-translational modification that is strongly associated with pathogenic α-synuclein in PD (Eo et al., 2024; Chapter 1, Figure 2A). Modifications in the C-terminal region, including pS129, can influence α-synuclein aggregation, with phosphorylation at this site accelerating fibril formation, enhancing membrane interactions, and increasing neurotoxic potential (Samuel et al., 2016). Importantly, the observed pS129 aggregation occurs without exogenous preformed fibrils or pharmacological stressors, underscoring the sufficiency of microglial dysfunction to initiate pathogenic α-synuclein accumulation. Taking advantage of the assembloid model described by Sabate-Soler et al (2022) and used in **Manuscript II**, the integration of microglia carrying the 3xSNCA mutation into human midbrain organoids enabled a detailed examination of how genetically predisposed immune cells shape the early course of disease.

Already, 3xSNCA microglia not only expressed total α-synuclein but also exhibited a loss of key homeostatic features, including impaired phagocytic capacity, altered pro-inflammatory signalling, and transcriptional changes in lysosomal and metabolic pathways (**Manuscript III, Figure 1, Figure S2**). Upon integration into the 3xSNCA midbrain organoid environment, these microglia adopted an activated, ameboid morphology, indicative of reduced homeostatic surveillance, in contrast to WT microglia in WT midbrain organoids, which maintained a more ramified, surveillant morphology (**Manuscript III, Figure 2D-E**). The 3xSNCA assembloids exhibited also a significant increase in intra- and extracellular α-synuclein as well as increased levels of its phosphorylated form (pS129) (**Manuscript III, Figure 3**). The interaction of the 3xSNCA microglia with neurons likely intensified proteostatic stress, either through the release of pro-inflammatory cytokines or insufficient clearance of extracellular α-synuclein. This initiates a pathological feedback loop in which neuroinflammation, and aggregation reciprocally exacerbate each other. Notably, this dysregulated phenotype was associated with the spontaneous accumulation of pS129, which aggregated by day 50 (**Manuscript III, Figure 4A**), substantially earlier than reported in comparable SNCA overexpression models (Birtele et al., 2025). The morphological diversity of the pS129-positive structures, as described by Lashuel et al. (2022), closely resembles Lewy body pathology observed in postmortem brain tissue of PD patients. Specifically, the filamentous- and dense-like structures resemble brainstem-type Lewy bodies and Lewy neurites in the substantia nigra of the brain (Koga et al., 2021). To confirm the pathological nature of these aggregates, we used a comprehensive panel of established aggregation markers (**Manuscript III, Figure 4B-F, Figure S3**). Their co-localization with pS129-positive structures confirms that the observed pathology involves aggregation

processes. This rapid onset suggests that microglial dysfunction in the context of the SNCA triplication accelerated pathological aggregation, likely by overwhelming endogenous clearance systems rather than responding secondarily to neuronal stress.

Further evidence for a microglia-driven mechanism was established using a chimeric assembloid system. Here, 3xSNCA microglia were integrated into WT midbrain organoids. Remarkably, these chimeric assembloids developed pS129-positive aggregates even without neuronal SNCA overexpression (**Manuscript III, Figure 5C**). This indicates that 3xSNCA microglia alone are sufficient to initiate disease-relevant pathology. Co-localization with aggregation markers in the chimeric model further confirmed the pathological relevance of the observed aggregates (**Manuscript III, Figure 5D-E, Figure S4**). These findings challenge conventional models that place neurons at the centre of disease onset and support the notion that non-neuronal cells, particularly microglia, can be primary contributors to PD-associated genetic alterations.

Together, these results demonstrate that microglial dysfunction driven by the SNCA gene triplication is not a secondary reaction to neuronal stress but a primary initiator of PD pathology. The assembloid model described here advances the field by providing a genetically defined and physiologically relevant model for studying microglia-neuron interactions in human synucleinopathies. This allows the investigation of early α-synuclein aggregation and its cellular drivers in the absence of artificial seeding of preformed fibrils.

Mechanistically, several factors may converge to explain the pathology. The overexpression of SNCA in microglia likely overwhelms intracellular clearance systems, including the autophagy-lysosome and ubiquitin-proteasome pathways, and impairs their ability to degrade α-synuclein and other protein aggregates (Plaza-Zabala et al., 2017; Lv et al., 2023; Eo et al., 2024). This proteostatic stress may be further exacerbated by the relatively limited degradative capacity of microglia compared to neurons, particularly under inflammatory conditions (Quick et al., 2023). In parallel, the pro-inflammatory state of microglia, marked by cytokine secretion or impaired clearance of cellular debris, can promote neuronal stress and facilitate α-synuclein aggregation in neighbouring cells (Gao et al., 2023; Eo et al., 2024). Notably, IL-1β and TNF-α have been shown to enhance α-synuclein expression and aggregation, suggesting a feed-forward loop between inflammation and proteotoxicity. The interplay between impaired proteostasis and chronic inflammation likely creates a permissive environment for neurodegeneration, particularly in vulnerable dopaminergic populations. However, the precise sequence and interdependence of these events remain unclear. For instance, whether α-synuclein accumulation in microglia

precedes or follow inflammatory activation is still debated and represents a key direction for further investigation (Sonninen et al., 2020; Lv et al., 2023; Eo et al., 2024).

Emerging longitudinal biomarker data in patients support a temporal progression of these dynamics. Baseline cerebrospinal fluid (CSF) α-synuclein levels predict subsequent decline in sensorimotor connectivity (Campbell et al., 2020), while dynamic changes in α-synuclein species correlate with worsening motor symptoms and cognitive decline (Majbour et al., 2016; Brockmann et al., 2021). These findings suggest that proteostatic and inflammatory imbalances evolve over the disease course and are detectable before overt pathology. Together, these patient biomarker studies and our assembloid findings point toward a temporal disease trajectory that can be intercepted therapeutically.

These insights have sparked the development of targeted therapeutic strategies to reduce α-synuclein burden and restoring proteostasis. Small molecules such as Minzasolmin (UCB0599) and Emrusolmin (Anle138b) interfere with α-synuclein misfolding and oligomerization, thus preventing the formation of toxic aggregates (Price et al., 2023; Heras-Garvin et al., 2019; Wegrzynowicz, et al., 2019). Other molecules, like squalamine and trodusquemine, displace α-synuclein from lipid membranes, thereby blocking its aggregation at the source (Perni et al., 2017; Rao et al., 2000; Yang et al., 2024). In parallel, strategies that enhance lysosomal degradation, such ambroxol, which increases glucocerebrosidase activity, offer complementary options for reducing intracellular burden and oxidative stress (Colucci et al., 2023).

Overall, the findings from **Manuscript II** and **Manuscript III** establish microglia carrying PD-associated mutations as central contributors to Parkinson's disease pathology. LRRK2-G2019S microglia promote dopaminergic neuron degeneration through metabolic reprogramming and heightened inflammatory signalling, whereas SNCA triplication drives early and robust α-synuclein aggregation through lysosomal dysfunction and impaired phagocytic capacity. Despite acting through distinct molecular pathways, both mutations result in a disease-promoting microglial phenotype, challenging the neuron-centric view of PD and positioning microglia as active initiators of neurodegeneration. This conceptual shift has significant implication for the field. It reframes PD not solely as a neuronal disorder, but as a multifaceted disease involving immune dysfunction and impaired proteostasis. Recognizing microglia as central players opens new avenues for understanding early pathogenic events and highlights the need to explore microglia-specific biomarkers and therapeutic targets. For example, inflammatory cytokine profiles, metabolic signatures, or phagocytic behaviour could serve as early indicators of disease onset or progression, particularly in genetically predisposed individuals. These biomarkers could also contribute

to patient stratification in clinical trials and enable personalized treatment approaches based on microglial dysfunction. Therapeutically, interventions aimed at restoring microglial homeostasis, whether by modulating inflammatory signalling, correcting metabolic imbalances, or enhancing proteostatic capacity, may complement neuron-focused strategies and potentially slow disease progression.

These insights underscore the importance of cell-type specific therapeutic strategies, as targeting microglial dysfunction may require fundamentally different approaches than those used for neurons. The integration of microglia into human midbrain organoids provides a physiologically relevant model to dissect neuroimmune interactions and test tailored interventions, bridging mechanistic understanding with translational potential.

Chapter 2: Materials and Methods

A detailed description of all materials and methods that were used in this thesis can be found in the original articles listed in Chapter 3: Results. The following section outlines the main experimental procedures I performed or contributed to in each study.

- iPSC culture
  - see Manuscript II and III
- Derivation and culture of NESCs
  - see Manuscript I, II and III
- Generation of midbrain organoids
  - see Manuscript I, II, and III
- Macrophage precursor derivation and microglia differentiation
  - see Manuscript II and III
- Co-culture of midbrain organoids with macrophage precursors
  - see Manuscript II and III
- Western Blotting and analysis
  - see Manuscript II and III
- Dot Blot for α-synuclein
  - see Manuscript III
- Flow Cytometry
  - see Manuscript III
- Immunofluorescence staining
  - see Manuscript I and III
- β-galactosidase assay
  - see Manuscript I
- Confocal microscopy
  - see Manuscript I and III
- High-Content Imaging and image analysis with MATLAB
  - see Manuscript I and III
- 3D reconstruction with IMARIS
  - see Manuscript I and III
- RNA extraction, library preparation and sequencing
  - see Manuscript I and III
- Bulk RNA sequencing data analysis
  - see Manuscript I and III

- Statistical analysis with R and GraphPad
    - see Manuscript I and III

Chapter 3: Results

Manuscript I: Reproducibility of PD patient-specific midbrain organoid data for *in vitro* disease modelling. (Zuccoli & Al Sawaf et al., 2025)

Manuscript II: The Parkinson's disease-associated LRRK2-G2019S variant restricts serine metabolism, leading to microglial inflammation and dopaminergic neuron degeneration. (Kurniawan et al., 2025)

Manuscript III: Parkinson's disease microglia induce endogenous α-synuclein pathology in patient-specific midbrain organoids. (Zuccoli et al., 2025)

3.1 Manuscript I

Reproducibility of PD patient-specific midbrain organoid data for *in vitro* disease modelling.

Elisa Zuccoli[1#], Haya Al Sawaf[1#], Mona Tuzza[1], Sarah Nickels[1], Alise Zagare[1], Jens C. Schwamborn[1*]

[1] Developmental and Cellular Biology, Luxembourg Centre for Systems Biomedicine (LCSB), University of Luxembourg, 6, Avenue du Swing, L-4367 Belvaux, Luxembourg.

#Co-first authors

*Corresponding author

This article has been published in iScience.

3.1.1 Contribution statement

In this study, I share first authorship with H. Al Sawaf. We both had an equal contribution to the development of the R scripts, data analysis, and writing of the manuscript. My specific contributions included performing cell culture and RNA extraction of midbrain organoids, extracting the counts from the fastQ files, and developing the R scripts for the bulk RNA sequencing. I also conducted correlation and principal component analysis of Dataset 1, with the results presented in Figure 2 (panels A, E-H). Additionally, I performed differential gene expression analysis of Dataset 1, integrated Dataset 2, and performed its gene expression analysis, as shown in Figure 3. I also acquired and analysed the immunofluorescence staining images for Figure 4 and prepared the manuscript figures. A. Zagare supervised the project and analysed the metabolomic data. The initial concept for the study was developed by J. C. Schwamborn.

3.1.2 Preface

The main aim of this manuscript was to evaluate the reproducibility of midbrain organoids derived from GBA-PD patient lines, focusing on multiple timepoints and both early and late NESC passages. For this study, we used three age- and sex-matched healthy control cell lines and three GBA-N370S PD cell lines. Midbrain organoids were generated from NESCs, and two complementary datasets were collected. Bulk RNA sequencing, metabolomic profiling, and high-content image analysis were then applied to capture molecular, metabolic, and cellular phenotypes associated with PD. Our objectives included assessing disease-specific transcriptomic and metabolic signatures, validating phenotypic markers at the protein level, and establishing the model as a robust and reproducible platform for PD *in vitro* research. Moreover, we aimed to quantify batch- and passage-dependent variability, thereby demonstrating the reproducibility of GBA-PD midbrain organoids across batches and timepoints.

Dataset 1 consisted of midbrain organoids cultured to day 30 and included four batches each at early (p10-p15) and late (p16-p20) passages. Bulk RNA sequencing revealed that disease, cell line, and sex were the most influential variables, with passage number also contributing strongly. The transcriptomic data highlighted genes associated with senescence and apoptosis, and these results were confirmed by image analysis, consistent with previous studies of GBA-PD midbrain organoids (Rosety et al., 2023; Zagare et al., 2024). Dataset 2 also comprised four batches, but the midbrain organoids were cultured at two different timepoints, day 30 and day 60. Transcriptomic analysis at both timepoints revealed consistent disease-specific phenotypes, emphasizing the reproducibility of the

GBA-PD model. Additionally, metabolic profiling of Dataset 2 demonstrated highly consistent metabolic expression patterns, underlining the robustness of the observed metabolic signature. Integration of transcriptomic data from both datasets showed a strong similarity between late passage batches at day 30 (Dataset 1) and those cultured until day 60 (Dataset 2), suggesting that number of passages contributed to an aging-related transcriptional shift. Finally, we performed a sample estimation power analysis for each data modality. Here we showed that 30 samples per group are required to reach optimal statistical power to detect true differences in the transcriptomic data. Metabolomics required 20 samples per group and imaging data 50 samples per group. These results emphasize the importance of incorporating multiple batches to ensure statistical power for reproducible and robust results, particularly critical when the availability of biological replicates (cell lines) is imitated. Our study highlights the potential of patient-specific organoids for advancing our understanding of disease mechanisms and accelerating the development of personalized treatments for Parkinson's disease.

iScience

Article

Reproducibility of PD patient-specific midbrain organoid data for *in vitro* disease modeling

Graphical abstract

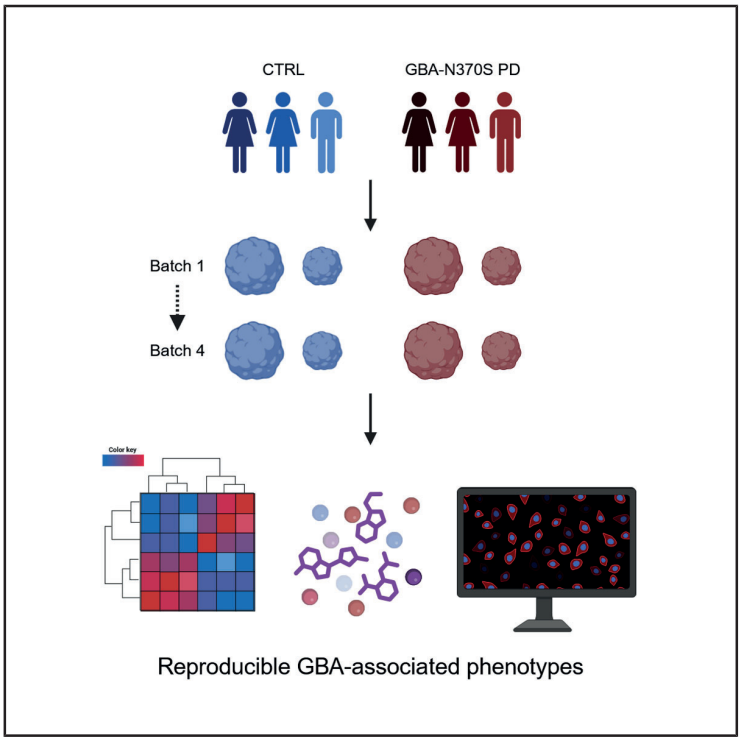

Authors

Elisa Zuccoli, Haya Al Sawaf, Mona Tuzza, Sarah L. Nickels, Alise Zagare, Jens C. Schwamborn

Correspondence

jens.schwamborn@uni.lu

In brief

Molecular biology; Neuroscience; Cell biology; Omics

Highlights

- Midbrain organoids provide a robust *in vitro* model for Parkinson's disease
- GBA-PD phenotypes are reproducible across midbrain organoid batches
- NESC passage has a greater impact on variability than organoid batches
- Disease signatures are consistent at transcriptomic, protein, and metabolic levels

Zuccoli et al., 2025, iScience *28*, 113541
October 17, 2025
https://doi.org/10.1016/j.isci.2025.113541

CellPress

iScience

CellPress
OPEN ACCESS

Article

Reproducibility of PD patient-specific midbrain organoid data for *in vitro* disease modeling

Elisa Zuccoli,[1,2] Haya Al Sawaf,[1,2] Mona Tuzza,[1] Sarah L. Nickels,[1] Alise Zagare,[1] and Jens C. Schwamborn[1,3,*]
[1]Developmental and Cellular Biology, Luxembourg Centre for Systems Biomedicine (LCSB), University of Luxembourg, 6, Avenue du Swing, 4367 Belvaux, Luxembourg
[2]These authors contributed equally
[3]Lead contact
*Correspondence: jens.schwamborn@uni.lu
https://doi.org/10.1016/j.isci.2025.113541

SUMMARY

Midbrain organoids are advanced *in vitro* cellular models for disease modeling. They have been used successfully over the past decade for Parkinson's disease (PD) research and drug development. The three-dimensional structure and multicellular composition allow disease research under more physiological conditions than is possible with conventional 2D cellular models. However, there are concerns in the field regarding the organoid batch-to-batch variability and thus the reproducibility of the results. In this manuscript, we generate multiple independent midbrain organoid batches derived from healthy individuals or glucocerebrosidase (GBA)-N370S mutation-carrying PD patients to evaluate the reproducibility of the GBA-N370S mutation-associated PD transcriptomic and metabolic signature as well as selected protein abundance. Our analysis shows that GBA-PD-associated phenotypes are reproducible across organoid generation batches and time points. This proves that midbrain organoids are not only suitable for PD *in vitro* modeling but also represent robust and highly reproducible cellular models.

INTRODUCTION

Parkinson's disease (PD) is a common neurodegenerative disorder characterized by the progressive loss of midbrain dopaminergic neurons, leading to motor symptoms such as bradykinesia, rigidity, and tremors, as well as cognitive impairments.[1] Conventional two-dimensional (2D) cell cultures and animal models have limitations in replicating the complexity of the human midbrain, hindering their utility in understanding PD pathogenesis, and developing effective therapies.[2] Specifically, 2D cultures lack intricate cell-to-cell interactions, which are present in three-dimensional structures, and are crucial for accurately modeling neural environments. Additionally, animal models, such as mice, do not naturally develop neurodegenerative diseases like Parkinson's, and their brain anatomy differs significantly from humans, which limits their effectiveness in studying complex human brain disease processes.[3] Recent breakthroughs in stem cell technologies have resulted in the development of three-dimensional (3D) midbrain organoids, which more closely mimic the architecture and cellular diversity of the human midbrain. Importantly, these organoids are derived from patient-specific induced pluripotent stem cells (iPSCs) and are generated via the differentiation of iPSCs into neuroepithelial stem cells (NESCs), which subsequently self-organize into midbrain-like structures.[4,5] This approach offers a physiologically relevant platform to study disease mechanisms and to test therapeutic interventions on patient-specific genetic backgrounds. Glucocerebrosidase (GBA)-associated PD, linked to mutations in the GBA (GBA1) gene, represents one of the most significant genetic risk factors for PD.[6] GBA mutations impair lysosomal function and autophagy, contributing to α-synuclein protein accumulation and dopaminergic neuron loss.[6] Additionally, cellular senescence has emerged as a contributing factor in PD, with evidence suggesting that senescent cells exacerbate neurodegeneration through pro-inflammatory pathways.[7–9] Midbrain organoids derived from GBA-PD patients have shown hallmarks of disease, including dopaminergic neuron loss, oxidative stress, impaired lipid metabolism, and a senescence-associated phenotype.[10] These findings underline the value of midbrain organoids as a robust platform to explore the interplay between genetic risk factors, cellular senescence, and neurodegeneration. iPSC-derived organoid models hold the potential to inform therapeutic strategies targeting the underlying mechanisms of GBA-associated PD and related neurodegenerative disorders.

Although midbrain organoid models hold significant promise, they also present certain limitations that must be carefully considered when designing experiments. Complex, multistep culturing protocols can increase sources of variability, thus increasing the number of replicates needed both within a batch and between independent batches. Therefore, it is important to be aware of variation sources in order to account for it. In this manuscript, we explore these sources of variation and inform on the relevance of cell passage in reducing batch-to-batch variability. Overall, our results show that key disease phenotypes are reproducible despite potential sources of variability.

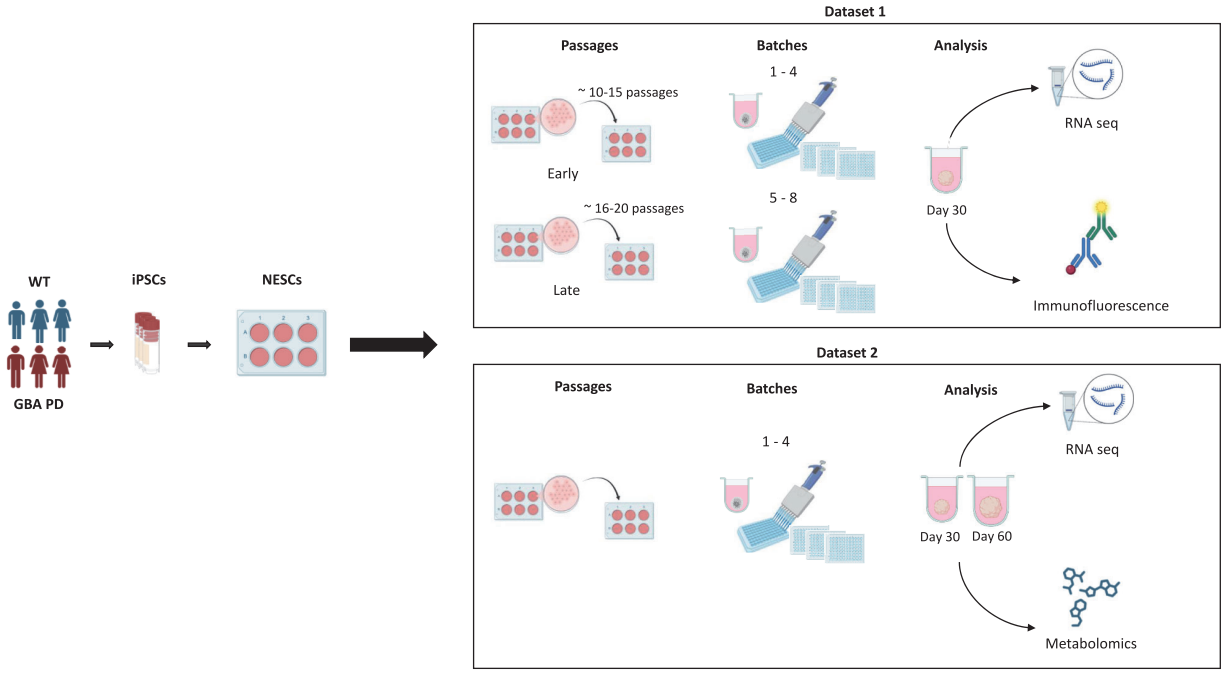

Figure 1. Overview of factors affecting midbrain organoid culture and dataset generation

Schematic overview of the factors affecting midbrain organoid culture and dataset generation. iPSCs from healthy control (WT) and GBA-PD patients were differentiated into NESCs. For dataset 1, midbrain organoids from early (~10–15) or late (~16–20) passages were generated in four independent batches. On day 30 of midbrain organoid culture, RNA-seq and immunofluorescence experiments were performed. For dataset 2, four independent batches of midbrain organoids were generated. On day 30 or day 60 of midbrain organoid culture, RNA-seq and metabolomic analysis were performed.

RESULTS

Disease and cell passage are key sources of variation in midbrain organoid culture

The midbrain organoid culture system is influenced by several factors, including cell line selection, initial passage number, donor sex, and potential batch effects from different experimental runs, all of which require careful consideration (Figure 1; Table 1). To investigate each factor's contribution to the data variance, we generated midbrain organoids from three healthy donors and three patients with PD carrying the GBA-N370S variant (GBA-PD) (Table S1). iPSCs derived from GBA-PD patients and healthy donors were differentiated into NESCs and patterned toward a midbrain identity to generate midbrain organoids.[4] In this study, two independent datasets were produced, where dataset 1 comprised RNA sequencing (RNA-seq) and immunofluorescence analyses performed on 30-day-old midbrain organoids and dataset 2 included metabolomic analysis and RNA-seq analysis performed on both day 30 and day 60 midbrain organoids cultures. While dataset 1 was used to define experimental and biological sources of variation, dataset 2 served to validate the reproducibility of key phenotypes across independent experiments (Figure 1).

Correlation analysis of transcriptomic signatures of eight independent organoid generation batches from early and late NESC passages revealed that the features such as disease, cell line, and donor sex are interdependent factors, representing the donor (patient or healthy individual). However, the passage of NESCs and the organoid generation batch are independent sources of variance (Figure 2A). Applying principal variance component analysis (PVCA), a statistical method for quantifying and prioritizing sources of variance, revealed that the interaction between disease and sex (31.7%) contributed most to the variance in the transcriptomic data. The passage (31%) appeared as the second highest contributor, followed by the residual variance (18.6%), which represents the variance that cannot be attributed to specific explanatory variables or known factors in our dataset. The variance attributed to batch (5%) or its interaction with passage (0.7%), sex (0%), or disease (0%) showed an insignificant role in the data variance (Figure 2B).

Considering the presumed role of the passage number in transcriptomic data variation, we divided the dataset in batches generated from early (pE10–15) or late NESC passages (pL16–20) to explore the effects of passage on data reproducibility in detail. The PVCA showed that the disease accounted for the largest proportion of the variance (32.8%) in organoid batches generated from early-passage NESCs, followed by the interaction between disease and sex (26.3%) and the unexplained residuals (26%). The percentage of the batch was elevated compared to the complete dataset (4%) (Figure 2C). Similarly, the disease-sex interaction with 55% was the highest contributor to the variance in the organoid batches produced from the late passages (B5–8), followed by the residual variance (21.2%). We observed that the proportion of variance of the batch doubled in organoids

Table 1. Nomenclature

Statistical term	Culture term	Definition
Biological replicate	individual	healthy or GBA-N370S mutation-carrying donor
	patient	donor with Parkinson's disease (PD) diagnosis
	cell line	an iPSC cell line is a population of pluripotent stem cells derived from a single donor through one reprogramming event. Multiple independent iPSC lines (clones, see below) from the same donor can be generated as biological replicates to account for variability
	passage	cell line passages refer to the number of times a cell culture is split (propagated) once it becomes confluent
	clone	a clone is a population of genetically identical cells derived from a single parent cell, typically originating from a specific donor; multiple clones can be derived from a single donor, but a single clone is often selected for experiments to ensure genetic and phenotypic consistency
	batch	each batch represents independent generations of midbrain organoids from different neuroepithelial stem cell (NESC) passages, accounting for variability in organoid maturation; within a batch, organoids serve as biological replicates, cultured and processed together under identical conditions to minimize batch effects and ensure reproducibility
	sample	a sample is a unique experimental unit used for analysis. Its origin depends on the experiment and assay, coming from either an independent organoid culture (batch), a pool of organoids within the same batch, or multiple batches (batch pooling); a sample is represented as a single data point in the analysis of an experiment
Technical replicate	section	sections obtained from a single organoid using a vibratome are considered technical replicates, i.e., repeated measurements of the same biological sample; they help to assess the reproducibility of the equipment and protocol, minimizing technical variability and error; unlike biological replicates, which capture variation between independent organoid cultures, technical replicates ensure differences are due to biological effects rather than inconsistencies in sample processing or analysis

generated from late-passage NESCs compared to the early-passage NESCs (8%) (Figures 2D and S1A), indicating that the increased batch-to-batch variability is due to the use of NESCs at later passage numbers during organoid generation. Next, we investigated the effects of passages and batches on each cell line's individual transcriptomic profile. Using principal-component analysis (PCA), we observed that organoid samples from healthy donors (wild type [WT]) tended to cluster separately, demonstrating biological variance, which is independent of passage. Only in the WT2 cell line, we observed an effect of passage, with WT2 progressively resembling the WT1 cell line with each passage. This indicates that the WT2 cell line may exhibit greater variability in the phenotype depending on the NESC passage (Figure 2E). In contrast, GBA-PD midbrain organoid samples clustered rather depending on the initial NESC passages, indicating that patient samples are more sensitive to experimental design and culture conditions (Figures 2F and S1B).

To explore the passage effect on a disease signature, we correlated the expression of significantly differentially expressed genes (DEGs) between healthy controls and GBA-PD midbrain organoids generated in batches from early or late NESC passages. Early-passage batches (B1–4) showed a significant correlation of DEG expression (0.74–0.82) (Figure 2G), while late-passage batches (B5–8) showed on average a moderate correlation (0.64–0.72) (Figure 2H). Similarly, looking at the expression of all shared genes across the late- or early-passage batches, we saw a higher (0.51–0.64) correlation for the early-passage batches than for the late-passage batches (0.42–0.50) (Figures S1C and S1D).

Overall, exploratory analysis of potential sources of variation in the transcriptomic data of midbrain organoids suggests that disease status and number of passages are major sources of gene expression variance, while batch effects are minimal. Moreover, early passages show more consistent transcriptomic profiles, while late passages lead to increased variability, emphasizing the need to consider NESC passage in study design.

Reproducible transcriptomic disease signature across independently generated datasets

The passage number showed a more considerable impact on data reproducibility than organoid batches. We further wanted to assess more in detail how the choice of NESC passages used for organoid generation might influence the reproducibility of disease phenotypes.

We grouped the early-passage batches (B1–4) and the late-passage batches (B5–8) and identified the significant DEGs within these data subsets. We found 27 overlapping DEGs in the early-passage set, whereas the late-passage batches did not show shared DEGs (Figures S2A and S2B). This could be due to the lower gene expression correlation between organoid batches from late-passage NESCs, representing higher data variability. Since the DEG expression signature at early passages appeared more consistent across organoid batches, we presumed 27 DEGs shared among the early-passage batches as a potential key GBA-PD disease signature and examined its reproducibility in both early- and late-passage batches. Here, we observed that the clustering of WT versus GBA-PD samples for the 27 DEGs was notably more distinct in the early-passage heatmap compared to the late-passage heatmap (Figures S2C and S2D), where we still observed adequate separation. Moreover, by combining all eight batches, the expression of selected 27 DEGs also separated WT and GBA-PD samples,

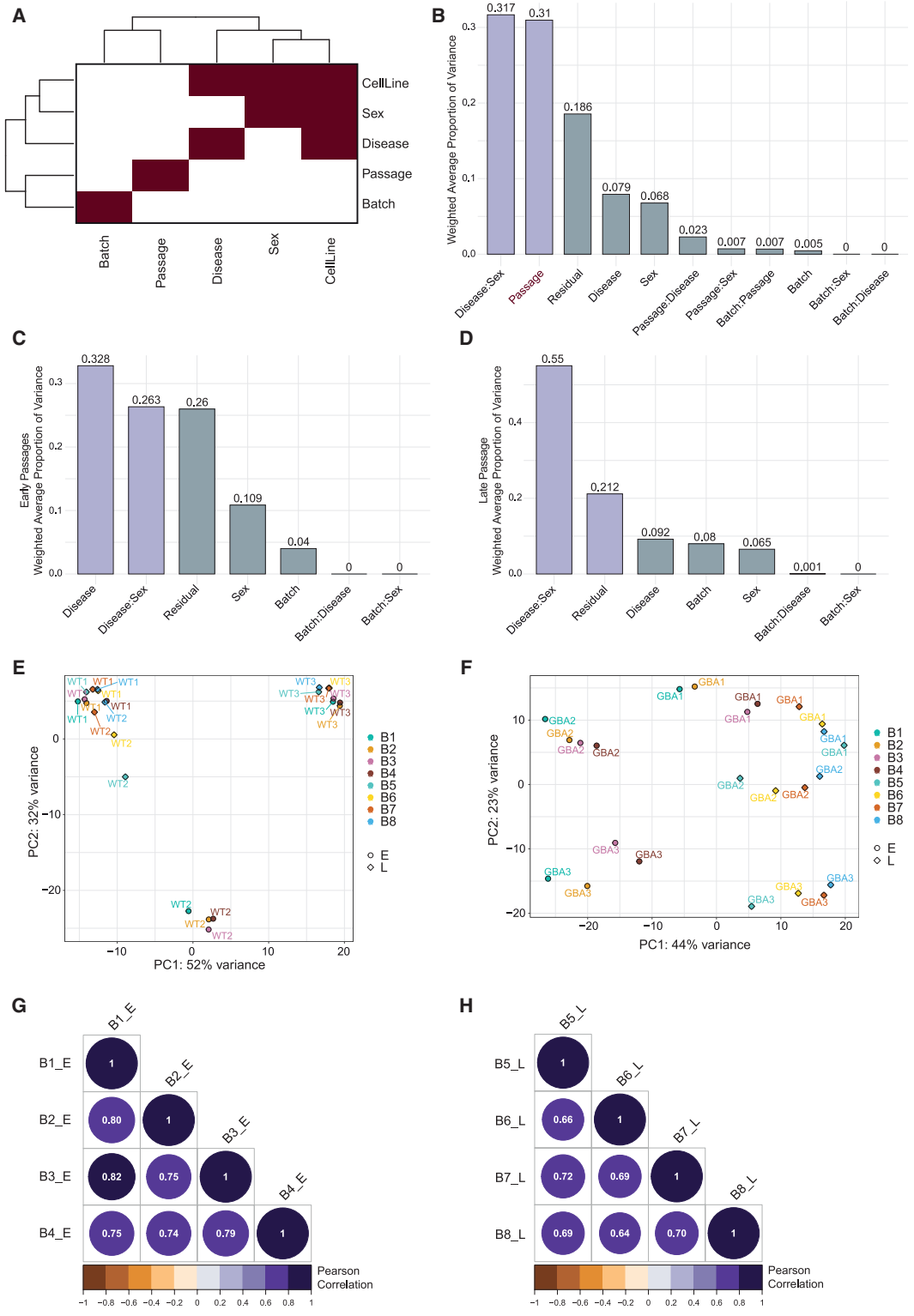

(legend on next page)

indicating the relevance of these genes in disease pathogenesis (Figure 3A). Enrichment analysis of the 27 significant DEGs between GBA-PD and WT samples revealed an association with Reactome pathways related to cellular senescence and apoptosis, consistent with findings of recent studies (Figure 3B).[10] Additionally, a Gene Ontology enrichment analysis supported these results and identified "bleb assembly," which is linked to apoptosis, as the most enriched pathway, further confirming the disease signature in GBA-PD (Figure 3C). Next, we classified the 27 genes into distinct functional categories. These included the senescence/apoptosis pathway, biological processes related to synapse and nervous system development, metabolic and oxidative stress processes, cell adhesion and extracellular matrix dynamics, and transcription and gene regulation. Importantly, the fold change (FC) of GBA-PD vs. WT demonstrated a highly similar dysregulation trend for all genes across all eight batches (Figure S2E).

The initial dataset included organoid transcriptomic data from a single time point—day 30 of organoid culture. We produced new independent organoid batches and performed RNA-seq and metabolomic analyses for organoids at two time points, day 30 and day 60 (dataset 2). These analyses were done to additionally assess how reproducible the phenotypes are at different time points of organoid culture and across independent experiments. The transcriptomic analysis allowed us to compare the two datasets, where the PCA showed, as expected, a tighter clustering for dataset 1 (day 30 organoids) compared to a broader pattern in dataset 2 (day 30 and day 60 organoids) (Figure 3D). Early passage samples (B1–4_Early) from dataset 1 clustered with day 30 samples from dataset 2 (B1–4_D30), showing a similar expression profile (Figure 3E). In contrast, late passage samples (B5–8_Late) from dataset 1 formed a separate cluster, highlighting the significant impact of passage number on gene expression (Figure 3E). To assess the similarity of specific data points to predefined clusters, we calculated the Euclidean distance of individual points from the centroids of designated groups. The analysis revealed that most late passage samples (B1–4_Late) aligned more closely with day 60 samples (B5–8_D60), except for "B7_Late," which clustered near day 30 (B1–4_D30) (Figure 3F). These findings indicate that late-passage midbrain organoids display phenotypes more similar to those observed in longer term midbrain organoid cultures, which may reflect age-related changes in the organoid system. Next, we wanted to determine whether the samples in the newly generated dataset shared the same disease signature defined by the 27 significant DEGs common to the early-passage NESC organoid batches. We observed that the WT and GBA-PD samples showed an even clearer clustering at day 60 compared to day 30. This finding aligns with expectations as day 60 midbrain organoids are more aged, leading to the accumulation of cellular, epigenetic, and transcriptional changes that enhance the distinction between sample groups (Figures 3G and 3H).

Altogether, our analysis shows that while NESC passage can influence phenotype detection, the disease signature identified in early passages is reproducible in later passages and across independent sequencing experiments from two distinct organoid culturing time points. This establishes the midbrain organoid model as a reliable tool for disease phenotyping and modeling.

Validation of dopaminergic neuron and senescence phenotypes at the protein level confirms the transcriptomic disease signature in midbrain organoids

Our transcriptomic analysis identified a distinct disease signature in GBA-PD, characterized by significant dysregulation of genes associated with pathways related to cellular senescence and apoptosis, as well as differences in synaptic and nervous system development. To validate these transcriptomic results and confirm phenotype reproducibility at the protein level, we performed whole-mount staining of midbrain organoids. We used the dopaminergic neuron marker TH (tyrosine hydroxylase), the neuronal marker MAP2 (microtubule-associated protein 2), and the DNA damage/senescence marker 53BP1 (p53-binding protein 1) to additionally assess dopaminergic neurons and the senescence phenotypes at the protein level. We observed that GBA-PD midbrain organoids exhibit a significantly reduced number of TH-positive dopaminergic neurons compared to WT midbrain organoids consistent with results previously reported[10,11] (Figures 4A and 4B). Similarly, 3D reconstruction of dopaminergic neurons showed that neurites in patient-specific organoids are shorter and less ramified compared to WT (Figure 4C). Assessing the TH transcript counts in the transcriptomic data, we observed a significant decrease in the GBA-PD cell lines, supporting the immunofluorescence findings (Figure S3A). The log2 FC of the TH expression in GBA-PD vs. WT appeared more heterogeneous in late-passage batches (B5–8) compared to the early-passage batches (B1–4) (Figure S3B), confirming that early-passage batches are more reproducible at day 30 of organoid culture. Additionally, we observed that increasing the sample size through individual batches plays a critical role in detecting even the most important phenotypes (Figures S3C and S3D).

Analysis of the DNA damage/senescence marker 53BP1 showed that the senescence phenotype at the protein level

Figure 2. PVCA identifies the disease and the passage to be the major sources of variation in midbrain organoid culture

Midbrain organoids were generated at early or late passage in four independent batches and transcriptomic analysis was performed.

(A) Correlation analysis of variance features including batch, passage, disease, sex, and cell line.

(B) Principal variance component analysis (PVCA) of transcriptomic data including all passages.

(C) PVCA of early passage transcriptomic data.

(D) PVCA of late passage transcriptomic data.

(E) Principal-component analysis (PCA) on healthy control (WT) samples from early and late passage and all eight batches.

(F) PCA on PD-GBA samples from early and late passage and all eight batches.

(G) Pearson correlation of log2 fold change (FC) of significant genes ($p < 0.05$) between batches derived from early-passage NESCs.

(H) Pearson correlation of log2 FC of significant genes ($p < 0.05$) between batches derived from late-passage NESCs.

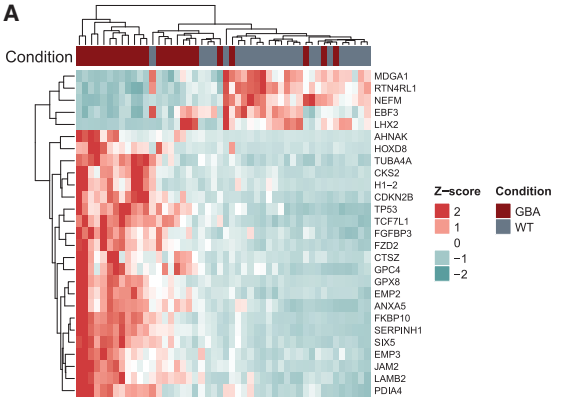

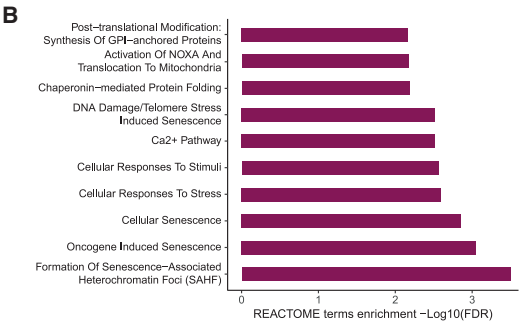

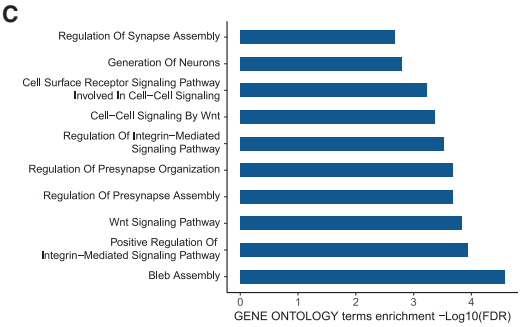

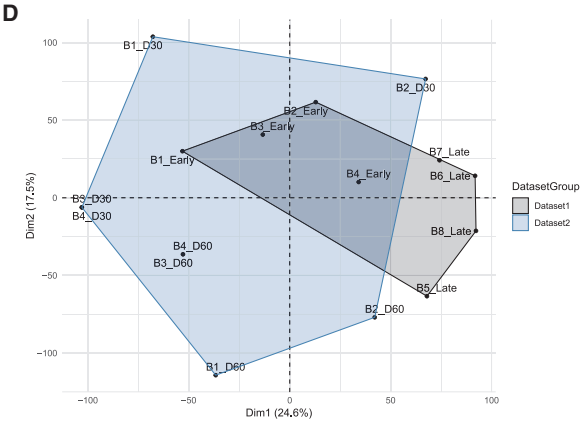

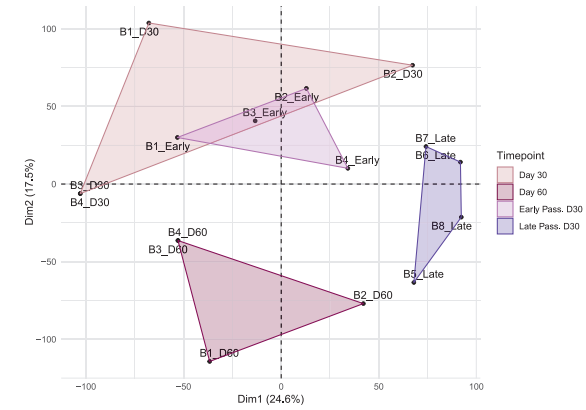

F

Batch	Distance to D30 (dataset 2)	Distance to D60 (dataset 2)	Closer to
B5_Late	159.4240661	93.12380304	Day 60
B6_Late	146.1657097	141.7848331	Day 60
B7_Late	127.0916286	134.1490476	Day 30
B8_Late	157.2472392	125.6148831	Day 60

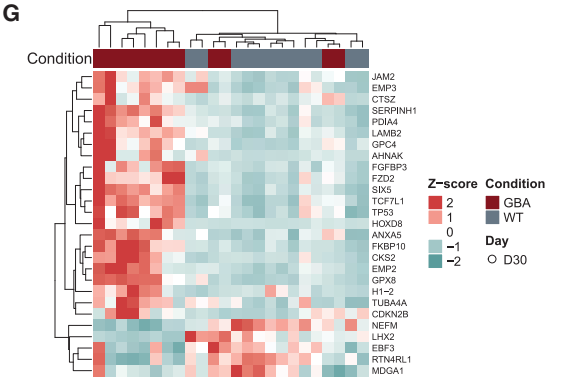

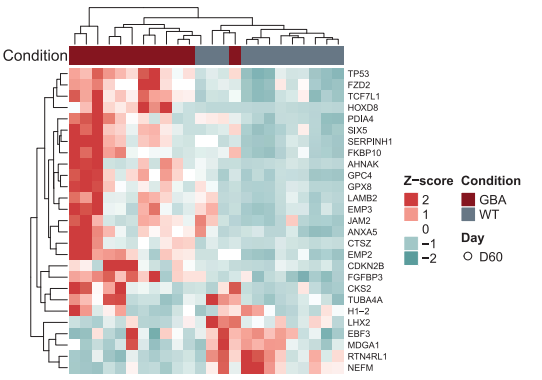

(legend on next page)

appears in the late-passage batches (B5–8), while the transcriptomic signature indicated a significant senescence-associated phenotype already in the early-passage batches (B1–4) (Figures 4D and 4E; Figures S4A and S4B). To further confirm the senescence phenotype in GBA-PD samples, we stained the organoids with β-galactosidase, a well-established marker for detecting cellular senescence.[12] We qualitatively observed a more intense β-galactosidase signal in GBA-PD midbrain organoids (Figure 4F), providing additional evidence of increased senescence in midbrain organoids derived from patients with PD.[10]

GBA-PD midbrain organoids demonstrate a reproducible metabolic profile

After confirming the phenotype reproducibility at the transcriptomic and protein levels, we wanted to assess how reproducible the GBA-PD metabolic signature was. Metabolism is highly dynamic, and therefore metabolite levels may exhibit greater variability between organoid batches compared to changes in transcript or protein abundance. Nevertheless, our data showed that the majority of measured metabolite expression patterns were consistent across four batches at both time points (Figures 5A and 5B). As an exception, we identified B4 to display the most distinct metabolite abundance profile compared to the other three batches at day 30 of organoid culture. Accordingly, correlation analysis showed a significant correlation of metabolite FCs (GBA-PD vs. WT) for B1, B2, and B3 (0.61–0.86), while B4 demonstrated a low correlation with any of these batches (0.12) (Figure 5C). However, at the later time point (day 60), all four batches showed a significant correlation (0.59–0.79), suggesting that the differences in B4 at day 30 might be due to an organoid differentiation path that transiently diverges from the other batches, but these differences even out in more mature organoid cultures (Figure 5D). Moreover, PCA analysis demonstrated that the metabolic profiles of WT and GBA-PD midbrain organoids are not influenced by batch effects but are instead driven by sample and disease state, further supporting the reliability and reproducibility of the data (Figure 5E).

In addition, we performed an integrative analysis between the metabolomics and transcriptomics datasets to identify the key molecular interactions across different omics levels at different organoid culturing stages (day 30 and day 60). Importantly, this analysis confirmed earlier findings, demonstrating that the top transcripts and metabolites more effectively distinguish samples by condition rather than by batch (Figure S5). We observed that pyruvic acid, urea, glycine, and glucose were reappearing among the top five metabolites separating the WT and GBA-PD samples at both time points (Figures 5A–5I). Moreover, at both time points, the change in glycine abundance between conditions was negatively correlated with a subset of the top 50 genes, suggesting that glycine metabolism and its transcriptional regulation play a substantial role in GBA-PD (Figures 5F and 5H). Aligned with overall metabolism adaptations usually observed during aging and the metabolic alterations associated with GBA mutation-driven dysregulation and senescence, we found improved sample separation based on top transcriptomic and metabolomic features at day 60 of organoid culture (Figures 5G and 5I). This finding suggests that the metabolic phenotype of GBA-PD intensifies over time (Figures 5G and 5I).

Altogether, these data suggest that even highly dynamic metabolic changes are reproducible in midbrain organoid models and therefore can reliably capture critical molecular interactions driving GBA-PD metabolic dysregulation.

Sample estimation using power analysis for iPSC-derived models

A considerable limitation of studies using iPSC-derived models is the availability of cell lines, particularly when it comes to patient-specific lines with a particular mutation. This leads to underpowered studies, increasing the risk of reporting false-negative results (type II error).[13] We observed exactly this in our example study on TH gene expression presented here, where a single batch with three samples per group failed to capture the true differences in TH expression levels between the control and GBA-PD samples. Therefore, using independent experimental batches can be used to enhance the experimental throughput by increasing sample sizes. Thus, in addition to assessing the reproducibility of the midbrain organoid model, we wanted to estimate the required sample size for RNA-seq, metabolomics, and imaging experiments to reach an optimal statistical power of 80%, considering the presented data as pilot experiments for future experimental designs using organoid models. 80% statistical power is, by convention, the target power of a study to reduce the probability of rejecting a false null hypothesis.[14] For RNA-seq datasets, we estimated how many samples per group are required to reach optimal statistical power based on the observed effect size as log2 FC between the significant DEGs in this study. While the absolute values of log2 FC ranged from 0.08 (min) to 8.21 (max), the median was 0.42, indicating that for most of the DEGs, the difference between the two groups is relatively small and 30 samples per group would be required to detect

Figure 3. Disease signature is reproducible across independent datasets at the transcriptomic level

For dataset 1, midbrain organoids were generated at early or late passage in four independent batches, and transcriptomic analysis was performed. For dataset 2, midbrain organoids were generated in four independent batches at two time points, and transcriptomic analysis was performed.

(A) Unsupervised hierarchical clustering of GBA-PD and healthy control (WT) samples based on normalized gene counts of 27 predefined genes of all passages.

(B) REACTOME pathway enrichment analysis of the DEGs between GBA-PD and healthy control (WT) samples.

(C) Gene Ontology pathway enrichment analysis of the DEGs between GBA-PD and healthy control (WT) samples.

(D) Integration of log2 fold change (FC) from dataset 1 and dataset 2 shown in principal-component analysis (PCA) plot. Samples are clustered by dataset.

(E) Integration of log2 FC from dataset 1 and dataset 2 shown in PCA plot. Samples are clustered by time point and passage.

(F) Euclidean distance table showing the batch, the calculated distance to day 30 or day 60, and the proximity to one of the two time points.

(G) Unsupervised hierarchical clustering of GBA-PD and healthy control (WT) samples based on normalized gene counts of 27 predefined genes at day 30.

(H) Unsupervised hierarchical clustering of GBA-PD and healthy control (WT) samples based on normalized gene counts of 27 predefined genes at day 30.

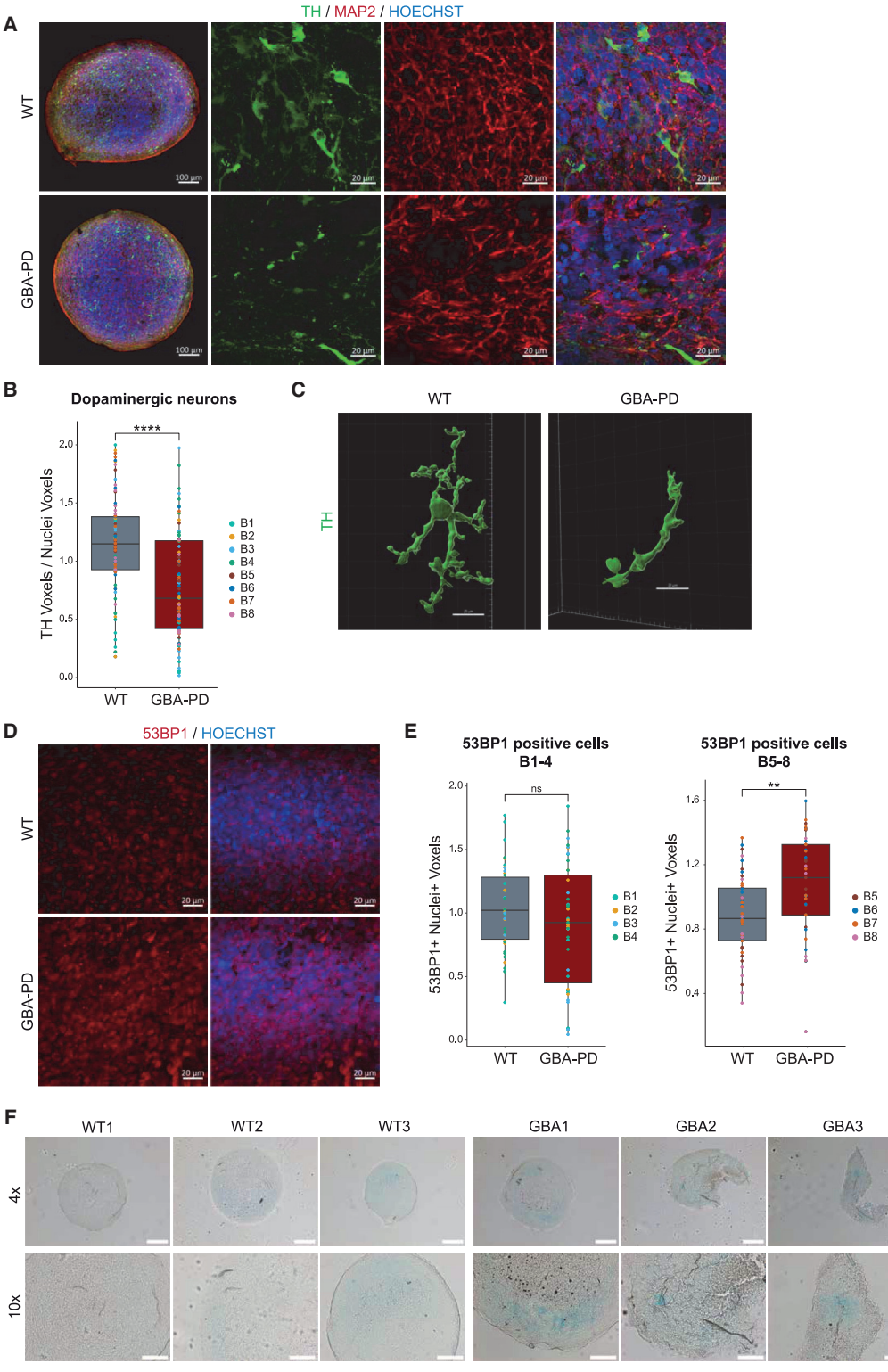

(legend on next page)

true differences in the gene expression (Figures 6A and 6D). This means that for the most differentially expressed transcripts, 10 batches must be generated to detect true significant differences between the groups if we have 3 cell lines from each group or condition available. For a larger effect size between groups (>1.5 log2 FC), the sample size required for optimal power of 80% decreases to 9 samples per group. Consequently, three independent rounds of organoid generation are required to detect significantly DEGs with an expected expression difference greater than 1.5-fold when three cell lines per group or condition are used. In the metabolomics dataset, we estimated the effect size as Cohen's *d* of each significantly differentially abundant metabolite. Median *d* was large (0.91), which would require 20 samples per sample group to reach optimal statistical power in the analysis (Figures 6B and 6D). The maximum *d* was 1.58, decreasing the required sample number to ten, while the smallest *d* was 0.73, increasing the required sample number to 35 per group (Figures 6B and 6D). In the imaging dataset, we estimated the required sample size based on the values of TH normalized by nuclei, as this is the expected imaging feature to be significantly different between the healthy control and GBA-PD samples. With the calculated effect size d = 0.56, 50 samples per group would be necessary to reach 80% statistical power (Figures 6C and 6D). In organoid studies, immunofluorescence staining is performed on organoid sections. Unlike RNA-seq or metabolomics experiments, where organoids are pooled into a single sample represented by one data point in the analysis, in imaging experiments, we consider each individual organoid as a biological replicate. This increases the sample size, which allows for optimal statistical power considering the rather low expected effect size between the sample groups in imaging.

For instance, in this pilot study, the use of three cell lines and eight batches per group increases the sample size to 24 per group. Similar approaches can be used to achieve the optimal sample size, considering the specific study objective and the standards required.[15]

This analysis highlights the importance of incorporating multiple batches to achieve statistically robust and reproducible results, when the availability of biological replicates (cell lines) is limited. However, increasing the number of cell lines is always preferred over adding more batches, as it results in more generalizable and translatable findings.

DISCUSSION

Our study establishes midbrain organoids as a reproducible *in vitro* model to study PD. By generating multiple independent organoid batches and examining both early and late passages, as well as different time points, we address a key challenge in the field: ensuring reproducibility and consistency in complex 3D culture systems.

Our findings reveal that, despite the inherent complexity of organoid models, batch effects can be successfully minimized. PVCA underscores that donor-related factors, disease state, and sex are prominent drivers of transcriptional variability, while passage of the NESCs emerges as a technical parameter contributing to transcriptional shifts. Notably, early-passage cultures consistently yield a more robust and stable disease-specific transcriptomic signature compared to late-passage organoids, which nonetheless still maintain core disease-related features. This signature, associated with TH-positive dopaminergic neurons loss and cellular senescence, aligns with previously reported phenotypes in GBA-PD models and reflects key pathogenic mechanisms implicated in disease progression.[10,11]

Crucially, we validated these transcriptomic differences at the protein and metabolic levels. Changes in dopaminergic neuron numbers, along with increased senescence-associated markers, were consistent with our gene expression data. Furthermore, the metabolic profiles were largely stable and reproducible across independent batches of organoid generation, particularly as the organoids matured. This evidence supports the notion that midbrain organoids can recapitulate key aspects of PD pathology reproducibly along multi-level analysis.

Although this study focused on PD patient midbrain organoid samples carrying the GBA-N370S genetic variant, we believe that the number of samples from independent organoid generation batches was sufficient to assess the overall variation in the organoid data. Thus, our conclusions on organoid reproducibility can likely be generalized to other organoid experiments involving two or more independent sample groups. Furthermore, our analysis incorporated sample size estimation to achieve optimal statistical power across bulk RNA-seq, immunofluorescence high-content imaging, and metabolomics experiments, offering guidelines for designing future organoid studies to ensure result accuracy and minimize false-positive results. It is important to note that midbrain organoids represent a guided brain organoid model, where variability between individual organoids and

Figure 4. Reproducible dopaminergic neuron and senescence phenotypes at the protein level in midbrain organoids

Midbrain organoids were generated at early or late passage in four independent batches, and whole-mount immunofluorescence and β-galactosidase staining were performed.

(A) Representative confocal images of TH (green), MAP2 (red), and nuclei (blue) of midbrain organoid section staining at day 30 (scale bars, 100 μm, 20×; 50 μm, 63×).

(B) High-content automated image analysis of immunofluorescence staining of TH+ dopaminergic neurons in midbrain organoids normalized by total nuclei. Data are shown as boxplots and represent a summary of eight independent batches normalized to the mean of the controls per batch ±SD. Wilcoxon t test; ****$p < 0.0001$.

(C) 3D reconstruction with IMARIS software showing the dopaminergic neuron (TH) in the healthy control (WT) and GBA-PD cell line (scale bars, 20 μm, 63×).

(D) Representative confocal images of 53BP1 (red) and nuclei (blue) in whole-mount staining of midbrain organoids at day 30 (scale bars, 20 μm, 63×).

(E) High-content automated image analysis of immunofluorescence staining of 53BP1 (53BP1+) and Nuclei (Nuclei+) double-positive cells in midbrain organoids. Data are shown as boxplots and represent early-passage (B1–4) or late-passage (B5–8) batches normalized to the mean of the controls per batch ±SD. Wilcoxon t test; **$p < 0.01$.

(F) Senescence-associated β-galactosidase staining (blue) of midbrain organoids (scale bars, 200 μm, 4×; 100 μm, 10×).

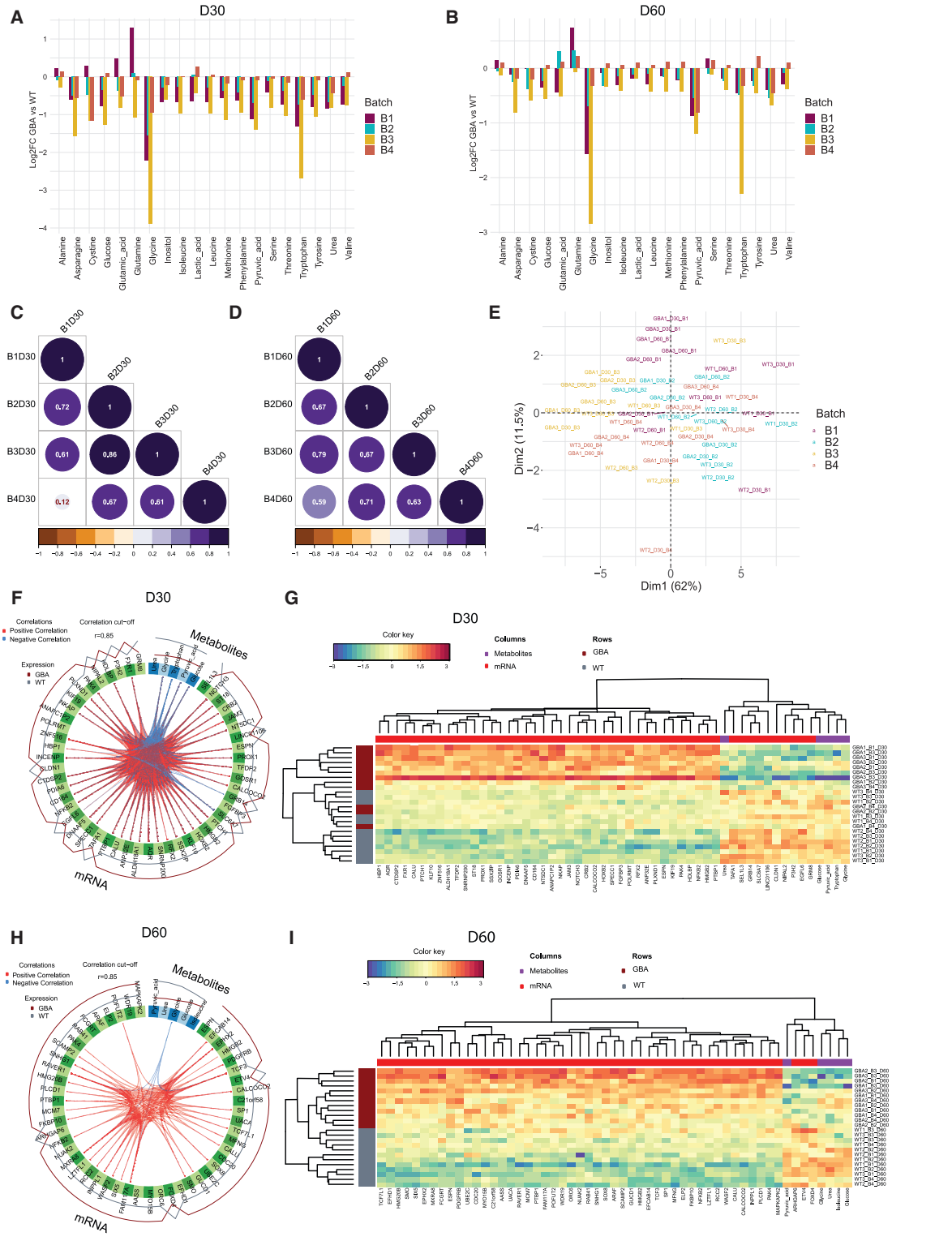

(legend on next page)

batches is expected to be lower compared to unguided brain organoid protocols. In such unguided models, larger sample sizes may be necessary to reliably detect true differences between sample groups.

While including batches can enhance the statistical power of a study, they should not be used to artificially inflate power. Instead, batches should serve as an additional replicate alongside multiple distinct cell lines (if available) or used as a strategy to help overcome the common challenge of limited cell line availability (e.g., in the case of rare mutations).

In conclusion, this study provides strong evidence that patient-derived midbrain organoids are not only an accurate model of GBA-PD pathology but are also a robust and reproducible experimental system. By highlighting and controlling critical sources of variability, these models can build a solid foundation for future work aimed at unraveling disease mechanisms and accelerating the development of personalized treatments for PD.

Limitations of the study

Despite the strengths of our study, several limitations should be acknowledged. While we used multiple organoid batches and time points, our analysis focused exclusively on midbrain organoids derived from patients with PD carrying the GBA-N370S mutation, which may limit generalizability to other PD genetic backgrounds. The relatively small number of distinct donor lines, though sufficient for detecting robust transcriptomic and phenotypic changes, may not fully capture the spectrum of patient heterogeneity. A key consideration is that NESC passage number introduced greater variability than organoid batch, which could affect reproducibility if not carefully controlled. Early-passage organoids showed more consistent phenotypes, making them more suitable for disease modeling. In contrast, late-passage organoids exhibited greater variability but also signs of transcriptional aging. This suggests their potential for modeling late-stage phenotypes, though early and late passages should be analyzed separately to preserve reproducibility. Although we implemented power calculations, limited cell line availability, especially for rare mutations, remains a challenge for study robustness. To further evaluate the generalizability of our findings, future studies should include organoids derived from patients carrying other GBA variants or additional PD-linked mutations (e.g., LRRK2, SNCA, and Miro1) to assess reproducibility across diverse genetic backgrounds. A more balanced inclusion of female and male donor lines, combined with minimized technical variability such as consistent passage number, would also enable systematic investigation of sex-specific transcriptomic effects in disease modeling. Together, these approaches would help validate midbrain organoids as a consistent and versatile *in vitro* model for studying PD.

RESOURCE AVAILABILITY

Lead contact

Further information and requests for resources should be directed to and will be fulfilled by the lead contact, Jens C. Schwamborn (jens.schwamborn@uni.lu).

Materials availability

This study did not generate new unique reagents.

Data and code availability

- All original and processed data as well as scripts that support the findings of this study are public available at https://doi.org/10.17881/4n7e-vc76.
- Gene expression datasets can be accessed on Gene Expression Omnibus under the accession codes GSE287566 and GSE269316.
- All scripts used to obtain, analyze, and plot the data are available at https://gitlab.com/uniluxembourg/lcsb/developmental-and-cellular-biology/reproducibility_2025.
- Any additional information required to reanalyze the data reported in this article is available from the lead contact upon request.

ACKNOWLEDGMENTS

We thank the LCSB Metabolomics and Lipidomics Platform for their service. We acknowledge Novogene for RNA sequencing. We would like to thank the LCSB Bioimaging Platform for supporting high-content imaging and image analysis workflow. We would also like to thank Dr. Sònia Sabaté Soler for the help with the 3D reconstruction using the IMARIS software and Dr. Matthieu Gobin for his critical contributions to the manuscript.

This project has received funding from the National Centre of Excellence in Research on Parkinson's Disease (NCER-PD), which is funded by the Luxembourg National Research Fund (FNR) (FNR/NCER13/BM/11264123). Further, FNR funding as part of the i2TRON Doctoral Training Unit (PRIDE19/14254520) and the CORE program (CORE 22_BM_17193204_MidStriPD) is acknowledged.

This research was funded in whole by the FNR Luxembourg. For the purpose of Open Access, the author has applied a CC BY public copyright license to any Author Accepted Manuscript (AAM) version arising from this submission.

Figure 5. Midbrain organoids from day 30 and day 60 show a reproducible metabolic profile

(A) Metabolite abundance difference in GBA-PD samples presented as log2 fold change (FC) compared to healthy control (WT) samples across four batches at day 30 of organoid culture.

(B) Metabolite abundance difference in GBA-PD samples presented as log2 FC compared to healthy control (WT) samples across four batches at day 60 of organoid culture.

(C) Pearson correlation of log2 FC for all metabolites across four batches at day 30 of organoid culture.

(D) Pearson correlation of log2 FC for all metabolites across four batches at day 60 of organoid culture.

(E) PCA of metabolomics data.

(F) Circos plot showing the correlation between metabolomics and transcriptomics features contributing to the variation of the component 1 at day 30 of organoid culture. Correlation threshold: r = 0.9.

(G) Unsupervised hierarchical clustering of the top discriminant metabolomics and transcriptomics features between the GBA-PD and healthy control (WT) samples at day 30 of organoid culture.

(H) Circos plot showing the correlation between metabolomics and transcriptomics features contributing to the variation of component 1 at day 60 of organoid culture. Correlation threshold: r = 0.84.

(I) Unsupervised hierarchical clustering of the top discriminant metabolomics and transcriptomics features between the GBA-PD and healthy control (WT) samples at day 30 of organoid culture.

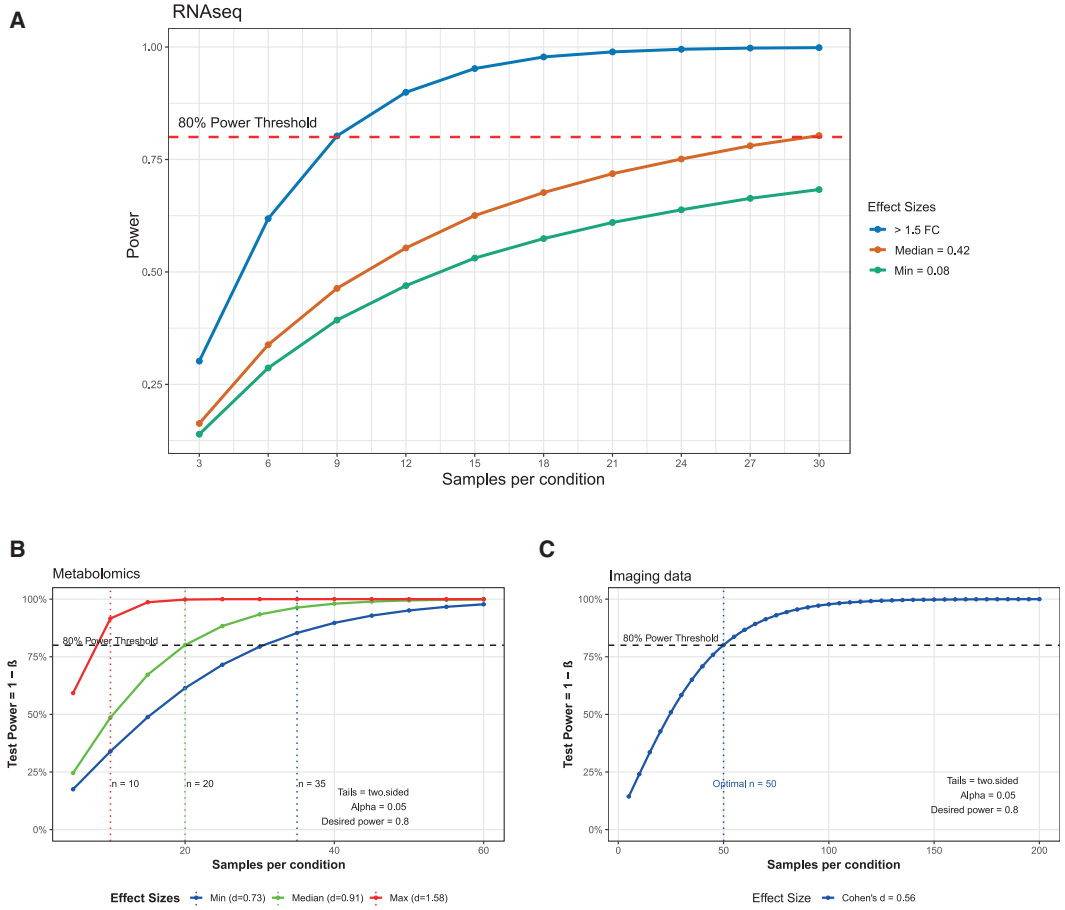

D

Experiment	Effect Size	Samples per condition	Estimated Power
RNAseq	Min (delta = 0.08)	30	0.683
	Median (delta = 0.42)	24	0.751
		27	0.780
		30	0.803
	Max (delta = 1.5)	9	0.802
Metabolomics	Min (d = 0.73)	30	0.794
		35	0.853
	Median (d = 0.91)	20	0.801
	Max (d = 1.58)	10	0.916
Imaging data	TH to nuclei feature (d = 0.56)	45	0.758
		50	0.801

Figure 6. Sample estimation using power analysis for three data types (RNA-seq, metabolomics, and imaging)

Each panel plots statistical power (1-β) against sample size per group at $\alpha = 0.05$, highlighting the sample sizes needed to reach the 80% power threshold (dashed line) for different effect sizes determined from this pilot study in each data type.

(A) RNA-seq shows effect sizes of >1.5-fold (blue), median = 0.42 (orange), and min = 0.08 (green).

(B) Metabolomics compares min ($d = 0.73$), median ($d = 0.91$), and max ($d = 1.58$) effect sizes; vertical lines mark the number of replicates at which each effect achieves 80% power.

(C) Imaging data illustrate a single effect size (Cohen's $d = 0.56$), requiring $\sim n = 50$ per group to reach 80% power.

(D) Table summarizing the power analysis results showing the effect size, the sample size per group, and the estimated power for each experiment performed in this study (RNA-seq, metabolomics, and imaging data).

AUTHOR CONTRIBUTIONS

E.Z. and A.Z. conceived, designed, and collected data. E.Z., H.A.S., and A.Z. performed data analysis and interpretation of results. M.T. contributed with experiments. E.Z., H.A.S., and A.Z. wrote the original manuscript. The work was supervised by J.C.S. S.L.N. and J.C.S. revised and edited the manuscript.

DECLARATION OF INTERESTS

J.C.S. declare no competing non-financial interests but declare competing financial interests as cofounders and shareholders of OrganoTherapeutics société à responsabilité limitée.

STAR★METHODS

Detailed methods are provided in the online version of this paper and include the following:

- KEY RESOURCES TABLE
- EXPERIMENTAL MODEL AND SUBJECT DETAILS
  - Ethical approval
  - Cell lines
  - Midbrain organoid culture
- METHOD DETAILS
  - Whole mount staining
  - Immunofluorescence staining of midbrain organoid sections
  - Image 3D reconstruction
  - β-galactosidase staining
  - Image acquisition and analysis
  - RNA extraction, library preparation and sequencing
  - Transcriptomic analysis
  - Analysis of explained variance
  - Transcriptomics and metabolomics integration
  - Sample size estimation using power analysis
- QUANTIFICATION AND STATISTICAL ANALYSIS
  - Statistical analysis

SUPPLEMENTAL INFORMATION

Supplemental information can be found online at https://doi.org/10.1016/j.isci.2025.113541.

Received: May 16, 2025
Revised: July 27, 2025
Accepted: September 8, 2025
Published: September 10, 2025

REFERENCES

1. Kalia, L.V., and Lang, A.E. (2015). Parkinson's disease. Lancet *386*, 896–912. https://doi.org/10.1016/S0140-6736(14)61393-3.
2. Kelava, I., and Lancaster, M.A. (2016). Dishing out mini-brains: Current progress and future prospects in brain organoid research. Dev. Biol. *420*, 199–209. https://doi.org/10.1016/j.ydbio.2016.06.037.
3. Dovonou, A., Bolduc, C., Soto Linan, V., Gora, C., Peralta III, M.R., and Lévesque, M. (2023). Animal models of Parkinson's disease: Bridging the gap between disease hallmarks and research questions. Transl. Neurodegener. *12*, 36. https://doi.org/10.1186/s40035-023-00368-8.
4. Monzel, A.S., Smits, L.M., Hemmer, K., Hachi, S., Moreno, E.L., van Wuellen, T., Jarazo, J., Walter, J., Brüggemann, I., Boussaad, I., et al. (2017). Derivation of human midbrain-specific organoids from neuroepithelial stem cells. Stem Cell Rep. *8*, 1144–1154. https://doi.org/10.1016/j.stemcr.2017.03.010.
5. Nickels, S.L., Modamio, J., Mendes-Pinheiro, B., Monzel, A.S., Betsou, F., and Schwamborn, J.C. (2020). Reproducible generation of human midbrain organoids for in vitro modeling of Parkinson's disease. Stem Cell Res. *46*, 101870. https://doi.org/10.1016/j.scr.2020.101870.
6. Smith, L., and Schapira, A.H.V. (2022). GBA variants and Parkinson disease: Mechanisms and treatments. Cells *11*, 1261. https://doi.org/10.3390/cells11081261.
7. Chinta, S.J., and Andersen, J.K. (2008). Redox imbalance in Parkinson's disease. Biochim. Biophys. Acta *1780*, 1362–1367. https://doi.org/10.1016/j.bbagen.2008.02.005.
8. Melo dos Santos, L.S., Trombetta-Lima, M., Eggen, B.J.L., and Demaria, M. (2024). Cellular senescence in brain aging and neurodegeneration. Ageing Res. Rev. *93*, 102141. https://doi.org/10.1016/j.arr.2023.102141.
9. Wang, Y., Kuca, K., You, L., Nepovimova, E., Heger, Z., Valko, M., Adam, V., Wu, Q., and Jomova, K. (2024). The role of cellular senescence in neurodegenerative diseases. Arch. Toxicol. *98*, 2393–2408. https://doi.org/10.1007/s00204-024-03768-5.
10. Rosety, I., Zagare, A., Saraiva, C., Nickels, S., Antony, P., Almeida, C., Glaab, E., Halder, R., Velychko, S., Rauen, T., et al. (2023). Impaired neuron differentiation in GBA-associated Parkinson's disease is linked to cell cycle defects in organoids. NPJ Parkinson's Dis. *9*, 166. https://doi.org/10.1038/s41531-023-00616-8.
11. Zagare, A., Hemedan, A., Almeida, C., Frangenberg, D., Gomez-Giro, G., Antony, P., Halder, R., Krüger, R., Glaab, E., Ostaszewski, M., et al. (2025). Insulin resistance is a modifying factor for Parkinson's disease. Mov. Disord. *40*, 67–76. https://doi.org/10.1002/mds.30039.
12. Hernandez-Segura, A., Nehme, J., and Demaria, M. (2018). Hallmarks of cellular senescence. Trends Cell Biol. *28*, 436–453. https://doi.org/10.1016/j.tcb.2018.02.001.
13. Brunner, J.W., Lammertse, H.C.A., van Berkel, A.A., Koopmans, F., Li, K.W., Smit, A.B., Toonen, R.F., Verhage, M., and van der Sluis, S. (2023). Power and optimal study design in iPSC-based brain disease modelling. Mol. Psychiatr. *28*, 1545–1556. https://doi.org/10.1038/s41380-022-01866-3.
14. Serdar, C.C., Cihan, M., Yücel, D., and Serdar, M.A. (2020). Sample size, power and effect size revisited: Simplified and practical approaches in pre-clinical, clinical and laboratory studies. Biochem. Med. *31*, 010502. https://doi.org/10.11613/BM.2021.010502.
15. Jensen, K.B., and Little, M.H. (2023). Organoids are not organs: sources of variation and misinformation in organoid biology. Stem Cell Rep. *18*, 1255–1270. https://doi.org/10.1016/j.stemcr.2023.05.009.
16. Reinhardt, P., Glatza, M., Hemmer, K., Tsytsyura, Y., Thiel, C.S., Höing, S., Moritz, S., Parga, J.A., Wagner, L., Bruder, J.M., et al. (2013). Derivation and expansion using only small molecules of human neural progenitors for neurodegenerative disease modeling. PLoS One *8*, e59252. https://doi.org/10.1371/journal.pone.0059252.
17. Bolognin, S., Fossépré, M., Qing, X., Jarazo, J., Ščančar, J., Moreno, E.L., Nickels, S.L., Wasner, K., Ouzren, N., Walter, J., et al. (2019). 3D cultures of Parkinson's disease-specific dopaminergic neurons for high content phenotyping and drug testing. Adv. Sci. *6*, 1800927. https://doi.org/10.1002/advs.201800927.
18. Hiltemann, S., Rasche, H., Gladman, S., Hotz, H.R., Larivière, D., Blankenberg, D., Jagtap, P.D., Wollmann, T., Bretaudeau, A., Goué, N., et al. (2023). Galaxy Training: A powerful framework for teaching. PLoS Comput. Biol. *19*, e1010752. https://doi.org/10.1371/journal.pcbi.1010752.
19. Doyle, M., Phipson, B., and Dashnow, H.. 1: RNA-Seq reads to counts. (Galaxy Training Materials). https://training.galaxyproject.org/training-material/topics/transcriptomics/tutorials/rna-seq-reads-to-counts/tutorial.html.
20. Love, M.I., Huber, W., and Anders, S. (2014). Moderated estimation of fold change and dispersion for RNA-seq data with DESeq2. Genome Biol. *15*, 550. https://doi.org/10.1186/s13059-014-0550-8.
21. Benjamini, Y., and Hochberg, Y. (1995). Controlling the false discovery rate: a practical and powerful approach to multiple testing. J. Roy. Stat. Soc. B *57*, 289–300.
22. Chen, E.Y., Tan, C.M., Kou, Y., Duan, Q., Wang, Z., Meirelles, G.V., Clark, N.R., Ma'ayan, A., and Ma'ayan, A. (2013). Enrichr: interactive and

collaborative HTML5 gene list enrichment analysis tool. BMC Bioinf. *14*, 128. https://doi.org/10.1186/1471-2105-14-128.

23. Kuleshov, M.V., Jones, M.R., Rouillard, A.D., Fernandez, N.F., Duan, Q., Wang, Z., Koplev, S., Jenkins, S.L., Jagodnik, K.M., Lachmann, A., et al. (2016). Enrichr: a comprehensive gene set enrichment analysis web server 2016 update. Nucleic Acids Res. *44*, W90–W97. https://doi.org/10.1093/nar/gkw377.
24. Milacic, M., Beavers, D., Conley, P., Gong, C., Gillespie, M., Griss, J., Haw, R., Jassal, B., Matthews, L., May, B., et al. (2024). The reactome pathway knowledgebase 2024. Nucleic Acids Res. *52*, D672–D678. https://doi.org/10.1093/nar/gkad1025.
25. Ashburner, M., Ball, C.A., Blake, J.A., Botstein, D., Butler, H., Cherry, J.M., Davis, A.P., Dolinski, K., Dwight, S.S., Eppig, J.T., et al. (2000). Gene ontology: tool for the unification of biology. Nat. Genet. *25*, 25–29. https://doi.org/10.1038/75556.
26. Gene Ontology Consortium, Aleksander, S.A., Balhoff, J., Carbon, S., Cherry, J.M., Drabkin, H.J., Ebert, D., Feuermann, M., Gaudet, P., Harris, N.L., et al. (2023). The gene ontology knowledgebase in 2023. Genetics *224*, iyad031. https://doi.org/10.1093/genetics/iyad031.
27. Shirkhorshidi, A.S., Aghabozorgi, S., and Wah, T.Y. (2015). A comparison study on similarity and dissimilarity measures in clustering continuous data. PLoS One *10*, e0144059. https://doi.org/10.1371/journal.pone.0144059.
28. Kim, T., Chen, I.R., Lin, Y., Wang, A.Y.Y., Yang, J.Y.H., and Yang, P. (2019). Impact of similarity metrics on single-cell RNA-seq data clustering. Brief. Bioinform. *20*, 2316–2326. https://doi.org/10.1093/bib/bby076.
29. Bushel, P. (2024). pvca: Principal Variance Component Analysis (PVCA). https://doi.org/10.18129/B9.bioc.pvca,Rpackageversion1.46.0. https://bioconductor.org/packages/pvca.
30. Rohart, F., Gautier, B., Singh, A., and Lê Cao, K.A. (2017). mixOmics: An R package for 'omics feature selection and multiple data integration. PLoS Comput. Biol. *13*, e1005752. https://doi.org/10.1371/journal.pcbi.1005752.
31. Singh, A., Shannon, C.P., Gautier, B., Rohart, F., Vacher, M., Tebbutt, S.J., and Lê Cao, K.A. (2019). DIABLO: an integrative approach for identifying key molecular drivers from multi-omics assays. Bioinformatics *35*, 3055–3062. https://doi.org/10.1093/bioinformatics/bty1054.

STAR★METHODS

KEY RESOURCES TABLE

REAGENT or RESOURCE	SOURCE	IDENTIFIER
Antibodies		
Chicken polyclonal anti-TH	Abcam	Cat#ab76442; RRID:AB_1524535
Rabbit polyclonal anti-TH	Abcam	Cat# ab112; RRID:AB_297840
Mouse monoclonal anti-TUJ1	BioLegend	Cat#801201; RRID:AB_2313773
Rabbit polyclonal anti-53BP1	Novus Biologicals	Cat# NB100-304; RRID:AB_10003037
Chicken polyclonal anti-MAP2	Abcam	Cat# ab92434; RRID:AB_2138147
Alexa Fluor® 488 AffiniPure® Donkey Anti-Chicken IgY (IgG) (H + L)	Jackson Immunoresearch	Cat#703-545-155; RRID:AB_2340375
Alexa Fluor® 647 AffiniPure® Donkey Anti-Chicken IgY (IgG) (H + L)	Jackson Immunoresearch	Cat#703-605-155; RRID:AB_2340379
Donkey anti-Rabbit IgG (H + L) Highly Cross-Adsorbed Secondary Antibody, Alexa Fluor™ 488	Invitrogen	Cat# A21206; RRID:AB_2535792
Donkey anti-Rabbit IgG (H + L) Highly Cross-Adsorbed Secondary Antibody, Alexa Fluor™ 568	Invitrogen	Cat# A-10042; RRID:AB_2534017
Donkey anti-Mouse IgG (H + L) Highly Cross-Adsorbed Secondary Antibody, Alexa Fluor™ 647	Invitrogen	Cat# A-31571; RRID:AB_162542
Chemicals, peptides, and recombinant proteins		
Geltrex	Gibco	A1413302
DMEM/F-12, no glutamine	Gibco	21331046
Neurobasal Medium	Gibco	21103049
GlutaMAX	Gibco	35050061
Penicillin-Streptomycin, liquid	Gibco	15140122
B-27 Supplement Minus Vitamin A (50×), Liquid	Gibco	12587001
N-2 Supplement (100×)	Gibco	17502001
L-Ascorbic acid	Sigma-Aldrich	A4544
CHIR99021	Axon Medchem BV	AXON1386
DONKEY SERUM Purmorphamin	Enzo Life Science	ALX-420-045
Accutase	Sigma-Aldrich	A6964
dbcAMP	STEMCELL Technologies	100–0244
hBDNF	PeproTech EC Ltd.	450–02
hGDNF	PeproTech EC Ltd.	450–10
TGF-β3	PeproTech EC Ltd.	100-36E
Paraformaldehyde	Sigma-Aldrich	P6148
Hoechst33342	Invitrogen	H21492
Triton X-100	Carl Roth	3051.3
Bovine Serum Albumin	Sigma-Aldrich	A4503
Donkey Serum	Sigma Aldrich	D9663
Sodium Azide	Carl Roth	K305.1
Fluoromount-G	Southern Biotech	SOUT0100-01
Critical commercial assays		
LookOut® Mycoplasma PCR Detection Kit	Sigma-Aldrich	MP0035-1 KT
Senescence Detection Kit	Abcam	ab65351

(*Continued on next page*)

Continued

REAGENT or RESOURCE	SOURCE	IDENTIFIER
RNeasy Mini Kit	Qiagen	74106
Deposited data		
Bulk RNA sequencing dataset 1	This paper	GSE287566
Bulk RNA sequencing dataset 2	This paper	GSE269316
Figures and Source codes	This paper	https://doi.org/10.17881/4n7e-vc76
Experimental models: Cell lines		
iPSC line WT1	IBBL/Max Planck Institute	N/A
iPSC line WT2	IBBL/Max Planck Institute	N/A
iPSC line WT3	Coriell Institute	GM23338
iPSC line GBA1	European Bank for induced pluripotent Stem Cells	UOXFi001-B
iPSC line GBA2	University College London	N/A
iPSC line GBA3	Coriell Institute	ND31630
Software and algorithms		
IMARIS	Bitplane software	Version 9.9.1.; RRID:SCR_007370
Fiji	https://fiji.sc/	RRID:SCR_002285
MATLAB	Matchworks, Inc.	R2021a; RRID:SCR_001622
Galaxy	Galaxy server	Version 23.2.rc1
HISAT2	https://daehwankimlab.github.io/hisat2/	RRID:SCR_015530
featureCounts	http://bioinf.wehi.edu.au/featureCounts/	RRID:SCR_001905
R Project for Statistical Computing	https://www.r-project.org/	Version 4.4.2.; RRID:SCR_001905
DESeq2 R package	https://bioconductor.org/packages/release/bioc/html/DESeq2.html	Version 1.42.1.; RRID:SCR_015687
dplyr R package	https://dplyr.tidyverse.org/	Version 1.1.4.; RRID:SCR_016708
PVCA R package	https://www.bioconductor.org/packages/release/bioc/html/pvca.html	Version 1.42.0.; RRID:SCR_001356
mixOmics R package	http://mixomics.org/access/	Version 6.22.0.; RRID:SCR_016889
Circos R package	http://circos.ca/	Version 0.69–9.; RRID:SCR_011798
PROPER R package	https://bioconductor.org/packages/release/bioc/html/PROPER.html	Version 1.30.0.
pwr R package	https://cran.r-project.org/web/packages/pwr/index.html	Version 1.3.0.; RRID:SCR_025480
effsize R package	https://cran.r-project.org/web/packages/effsize/effsize.pdf	Version 0.8.1.
EnrichR tool	https://maayanlab.cloud/Enrichr/	RRID:SCR_001575
Illustrator	Adobe Systems, Inc.	Version 29.5.1.; RRID:SCR_010279
Photoshop	Adobe Systems, Inc.	Version 26.6.1.; RRID:SCR_014199

EXPERIMENTAL MODEL AND SUBJECT DETAILS

Ethical approval

The work with iPSCs has been approved by the Ethics Review Panel (ERP) of the University of Luxembourg and the national Luxembourgish Research Ethics Committee (CNER, Comité National d'Ethique de Recherche) under CNER No. 201901/01 (ivPD) and No. 202406/03 (AdvanceOrg).

Cell lines

The patient GBA1 cell line was obtained from the European Bank for induced pluripotent Stem Cells (EBiSC), the patient GBA2 cell line was provided by the University College London and the patient GBA3 cell line from the Coriell Institute. The healthy control 1 and 2 were generated at the Max Planck Institute and healthy control 3 was provided by the Coriell Institute (see Table S1).

Midbrain organoid culture

One iPSC line from each donor was used, which was derived into NESCs as described by Reinhardt et al.[16] Midbrain organoids were generated from NESCs according to a protocol published by Monzel et al.[4] and Nickels et al.[5] until day 30 or day 60 of organoid culture depending on the experiment. NESCs were cultured in N2B27 maintenance media in 6-well Geltrex (Gibco, cat. no. A1413302) precoated plates. The N2B27 base media consists of DMEM/F-12 (Gibco cat. no. 21331046) and Neurobasal (Gibco, cat. no. 21103049) in a 50:50 ratio and is supplemented with 1% GlutaMAX (Gibco, cat. no. 35050061), 1% penicillin/streptomycin (Gibco, cat. no. 15140122), 1% B27 supplement w/o Vitamin A (Gibco, cat. no. 12587001) and 2% N2 supplement (Gibco, cat. no. 17502001). For the maintenance of NESCs, the N2B27 base media was supplemented with 150 μM ascorbic acid (Sigma-Aldrich, cat. no. A4544), 3 μM CHIR-99021 (Axon Medchem BV, cat. no. AXON1386), and 0.75 μM purmorphamine (Enzo Life Science, cat. no. ALX-420-045). The NESC maintenance media was exchanged every second day. For the generation of midbrain organoids, NESCs were detached at 80% confluence with Accutase (Sigma-Aldrich, cat. no. A6964). Trypan Blue was used to count the number of viable cells. 9,000 live cells were seeded into each well of a 96-well ultra-low attachment plate (faCellitate, cat. no. F202003) in 150 μL of NESC maintenance media to initiate spheroid formation, marking day 0 of organoid culture. On the 2nd day of midbrain organoid culture, the maintenance media was changed to patterning media, where N2B27 base media was supplemented with 200 μM ascorbic acid (Sigma-Aldrich, cat. no. A4544), 500 μM dbcAMP (STEMCELL Technologies, cat. no. 100–0244), 10 ng/mL hBDNF (PeproTech EC Ltd., cat. no. 450-02), 10 ng/mL hGDNF (PeproTech EC Ltd., cat. no. 450-10), 1 ng/mL TGF-β3 (PeproTech EC Ltd., cat. no. 100-36E) and 1 μM purmorphamine (Enzo Life Science, cat. no. ALX-420-045). The next media change with the pattering media was done on the 5th day of organoid culture. On the 8th day of organoid culture, the patterning media was replaced by the differentiation media, which excluded PMA from the patterning media composition. Further media changes were done every 3–4 days until sample collection. NESC and midbrain organoid cultures were regularly (once per month) tested for mycoplasma contamination using LookOut Mycoplasma PCR Detection Kit (Sigma-Aldrich, cat. no. MP0035-1 KT).

METHOD DETAILS

Whole mount staining

Midbrain organoids were collected at day 30, fixed with 4% paraformaldehyde (PFA) (Sigma-Aldrich, cat. no. P6148) overnight at 4 °C and washed 3× with PBS for 10 min. The whole organoids were permeabilized and blocked with 1% Triton X-100 (Carl Roth, cat. no. 3051.3) and 10% donkey serum (Sigma-Aldrich, cat. no D9663) in PBS for 24 h at room temperature (RT) and washed with 0.01% Triton X-100 in PBS for 30 min at RT on an orbital shaker. The organoids were incubated for 4 days at 4 °C on an orbital shaker with the primary antibodies (Table S2) diluted in 0.5% Triton X-100 and 3% donkey serum in PBS. They were washed 3× with PBS for 1 h before incubation for 2 days at 4 °C on an orbital shaker with secondary antibodies (Table S2) diluted in 0.5% Triton X-100 and 3% donkey serum in PBS. The whole organoids were washed 3× with 0.05% Triton X-100 in PBS and once with Milli-Q water for 5 min at RT before mounting them with Fluoromount-G mounting medium (Southern Biotech, cat. no. SOUT0100-01).

Immunofluorescence staining of midbrain organoid sections

Midbrain organoids were collected at day 30, fixed with 4% paraformaldehyde (PFA) overnight at 4 °C and washed 3× with PBS for 10 min. Four midbrain organoids per cell line were embedded in 3% low-melting point agarose (Biozym, cat. no. 840100) and the solid agarose block with the assembloid was sectioned at 60 μm using the vibrating blade microtome (Leica VT1000s, RRID:SCR_016495). The sections were permeabilized for 30 min in 0.5% Triton X-100 at RT, followed by one quick wash with 0.01% Triton X-100 in PBS. The sections were then blocked for 2h at RT with blocking buffer containing 2.5% BSA (Sigma-Aldrich, cat. no. A4503), 2.5% donkey serum, 0.01% Triton X-100 and 0.1% sodium azide (Carl Roth, cat. no. K305.1) in PBS. Primary antibody (Table S2) was diluted in blocking buffer and the sections were incubated with the primary antibody dilutions for 48h at 4°C on an orbital shaker. Incubation with secondary antibodies and mounting of the sections were performed as previously described.[5]

Image 3D reconstruction

The 3D structure of the dopaminergic neuron was reconstructed from whole mount stainings using IMARIS software (version 9.9.1., (Bitplane, RRID:SCR_007370). z stack planes were used to visualise the fragmentation of dopaminergic neurons positive to tyrosine hydroxylase (TH) in GBA-PD compared to hearty control (WT) midbrain organoids.

β-galactosidase staining

60 μm sections from midbrain organoids were used in the β-galactosidase staining, using the Senescence Detection Kit (Abcam, cat. no. ab65351). Two sections from one midbrain organoid per cell line were used. Images were acquired at 4× and 10× on an Olympus IX83 Automated Fluorescence Microscope (RRID:SCR_020344) for qualitative images and enhanced using Fiji software (RRID: SCR_002285) to account solely for differences in the background levels of light.

Image acquisition and analysis

For high-content imaging, mounted organoids were scanned using the Yokogawa CellVoyager CV8000 microscope (RRID: SCR_023270). A 4× pre-scan in the 405 channel identified organoid-containing wells, enabling the creation of masks to outline organoids. These masks guided the selection of the field for imaging at different wavelengths with a 20× objective. For all stainings, three to four organoids per condition and four batches were analyzed, with details provided in figure legends. Qualitative images were captured using a Zeiss LSM 710 Confocal Inverted Microscope (RRID:SCR_018063) with 20×, or 60× objectives.

Immunofluorescence images of the whole mount organoids from the Yokogawa microscope were analyzed in MATLAB (2021a, Mathworks, RRID:SCR_001622) using a custom image-analysis algorithm as described by Bolognin et al.[17] The algorithm merges overlapping sections into mosaic images, smoothes and combines color channels and removes small objects. Masks were created and refined for each marker based on pixel intensity to quantify marker areas in 3D space (voxels). Representative images were edited with Adobe Illustrator (version 29.5.1., RRID:SCR_010279) and Adobe Photoshop (version 26.6.1, RRID:SCR_014199) for visualization purposes.

RNA extraction, library preparation and sequencing

Total RNA was extracted from each organoid generation batch, with 15–20 midbrain organoids pooled per batch at either day 30 or day 60. RNA isolation was done using the RNeasy Mini Kit (Qiagen, cat. no. 74106) following the manufacturer's protocol. Messenger RNA was purified from total RNA using poly-T oligo-attached magnetic beads. After fragmentation, the first strand cDNA was synthesized using random hexamer primers, followed by the second strand cDNA synthesis using either dUTP for directional library or dTTP for non-directional library. Library preparations were sequenced on an Illumina platform by Novogene's sequencing service.

Transcriptomic analysis

RNA sequencing data were pre-processed on the Galaxy server (version 23.2.rc1) following Galaxy training tutorial.[18,19] Reads were mapped to the human reference genome hg38 using the HISAT2 tool (RRID:SCR_015530). Mapped reads were counted using the featureCounts (RRID:SCR_001905) function on the BAM output files of HISAT2. Differential expression analysis was conducted in the R Project for Statistical Computing (version 4.4.2., RRID:SCR_001905) using the software package ''DESeq2'' (version 1.42.1., RRID:SCR_015687) (Love et al.[20]). *P*-value significance scores for differential expression were adjusted for multiple hypothesis testing according to the Benjamini and Hochberg method.[21] Pathway enrichment analysis was performed with the EnrichR tool (RRID:SCR_001575)[22,23] using the gene-level differential expression results table obtained with the DESeq2. We made use of two Gene-set libraries: the ''Reactome Pathways 2024'' library[24] and the ''GO Biological process 2023'' library.[25,26] Euclidean distance analysis was performed in R using base functions for distance computation and the ''dplyr'' package (version 1.1.4., RRID:SCR_016708) for data manipulation, ensuring precise distance measurements through established statistical functions.[27,28] This approach allowed us to quantify the relative positioning of the data points within the multidimensional space defined by the clusters, providing insight into its similarity to each group.

Analysis of explained variance

To assess the sources of variability in gene expression data, Principal Variance Component Analysis (PVCA) was performed in R using the ''PVCA'' package (version 1.42.0., RRID:SCR_001356).[29] PVCA performs the dual analysis Principal Component Analysis (PCA) and Variance Component Analysis (VCA). This results in a reduction in data dimensionality while retaining most of its variability. A mixed linear model is then applied, treating all factors of interest as random effects, including two-way interaction terms, to estimate and partition the total variance attributed to each term. This method accounts for all defined sources of variability, including both experimental (cell line, passage, batch) and biological (disease status, patient sex) factors. Both, biological and experimental variates were treated as random factors and the variance attributed to other technical variables was assigned to a residual variance category.

Transcriptomics and metabolomics integration

RNA sequencing and metabolomics data were integrated using ''mixOmics'' package (version 6.22.0., RRID:SCR_016889)[30] in R with DIABLO framework.[31] The separation between sample groups was assessed using the correlation of the top 50 genes with the top five metabolites from the first component of Partial Least Squares Discriminant Analysis (PLS-DA). Pearson correlation (abs(r) = 0.85) between metabolomics and transcriptomics features was further visualized in a Circos plot (version 0.69–9., RRID: SCR_011798).

Sample size estimation using power analysis

For the RNAseq dataset statistical power based on sample size was estimated using ''PROPER'' package (version 1.30.0.) in R. Library size dispersion and baseline expression values were determined based on the complete RNAseq data (Dataset 1) of midbrain organoid samples from eight independent organoid batches with 48 samples per group (3 cell lines x 2 independent groups (WT and GBA-PD) x 8 independent organoid batches). 20 simulations were run using ''DESeq2'' (version 1.42.1, RRID: SCR_015687) (Love et al.[20]) as a differential expression analysis method for possible sample sizes considering that we have three

independent cell lines per group (WT or GBA-PD), thus sample size can increase by three for each batch (3 cell lines x 2 batches = 6 samples per group). To determine the relevant effect sizes between the two groups, we estimated the median, min and max log2 fold change of significantly differentially expressed genes between GBA and control sample groups. The false discovery rate was set to 5%.

For metabolomics and imaging experiments, sample size estimation was done using ''pwr'' package (version 1.3.0., RRID: SCR_025480) with a defined significance of alpha = 0.05 and power = 0.8. For both datasets Cohen's effect size was calculated using the ''effsize'' package (version 0.8.1.) for significantly different abundant metabolites and TH normalised to nuclei of imaging features respectively. Based on normal data distribution of metabolomics data, we applied pwr.t.test function, while considering potential unequal sample sizes in each group and non-normal data distribution of imaging data, function pwr.2p.test of the pwr package was applied to imaging data.

QUANTIFICATION AND STATISTICAL ANALYSIS

Statistical analysis

Statistical significance was calculated using Wilcoxon T-test in R Project for Statistical Computing (version 4.4.2., RRID: SCR_001905). Statistically significant results were indicated when *p* values were * <0.05, ** <0.01, *** <0.001 and **** <0.0001. When data was found not significant, it is not specifically stated in the figures and is expressed as ns, not significant. Error bars represent mean +standard deviation (SD). All statistical details of experiments can be found in the Figure legends.

iScience, Volume *28*

Supplemental information

Reproducibility of PD patient-specific midbrain organoid data for *in vitro* disease modeling

Elisa Zuccoli, Haya Al Sawaf, Mona Tuzza, Sarah L. Nickels, Alise Zagare, and Jens C. Schwamborn

Supplemental Figures

Figure S1

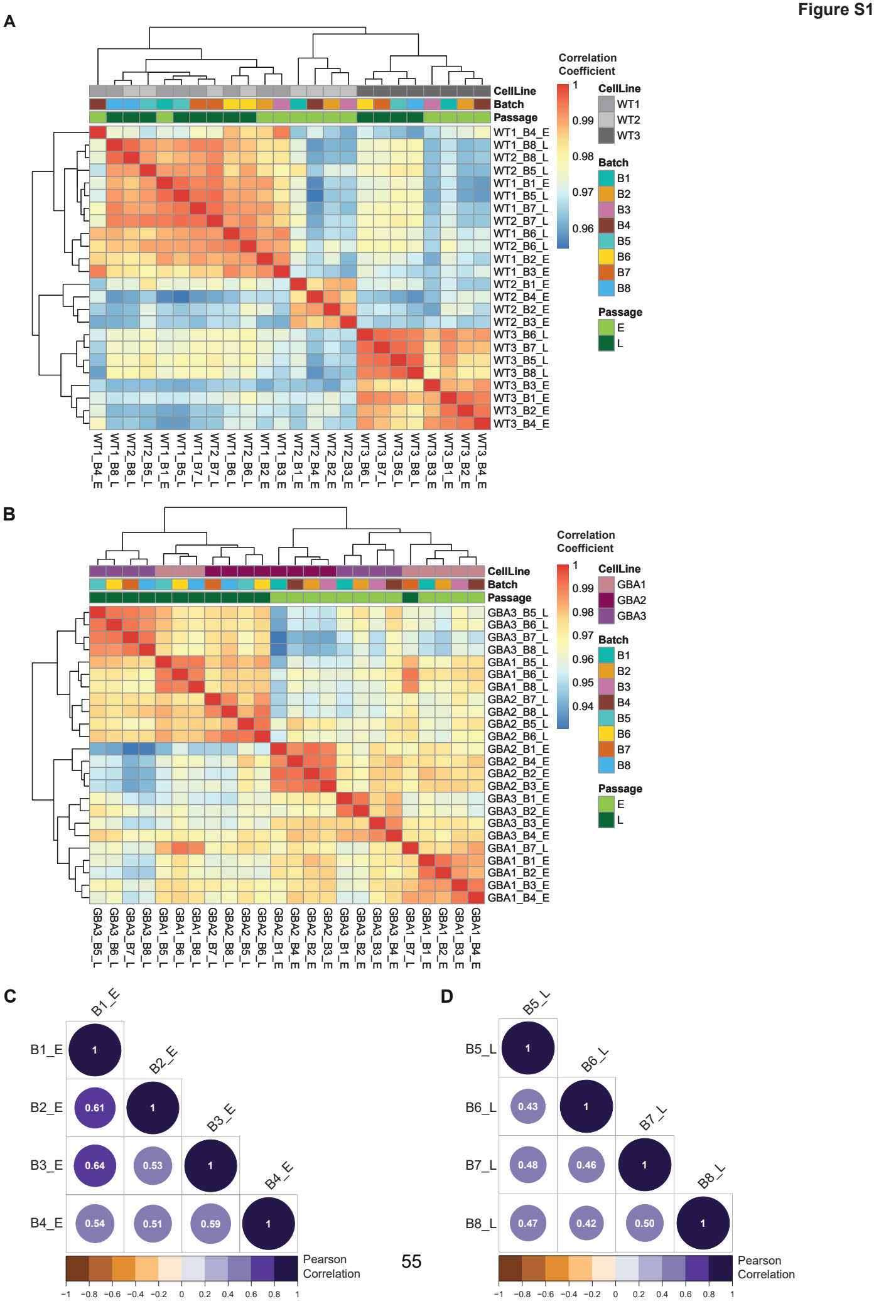

Figure S1: Correlation analysis of healthy control (WT) and GBA-PD samples. Related to Figure 2.

(A) Unsupervised hierarchical clustering plot showing the correlation of healthy control (WT) samples from early and late passage and all eight batches.

(B) Unsupervised hierarchical clustering plot showing the correlation of GBA-PD samples from early and late passage and all eight batches.

(C) Pearson Correlation of log2 fold changes (FC) of all genes between batches derived from early passage NESCs.

(D) Pearson Correlation of log2 fold changes (FC) of all genes between batches derived from late passage NESCs.

A

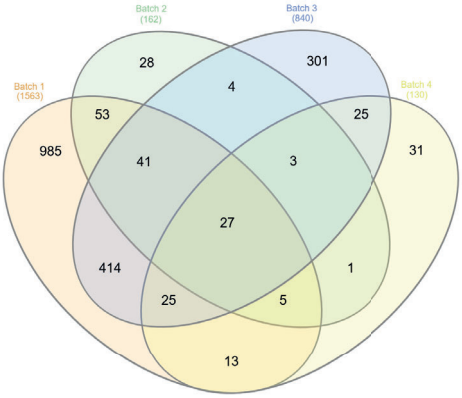
Dataset 1 - Early Passage
Batch 1 (1563)
Batch 2 (162)
Batch 3 (840)
Batch 4 (130)
985
28
301
31
53
4
25
41
3
27
414
1
25
5
13

B

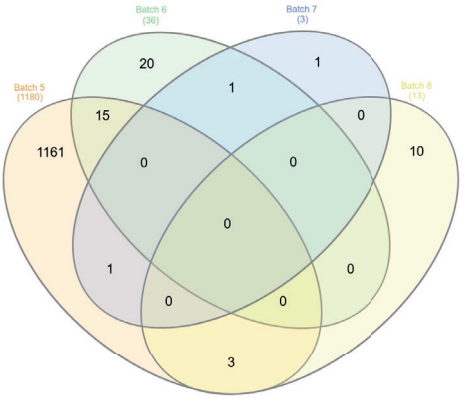
Dataset 1 - Late Passage
Batch 5 (1180)
Batch 6 (36)
Batch 7 (3)
Batch 8 (13)
1161
20
1
15
1
0
10
0
0
0
1
0
0
0
3

C

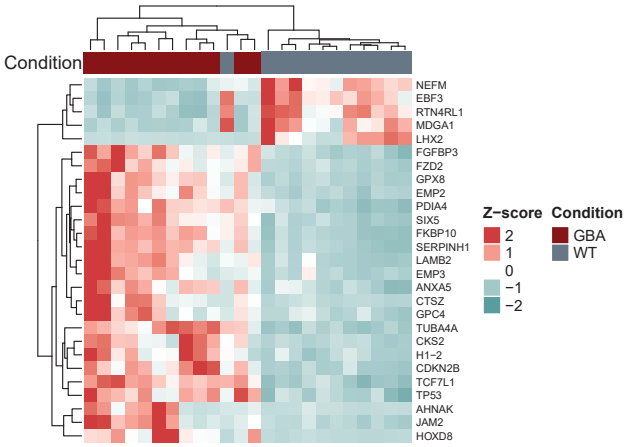
27 DEGs - Early Passage
Condition
NEFM
EBF3
RTN4RL1
MDGA1
LHX2
FGFBP3
FZD2
GPX8
EMP2
PDIA4
SIX5
FKBP10
SERPINH1
LAMB2
EMP3
ANXA5
CTSZ
GPC4
TUBA4A
CKS2
H1−2
CDKN2B
TCF7L1
TP53
AHNAK
JAM2
HOXD8
Z−score
2
1
0
−1
−2
Condition
GBA
WT

D

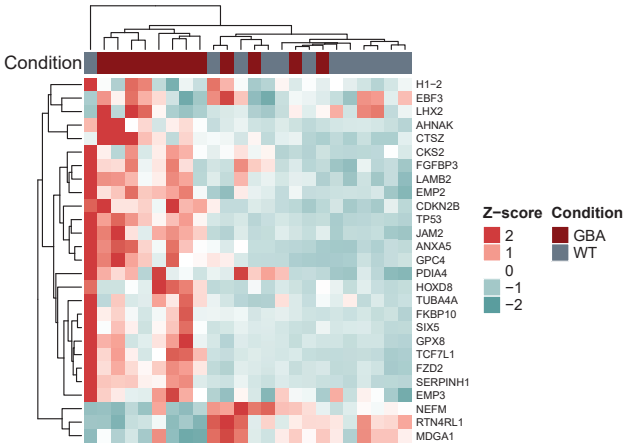
27 DEGs - Late Passage
Condition
H1−2
EBF3
LHX2
AHNAK
CTSZ
CKS2
FGFBP3
LAMB2
EMP2
CDKN2B
TP53
JAM2
ANXA5
GPC4
PDIA4
HOXD8
TUBA4A
FKBP10
SIX5
GPX8
TCF7L1
FZD2
SERPINH1
EMP3
NEFM
RTN4RL1
MDGA1
Z−score
2
1
0
−1
−2
Condition
GBA
WT

E

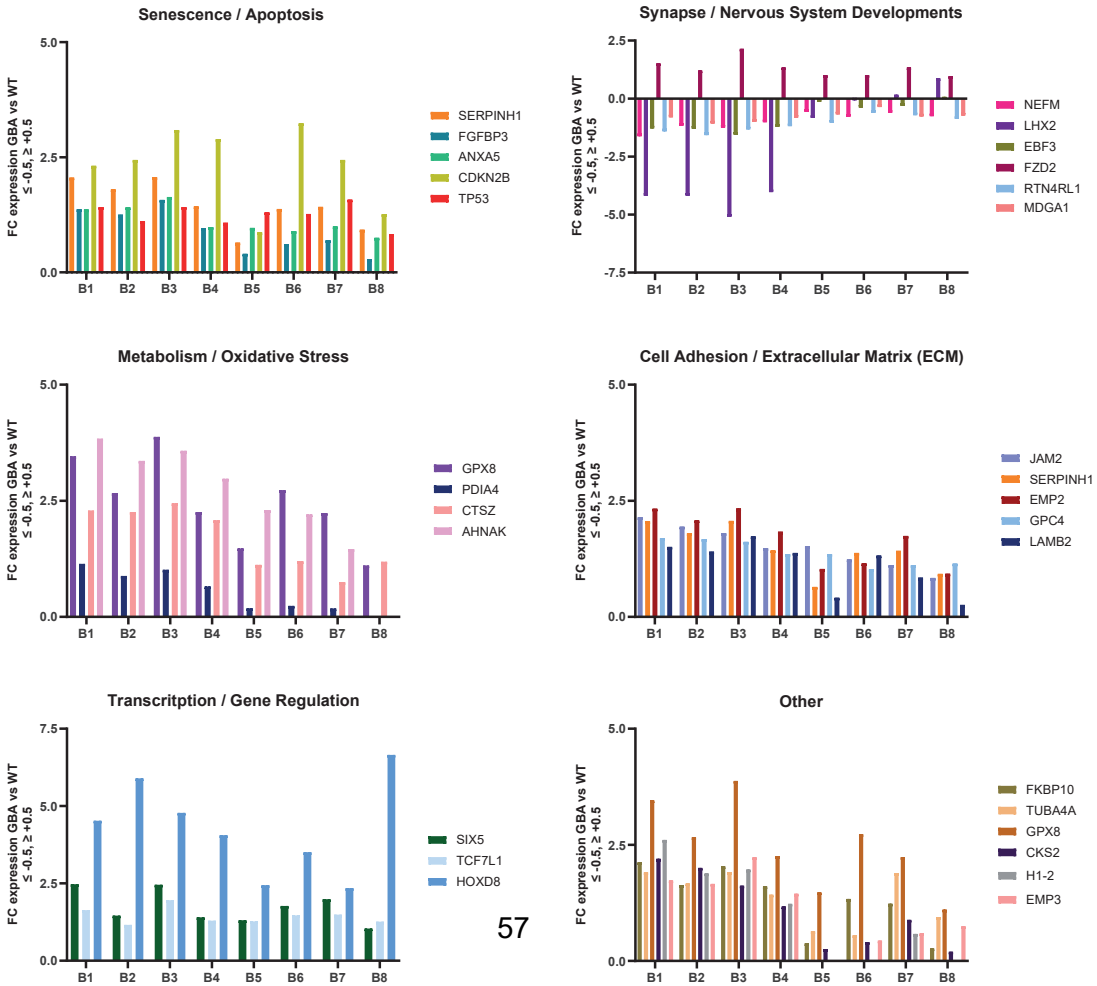
Senescence / Apoptosis
FC expression GBA vs WT
≤ -0.5; ≥ +0.5
SERPINH1
FGFBP3
ANXA5
CDKN2B
TP53
Synapse / Nervous System Developments
NEFM
LHX2
EBF3
FZD2
RTN4RL1
MDGA1
Metabolism / Oxidative Stress
GPX8
PDIA4
CTSZ
AHNAK
Cell Adhesion / Extracellular Matrix (ECM)
JAM2
SERPINH1
EMP2
GPC4
LAMB2
Transcritption / Gene Regulation
SIX5
TCF7L1
HOXD8
Other
FKBP10
TUBA4A
GPX8
CKS2
H1-2
EMP3
B1
B2
B3
B4
B5
B6
B7
B8

Figure S2: Identification of 27 differentially expressed genes (DEGs) in early passage batches and assignment to distinct functional categories. Related to Figure 3.

(A) Venn diagram of DEGs showing the batches derived from early passage NESCs, with 27 genes in common.

(B) Venn diagram of DEGs showing the batches derived from early passage NESCs.

(C) Unsupervised hierarchical clustering of GBA-PD and healthy control (WT) samples based on normalised gene counts of 27 predefined genes for early passage batches.

(D) Unsupervised hierarchical clustering of GBA-PD and healthy control (WT) samples based on normalised gene counts of 27 predefined genes for late passage batches.

(E) Log2 fold changes (FC) of 27 predefined genes divided into distinct functional categories. The genes were assigned to the senescence/apoptosis pathway, synapse and nervous system development, metabolic and oxidative stress processes, cell adhesion and extracellular matrix (ECM) dynamics, and transcription and gene regulation. Each category shows the FC per batch with eight batches in total.

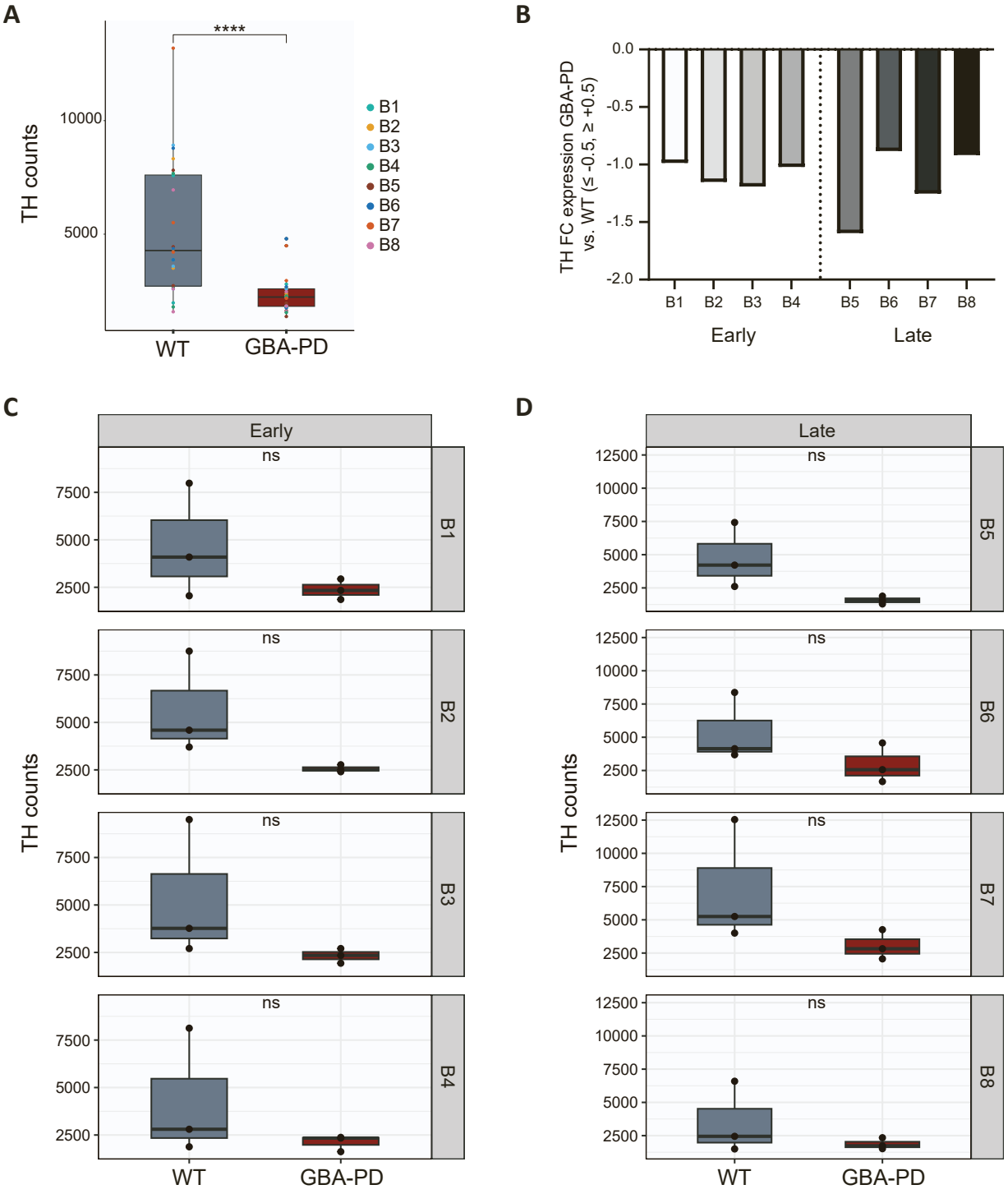
A
****
TH counts
10000
5000
B1
B2
B3
B4
B5
B6
B7
B8
WT
GBA-PD
B
TH FC expression GBA-PD
vs. WT (≤ -0.5, ≥ +0.5)
0.0
-0.5
-1.0
-1.5
-2.0
B1 B2 B3 B4 B5 B6 B7 B8
Early
Late
C
Early
ns
B1
B2
B3
B4
TH counts
7500
5000
2500
WT
GBA-PD
D
Late
ns
B5
B6
B7
B8
12500
10000
7500
5000
2500
TH counts
WT
GBA-PD

Figure S3: Transcriptomic analysis of dopaminergic neuron phenotype supports imaging analysis. Related to Figure 4.

(A) TH counts from all eight batches pooled. Data is shown as boxplots ± SD. Wilcoxon T-test; ****p < 0.0001.

(B) Log2 fold change (FC) of TH expressed in early passage batches (B1-4) and late passage batches (B5-8).

(C) TH counts from early passage batches (B1-4). Pooled healthy control (WT) or GBA-PD lines are shown per batch. Data is shown as boxplots ± SD. Wilcoxon T-test; ns, not significant.

(D) TH counts from late passage batches (B5-8). Pooled healthy control (WT) or GBA-PD lines are shown per batch. Data is shown as boxplots ± SD. Wilcoxon T-test; ns, not significant.

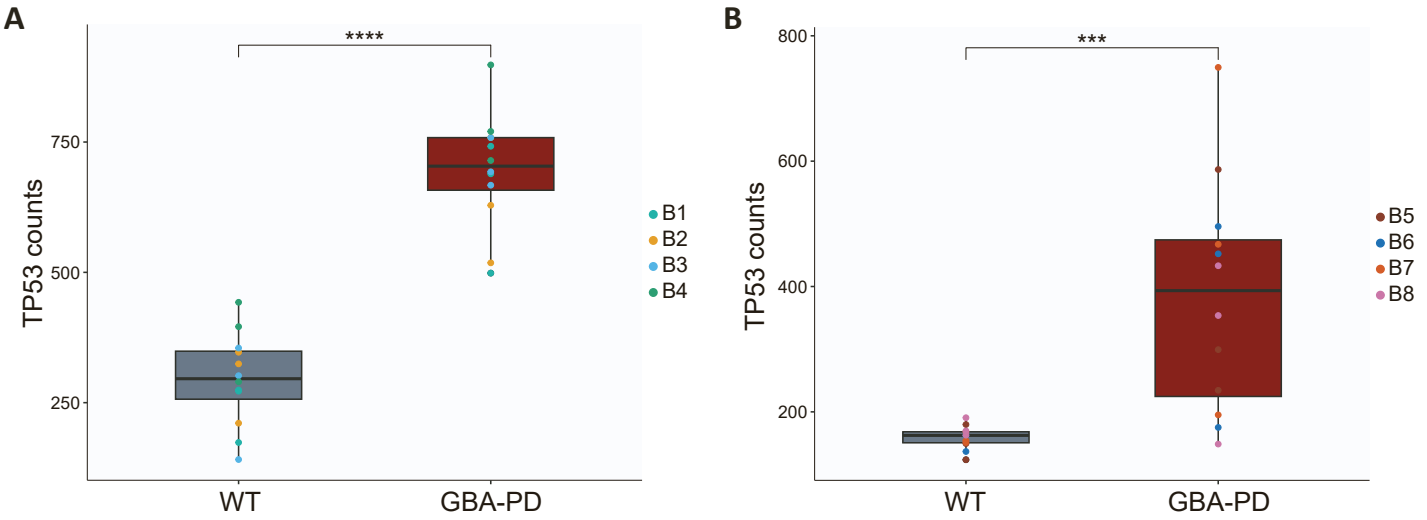
A
****
TP53 counts
750
500
250
WT
GBA-PD
B1
B2
B3
B4
B
***
TP53 counts
800
600
400
200
WT
GBA-PD
B5
B6
B7
B8

Figure S4: Transcriptomic analysis of senescence phenotype supports imaging analysis. Related to Figure 4.

(A) TP53 counts from early passage batches (B1-4) pooled. Data is shown as boxplots ± SD. Wilcoxon T-test; ****p < 0.0001.

(B) TP53 counts from late passage batches (B5-8) pooled. Data is shown as boxplots ± SD. Wilcoxon T-test; ***p < 0.001.

A

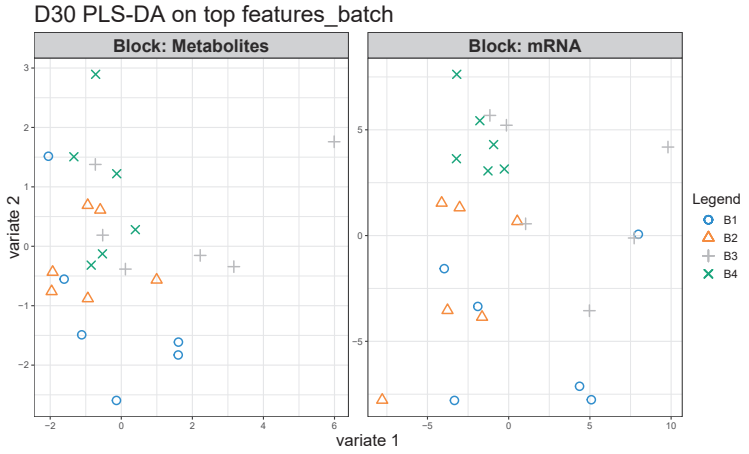
D30 PLS-DA on top features_batch
Block: Metabolites
Block: mRNA
variate 2
variate 1
Legend
B1
B2
B3
B4

B

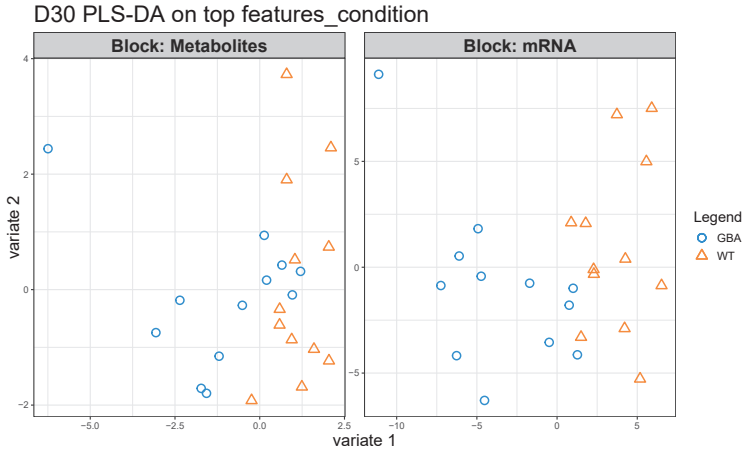
D30 PLS-DA on top features_condition
Block: Metabolites
Block: mRNA
variate 2
variate 1
Legend
GBA
WT

C

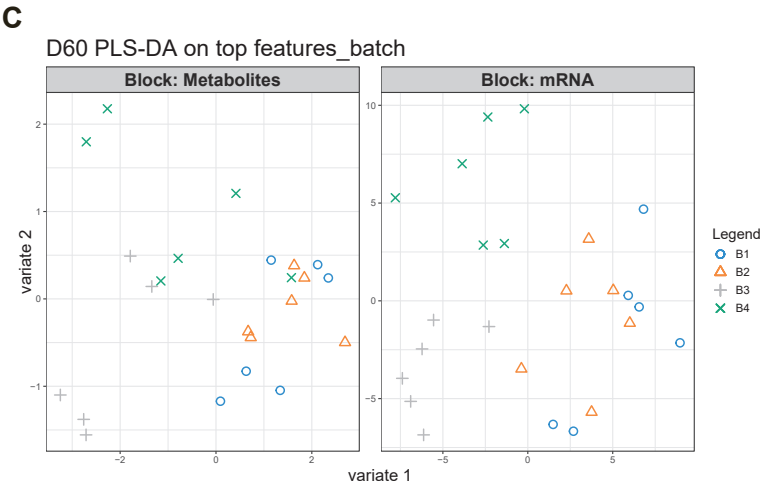
D60 PLS-DA on top features_batch
Block: Metabolites
Block: mRNA
variate 2
variate 1
Legend
B1
B2
B3
B4

D

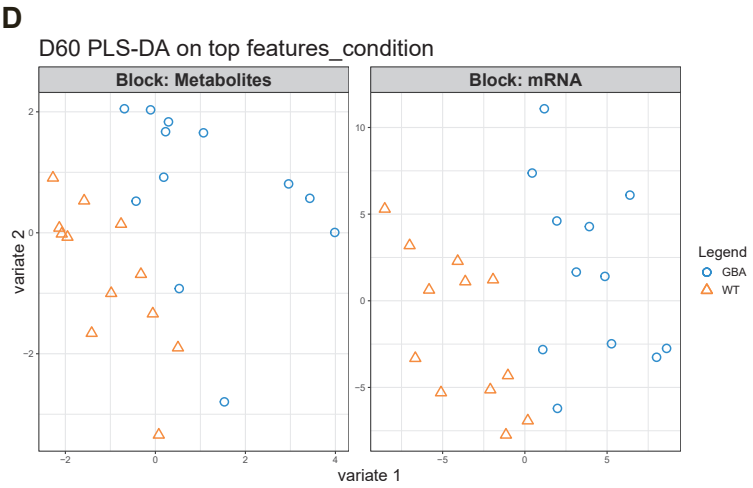
D60 PLS-DA on top features_condition
Block: Metabolites
Block: mRNA
variate 2
variate 1
Legend
GBA
WT

Figure S5: Partial Least Squares Discriminant Analysis (PLS-DA). Related to Figure 5.

(A) Day 30 sample discrimination by batch.

(B) Day 30 sample discrimination by condition.

(C) Day 60 sample discrimination by batch.

(D) Day 60 sample discrimination by condition.

Supplemental Tables

Table S1. Cell lines used in this study. Related to STAR Methods.

Sample ID	Diagnosis	Genotype	Sex	Age of onset	Age of sampling	Source of iPSC
WT1	Healthy	wt/wt	F	/	63	IBBL / Max Planck Institute
WT2	Healthy	wt/wt	F	/	68	IBBL / Max Planck Institute
WT3	Healthy	wt/wt	M	/	55	Coriell Institute
GBA1	PD	GBA-N370S/wt	F	77	81	European Bank for induced pluripotent Stem Cells
GBA2	PD	GBA-N370S/wt	F	55	55	University College London
GBA3	PD	GBA-N370S/wt	M	63	66	Coriell Institute

Table S2. Primary and secondary antibodies used for immunofluorescence stainings. Related to STAR Methods.

Antibody	Source	Cat. no.	RRID	Species	Dilution
TH	Abcam	ab76442	*AB_1524535*	Chicken	1:250
TH	Abcam	Ab112	*AB_297840*	Rabbit	1:1000
TUJ1	BioLegend	801201	*AB_2313773*	Mouse	1:300
53BP1	Novus BIologicals	NB100-304	*AB_10003037*	Rabbit	1:250
MAP2	Abcam	ab92434	*AB_2138147*	Chicken	1:250 1:1000
Anti-chicken 488	Jackson Immunoresearch	703-545-155	*AB_2340375*	Donkey	1:1000
Anti-chicken 647	Jackson Immunoresearch	703-605-155	*AB_2340379*	Donkey	1:1000
Anti-rabbit 488	Invitrogen	A21206	*AB_2535792*	Donkey	1:1000
Anti-rabbit 568	Invitrogen	A-10042	*AB_2534017*	Donkey	1:1000
Anti-mouse 647	Invitrogen	A-31571	*AB_162542*	Donkey	1:1000

3.2 Manuscript II

The Parkinson's disease-associated LRRK2-G2019S variant restricts serine metabolism, leading to microglial inflammation and dopaminergic neuron degeneration.

Henry Kurniawan[1*#], Sarah L. Nickels[1], Alise Zagare[1], Elisa Zuccoli[1], Isabel Rosety[1], Enrico Glaab[2], Jens C. Schwamborn[1#]

[1] Developmental and Cellular Biology, Luxembourg Centre for Systems Biomedicine (LCSB), University of Luxembourg, 6, Avenue du Swing, L-4367 Belvaux, Luxembourg.

[2] Biomedical Data Science Group, Luxembourg Centre for Systems Biomedicine, University of Luxembourg, Esch-sur-Alzette, Luxembourg.

* First author

[#] Corresponding author

This article is published in the Journal of Neuroinflammation.

3.2.1 Contribution statement

In this article, I supported the first author by generating and maintaining cultures. I collected samples, performed protein extraction and Western blots, which were necessary for the revision of the paper. I also contributed with the manuscript revision. The initial concept for the study was developed by J. C. Schwamborn, and the project was carried out by H. Kurniawan.

3.2.2 Preface

The main aim of this study was to investigate how patient-derived microglia carrying the LRRK2-G2019S mutation contribute to Parkinson's disease pathogenesis. Using iPSC-derived microglia from LRRK2-G2019S patients and healthy controls, we first characterized the impact of the mutation on microglial identity, physiology, and function. Subsequently, we assessed how LRRK2-G2019S microglia affect the cellular and molecular environment of healthy midbrain organoids, with a particular focus on dopaminergic neuron integrity.

Our findings show that the LRRK2-G2019S mutation does not impair microglial differentiation or structural integrity but significantly alters microglial function. Mutant microglia exhibited increased immune activity, including increased TNF-α production and enhanced phagocytosis. Bulk RNA sequencing revealed transcriptional signatures consistent with inflammatory activation and metabolic reprogramming, with notable enrichment in TNF and IL-1 signalling pathways. Further metabolic profiling revealed a shift toward glycolysis and reduced glucose-derived biosynthesis, indicating an inflammatory immunometabolic state. Interestingly, mitochondrial function was largely preserved, suggesting that the observed metabolic reprogramming reflects a deliberate shift rather than mitochondrial dysfunction.

To assess the functional impact of this altered microglial state, we co-cultured LRRK2-G2019S microglia with healthy control midbrain organoids. The presence of the mutant microglia led to the degeneration of dopaminergic neurons, recapitulating a key aspect of PD pathology. The neuronal loss was mediated by TNF-α-dependent mechanisms, as pharmacological inhibition of TNF-α restored neuronal viability. Furthermore, targeting glycolysis with oxamic acid, a lactate dehydrogenase inhibitor, attenuated microglial immune activity and prevented loss of dopaminergic neuron. These results suggest that microglial metabolic rewiring is not only a consequence of immune activation, but also an active driver of microglia-mediated neurotoxicity in LRRK2-associated PD.

Together, our findings demonstrate a patient-specific iPSC-derived assembloid model provides a mechanistic platform for studying neuroinflammation in PD. They highlight the

critical role of immunometabolic reprogramming in LRRK2-G2019S microglia and identify microglial metabolism as a promising therapeutic target for modifying disease progression.

Kurniawan *et al. Journal of Neuroinflammation* (2025) 22:244
https://doi.org/10.1186/s12974-025-03577-2

Journal of Neuroinflammation

RESEARCH Open Access

The Parkinson's disease-associated LRRK2-G2019S variant restricts serine metabolism, leading to microglial inflammation and dopaminergic neuron degeneration

Henry Kurniawan[1*], Sarah L. Nickels[1], Alise Zagare[1], Elisa Zuccoli[1], Isabel Rosety[1], Gemma Gomez-Giro[1], Enrico Glaab[2] and Jens C. Schwamborn[1*]

Abstract

A growing body of evidence implicates inflammation as a key hallmark in the pathophysiology of Parkinson's disease (PD), with microglia playing a central role in mediating neuroinflammatory signaling in the brain. However, the molecular mechanisms linking microglial activation to dopaminergic neuron degeneration remain poorly understood. In this study, we investigated the contribution of the PD-associated LRRK2-G2019S mutation to microglial neurotoxicity using patient-derived induced pluripotent stem cell (iPSC) models. We found that LRRK2-G2019S mutant microglia exhibited elevated activation markers, enhanced phagocytic capacity, and increased secretion of pro-inflammatory cytokines such as TNF-α. These changes were associated with metabolic dysregulation, including upregulated glycolysis and impaired serine biosynthesis. In 3D midbrain organoids, these overactivated microglia resulted in dopaminergic neuron degeneration. Notably, treating LRRK2-G2019S microglia with oxamic acid, a glycolysis inhibitor, attenuated microglial inflammation and reduced neuronal loss. Our findings underscore the link between metabolic targeting in microglia and dopaminergic neuronal loss in LRRK2-G2019S mutation, and highlight a potential strategy that warrants further preclinical evaluation.

Keywords LRRK2-G2019S, Microglia, Parkinson's disease, Metabolism, Serine, Glycolysis, IPSC, Organoids

*Correspondence:
Henry Kurniawan
henry.kurniawan@uni.lu
Jens C. Schwamborn
Jens.Schwamborn@uni.lu
[1]Developmental and Cellular Biology, Luxembourg Centre for Systems Biomedicine (LCSB), University of Luxembourg, Esch-Sur-Alzette, Luxembourg
[2]Biomedical Data Science Group, Luxembourg Centre for Systems Biomedicine, University of Luxembourg, Esch-Sur-Alzette, Luxembourg

Introduction

Parkinson's disease (PD) stands as the second most common neurodegenerative disorder, with its incidence steadily rising over time [1]. While mitochondrial dysfunction, oxidative stress, calcium imbalance, and impaired autophagy and mitophagy have long been recognized as key contributors to dopaminergic neuron loss [2], neuroinflammation has emerged in recent years as a prominent and unifying feature across PD subtypes [3]. Accordingly, targeting neuroinflammatory pathways presents a promising therapeutic strategy for PD.

Microglia, the brain's resident immune cells, play essential roles in both immune defense and neuronal homeostasis. In response to pathogen-associated molecular patterns, microglia activate and release cytokines to recruit peripheral immune cells and contain damage. Beyond immune surveillance, microglia support neuronal development by regulating neuronal progenitor cells, guiding dopaminergic axon growth, and releasing neurotrophic factors [4]. Importantly, they are also key mediators of aggregated α-synuclein clearance – another pathological hallmark of PD [5]. However, chronic engagement in α-synuclein clearance can perpetuate a cycle of inflammation, ultimately resulting in neurotoxicity and neuronal death [6, 7]. This vicious cycle is increasingly recognized as a critical driver of PD progression.

Immune cells, including microglia, shift from a resting state to an activated state upon receiving stimulatory signals, accompanied by adaptations in their metabolic pathways – a process known as metabolic reprogramming. This metabolic shift is fundamental for providing the energy required for cell proliferation, differentiation, and activation. Studies have shown that peripheral immune cells, including microglia, switch from a highly efficient ATP production via mitochondrial oxidative phosphorylation to faster ATP production through glycolysis [8]. The fine-tuning of cellular metabolism is crucial for normal immune cell functions in both health and disease [9, 10]. In addition to glucose metabolism, glucose is diverted to the pentose phosphate pathway to produce NADPH and ribose 5-phosphate, a precursor for nucleotide synthesis. Additionally, glucose can also be channeled into serine synthesis and one-carbon metabolism, supplying proteins, nucleic acids, lipids, and macromolecules to support cell proliferation and growth [11]. Microglia can also utilize free fatty acids as alternative energy sources in the absence of glucose, indicating their metabolic flexibility [12]. These metabolic dynamics highlight the importance of metabolic rewiring to provide sufficient precursors and energy to maintain normal microglial function. It has been hypothesized that during chronic inflammation in PD, microglial metabolism becomes compromised [8, 13, 14]. However, due to the complex etiology of PD, the precise link between PD pathology and microglial metabolic rewiringr remains unclear.

In this study, we examined how the LRRK2-G2019S mutation, one of the most common genetic causes of familial and sporadic PD, affects microglial physiology. Our results show that LRRK2-G2019S drives a proinflammatory phenotype in microglia by reprogramming their metabolism, notably enhancing glycolysis and impairing serine biosynthesis. These changes contribute to dopaminergic neurotoxicity in otherwise healthy midbrain organoids. Importantly, pharmacological targeting of glucose metabolism with oxamic acid ameliorated microglial activation and protected neurons. These findings are consistent with a functional connection between microglial immunometabolism and dopaminergic neuron vulnerability, and suggest avenues to explore for restoring microglial homeostasis.

Table 1 List of human iPSCs used in this study with details of the gender and age of sampling. The study uses four healthy and four patient-derived iPSCs

Original ID	Diagnosis	Sex	Age
DB 202	LRRK2-WT	M	55–59
DB 262	LRRK2-WT	F	57
DB 389	LRRK2-WT	M	-
DB 201	LRRK2-WT	F	-
DB 209	LRRK2-G2019S	F	81
DB 228	LRRK2-G2019S	F	40
DB 222	LRRK2-G2019S	F	66
DB 226	LRRK2-G2019S	M	79

Materials and methods

Cell cultures

Human induced pluripotent stem cells (iPSCs) culture

iPSCs (Table 1) were generated as previously described [15] and maintained on GelTrex™ hESC-qualified coated 6-well plates (ThermoFisher Scientific, A1569601) in Essential 8 Basal medium (ThermoFisher Scientific, A157001) supplemented with ROCK inhibitor (Y-27632, Merck Millipore, SCM075) for the first 24 h post-passaging. Medium was exchanged daily. At ~ 80% confluence, iPSCs were split dissociated using Accutase® (Sigma, A6964) and reseeded at approximately 500,000 cells per well.

Macrophage precursors were generated from iPSCs based on previous protocols [16]. Briefly, 4×10^6 iPSCs were seeded into AggreWell™ 800 plate pre-treated with Anti-Adherence Rinsing Solution (Stemcell Technologies, 34860). Cells were cultured for 4 days in embryoid body (EB) medium, consisting of Essential 8 Basal medium supplemented with ROCK inhibitor, 50 ng/ml bone morphogenetic protein 4 (BMP4, Biolegend, 795606), 50 ng/ml vascular endothelial growth factor 165 (VEGF-165, Biolegend, 583708), and 20 ng/ml stem

cell factor (SCF, Miltenyi Biotec, 130–096–695). EBs were harvested and transferred to ultra-low attachment 6-well plates (ThermoFisher Scientific, 07–200–601) and cultured for an additional 3 days in EB medium. Subsequently, EBs were transferred to a T75 flask and cultured in Factory medium (X-VIVO15 supplemented with 100 ng/ml macrophage colony-stimulating factor M-CSF, Biolegend 574808 and 25 ng/ml IL-3, Biolegend 578008) to generate macrophage precursors.

Microglia differentiation

Macrophage precursors were harvested biweekly and plated at either 50,000 (96-well) or 1×10^6 (6-well) cells/well. Cells were cultured for 14 days in basal microglia differentiation medium composed of Advanced DMEM/F12 (ThermoFisher Scientific, 35050061), 1 × N2 (ThermoFisher Scientific, 17502001), 1 × Pen/Strep (Invitrogen, 15140122), 1 × GlutaMax (ThermoFisher Scientific, 35050061), 50 µM β-Mercaptoethanol (ThermoFisher Scientific, 31350–010) supplemented with 100 ng/ml IL-34 (Biolegend, 577906), and 10 ng/ml GM-CSF (Biolegend, 572905) as described previously [17]. Medium was changed twice weekly. At day 14, microglia were detached with Accutase® for 15 min, washed twice in serum free media, or FACS buffer, and processed for downstream applications.

Midbrain organoid generation and culture

Neural epithelial stem cells (NESCs; 6,000 cells/well) were seeded into BIOFLOAT™ 96-well plates (faCellitate, F202003), and cultured in maintenance medium consisting of N2B27 supplemented with 3 µM CHIR (Axon CT 99021), 0.2 mM ascorbic acid (Sigma, A4544-100G), 0.5 µM smoothened agonist (SAG, Stemcell Technologies 73412), 2.5 µM SB-431542 (Abcam, ab120163), and 0.1 µM LDN-193189 (Sigma, SML0559) for 2 days.

From day 2 to 4, cells were cultured in patterning medium I (N2B27 supplemented with 0.2 mM Ascorbic Acid, 3 µM CHIR, and 0.5 µM SAG), then in patterning medium II from day 4 to 8 (N2B27 supplemented with 0.2 mM ascorbic acid, 0.7 µM CHIR, and 0.5 µM SAG). From day 8 onward, organoids were cultured in maturation medium of N2B27 supplemented with 0.2 mM ascorbic acid, 10 ng/ml Brain-Derived Neurotrophic Factor (BDNF, Peprotech, 450–02), 10 ng/ml Glial-Derived Neurotrophic Factor (GDNF, Peprotech, 450–10), 1 pg/ml TGF-β3 (Peprotech, 100-36E), 0.5 mM Dibutyryl cyclic-AMP (Biosynth SRO, ND07996), 10 µM DAPT (R&D Systems, 2634/10) and 2.5 ng/ml Activin A (ThermoFisher Scientific, PHC9564). Organoids were maintained under static conditions with biweekly medium changes until day 15 of differentiation.

Coculture of midbrain organoids and macrophage precursors (assembloids)

On day 15 of dopaminergic differentiation, 150,000 macrophage precursors were added to each organoid as previously described [17]. Co-culture was maintained in basal microglia differentiation medium supplemented with 100 ng/ml IL-34 (Biolegend, 577906), 10 ng/ml GM-CSF (Biolegend, 572905), 10 ng/ml BDNF, 10 ng/ml GDNF, 10 µM DAPT, and 2.5 ng/ml Activin A. Media were exchanged twice weekly. The duration of co-culture depended on the experimental design (D20 or D75).

2D microglia analysis

Flow cytometry

For surface marker analysis, microglia were stained in FACS buffer (PBS supplemented with 1% FCS and 5 mM EDTA pH 8.0) with fluorescently conjugated antibodies (Materials, Table S1) for at least 30 min at 4 °C, protected from light. Cells were washed twice, resuspended in FACS buffer and analyzed on a flow cytometer.

For intracellular phosphoprotein detection, cells were fixed in 2% formaldehyde for 10 min, and permeabilized with 0.01% saponin in FACS buffer. Staining and subsequent analysis were performed in 0.01% saponin.

For intracellular cytokine measurement, microglia were stimulated with 100 ng/ml lipopolysaccharide (LPS) for 24 h at D13 of differentiation, with BD GolgiPlug™ (BD Biosciences, 555029) added during the last 6 h of stimulation. Microglia were fixed and permeabilized using the BD Pharmingen™ Transcription Buffer Set (BD Biosciences, 562574) according to the manufacturer's protocol. This kit was also used to stain intracellular nuclear proteins.

For ROS/mitochondrial analysis, microglia were stained with dichlorofluorescein diacetate (H2-DCF-DA, ThermoFisher Scientific D399) or Mitotracker™ Deep Red and Green (ThermoFisher Scientific, M46753; M46750) for 30 min in non-supplemented DMEM-F12. The cells were washed twice in PBS and analyzed immediately in flow cytometer.

Phagocytosis assay

Microglia were incubated with 10 µg/ml Zymosan A (*S.cerevisiae*) BioParticles™ (ThermoFisher Scientific, Z23373) or pHRodo™-Zymosan BioParticles™ Conjugate (ThermoFisher Scientific, P35364) in HBSS medium supplemented with 20mM HEPES and 10% FCS. Cells were incubated for at least 30 min at 37 °C, washed 2 × with PBS, and analyzed by flow cytometry.

Glucose uptake assay

Cells were incubated in glucose free DMEM-F12 (non-supplemented) with 50 µM 2-NBDG (ThermoFisher

Scientific, N13195) for 1 h at 37°C. Cells were immediately analyzed using a flow cytometer.

Metabolic profiling

Microglia (2×10^5 cells/well) were plated in Agilent Seahorse XF DMEM medium (Agilent, 103575–100). The extracellular acidification rate (ECAR) and oxygen consumption rate (OCR) were measured using the XF Glycolytic Stress Test and the XF Cell Mitochondrial Stress Test kits according to the manufacturer's protocols.

Isotopic labelling

Microglia were cultured for 24 h in DMEM-F12 containing [U-$^{13}C_6$]-glucose (11.1 mmol/L; Cambridge Isotope Laboratories). Metabolite extraction, mass spectrometry, mass isotopomer quantification and determination of fractional carbon contributions were performed as previously described [18], using MetaboliteDetector software package.

Cytokine quantification

Proinflammatory cytokines were assessed using Human Inflammatory Cytokine Multiplex ELISA Kit (Arigo Biolaboratories, ARG80929) according to the manufacturer's protocol. In addition, TNF-α and IL-1β were quantified using human uncoated ELISA Kits from ThermoFisher Scientific (88–7346-77 and 88–7261-77).

2D Immunofluorescence staining

Microglia were differentiated and plated in 96-well glass bottom plate (Cellvis, P96-0-N). The cells were then fixed for 10 min with 4% formaldehyde (Sigma, 100496), and permeabilized using 0.3% Triton X-100 in PBS for 15 min. Microglia were washed three times with PBS and blocked with blocking buffer (3%BSA + 0.3% Triton X-100 in PBS). The cells were stained overnight at 4 °C with primary antibodies diluted in blocking buffer. The cells were rinsed three times and incubated with secondary antibodies in blocking buffer for 2 h at room temperature. After two PBS washes, the samples were resuspended in PBS + 0.1% Na-Azide and imaged using Zeiss LSM710 Confocal Laser Scanning Microscope.

RNA extraction and RT-PCR

RNA isolation was done using RNeasy Mini Kit (Qiagen, 74104) according to the manufacturer's protocol. cDNA was prepared using High-Capacity RNA-to-cDNA™ Kit (ThermoFisher Scientific, 4387406). RT-PCR was performed using Green-Taq polymerase with 50ng of cDNA per reaction. The primers used are listed under 'Oligonucleotides'. The reactions were run on an ABI 7500 HT Fast qRT-PCR instrument. Data were normalized to control gene and analyzed using ΔΔCt method as previously described.

RNA sequencing

Libraries were prepared using Novogene's property library prep protocols (Novogene NGS RNA Library Prep Set PT042 for 250–300 bp insert cDNA library). The indices were incorporated to multiplex multiple samples. mRNA was purified using poly-T oligo-attached magnetic beads. After fragmentation, the first strand cDNA was synthesized using random hexamer primers, followed by a second strand cDNA synthesis. Library preparation was finalized following end repair, A-tailing, adapter ligation, and size selection. After amplification and purification, the insert size of the library was validated on an Agilent 2100 and quantified using RT-PCR. Libraries were sequenced using Illumina NovaSeq 6000 S4 flow cell with PE150.

Transcriptomic analysis

The data were analyzed and visualized with RStudio (R version 4.3.3). Raw sequencing reads were processed using the Rsubread package (version 2.10.4) for alignment and quantification. Paired-end reads were aligned to the human reference genome GRCh38 using the Subread aligner with default parameters. The alignment quality showed high mapping rates with over 98% of reads successfully mapped across all samples. Gene-level counts were generated using the featureCounts function from Rsubread. Differential gene expression analysis was done using the DESeq2 pipeline [19]. GeneGO Metacore was used for gene set enrichment analysis (https://clarivate.com; https://portal.genego.com). The GEO accession number for the RNA-seq data from the healthy and mutant microglia in this study is GSE282494.

Metabolic modelling

Context-specific metabolic models were reconstructed by integration of RNA sequencing data into the Recon 3 generic human metabolic model [20] using rFASTCORMICS pipeline [21]. With this workflow, transcripts per million (TPM) normalized gene expression was used as a determinant of the presence of metabolic reactions models. In addition, metabolic networks were constrained by the composition of cell culture media, defying the availability of metabolites which can be taken up by cells. A separate metabolic model was generated for each LRRK2-WT and LRRK2-G2019S microglia. Models were generated and analyzed in MATLAB (MathWorks, v.2019b) using the COBRA toolbox [22]. Using the setdiff function in MATLAB shared reactions across the WT and MUT models were identified. Unique reactions for each condition (only present in the WT or MUT condition) were determined by the intersect function in MATLAB and assigned to the corresponding subsystem of Recon 3. Subsystems with five or more unique reactions, representing at least 10% of the total reaction number

in the respective subsystem in Recon 3 for WT or MUT conditions, were selected for further investigation.

3D assembloid analysis

Flow cytometry

The assembloids were incubated for 30 min at 37 °C in 100 µl Accutase® under an orbital shaker. The assembloid underwent mechanical dissociation into a single cell suspension with a 1000 µl pipette followed by a 200 µl pipette. The cell suspensions were washed twice with assay media or PBS. The assembloids were fixed and permeabilized with a BD Pharmingen™ Transcription Buffer Set. The cells were stained for neuronal markers: dopaminergic neurons (TH), neurons (MAP2). The samples were analyzed using flow cytometer BD LSR Fortessa ™.

Immunofluorescence staining

The assembloids were fixed overnight in 4% paraformaldehyde at RT and washed 3 × with PBS for 15 min. The assembloids were then embedded in 3% low melting point agarose (Biozym Scientific GmbH, 840100) and cut into 70 µm sections using Leica VT1000s vibratome. One assembloid was sliced into approximately 10–15 sections depending on the size. The sections were permeabilized in 0.5% Triton X-100 in PBS for 2 h. The samples were blocked with a mixture of 2.5% BSA and 2.5% donkey serum in PBS for 2 h at RT. The sections were then incubated for 48 h at 4 °C with primary antibodies diluted in blocking buffer. The sections were washed 3 × for 10 min with 0.01% Triton X-100 in PBS and incubated with secondary antibody for 2 h diluted in blocking buffer. The list of the primary and secondary antibodies is listed in Materials. The sections were washed 3 × for 10 min with 0.01% Triton X-100 in PBS, followed by one wash with H_2O. Finally, the sections were mounted on DBM Teflon® slides (De Beer Medicals, BM-9244) using Fluoromount-G® mounting media (Southern Biotech, 0100–01).

Image analysis

Image acquisition and analysis was done using the established pipeline in the group [23]. All sections of the assembloid (x, y and z fields) were acquired with a 20 × objective using Yokogawa CV8000 standalone high content screening confocal microscope and the Cell Voyager coupled with Wako software. Image quantification was done using in-housed MATLAB scripts, from two sections per organoid per cell line and from at least three independent assembloid derivations.

Data analysis and statistics

The data were analyzed using GraphPad Prism 10.1.2. A normality test was performed using the Shapiro test. If not stated otherwise, outlier removal was performed using the ROUT method Q 1% in GraphPad. For nonnormally distributed data, two-sided Wilcoxon test or Kruskal–Wallis with Dunn's multiple comparison test and Benjamini–Hochberg correction was implemented. For normally distributed data, Welch's t-test or one-way ANOVA with Tukey's multiple comparison test were performed. Significant P values are represented with asterisks in the order $P < 0.05$ *, $P < 0.01$ **, $P < 0.001$ ***, $P < 0.0001$ ****. The error bars represent mean ± SD.

Results

LRRK2-G2019S mutation does not affect iPSC-derived microglial differentiation and identity

In this study, we used iPSCs from four healthy individuals and four PD patients harboring the LRRK2-G2019S mutation (Table 1). Initially, embryoid bodies were formed from the iPSCs and cultured in a flask to produce macrophage precursors (Fig. 1A). These precursors were harvested and differentiated for 14 days to generate mature microglia, according to the previously established protocol [17, 24]. Healthy iPSC derived microglia expressed typical macrophage and microglial markers such as IBA1 and PU1 (Fig. 1B). After validating our robust microglial generation protocol, we compared microglia from healthy individuals and those with the LRRK-G2019S mutation.

Despite reports of LRRK2-related toxicity resulting in 10–70% cell death, other studies found no effect on cell viability [25]. In our system, we observed no differences in cell viability as assessed by flow cytometry (Fig. 1C), or total ATP levels using CellTiter-GLO® luminescence assay (Fig. 1D). Additionally, the presence of the LRRK2-G2019S mutation did not impact embryoid body formation or the yield of macrophage precursors (Figure S1A). Furthermore, morphological assessments via flow cytometry (FSC/SSC) revealed no differences in cell size or complexity between healthy and mutant microglia (Figure S1B).

Upon stimulation IL-34 and GM-CSF, macrophage precursors mature into microglial cells [24]. Mature microglia express markers, including general macrophage markers (CD11b, CD45, IBA1, PU1) as well as specific microglial markers (P2RY12, CX3CR1, and TMEM119) [26]. Both wild-type (WT) and LRRK2-G2019S microglia showed comparable expressions of these markers, as confirmed by immunofluorescence and flow cytometry (Fig. 1E-G, S1C). Together, these data indicate that the LRRK2-G2019S mutation does not alter the differentiation efficiency, identity, or basic morphology of iPSC-derived microglia.

LRRK2-G2019S microglia exhibit heightened immune activation and inflammatory phenotypes

Despite normal differentiation, LRRK2-G2019S microglia exhibit increased immune activation and

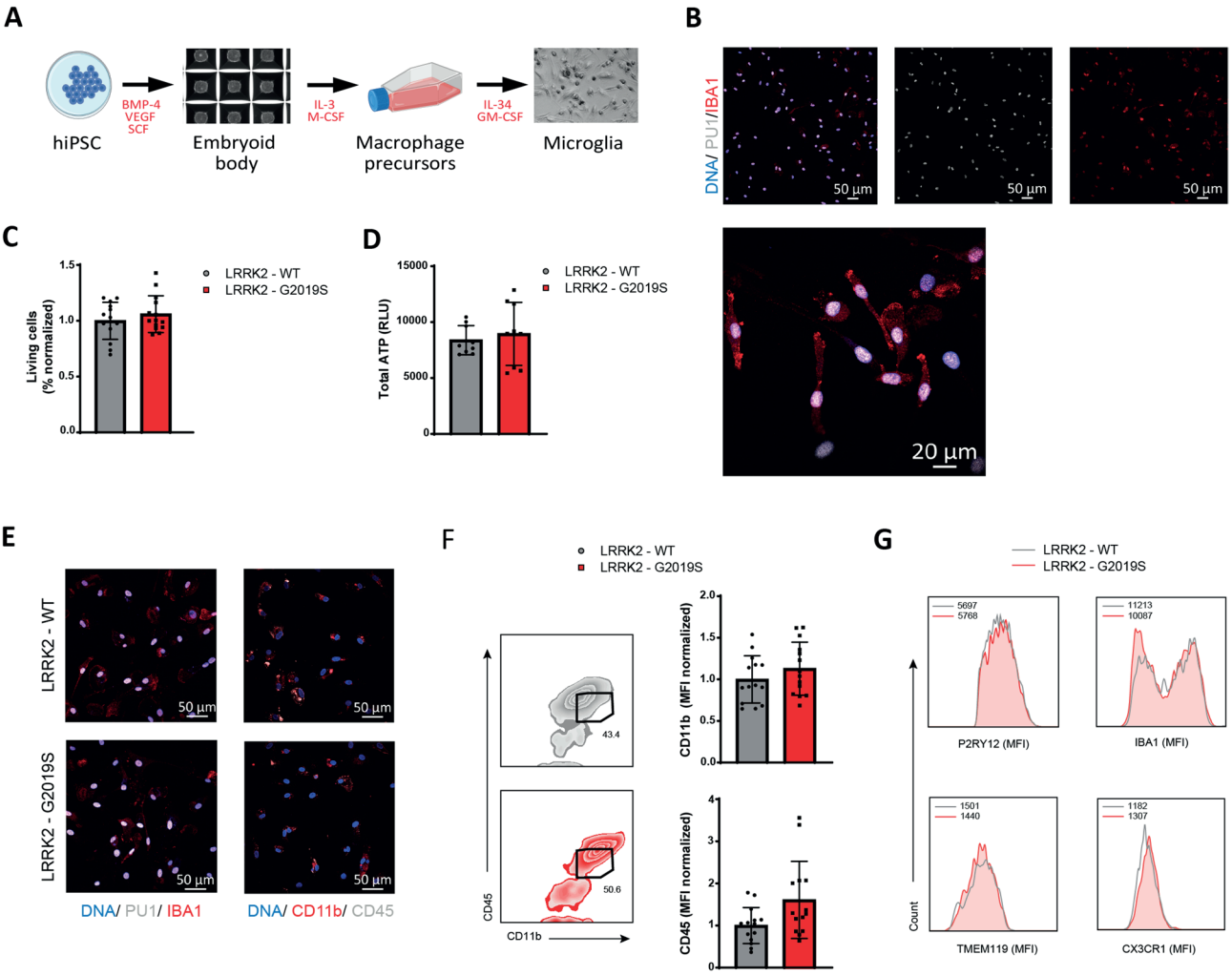

Fig. 1 Generation and characterization of iPSC-derived microglia identity show no alteration in microglia harboring the LRRK2-G2019S mutation. **A** Schematic representation of the generation of iPSC-derived microglia. **B** Representative immunostaining image of healthy iPSC-derived microglia with Hoechst, PU1, and IBA1. **C** Flow cytometry analysis of LRRK2-WT and LRRK2-G2019S microglia viability upon differentiation using the Zombie NIR™ Fixable viability kit. Data are shown as mean ± SD ($n = 3–4$), pooled from three independent trials **D** Luminescence-based quantification of cellular ATP levels in LRRK2-WT and LRRK2-G2019S microglia. Data are shown mean ± SD ($n = 3–4$), pooled from three independent trials. **E** Representative immunostaining images of LRRK2-WT and LRRK2-G2019S microglia with Hoechst, PU1, IBA1 (left) and Hoechst, CD11b, CD45 (right). **F** Flow cytometry analysis of mature microglia ($CD11b^{hi}CD45^{int}$) (left) and representative analysis of mean fluorescence intensity of CD11b and CD45 (right) in LRRK2-WT and LRRK2-G2019S microglia. Data are shown as mean ± SD ($n = 3–4$), pooled from three independent trials. **G**. Representative analysis of mean fluorescence intensity of microglia identity markers (P2RY12, IBA1, TMEM119, CX3CR1) in mature LRRK2-WT vs LRRK2-G2019S microglia using flow cytometry

proinflammatory properties. Previous studies have implicated LRRK2 polymorphisms in autoinflammatory diseases including inflammatory bowel disease (IBD), Crohn's disease, and tuberculosis, indicating a significant connection to immune functions [27]. Notably, increased expression of LRRK2 has been observed in immune cells in response to proinflammatory signals [28]. We therefore sought to determine the impact of LRRK2-G2019S mutation on microglial inflammatory functions in iPSC-derived microglia.

Flow cytometry analysis showed that CD68, a lysosomal protein indicative of phagocytic activity, was significantly upregulated in LRRK2-G2019S microglia compared to healthy controls (Fig. 2A). Markers associated with antigen presentation and costimulation, including HLA-DR, CD80 and CD86, were elevated in mutant microglia relative to that in control microglia (Fig. 2A). However, other activation markers such as CD69, CCR6, and the exhaustion marker PD-1 were unchanged (Figure S2A).

One of the key functions of microglia is the uptake of antigens for removal or presentation. Microglia possess several pathogen recognition receptors, namely Toll-like receptors (TLRs). TLR signaling and phagocytosis are hallmarks of the microglia-mediated immune response to infections [29]. The activation of TLR2 has been

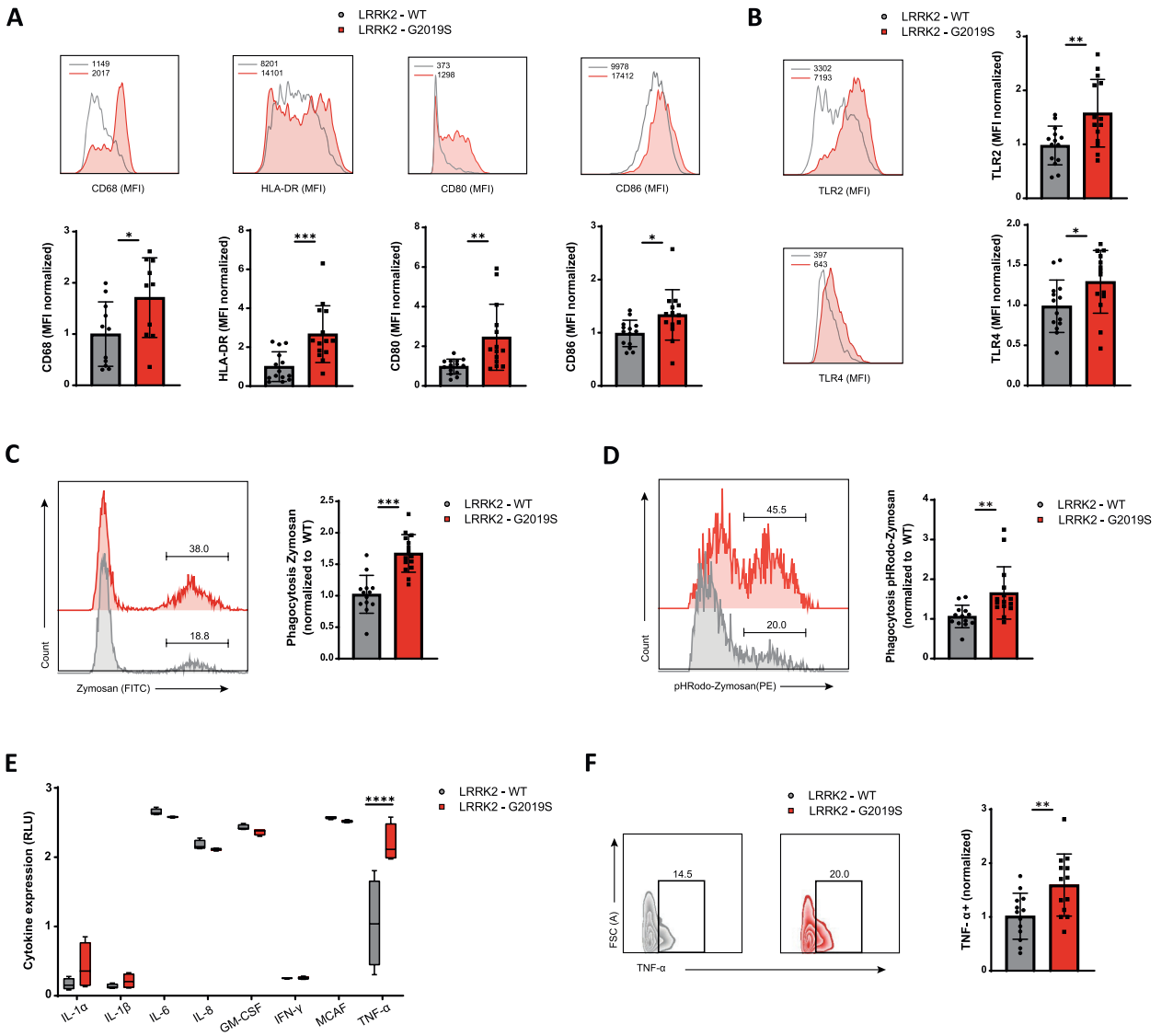

Fig. 2 Immunological phenotyping of LRRK2-G2019S microglia showed heightened activation and inflammatory profiles. **A** Representative analysis of mean fluorescence intensity (top) and the quantification (bottom) of activation markers (CD68, HLA-DR, CD80, and CD86) of LRRK2-WT and LRRK2-G2019S microglia. Data are shown as mean ± SD ($n = 3–4$), pooled from four independent trials. **B** Representative analysis of mean fluorescence intensity (left) and the quantification (right) of pathogen recognition receptors TLR2 and TLR4 in LRRK2-WT and LRRK2-G2019S microglia. Data are shown as mean ± SD ($n = 3–4$), pooled from four independent trials. **C** Flow cytometry analysis of microglia phagocytosis in LRRK2-WT and LRRK2-G2019S microglia using fluorescently labelled Zymosan beads. Representative images are shown on the left, quantification on the right. Data are shown as mean ± SD ($n = 3–4$), pooled from four independent trials. **D** Flow cytometry analysis of microglia phagocytosis in LRRK2-WT and LRRK2-G2019S microglia using pH-sensitive fluorescent Zymosan beads. Representative images are shown on the left, quantification on the right. Data are shown as mean ± SD ($n = 3–4$), pooled from four independent trials. **E** Enzyme-linked immunosorbent assay of human inflammatory cytokines in LRRK2-WT and LRRK2-G2019S microglia using the Human Inflammatory Cytokine Multiplex ELISA Kit from Arigo Biolaboratories. Data are shown as mean ± SD ($n = 4$), representative of two independent trials. **F** Flow cytometry analysis of intracellular TNF-α in LRRK2-WT and LRRK2-G2019S microglia upon 24 h stimulation with LPS. Representative images are shown on the left, quantification on the right. Data are shown as mean ± SD ($n = 3–4$), pooled from four independent trials. *$p < 0.05$, **$p < 0.01$, ***$p < 0.001$, ****$p < 0.0001$

associated with neuronal injury [30]. Our data revealed that LRRK2-G2019S microglia presented increased levels of both TLR2 and TLR4, suggesting a potential increase in phagocytic activity (Fig. 2B). To assess microglial phagocytosis, we used fluorescence labelled Zymosan, a TLR2 agonist derived from yeast. Following incubation and thorough washing to remove unbound particles, LRRK2-G2019S microglia showed significantly greater uptake of zymosan than healthy microglia did (Fig. 2C). Using a more advanced fluorescence Zymosan particle coupled with a pH-sensitive pHRodo, which fluoresces only when the particle is digested in the lysosome, we confirmed an increased phagocytic rate in LRRK2-G2019S microglia (Fig. 2D).

Another critical function of microglia is the production of cytokines. In response to environmental cues, microglia can produce a range of pro- and anti-inflammatory cytokines. Proinflammatory cytokines such as IL-1, IL-6, IFN, and TNF-α have been implicated in the pathogenesis of PD [31]. Our results indicated that various inflammatory cytokines were similarly expressed between healthy and LRRK2-G2019S microglia. However, upon LPS stimulation, LRRK2-G2019S microglia uniquely secreted higher levels of TNF-α into the culture media than the control microglia (Fig. 2E). This finding was corroborated by flow cytometry, which revealed significant upregulation of intracellular TNF-α in LRRK2-G2019S microglia (Fig. 2F, Figure S2B). Interestingly, other inflammatory cytokines were expressed at similar levels in both groups (Fig. 2E, Figure S2B). In summary, our data suggest that the LRRK2-G2019S mutation enhances the inflammatory activity and function of microglia, which is primarily mediated by increased TNF-α expression.

Transcriptomic profiling reveals altered inflammatory profiles and ROS metabolism in LRRK2-G2019S microglia

To gain a deeper understanding of the molecular changes induced by the LRRK2-G2019S mutation in microglia, we performed a bulk RNA sequencing analysis. We included four healthy controls and four iPSC-derived microglia carrying the LRRK2-G2019S mutation. The transcriptomic data identified over 970 genes whose expression significantly differed between control and mutant microglia (Fig. 3A, B). Pathway analysis revealed that several inflammatory signaling pathways were differentially regulated in LRRK2-G2019S microglia compared with healthy controls. Among these, TNF and IL-1 signaling, both of which are critical mediators of immune responses and inflammation, were notably altered (Fig. 3C).

Our transcriptomic analysis also revealed distinct alterations in genes related to microglial inflammatory processes such as phagocytosis and inflammation (Fig. 3C). Genes involved in pathogen recognition and phagocytosis including TLR2, TLR4, TLR8, TLR9, and TLR10 – exhibited altered expression in LRRK2-G2019S microglia. Similarly, the expression of ZAP70, a key molecule involved in immune synapse formation, was altered (Fig. 3D, Figure S3A). Additionally, genes involved in antigen presentation, such as HLA-DRB5, HLA-DOB, and CD209 (DC-SIGN) also displayed increased expression in mutant microglia (Fig. 3D, Figure S3A). These findings highlight the broad impact of the LRRK2-G2019S mutation on microglial profiles.

Given the observed upregulation of inflammatory markers at both the RNA and protein levels in LRRK2-G2019S microglia, we further investigated the underlying cellular mechanism contributing to this heightened immune response. Recent studies have emphasized the pivotal role of immune metabolism in regulating cell development, proliferation, and function. Immune cells dynamically rewire their metabolic preferences in response to environmental cues and functional demands. We hypothesized that the LRRK2-G2019S mutation might impair microglial metabolism, contributing to their abnormal immune function.

Enrichment analysis identified several altered pathways in LRRK2-G2019S microglia, many of which were related to metabolism *(Supplemental information* Table 1). Notably, pathways such as reactive oxygen species (ROS) metabolism and mammalian target of rapamycin complex 1 (mTORC1) signaling were enriched in mutant microglia (Fig. 3E). mTORC1, which plays a key role in regulating cellular metabolism and immune responses, has been implicated in microglial functions [32, 33]. Similarly, our data revealed that genes regulating mTORC1 activity, including TSC1, TSC2, and RPTOR, were differentially expressed in LRRK2-G2019S microglia (Fig. 3F).

To gain a more comprehensive view of the metabolic changes associated with the LRRK2-G2019S mutation, we constructed context-specific metabolic models by integrating the RNA sequencing data with the Recon3 generic human metabolic model, using the rFASTCORMICS pipeline [20]. This model predicted significant alterations in several metabolic pathways, including energy metabolism, sugar metabolism, amino acid metabolism, and lipid metabolism. Importantly, the mutant microglia exhibited unique metabolic reactions that were absent in the healthy controls (Figure S3B). Further analysis identified the most dysregulated metabolic subsystems in LRRK2-G2019S microglia. These included ROS metabolism (particularly glutathione metabolism), lipid metabolism and glycolysis, all of which play key roles in maintaining cellular homeostasis and responding to stress (Figure S3C). Dysregulation of these metabolic pathways is likely to contribute to the pathological phenotypes observed in LRRK2-G2019S microglia.

LRRK2-G2019S microglia upregulate glycolysis and downregulate glucose-derived serine synthesis

In our previous analysis, transcriptomic profiling and metabolic modelling showed changes in microglia harboring the LRRK2-G2019S mutation. mTOR plays a crucial role in integrating extracellular and intracellular signals to regulate cellular metabolism and growth [34]. Given the observed changes in metabolic homeostasis at the transcriptomic level, we next sought to determine the functional status of mTOR by measuring its phosphorylation using flow cytometry. Interestingly, the phosphorylation of mTOR was comparable in LRRK2-G2019S microglia (Figure S4A). However, we detected a significant increase in the expression of phosphorylated S6 (pS6), a key downstream target of mTORC1 in

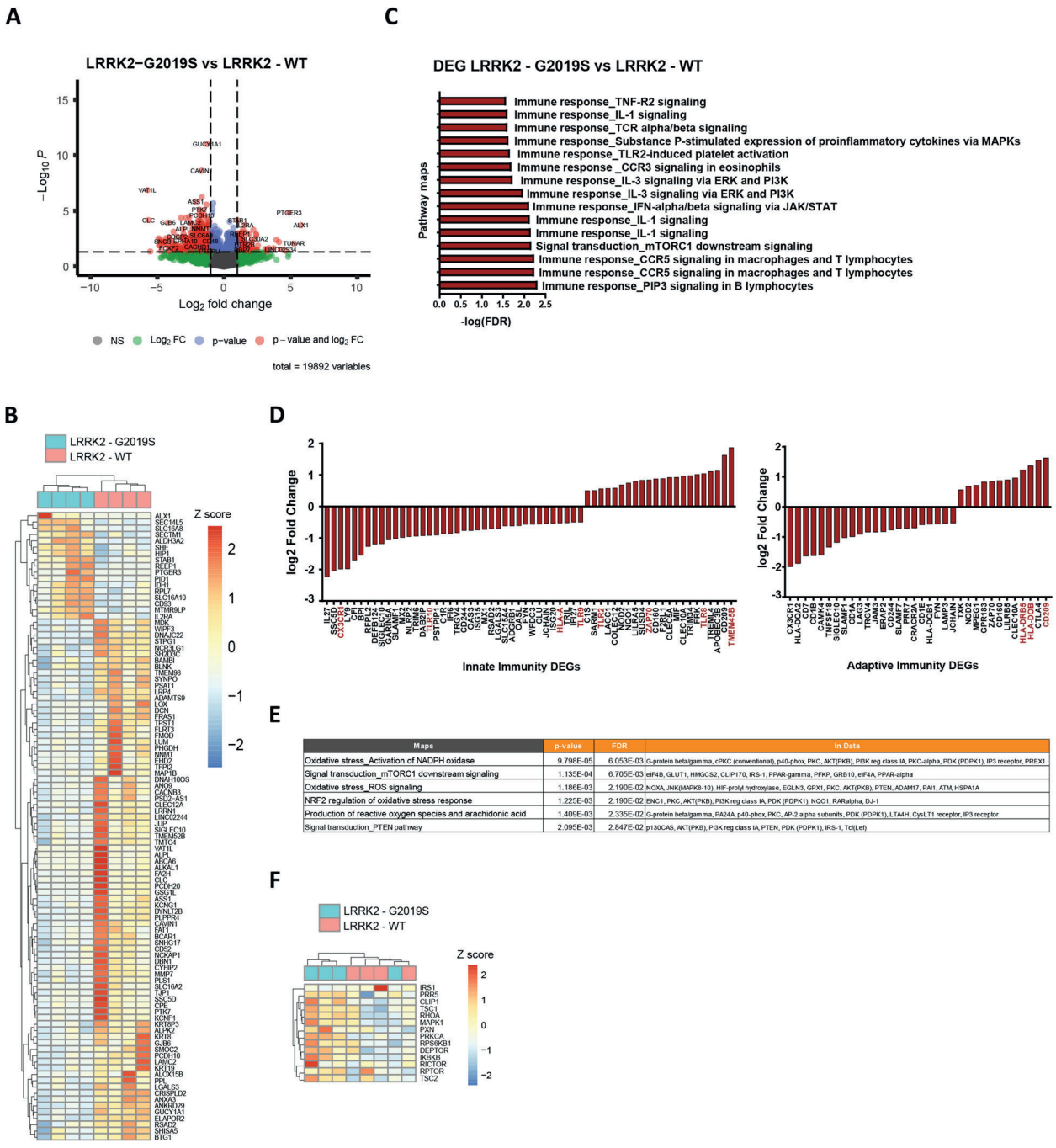

Maps	p-value	FDR	In Data
Oxidative stress_Activation of NADPH oxidase	9.798E-05	6.053E-03	G-protein beta/gamma, cPKC (conventional), p40-phox, PKC, AKT(PKB), PI3K reg class IA, PKC-alpha, PDK (PDPK1), IP3 receptor, PREX1
Signal transduction_mTORC1 downstream signaling	1.135E-04	6.705E-03	eIF4B, GLUT1, HMGCS2, CLIP170, IRS-1, PPAR-gamma, PFKP, GRB10, eIF4A, PPAR-alpha
Oxidative stress_ROS signaling	1.186E-03	2.190E-02	NOXA, JNK(MAPK8-10), HIF-prolyl hydroxylase, EGLN3, GPX1, PKC, AKT(PKB), PTEN, ADAM17, PAI1, ATM, HSPA1A
NRF2 regulation of oxidative stress response	1.225E-03	2.190E-02	ENC1, PKC, AKT(PKB), PI3K reg class IA, PDK (PDPK1), NQO1, RARalpha, DJ-1
Production of reactive oxygen species and arachidonic acid	1.409E-03	2.335E-02	G-protein beta/gamma, PA24A, p40-phox, PKC, AP-2 alpha subunits, PDK (PDPK1), LTA4H, CysLT1 receptor, IP3 receptor
Signal transduction_PTEN pathway	2.095E-03	2.847E-02	p130CAS, AKT(PKB), PI3K reg class IA, PTEN, PDK (PDPK1), IRS-1, Tcf(Lef)

Fig. 3 Transcriptomic profiling of LRRK2-G2019S microglia revealed more pro-inflammatory microglia phenotypes. **A** Volcano plot showing all genes with genes having $\log_2$FC > 1 and *p*-value < 0.05 highlighted, indicating differentially expressed genes between LRRK2-WT and LRRK2-G2019S microglia. **B** Top 50 differentially expressed genes (DEGs) between LRRK2-WT and LRRK2-G2019S microglia with the lowest *p* value. **C** Enrichment analysis using Metacore, showing top pathway maps involved in immunity. **D** Fold changes of genes from the GO term of innate and adaptive immunity with $\log_2$FC > 0.5. **E** Metacore enrichment analysis of pathways associated with cellular metabolism. **F** Heatmap of mTOR-regulated genes distinguishing LRRK2-WT from LRRK2-G2019S microglia upon hierarchical clustering

LRRK2-G2019S microglia compared with that in healthy controls (Fig. 4A).

Since mTORC1 signaling is known to regulate major metabolic pathways, such as mitochondrial respiration and glycolysis, the upregulation of mTORC1 in LRRK2-G2019S microglia could impact these processes. To assess mitochondrial function, we performed a mitochondrial stress test using Seahorse flux analysis. Although the spare respiratory capacity remained similar, the maximum respiration rate as well as proton leak was

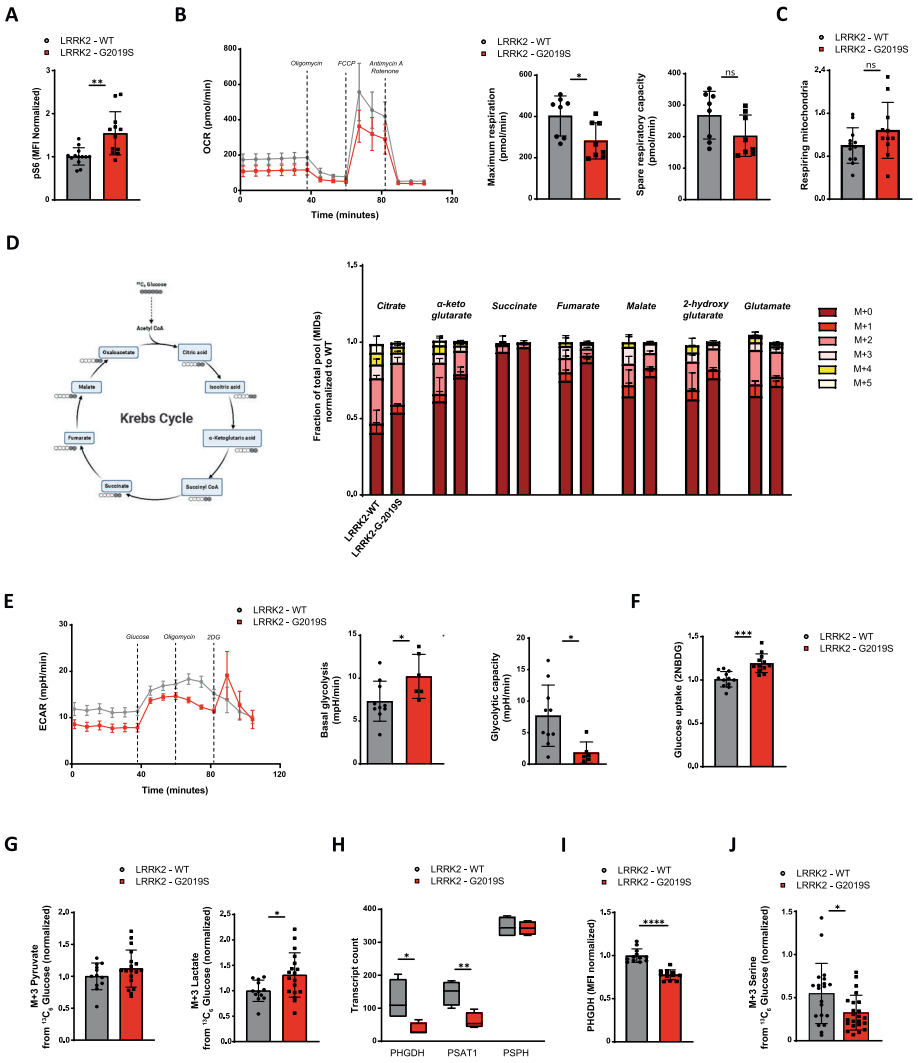

Fig. 4 Metabolic analysis indicated metabolic reprogramming in LRRK2-G2019S microglia. **A** Flow cytometry analysis of protein S6 phosphorylation in LRRK2-WT and LRRK2-G2019S microglia. Data are shown as mean ± SD ($n = 3–4$), pooled from four independent trials. **B** Measurement of oxygen consumption rate (OCR) in LRRK2-WT and LRRK2-G2019S microglia using the Seahorse Cell Mitochondrial Stress Test. Maximum respiration and spare respiratory capacity were quantified (right). Data are shown as mean ± SD ($n = 3–4$), representative from three independent trials. **C** Flow cytometry analysis of respiring mitochondria, calculated by the ratio between Mitotracker Deep Red™ (marking active mitochondria) and Mitotracker Green ™ (marking total mitochondria). Data are shown as mean ± SD ($n = 3–4$), pooled from four independent trials. **D** Flux map of carbon metabolism (left) and mass isotopomer distribution of TCA cycle metabolites in LRRK2-WT and LRRK2-G2019S microglia incubated with U-$^{13}C_6$-glucose during the final 24 h of differentiation. Data are shown as mean ± SD ($n = 3–4$), pooled from three independent trials. **E** Measurement of extracellular acidification rate (ECAR) in LRRK2-WT and LRRK2-G2019S microglia using Seahorse Glycolysis Stress Test. Basal glycolysis and glycolytic capacity were quantified (right). Data are shown as mean ± SD ($n = 3–4$), representative from three independent trials. **F** Flow cytometry analysis of glucose uptake rate in LRRK2-WT and LRRK2-G2019S microglia using fluorescent glucose 2-NBDG. Data are shown as mean ± SD ($n = 3–4$), pooled from four independent trials. **G** Mass isotopomer distribution of pyruvate (M + 3) and lactate (M + 3) in LRRK2-WT and LRRK2-G2019S microglia incubated with U-$^{13}C_6$-glucose during the final 24 h of differentiation. Data are shown as mean ± SD ($n = 3–4$), pooled from three independent trials. **H** Transcript count of serine synthesis genes PHGDH, PSAT1, and PSPH in LRRK2-WT and LRRK2-G2019S microglia. **I** Flow cytometry analysis of intracellular protein PHGDH in LRRK2-WT and LRRK2-G2019S microglia. Data are shown as mean ± SD ($n = 3–4$), pooled from four independent trials. **J** Mass isotopomer distribution of serine synthesis (M + 3) in LRRK2-WT and LRRK2-G2019S microglia incubated with U-.$^{13}C_6$-glucose during the final 24 h of differentiation. Data are shown as mean ± SD ($n = 3–4$), pooled from three independent trials. *$p < 0.05$, **$p < 0.01$, ***$p < 0.001$, ****$p < 0.0001$

significantly lower in LRRK2-G2019S microglia (Fig. 4B, SF4B).

Interestingly, the ratio of mitochondria with intact membrane potential (stained with MitoTracker DeepRed ™) to total mitochondrial mass (stained with MitoTracker Green™) was comparable between the mutant and control microglia, suggesting that mitochondrial quantity and membrane integrity were not compromised (Fig. 4C). Furthermore, the level of Ki-67 staining, a marker for cell proliferation, showed no differences

between LRRK2-G2019S and healthy microglia (Figure S4C). Similarly, total ROS levels, as assessed using H2-DCFDA probe (Figure S4D), as well as mitochondria ROS (data not shown), were also comparable between the two groups. Normal ROS levels suggest that LRRK2-G2019S microglia do not experience excessive oxidative stress, despite their heightened metabolism and immune activity. These results indicate that mitochondrial function is largely preserved in LRRK2-G2019S microglia, and that the reduced reliance on mitochondrial respiration suggests a shift toward alternative energy pathways to sustain microglial activity.

To further explore the altered metabolic flux in LRRK2-G2019S microglia, we performed metabolic tracing using uniformly labelled $^{13}C_6$ glucose. This approach allowed us to track the fate of glucose through various metabolic pathways. Pyruvate, the primary end product of glycolysis, can be used in the mitochondria to fuel the tricarboxylic acid (TCA) cycle. The mass isotopologue distribution (MID) showed no significant differences in the levels of TCA cycle intermediates – such as citrate, α-ketoglutarate, succinate, fumarate, and malate – between healthy and LRRK2-G2019S microglia (Fig. 4D). These findings align with the mitochondrial respiration results, further highlighting that the LRRK2-G2019S mutation does not significantly affect mitochondrial metabolism in microglia.

In resting immune cells, including microglia, energy production is typically reliant on mitochondrial metabolism; however, upon activation, these cells rewire their metabolism into glycolysis, a faster but less efficient metabolic pathway, to meet the increased energy demands [8]. Given the elevated immune activation in LRRK2-G2019S microglia, we suspected that glycolysis might be upregulated in these cells. To test this hypothesis, we performed a glycolytic stress test using Seahorse flux analysis. Indeed, basal glycolysis was elevated in LRRK2-G2019S microglia compared with healthy controls (Fig. 4E). However, their glycolytic capacity, defined as the maximum rate of glycolysis under stress conditions, was significantly reduced (Fig. 4E).

We further confirmed this metabolic shift by assessing glucose uptake using 2-NBDG, a fluorescent glucose analog. Compared with healthy microglia, LRRK2-G2019S microglia exhibited significantly greater glucose uptake (Fig. 4F). Instead of entering the TCA cycle, a significant portion of pyruvate generated from glycolysis was converted into lactate, as indicated by increased levels of M + 3 glucose-derived lactate (Fig. 4G). These data suggest that LRRK2-G2019S microglia undergo metabolic reprogramming and rely more on glycolysis to support their hyperactive immune function.

Glycolysis not only generates pyruvate but also produces intermediate metabolites that serve as precursors for other biosynthetic pathways. Specifically, 3-phosphoglycerate serves as a substrate for serine biosynthesis. Interestingly, two key genes involved in serine biosynthesis – PHGDH and PSAT1 – were significantly downregulated in LRRK2-G2019S microglia (Fig. 4H). PHGDH catalyzes the first and rate-limiting steps of serine synthesis. Flow cytometry confirmed a significant reduction in PHGDH expression in LRRK2-G2019S microglia compared with that in control microglia (Fig. 4I).

To further validate these findings, we traced the incorporation of glucose into serine using $^{13}C_6$ glucose. The results revealed significantly lower levels of M + 3 glucose-derived serine in LRRK2-G2019S microglia than in control microglia, indicating an impaired serine biosynthetic pathway (Fig. 4J). The reduction in serine production may reflect a compensatory shift to drive enhanced glycolysis due to the LRRK2-G2019S mutation, which needs to be further elaborated. In summary, our data show that LRKR2-G2019S microglia exhibit metabolic reprogramming, characterized by elevated glycolysis and impaired serine synthesis, which might be targeted to restore normal microglial functions in PD.

LRRK2-G2019S microglia induce degeneration of dopaminergic neurons in midbrain organoids

Neuroinflammation has been implicated in the progressive degeneration of dopaminergic neurons in PD [35, 36]. Here, we demonstrated that LRRK2-G2019S microglia upregulate immune activity, which is characterized by increased phagocytosis and elevated production of the proinflammatory cytokine TNF-α. Given the established role of neuroinflammation in neuronal injury, we sought to explore how microglial immune activation contributes to dopaminergic neuron loss, with a specific focus on the pathological effects of the LRRK2-G2019S mutation.

To do so, we used midbrain organoids derived from healthy individual iPSCs [23]. To simulate the inflammatory conditions associated with LRRK2-G2019S microglia, we treated these healthy midbrain organoids with exogenous TNF-α. This cytokine exposure led to a significant reduction in the number of dopaminergic neurons, by up to 30% compared with that in untreated controls (Fig. 5A). Interestingly, in the co-culture of organoids with LRRK2-G2019S microglia, TNF-α neutralizing antibody rescued dopaminergic neuron degeneration to the WT level (*SF4E*). This result suggests that inflammatory signaling alone is sufficient to induce neuronal injury, mimicking aspects of LRRK2-G2019S microglial inflammation in a TNF-α-dependent manner and that blocking TNF-α protect dopaminergic neurons.

To further capture the complexity of the brain's microenvironment and the contribution of microglia to dopaminergic neuron loss, we integrated iPSC-derived microglia into the midbrain organoids [17]. This

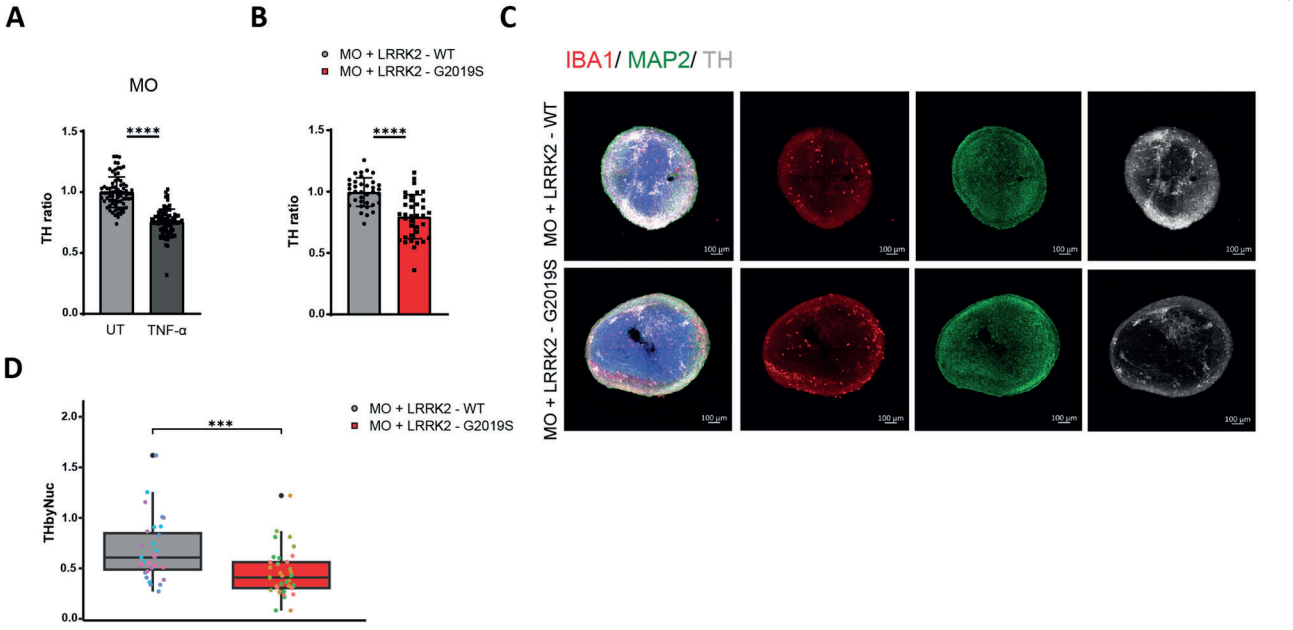

Fig. 5 LRRK2-G2019S microglia induced dopaminergic neuron degeneration in midbrain organoids. **A** The number of dopaminergic neurons, represented by the total TH + cells over total MAP2 + neurons, in midbrain organoids treated with or without 100 pg/ml TNF-α. Data are shown as mean ± SD ($n = 3$), pooled from three independent trials. **B** The number of dopaminergic neurons in midbrain organoids co-cultured with LRRK2-WT and LRRK2-G2019S microglia. Data are shown as mean ± SD ($N = 3$, $n = 4$), pooled from three independent trials. **C** Representative confocal image of a 70 µm midbrain organoids section with LRRK2-WT (top) or LRRK2-G2019S (bottom) microglia, immunostained with Hoechst, TH, MAP2, and IBA1. **D** High-content automated image analysis of immunofluorescence staining of dopaminergic neurons in assembloids (shown in C), expressed as the proportion of TH + cells normalized by total nuclei. Dotted color showed individual midbrain organoids. Data are shown as mean ± SD ($N = 3$, $n = 4$), pooled from three independent trials. $p < 0.05$, $^{**}p < 0.01$, $^{***}p < 0.001$, $^{****}p < 0.0001$

coculture approach allowed us to assess the direct effects of both healthy and LRRK2-G2019S mutant microglia on neuronal health and survival. Flow cytometry analysis showed that healthy midbrain organoids cocultured with LRRK2-G2019S microglia had significantly lower levels of tyrosine hydroxylase (TH) positive cells, the rate-limiting enzyme in dopamine synthesis and a surrogate marker of dopaminergic neurons. In contrast, organoids cocultured with healthy control microglia retained higher levels of TH, suggesting that the mutant microglia had a neurotoxic effect on dopaminergic neurons (Fig. 5B).

This trend was further confirmed by imaging analysis. Immunostaining of the organoids revealed that the incorporation of both healthy and LRRK2-G2019S microglia was comparable. The total number of MAP2 neurons in both organoids were comparable. In contrast, the number of TH positive dopaminergic neurons was significantly reduced in LRRK2-G2019S microglia containing midbrain organoids (Fig. 5C, D). These data demonstrate that neuroinflammation driven by LRRK2-G2019S microglia is associated with reduced dopaminergic neuron markers in co-cultured midbrain organoids. Elevated levels of TNF-α produced by the mutant microglia appear to play a central role in this neurotoxicity.

Oxamic acid reduces immune activity and attenuates dopaminergic neuron loss

The finding that midbrain organoids cocultured with LRRK2-G2019S microglia experienced significant dopaminergic neuronal loss (Fig. 5B, C), indicates that microglia-mediated neuroinflammation plays a central role in PD pathogenesis. These results underscore the potential of targeting microglia as a strategy for disease modification. Given that impaired serine biosynthesis results in increased levels of mTOR and glycolysis, we speculated that targeting the metabolic dysregulation could mitigate neuroinflammation and prevent dopaminergic neuron loss.

To address this hypothesis, we aimed to target the serine-mTOR-glycolysis axis. We used oxamic acid, a pyruvate analog that inhibits lactate dehydrogenase by forming an inactive complex with the enzyme [37, 38]. Oxamic acid-mediated inhibition of lactate dehydrogenase has been shown to reduce glycolysis and mTOR-dependent metabolic reprogramming in cancer cells [39, 40]. Here, we aimed to determine whether targeting glycolysis in LRRK2-G2019S microglia would alleviate their inflammatory toxicity and rescue TH neuronal levels.

As predicted, compared with no treatment, oxamic acid significantly reduced glucose uptake in LRRK2-G2019S mutant microglia (Fig. 6A). This effect was selective, as

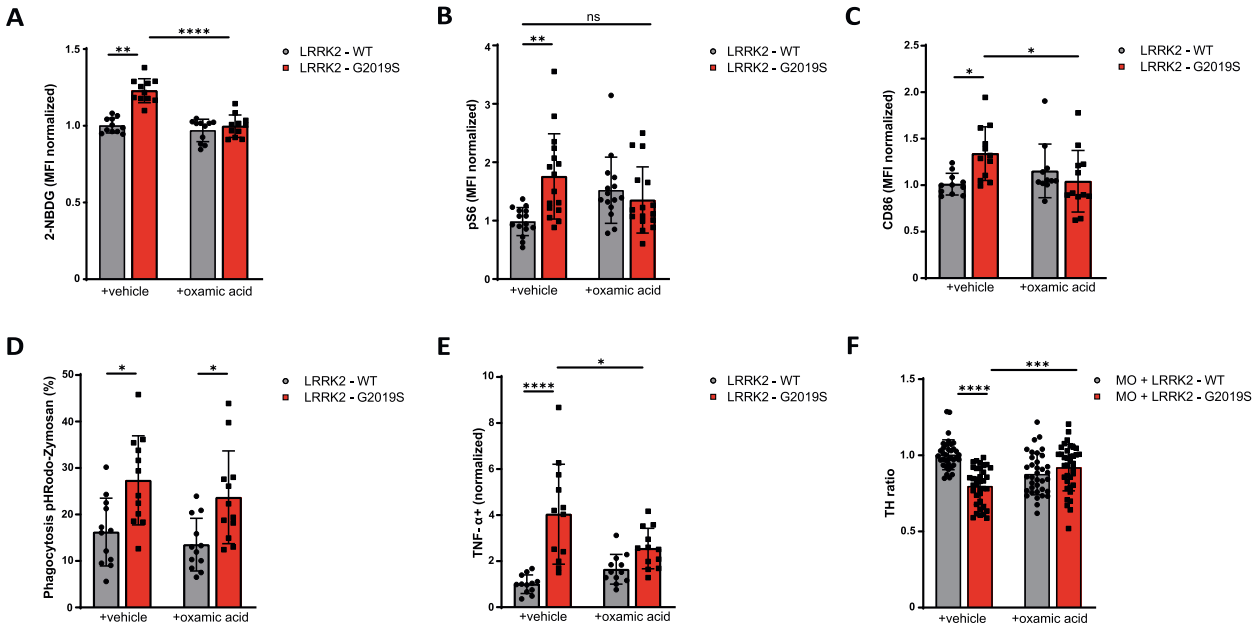

Fig. 6 Targeting microglia metabolism with oxamic acid rescued LRRK2-G2019S microglia overt activation and preserved dopaminergic neurons in midbrain organoids. **A** Flow cytometry analysis glucose uptake rate using fluorescent glucose 2-NBDG in LRRK2-WT and LRRK2-G2019S microglia treated with or without oxamic acid. Data are shown as mean ± SD ($n = 3–4$), pooled from three independent trials. **B** Flow cytometry analysis of protein S6 phosphorylation in LRRK2-WT and LRRK2-G2019S microglia treated with or without oxamic acid. Data are shown as mean ± SD ($n = 3–4$), pooled from three independent trials. **C** Flow cytometry analysis of CD86 in LRRK2-WT and LRRK2-G2019S microglia treated with or without oxamic acid. Data are shown as mean ± SD ($n = 3–4$), pooled from three independent trials. **D** Flow cytometry analysis of microglia phagocytosis using pH-sensitive fluorescently labelled Zymosan beads in LRRK2-WT and LRRK2-G2019S microglia treated with or without oxamic acid. Data are shown as mean ± SD ($n = 3–4$), pooled from three independent trials. **E** Flow cytometry analysis of intracellular TNF-α in LRRK2-WT and LRRK2-G2019S microglia treated with or without oxamic acid. Data are shown as mean ± SD ($n = 3–4$), pooled from three independent trials. **F** Number of dopaminergic neurons in midbrain organoids co-cultured with LRRK2-WT and LRRK2-G2019S microglia treated with or without oxamic acid. Data are shown as mean ± SD ($N = 3$, $n = 4$), pooled from three independent trials

glucose uptake in healthy microglia remained unaffected by the treatment, suggesting that oxamic acid specifically targets hyperactive glycolysis in LRRK2-G2019S microglia. Additionally, the elevated levels of pS6 in LRRK2-G2019S microglia were normalized to the control level upon treatment with oxamic acid (Fig. 6B).

Next, we examined whether oxamic acid attenuate LRRK2-G2019S microglia immune hyperactivity. Flow cytometry analysis showed a significant reduction in the expression of the costimulatory molecules CD86 in LRRK2-G2019S microglia following oxamic acid treatment (Fig. 6C). Interestingly, while the inflammatory markers were suppressed, oxamic acid treatment did not affect the phagocytic capacity of LRRK2-G2019S microglia (Fig. 6D). However, the levels of the inflammatory cytokine TNF-α were significantly reduced in LRRK2-G2019S microglia than in the untreated microglia (Fig. 6E). These findings confirm that targeting microglial metabolism can alter the course of immune activation, possibly mitigating the toxic effect of LRRK2-G2019S microglia on dopaminergic neurons.

Finally, to determine whether the rescue of metabolic and inflammatory phenotypes in LRRK2-G2019S microglia has a neuroprotective effect, we assessed dopaminergic neuron survival in midbrain organoids cocultured with microglia and treated with or without oxamic acid. Compared with organoids cultured with healthy microglia, midbrain organoids cultured with LRRK2-G2019S microglia showed significant dopaminergic neuron loss (Fig. 6F). However, treatment with oxamic acid substantially increased the number of dopaminergic neurons in midbrain organoids cultured with LRRK2-G2019S microglia, ameliorating the detrimental impact of LRRK2-G2019S microglia. These data indicate that targeting microglia metabolism in LRRK2-G2019S microglia not only reduces their inflammatory phenotype but also prevents neurotoxicity, demonstrating the potential of immunometabolic approaches that may slow neurodegeneration, pending further validation.

Discussion

The G2019S mutation in LRRK2 represents one of the most common causes of familial PD [41]. LRRK2 regulates a variety of cellular functions, including mitochondrial function, vesicle trafficking, autophagy, cell growth, differentiation, and metabolism [27]. Despite extensive research, the exact mechanism by which LRRK2 contributes to PD pathogenesis remains unclear. Notably,

neuroinflammation has emerged as an important characteristic of PD. LRRK2 is also highly expressed in various immune cells, where its expression correlates with immune activity, suggesting a potential role in neuroinflammation and neurodegeneration associated with PD.

This study investigated the impact of the LRRK2-G2019S mutation on microglial function in human iPSCs-derived models. Specifically, we employed in vitro midbrain organoids to evaluate the effects of LRRK2-G2019S microglia on dopaminergic neuron integrity and PD pathogenesis. While previous studies have shown altered microglial activity in both murine and human iPSC-derived microglia [42–44], details on the molecular mechanism driving this altered activity are limited. In particular, the interaction between LRRK2-G2019S microglia and dopaminergic neurons in a representative brain organoid model has been underexplored.

Our results demonstrated for the first time that LRRK2-G2019S mutant microglia exhibit increased proinflammatory activities, which are associated with changes in their cellular metabolism. Proinflammatory microglia induces neurotoxicity and dopaminergic neuron loss in midbrain organoids. Importantly, restoring microglial function by targeting metabolic pathways prevents dopaminergic neuronal loss, suggesting a potential therapeutic avenue.

Our findings reveal that iPSC-derived microglia with the LRRK2-G2019S mutation exhibit increased expression of inflammatory markers and altered function, without changes in their differentiation or identity. Previous studies have indicated that LRRK2 expression increases upon stimulation with the TLR ligand LPS in bone marrow-derived macrophages and primary murine microglia [44, 45]. LRRK2 mutations in PD have also been shown to exacerbate inflammatory responses [46], while the loss of LRRK2 has been associated with decreased proinflammatory signaling and neuroprotective effects against LPS and α-synuclein-induced neurodegeneration [47]. TLR-driven neuroinflammation is linked to dopaminergic neuron loss in PD, and TLR modulation has been shown to reduce inflammation and improve PD symptoms [48]. Murine and human models harboring LRRK2 mutations resulted in significant increases in the levels of proinflammatory cytokines such as IFN-γ, TNF-α, IL-1α, IL-1β, IL-6, IL-8, IL-10, and CXCL-1, among many others [49, 50]. Interestingly, we observed exclusively the upregulation of TNF-α in microglia harboring LRRK2-G2019S mutation. TNFα is not only a key regulator of inflammatory responses, but also in certain circumstances can cause cell death by apoptosis and necroptosis [51]. In the CNS, TNFα is linked to neuronal loss, which is mediated by microglial phagocytosis, as well as neuronal necroptosis [52, 53], possibly a key driver of dopaminergic neuron degeneration in PD.

Pathway analysis highlighted altered ROS metabolism, the NRF2 antioxidant pathway, and mTOR signaling in LRRK2-G2019S microglia. Changes in ROS-associated pathways could be due to compensatory mechanism, as elevated metabolism will produce higher ROS levels, which need to be buffered in LRRK2-G2019S microglia. This is also reflected by unchanged cytoplasmic ROS nor mitochondrial ROS in LRRK2-G2019S microglia compared to WT microglia. Context-specific metabolic models predicted metabolic remodeling in these mutant microglia, linking immune dysfunction to cellular metabolic changes. Dysregulated metabolic pathways in immune cells contribute to a wide range of diseases from autoinflammatory diseases to cancers [10, 54, 55]. Altered metabolism likely drives increased inflammatory activity in LRRK2-G2019S microglia, a mechanism implicated in various diseases.

Our data showed mTOR upregulation in LRRK2-G2019S microglia. mTOR senses the intra- and extracellular nutrient status, growth factor, and cell stress-related changes to coordinate cellular metabolism and balance immunological functions [56, 57]. Cheng et al. demonstrated that glycolytic reprogramming controls microglial inflammatory activation, and that glycolysis inhibition reduces NF-κB transcriptional activity and neuroinflammation [58]. We observed upregulated mTOR shifted LRRK2-G2019S microglial metabolism toward glycolysis, driving microglial inflammation. In fact, on adipocytes, LRRK2 substrates RAB10 has been shown as a downstream target of AS160 and a positive regulator of GLUT4 trafficking to the cell surface upon insulin stimulation, where RAB10 knockdown led to twofold decrease in GLUT4 exocytosis rate [59]. Moreover, Panagiotakopoulou et al., also showed that LRRK2-G2019S mutation led to changes in cytokine production and glycolytic switch in NFAT-independent manner, further highlighting the close relation between LRRK2, microglia inflammation and metabolic remodeling [60].

We noted impaired serine synthesis in LRRK2-G2019S microglia with reduced expression of the key genes PHGDH and PSAT1. In addition, metabolic tracing of labelled $^{13}C_6$ glucose confirmed decreased glucose-derived serine in LRRK2-G2019S microglia. Serine is a nonessential amino acid that play diverse physiological functions, including one carbon metabolism for nucleotide synthesis and epigenetic modification, as well as redox balance [61, 62]. Previously, serine deprivation was shown to impair mTOR signaling, IL-1β secretion and inflammasome activation [63]. In fact, altered serine metabolism between the conversion of L and D serine by serine racemase enzyme has also been explored in neuroepithelial stem cells harboring LRRK2-G2019S mutation [64]. Interestingly, LRRK2-G2019S microglia showed increased mTOR activity, shifting toward glycolysis, and

heightened immune activation. This metabolic adaptation may exacerbate neuroinflammation and impair dopaminergic neuron health.

In 3D midbrain organoid models, the addition of LRRK2-G2019S microglia led to dopaminergic neuron loss compared with that in midbrain organoids with healthy microglia, highlighting the neurotoxic effect of LRRK2-G2019S mutant microglia on dopaminergic neurons. Treating these microglia with oxamic acid, a known mTOR and glycolysis inhibitor [39, 40], normalized their metabolism, reduced inflammation, and preserved their phagocytic function. Phagocytosis is known to be beneficial for clearing cellular debris and protein aggregates, thereby protecting the CNS microenvironment and neurons from stress [65]. The uncoupling of phagocytosis and inflammation by oxamic acid undoubtedly adds an extra dimension in ensuring normal cellular clearance and inflammatory activity by microglia. Oxamic acid notably lowered TNF-α levels, thus preventing dopaminergic neuronal loss in organoid models with LRRK2-G2019S microglia. These findings suggest inhibiting glucose metabolism in LRRK2-G2019S microglia could mitigate their TNF-α dependent neurotoxic effects on dopaminergic neurons, demonstrating its neuroprotective potential.

In summary, this study provides new insights into the role of the LRRK2-G2019S mutation in modulating microglial function and PD pathogenesis. LRRK2 mutations promote immune hyperactivation and metabolic alterations, contributing to neuroinflammation and dopaminergic neuronal degeneration in healthy midbrain organoids. Targeting microglial metabolism with oxamic acid reduces TNF-α-dependent neuroinflammation while maintaining normal phagocytic function, underscoring the ideal therapeutic potential for disease-modifying strategies in PD.

Limitations

While our study provides novel insight into how LRRK2-G2019S microglia contribute to dopaminergic neuron degeneration through metabolic changes and inflammatory activation, several limitations should be considered. First, although we identified associations between glycolytic rewiring, impaired serine metabolism, increased inflammation, and neuronal vulnerability, our study does not establish direct causality between these processes. Whether metabolic reprogramming is the primary driver of inflammatory activation or a parallel consequence of LRRK2-G2019S signaling remains to be explored. Second, the altered pathways we identified such as ROS and mTOR signaling, may represent secondary or compensatory responses to the mutation rather than primary pathogenic mechanisms. Dissecting the temporal sequence of these changes will require more targeted perturbation or gene editing studies. Third, our analyses centered primarily on glycolysis and serine metabolism, but microglia also utilize broad metabolic networks including glutamine or lipid metabolism, which may also shape inflammatory phenotypes in LRRK2-G2019S context. A more comprehensive metabolic profiling, including isotope tracing and lipidomics, will be essential to fully capture the extent of metabolic vulnerabilities.

Moreover, while oxamic acid treatment was able to rescue aberrant microglial phenotypes and dopaminergic neuron loss in midbrain organoid, its off-target effects and translational feasibility remain to be validated in animal models. Thus, future studies employing alternative and more selective metabolic modulators will be required to confirm specificity and translational potential. Despite these limitations, our findings advance understanding of how LRRK2-G2019S mutations alter microglial metabolism and inflammatory response, and they underscore the potential of targeting immunometabolic pathways as a therapeutic avenue in PD.

Supplementary Information

The online version contains supplementary material available at https://doi.org/10.1186/s12974-025-03577-2.

Supplementary material 1.

Acknowledgements

We thank C. Jager and the metabolomics and lipidomics platform members of the Luxembourg Centre for Systems Biomedicine for metabolomic analyses. We thank Novogene Europe for RNA sequencing.

Authors' contributions

H.K.: study conception, experiment and data generation, analysis, and manuscript writing. S.L.N., E.G.: RNAseq data analysis. A.Z.: metabolic model generation and analysis. E.Z.: data generation. J.C.S: project supervision.

Funding

The study is supported by the Luxembourg National Research Fund (FNR) (INTER/FWF/19/14117540/PDage). EG is funded by the Luxembourg National Research Fund (FNR) as part of the projects RECAST (INTER/22/17104370/RECAST) and PreDYT (INTER/EJPRD22l1/7027921/PreDYT).

Data availability

All original and processed data as well as the scripts generated from the study are publicly available under this DOI: 10.17881/b3yf-xt27 **.** The bulk RNAseq gene expression dataset generated for this manuscript can be accessed in the Gene Expression Omnibus database under the identifier GSE282494.

Declarations

Ethics approval and consent to partipate

All work with human stem cells was done after the approval of the national ethics board, Comité National d'Ethique de Recherche (CNER), under the approval numbers 201305/04 and 201901/0.

Competing interests
The author J.C.S. declare no competing nonfinancial interests but declare competing financial interests as cofounders and shareholders of OrganoTherapeutics société à responsabilité limitée (SARL). The remaining authors declare no competing interests.

Received: 2 January 2025 / Accepted: 29 September 2025
Published online: 27 October 2025

References

1. Ou Z, et al. Global trends in the incidence, prevalence, and years lived with disability of Parkinson's disease in 204 countries/territories from 1990 to 2019. Front Public Health. 2021;9:776847.
2. Antony PM, et al. The hallmarks of Parkinson's disease. FEBS J. 2013;280(23):5981–93.
3. Gelders G, Baekelandt V, Van der Perren A. Linking neuroinflammation and neurodegeneration in Parkinson's disease. J Immunol Res. 2018;2018:4784268.
4. Park DS, et al. iPS-cell-derived microglia promote brain organoid maturation via cholesterol transfer. Nature. 2023;623(7986):397–405.
5. Lee HJ, et al. Clearance and deposition of extracellular alpha-synuclein aggregates in microglia. Biochem Biophys Res Commun. 2008;372(3):423–8.
6. Wang Y, et al. LRRK2-NFATc2 pathway associated with neuroinflammation may be a potential therapeutic target for Parkinson's disease. J Inflamm Res. 2021;14:2583–6.
7. Scheiblich H, et al. Microglia jointly degrade fibrillar alpha-synuclein cargo by distribution through tunneling nanotubes. Cell. 2021;184(20):5089-5106 e21.
8. Lauro C, Limatola C. Metabolic reprograming of microglia in the regulation of the innate inflammatory response. Front Immunol. 2020;11:493.
9. Chi H. Immunometabolism at the intersection of metabolic signaling, cell fate, and systems immunology. Cell Mol Immunol. 2022;19(3):299–302.
10. Kurniawan H, Soriano-Baguet L, Brenner D. Regulatory t cell metabolism at the intersection between autoimmune diseases and cancer. Eur J Immunol. 2020;50(11):1626–42.
11. Pan S, et al. Serine, glycine and one-carbon metabolism in cancer (Review). Int J Oncol. 2021;58(2):158–70.
12. Churchward MA, Tchir DR, Todd KG. Microglial function during glucose deprivation: inflammatory and neuropsychiatric implications. Mol Neurobiol. 2018;55(2):1477–87.
13. Sangineto M, et al. Metabolic reprogramming in inflammatory microglia indicates a potential way of targeting inflammation in Alzheimer's disease. Redox Biol. 2023;66:102846.
14. Sabogal-Guaqueta AM, et al. Species-specific metabolic reprogramming in human and mouse microglia during inflammatory pathway induction. Nat Commun. 2023;14(1):6454.
15. Reinhardt P, et al. Genetic correction of a LRRK2 mutation in human iPSCs links parkinsonian neurodegeneration to ERK-dependent changes in gene expression. Cell Stem Cell. 2013;12(3):354–67.
16. van Wilgenburg B, et al. Efficient, long term production of monocyte-derived macrophages from human pluripotent stem cells under partly-defined and fully-defined conditions. PLoS ONE. 2013;8(8):e71098.
17. Sabate-Soler, S., et al., Microglia integration into human midbrain organoids leads to increased neuronal maturation and functionality. Glia, 2022.
18. Battello N, et al. The role of HIF-1 in oncostatin M-dependent metabolic reprogramming of hepatic cells. Cancer Metab. 2016;4:3.
19. Love MI, Huber W, Anders S. Moderated estimation of fold change and dispersion for RNA-seq data with DESeq2. Genome Biol. 2014;15(12):550.
20. Brunk E, et al. Recon3d enables a three-dimensional view of gene variation in human metabolism. Nat Biotechnol. 2018;36(3):272–81.
21. Pacheco MP, et al. Identifying and targeting cancer-specific metabolism with network-based drug target prediction. EBioMedicine. 2019;43:98–106.
22. Heirendt L, et al. Creation and analysis of biochemical constraint-based models using the COBRA Toolbox v.3.0. Nat Protoc. 2019;14(3):639–702.
23. Monzel AS, et al. Derivation of human midbrain-specific organoids from neuroepithelial stem cells. Stem Cell Reports. 2017;8(5):1144–54.
24. Haenseler W, et al. A highly efficient human pluripotent stem cell microglia model displays a neuronal-co-culture-specific expression profile and inflammatory response. Stem Cell Rep. 2017;8(6):1727–42.
25. Lobbestael E, et al. Pathogenic LRRK2 requires secondary factors to induce cellular toxicity. Biosci Rep, 2020. 40(10).
26. Jurga AM, Paleczna M, Kuter KZ. Overview of general and discriminating markers of differential microglia phenotypes. Front Cell Neurosci. 2020;14:198.
27. Wallings RL, Tansey MG. LRRK2 regulation of immune-pathways and inflammatory disease. Biochem Soc Trans. 2019;47(6):1581–95.
28. Cook DA, et al. *LRRK2* levels in immune cells are increased in Parkinson's disease. NPJ Parkinsons Dis. 2017;3:11.
29. Doyle SE, et al. Toll-like receptors induce a phagocytic gene program through p38. J Exp Med. 2004;199(1):81–90.
30. Lehnardt S, et al. Activation of innate immunity in the CNS triggers neurodegeneration through a toll-like receptor 4-dependent pathway. Proc Natl Acad Sci U S A. 2003;100(14):8514–9.
31. Dzamko N. Cytokine activity in Parkinson's disease. Neuronal Signal. 2023;7(4):NS20220063.
32. Keane L, et al. mTOR-dependent translation amplifies microglia priming in aging mice. J Clin Invest. 2021;131(1).
33. Shi Q, et al. Microglial mTOR activation upregulates Trem2 and enhances beta-amyloid plaque clearance in the 5XFAD Alzheimer's disease model. J Neurosci. 2022;42(27):5294–313.
34. Laplante M, Sabatini DM. mTOR signaling at a glance. J Cell Sci. 2009;122(Pt 20):3589–94.
35. Wang Q, Liu Y, Zhou J. Neuroinflammation in Parkinson's disease and its potential as therapeutic target. Transl Neurodegener. 2015;4:19.
36. Tansey MG, Goldberg MS. Neuroinflammation in Parkinson's disease: its role in neuronal death and implications for therapeutic intervention. Neurobiol Dis. 2010;37(3):510–8.
37. Rodriguez-Paez L, et al. Oxamic acid analogues as LDH-C4-specific competitive inhibitors. J Enzyme Inhib Med Chem. 2011;26(4):579–86.
38. Altinoz MA, Ozpinar A. Oxamate targeting aggressive cancers with special emphasis to brain tumors. Biomed Pharmacother. 2022;147:112686.
39. Zhao Z, et al. Oxamate-mediated inhibition of lactate dehydrogenase induces protective autophagy in gastric cancer cells: involvement of the Akt–mTOR signaling pathway. Cancer Lett. 2015;358(1):17–26.
40. Fiume L, et al. Inhibition of lactic dehydrogenase as a way to increase the anti-proliferative effect of multi-targeted kinase inhibitors. Pharmacol Res. 2011;63(4):328–34.
41. Zimprich A, et al. Mutations in *LRRK2* cause autosomal-dominant parkinsonism with pleomorphic pathology. Neuron. 2004;44(4):601–7.
42. Yadavalli N, Ferguson SM. LRRK2 suppresses lysosome degradative activity in macrophages and microglia through MiT-TFE transcription factor inhibition. Proc Natl Acad Sci U S A. 2023;120(31):e2303789120.
43. Kim C, et al. LRRK2 mediates microglial neurotoxicity via NFATc2 in rodent models of synucleinopathies. Sci Transl Med, 2020. 12(565).
44. Moehle MS, et al. LRRK2 inhibition attenuates microglial inflammatory responses. J Neurosci. 2012;32(5):1602–11.
45. Hakimi M, et al. Parkinson's disease-linked LRRK2 is expressed in circulating and tissue immune cells and upregulated following recognition of microbial structures. J Neural Transm (Vienna). 2011;118(5):795–808.
46. Gillardon F, Schmid R, Draheim H. Parkinson's disease-linked leucine-rich repeat kinase 2(R1441G) mutation increases proinflammatory cytokine release from activated primary microglial cells and resultant neurotoxicity. Neuroscience. 2012;208:41–8.
47. Daher JP, et al. Abrogation of alpha-synuclein-mediated dopaminergic neurodegeneration in LRRK2-deficient rats. Proc Natl Acad Sci U S A. 2014;111(25):9289–94.
48. Heidari A, Yazdanpanah N, Rezaei N. The role of toll-like receptors and neuroinflammation in Parkinson's disease. J Neuroinflammation. 2022;19(1):135.
49. Dzamko N, Rowe DB, Halliday GM. Increased peripheral inflammation in asymptomatic leucine-rich repeat kinase 2 mutation carriers. Mov Disord. 2016;31(6):889–97.
50. Kozina E, et al. Mutant LRRK2 mediates peripheral and central immune responses leading to neurodegeneration in vivo. Brain. 2018;141(6):1753–69.
51. Brenner D, Blaser H, Mak TW. Regulation of tumour necrosis factor signalling: live or let die. Nat Rev Immunol. 2015;15(6):362–74.
52. Jayaraman A, et al. TNF-mediated neuroinflammation is linked to neuronal necroptosis in Alzheimer's disease hippocampus. Acta Neuropathol Commun. 2021;9(1):159.
53. Neniskyte U, Vilalta A, Brown GC. Tumour necrosis factor alpha-induced neuronal loss is mediated by microglial phagocytosis. FEBS Lett. 2014;588(17):2952–6.
54. Kurniawan H, et al. Glutathione restricts serine metabolism to preserve regulatory T cell function. Cell Metab. 2020;31(5):920-936 e7.

55. Teng X, et al. Metabolic regulation of pathogenic autoimmunity: therapeutic targeting. Curr Opin Immunol. 2019;61:10–6.
56. Braun C, Weichhart T. Mtor-dependent immunometabolism as Achilles' heel of anticancer therapy. Eur J Immunol. 2021;51(12):3161–75.
57. Hu Y, et al. mTOR-mediated metabolic reprogramming shapes distinct microglia functions in response to lipopolysaccharide and ATP. Glia. 2020;68(5):1031–45.
58. Cheng J, et al. Early glycolytic reprogramming controls microglial inflammatory activation. J Neuroinflammation. 2021;18(1):129.
59. Sano H, et al. Rab10, a target of the AS160 Rab GAP, is required for insulin-stimulated translocation of GLUT4 to the adipocyte plasma membrane. Cell Metab. 2007;5(4):293–303.
60. Panagiotakopoulou V, et al. Interferon-gamma signaling synergizes with LRRK2 in neurons and microglia derived from human induced pluripotent stem cells. Nat Commun. 2020;11(1):5163.
61. Zeng JD, et al. Serine and one-carbon metabolism, a bridge that links mTOR signaling and DNA methylation in cancer. Pharmacol Res. 2019;149:104352.
62. Kurniawan H, Kobayashi T, Brenner D. The emerging role of one-carbon metabolism in T cells. Curr Opin Biotechnol. 2021;68:193–201.
63. Chen S, et al. Serine supports IL-1beta production in macrophages through mTOR signaling. Front Immunol. 2020;11:1866.
64. Nickels SL, et al. Impaired serine metabolism complements LRRK2-G2019S pathogenicity in PD patients. Parkinsonism Relat Disord. 2019;67:48–55.
65. Lim J, Yue Z. Neuronal aggregates: formation, clearance, and spreading. Dev Cell. 2015;32(4):491–501.

Publisher's Note

Supplementary Information

The Parkinson's disease-associated LRRK2-G2019S variant restricts serine metabolism, leading to microglial inflammation and dopaminergic neuron degeneration

Henry Kurniawan, Sarah L. Nickels, Alise Zagare, Elisa Zuccoli, Isabel Rosety, Enrico Glaab, Jens C. Schwamborn

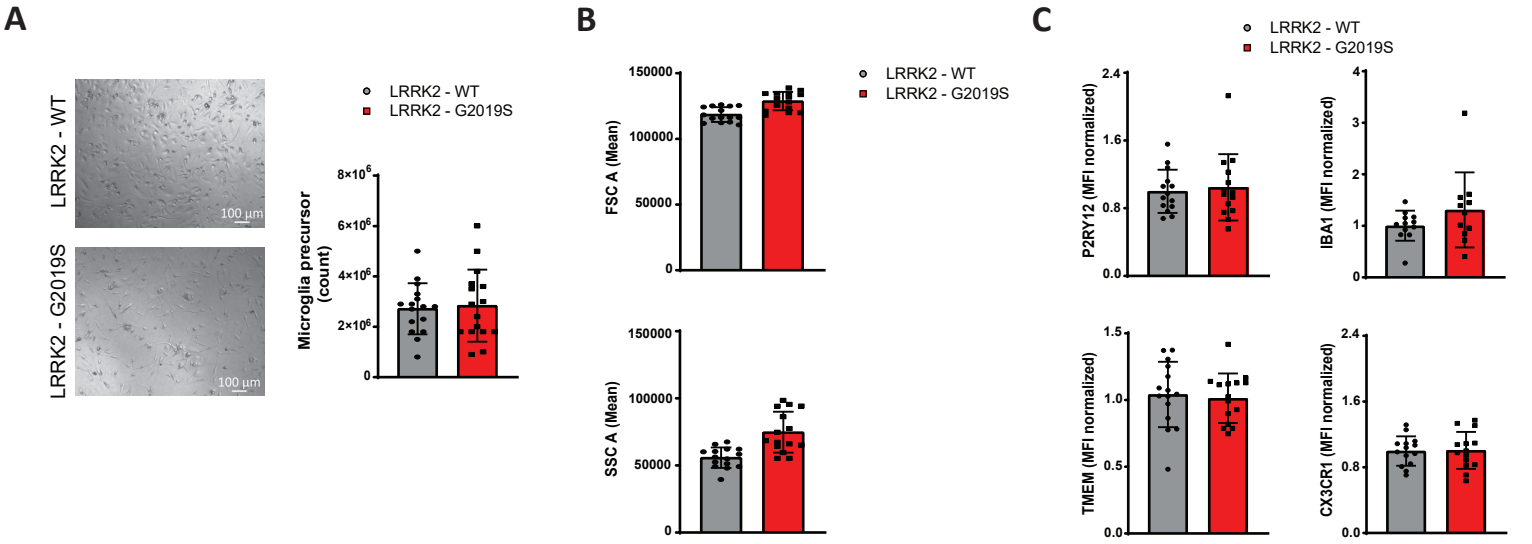
A
LRRK2 - WT
LRRK2 - G2019S
100 µm
100 µm
LRRK2 - WT
LRRK2 - G2019S
Microglia precursor (count)
8×10^6
6×10^6
4×10^6
2×10^6
0
B
LRRK2 - WT
LRRK2 - G2019S
FSC A (Mean)
150000
100000
50000
0
SSC A (Mean)
150000
100000
50000
0
C
LRRK2 - WT
LRRK2 - G2019S
P2RY12 (MFI normalized)
2.4
1.6
0.8
0.0
IBA1 (MFI normalized)
4
3
2
1
0
TMEM (MFI normalized)
1.5
1.0
0.5
0.0
CX3CR1 (MFI normalized)
2.4
1.6
0.8
0.0

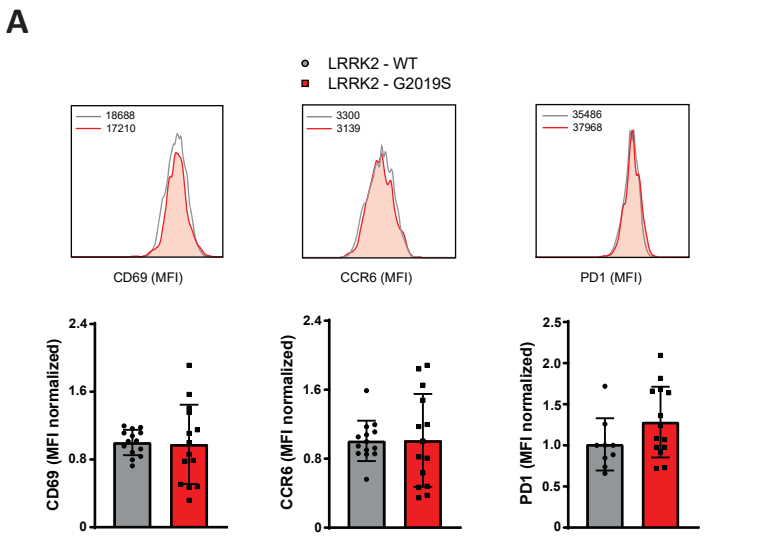
A
LRRK2 - WT
LRRK2 - G2019S
18688
17210
3300
3139
35486
37968
CD69 (MFI)
CCR6 (MFI)
PD1 (MFI)
CD69 (MFI normalized)
CCR6 (MFI normalized)
PD1 (MFI normalized)
2.4
1.6
0.8
0
2.5
2.0
1.5
1.0
0.5

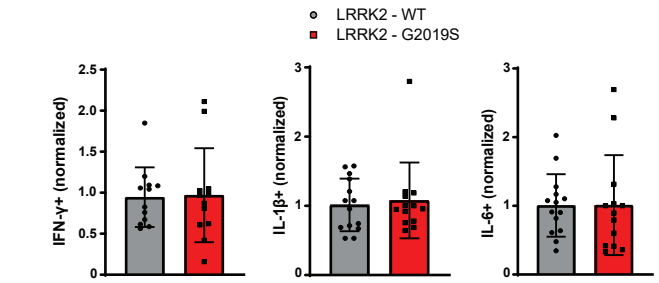
B
LRRK2 - WT
LRRK2 - G2019S
IFN-γ+ (normalized)
IL-1β+ (normalized)
IL-6+ (normalized)
2.5
2.0
1.5
1.0
0.5
0
3
2
1

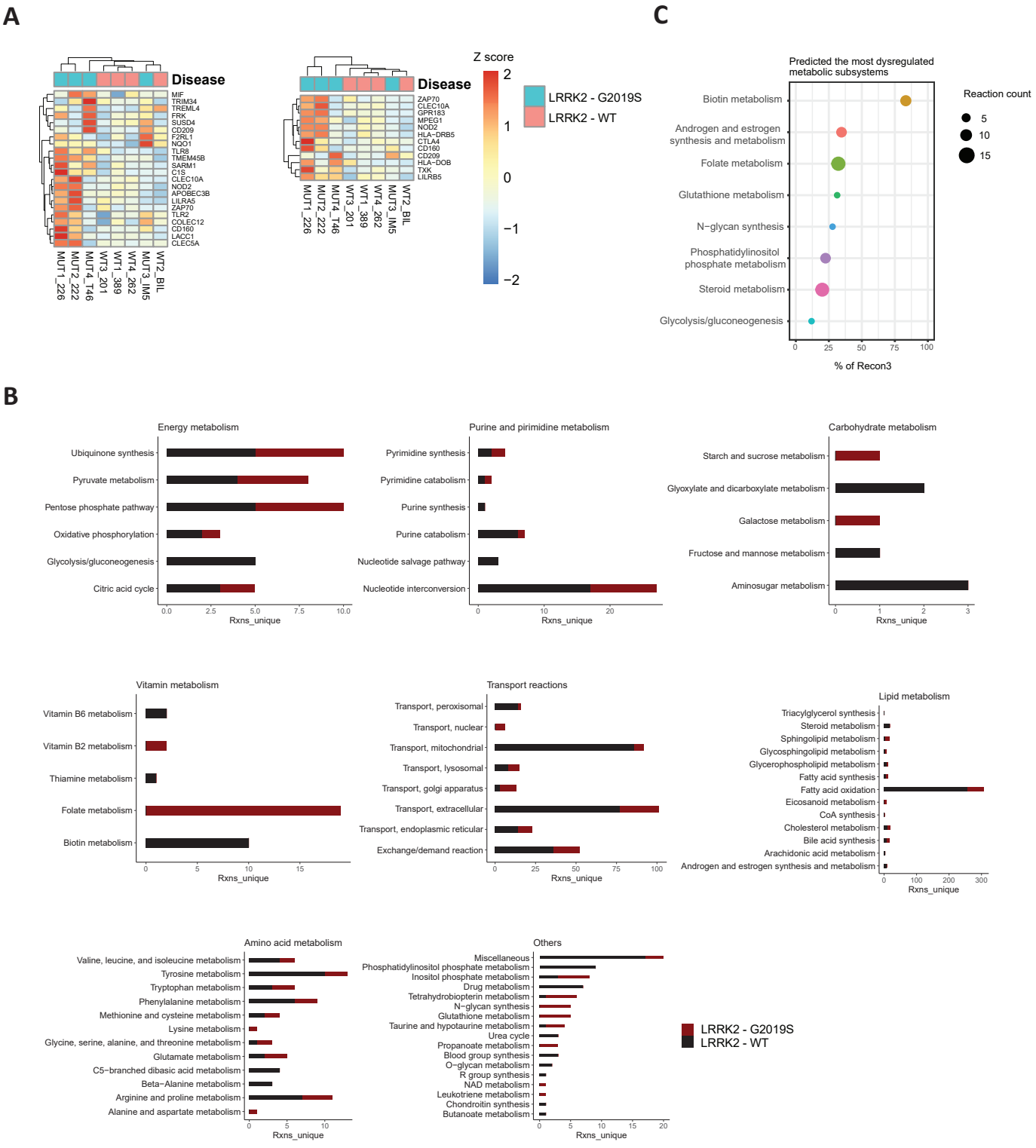
A
Disease
MIF
TRIM34
TREML4
FRK
SUSD4
CD209
F2RL1
NQO1
TLR8
TMEM45B
SARM1
C1S
CLEC10A
NOD2
APOBEC3B
LILRA5
ZAP70
TLR2
COLEC12
CD160
LACC1
CLEC5A
MUT1_226
MUT2_222
MUT4_T46
WT3_201
WT1_389
WT4_262
MUT3_IM5
WT2_BIL
Disease
ZAP70
CLEC10A
GPR183
MPEG1
NOD2
HLA−DRB5
CTLA4
CD160
CD209
HLA−DOB
TXK
LILRB5
Z score
2
1
0
−1
−2
LRRK2 - G2019S
LRRK2 - WT
C
Predicted the most dysregulated metabolic subsystems
Biotin metabolism
Androgen and estrogen synthesis and metabolism
Folate metabolism
Glutathione metabolism
N−glycan synthesis
Phosphatidylinositol phosphate metabolism
Steroid metabolism
Glycolysis/gluconeogenesis
0
25
50
75
100
% of Recon3
Reaction count
5
10
15
B
Energy metabolism
Ubiquinone synthesis
Pyruvate metabolism
Pentose phosphate pathway
Oxidative phosphorylation
Glycolysis/gluconeogenesis
Citric acid cycle
0.0
2.5
5.0
7.5
10.0
Rxns_unique
Purine and pirimidine metabolism
Pyrimidine synthesis
Pyrimidine catabolism
Purine synthesis
Purine catabolism
Nucleotide salvage pathway
Nucleotide interconversion
0
10
20
Rxns_unique
Carbohydrate metabolism
Starch and sucrose metabolism
Glyoxylate and dicarboxylate metabolism
Galactose metabolism
Fructose and mannose metabolism
Aminosugar metabolism
0
1
2
3
Rxns_unique
Vitamin metabolism
Vitamin B6 metabolism
Vitamin B2 metabolism
Thiamine metabolism
Folate metabolism
Biotin metabolism
0
5
10
15
Rxns_unique
Transport reactions
Transport, peroxisomal
Transport, nuclear
Transport, mitochondrial
Transport, lysosomal
Transport, golgi apparatus
Transport, extracellular
Transport, endoplasmic reticular
Exchange/demand reaction
0
25
50
75
100
Rxns_unique
Lipid metabolism
Triacylglycerol synthesis
Steroid metabolism
Sphingolipid metabolism
Glycosphingolipid metabolism
Glycerophospholipid metabolism
Fatty acid synthesis
Fatty acid oxidation
Eicosanoid metabolism
CoA synthesis
Cholesterol metabolism
Bile acid synthesis
Arachidonic acid metabolism
Androgen and estrogen synthesis and metabolism
0
100
200
300
Rxns_unique
Amino acid metabolism
Valine, leucine, and isoleucine metabolism
Tyrosine metabolism
Tryptophan metabolism
Phenylalanine metabolism
Methionine and cysteine metabolism
Lysine metabolism
Glycine, serine, alanine, and threonine metabolism
Glutamate metabolism
C5−branched dibasic acid metabolism
Beta−Alanine metabolism
Arginine and proline metabolism
Alanine and aspartate metabolism
0
5
10
Rxns_unique
Others
Miscellaneous
Phosphatidylinositol phosphate metabolism
Inositol phosphate metabolism
Drug metabolism
Tetrahydrobiopterin metabolism
N−glycan synthesis
Glutathione metabolism
Taurine and hypotaurine metabolism
Urea cycle
Propanoate metabolism
Blood group synthesis
O−glycan metabolism
R group synthesis
NAD metabolism
Leukotriene metabolism
Chondroitin synthesis
Butanoate metabolism
0
5
10
15
20
Rxns_unique
LRRK2 - G2019S
LRRK2 - WT

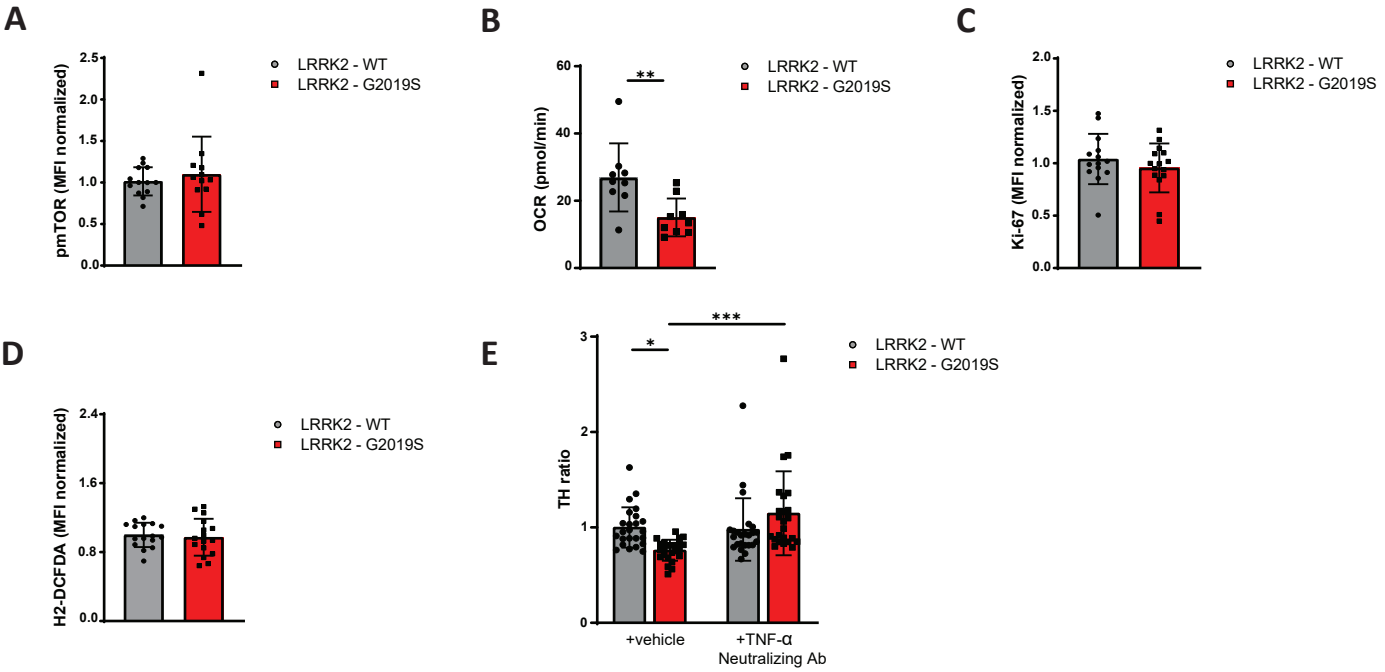
A
pmTOR (MFI normalized)
LRRK2 - WT
LRRK2 - G2019S
B
OCR (pmol/min)
**
C
Ki-67 (MFI normalized)
D
H2-DCFDA (MFI normalized)
E
TH ratio
*
***
+vehicle
+TNF-α
Neutralizing Ab

Supplementary Figure Legends

Figure SF1: Similar properties of iPSC-derived microglia harboring the LRRK2-G2019S mutation. (A) Brightfield images of microglia differentiated from LRRK2-WT and LRRK2-G2019S iPSCs (left). Quantification of macrophage precursors from LRRK2-WT and LRRK2-G2019S iPSCs (right). Data are shown as mean ± SD (n = 3-4), pooled from three independent trials. (B) Flow cytometry analysis of morphological features of LRRK2-WT and LRRK2-G2019S microglia, showing forward scatter area (size, top) and side scatter area (complexity, bottom). Data are shown as mean ± SD (n = 3-4), pooled from three independent trials. (C) Quantification of mean fluorescence intensity of identity markers (P2RY12, IBA1, TMEM119, CX3CR1) of mature LRRK2-WT vs LRRK2-G2019S microglia using flow cytometry. Data are shown as mean ± SD (n = 3-4), pooled from three independent trials.

Figure SF2: Similar expression of microglia associated markers and pro-inflammatory cytokines in LRRK2-G2019S microglia. (A) Representative analysis (top) and quantification of mean fluorescence intensity (bottom) of markers (CD69, CCR6, PD1) of LRRK2-WT vs LRRK2-G2019S microglia using flow cytometry. Data are shown as mean ± SD (n = 3-4), pooled from three independent trials. (B) Flow cytometry analysis of intracellular cytokine IFN-γ, IL-1β, and IL-6 in LRRK2-WT and LRRK2-G2019S microglia after 24h stimulation with LPS. Data are shown as mean ± SD (n = 3-4), pooled from three independent trials.

Figure SF3: Systemic changes of metabolic pathways based on the metabolic modelling in LRRK2-G2019S microglia. (A) Heatmap of innate immunity genes (left) and adaptive immunity genes (right) differentiating LRRK2-WT and LRRK2-G2019S microglia upon hierarchical clustering with FC>0.5. (B) Comparison of LRRK2-WT and LRRK20G2019S microglia metabolic model composition. Reactions found exclusively in LRRK2-WT microglia (black) or in LRRK2-G2019S microglia (red) were assigned to corresponding Recon 3 subsystems. (C) The most predicted dysregulated metabolic subsystems between LRRK2-WT and LRRK2-G2019S microglia after pooling the exclusive reactions from both conditions. Dot size and color indicate the number of reactions per subsystem. The location on y axis indicates how many reactions of the total subsystems in Recon 3 are affected.

Figure SF4: Similar upstream mTOR activity and proliferative capacity in LRRK2-G2019S microglia. (A) Flow cytometry analysis of mTOR phosphorylation in LRRK2-WT and LRRK2-G2019S microglia. Data are shown as mean ± SD (n = 3-4), pooled from three independent trials. (B) Measurement of oxygen consumption rate (OCR) in LRRK2-WT and LRRK2-G2019S microglia using the Seahorse Cell Mitochondrial Stress Test. Proton leak was quantified. Data are shown as mean ± SD (n = 3-4), pooled from three independent trials. (C) Flow cytometry analysis of intracellular protein Ki-67 in LRRK2-WT and LRRK2-G2019S microglia. Data are shown as mean ± SD (n = 3-4), pooled from three independent trials. (D) Flow cytometry analysis of reactive oxygen species levels using H2-DCFDA in LRRK2-WT and LRRK2-G2019S microglia. Data are shown as mean ± SD (n = 3-4), pooled from three independent trials. (E) The ratio of dopaminergic neurons, represented by the total TH+ cells over total MAP2+ neurons, in midbrain organoids treated with or without 1 ng/ml TNF-α neutralizing antibody. Data are shown as mean ± SD (n = 3), pooled from three independent trials.

Supplementary Table 1: List of materials (antibody, small molecules, probes, and commercial kits) used in this study.

REAGENT or RESOURCE	SOURCE	Cat#	RRIDS
Antibodies			
PU.1	Cell signalling	2258S	AB_2186909
IBA1	Abcam	Ab5076	AB_2224402
CD11b	Biolegend	101206	AB_312789
CD45	Biolegend	304007	AB_314395
P2RY12	Biolegend	392106	AB_2783921
TMEM119	Abcam	Ab225497	AB_3665680
CX3CR1	Biolegend	341627	AB_2810534
CD68	Biolegend	333822	AB_2571965
HLA-DR	Biolegend	307606	AB_314684
CD80	Biolegend	305218	AB_2076148
CD86	Biolegend	374214	AB_2734430
CD282	Biolegend	148604	AB_2564120
CD284	Biolegend	312816	AB_2562487
TNF-α	Biolegend	506344	AB_2565953
RPS6 phospho (Ser244)	Biolegend	935706	AB_3665682
PHGDH	Cell signalling	66350S	AB_2737030
TH	Abcam	Ab112	AB_297840
MAP2	Abcam	Ab92434	AB_2138147
IBA1	Abcam	Ab5076	AB_2224402
CD69	Biolegend	310904	AB_314839
CD196	Biolegend	353406	AB_10918437
CD279	Biolegend	329916	AB_2283437
IFN-γ	Biolegend	506528	AB_2566187
IL-6	Biolegend	501120	AB_2572042
IL-1β	Biolegend	508208	AB_604135
Phospho-mTOR (Ser2448)	Biolegend	48-9718-42	AB_2574127
Ki-67	Biolegend	350504	AB_10660752

donkey anti-goat Alexa Fluor ®488	Invitrogen	A11057	AB_142581
donkey anti-rabbit Alexa Fluor ®568	Invitrogen	A10042	AB_2534017
goat anti-rabbit Alexa Fluor ®488	Invitrogen	A11034	AB_2576217
goat anti-mouse Alexa Fluor®568	Invitrogen	A11031	AB_144696
goat anti-chicken Alexa Fluor®647	Invitrogen	A-21449	AB_2535866
goat anti-mouse Alexa Fluor ®488	Invitrogen	A-11001	AB_2534069
goat anti-rabbit Alexa Fluor ®647	Invitrogen	A-21244	AB_2535812
Chemicals, Peptides, and Recombinant Proteins			
MitoTracker™ Green FM	ThermoFisher Scientific	M7514	
MitoTracker™ Deep Red FM	ThermoFisher Scientific	M22426	
H2DCFDA	ThermoFisher Scientific	D399	
Zombie Green™ Fixable Viability Kit	Biolegend	423112	
Zombie NIR™ Fixable Viability Kit	Biolegend	423106	
2-(N-(7-Nitrobenz-2-oxa-1,3-diazol-4-yl)Amino)-2-Deoxyglucose	ThermoFisher Scientific	N13195	
Hoechst33342	Thermo Fisher Scientific	62249	
Zymosan A S.cerevisiae BioParticles™	ThermoFisher Scientific	Z2841	
pHrodo™ Red Zymosan BioParticles™	ThermoFisher Scientific	P35364	
Oligomycin A	Sigma-Aldrich	75351-5MG	
FCCP	Sigma-Aldrich	C2920-10MG	
Antimycin A	Sigma-Aldrich	A8674-25MG	
Rotenone	Sigma-Aldrich	R8875-1G	
D-Glucose (U-$^{13}C_6$, 99%)	Cambridge Isotope Laboratories, Inc	CLM-1396-1	
D-Glucose	Sigma-Aldrich	G8270-5KG	
2-Deoxy-D-glucose	Sigma-Aldrich	D6134-1G	
EDTA	Sigma-Aldrich	E9884-100G	
Saponin	Sigma-Aldrich	S4521-25G	
Formaldehyde	Sigma-Aldrich	252549-1L	
HEPES	Sigma-Aldrich	H4034-100G	
Methanol	Sigma-Aldrich	1060351000	

Chloroform	Sigma-Aldrich	34584-1L-M	
GolgiPlug™	BD Biosciences	555029	
Corning™ Cell-Tak Cell and Tissue Adhesive	ThermoFisher Scientific	10317081	
Sodium pyruvate	GIBCO	12539059	
2-mercaptoethanol	GIBCO	11508916	
Penicillin/Streptomycin	ThermoFisher Scientific	15140122	
DMEM/F12 Advanced medium	ThermoFisher Scientific	12634010	
Essential 8	ThermoFisher Scientific	A1517001	
DMEM/F12 (1:1) W/O L-GLUT	ThermoFisher Scientific	21331046	
Neurobasal medium	ThermoFisher Scientific	21103049	
B27 – vitamin A	ThermoFisher Scientific	12587001	
GlutaMAX	ThermoFisher Scientific	35050061	
Human IL-34 Recombinant Protein	Biolegend	577906	
Human GM-CSF Recombinant Protein	Biolegend	572905	
Human IL-3 Recombinant Protein	Biolegend	578008	
Human M-CSF Recombinant Protein	Biolegend	574808	
Human BMP-4 Recombinant Protein	Biolegend	795606	
Human VEGF-165 Recombinant Protein	Biolegend	583708	
Human SCF	Miltenyi Biotec	130-096-695	
BIOFLOAT™ 96 well plate U-bottom	Facellitate	F202003	
Aggrewell 800 24 well plate	StemCell technologies	34815	
L-Ascorbic acid	Sigma-Aldrich	A4544-100G	
SB431542	Sigma-Aldrich	ab120163	
CHIR99021	Axon	CT 99021	
Smoothened agonist	Merck	566660-1MG	
LDN193189	Sigma-Aldrich	SML0559-5MG	
ROCK inhibitor Y-27632 2HCl [146986-50-7, 129830-38-2]	CliniSciences	A11001-50	

pluriStrainer® 40 µm (Cell Strainer)	PluriSelect	SKU 43-50040-51	
N2 supplement 100x 50ml	ThermoFisher Scientific	17502001	
Recombinant Human GDNF	Peprotech	450-10-1mg	
Recombinant Human BDNF	Peprotech	450-02 - 1mg	
DAPT	R&D Systems	2634/50	
Human ActivinA Recombinant Protein	ThermoFisher Scientific	PHC9561	
X-VIVO 15 with Gentamicin and Phenol Red, 1 L	Lonza	LO BE02-060Q	
Critical Commercial Assays			
RNeasy kit	Qiagen	74106	
Human Inflammatory Cytokine Multiplex ELISA Kit	Arigo Laboratories	ARG80929	
CellTiter-Glo® Luminescent Cell Viability Assay	Promega	G7571	
Seahorse XFe96 Fluxpak	Agilent Technologies	102416-100	
BD Pharmingen™ Transcription Factor Buffer Set	BD Biosciences	554656	AB_2869424
Software and Algorithms			
R			
Graphpad Prism			
Matlab			
Image J			
Seahorse Wave			
FlowJo			
Zen blue/black			

3.3 Manuscript III

Parkinson's disease microglia induce endogenous α-synuclein pathology in patient-specific midbrain organoids.

Elisa Zuccoli[1]*, Henry Kurniawan[1], Isabel Rosety[1], Alise Zagare[1], Sonia Sabate-Soler[1], Anna-Sophie Zimmermann[1], Jens C. Schwamborn[1#]

[1] Developmental and Cellular Biology, Luxembourg Centre for Systems Biomedicine (LCSB), University of Luxembourg, 6, Avenue du Swing, L-4367 Belvaux, Luxembourg.

* First authors

[#] Corresponding author

This article is under revision in Nature Communications.

3.3.1 Contribution statement

This study is the result of my main PhD project. I carried out the experimental planning, execution of experiments, manuscript writing and figure preparation. Bulk RNA sequencing was performed by Novogene, while I extracted the counts and analysed the data. Flow cytometry experiments were performed by H. Kurniawan (Figure 1D-E). The MATLAB script for IBA1 skeleton image analysis was created by A. Zagare (Figure 2E), and 3D reconstruction using IMARIS was performed by S. Sabate-Soler (Figure 2D). Analysis of high-content imaging of α-synuclein, p62, and Proteostat staining was done by I. Rosety (Figure 4D, Figure 5E, Supplementary Figure 3D-E and Supplementary Figure 4A-B). A. Zimmermann contributed to the generation and collection of assembloids. The initial concept for the study was developed by J.C. Schwamborn.

3.3.2 Preface

The main objective of this study was to explore how patient-derived microglia harbouring the SNCA triplication (3xSNCA) contribute to Parkinson's disease pathogenesis, with a particular focus on α-synuclein aggregation and neuroinflammation within the midbrain organoid context.

We first confirmed that 3xSNCA microglia express α-synuclein and exhibit a significant reduction in phagocytic capacity. These microglia also showed an altered inflammatory signature, characterized by increased IL-1β production. Transcriptomic profiling revealed dysregulation of lysosomal pathways and metabolic processes, highlighting impairment in cellular clearance and homeostasis.

To better mimic physiological conditions, we integrated 3xSNCA microglia into midbrain organoids. Here, the mutant microglia displayed a pronounced morphological shift from the ramified, surveillant form characteristic of resting microglia to an ameboid, activated phenotype. This activation correlated with increased levels of both total and phosphorylated α-synuclein, particularly at serine 129, a post-translational modification linked to Lewy body formation. Remarkably, 3xSNCA assembloids spontaneously developed a variety of pS129-positive α-synuclein aggregate structures, including ring-like, filamentous and dense formations. These structures were consistently detected using multiple independent anti-pS129 antibodies, confirming the reproducibility of these pathological features. To further validate their pathological nature, we showed co-localization of the α-synuclein aggregates with key markers of protein aggregation, including p62, Proteostat, Ubiquitin and Thioflavin S, supporting the presence of misfolded α-synuclein.

Strikingly, the introduction of 3xSNCA microglia into healthy control midbrain organoids was sufficient to induce endogenous α-synuclein pathology. This included appearance of aggregated, misfolded, and phosphorylated α-synuclein, despite the absence of the neuronal SNCA mutation.

These findings demonstrate that 3xSNCA microglia actively contribute to initiation and propagation of Parkinson's disease pathology, underscoring their pivotal role in the neuroinflammatory and proteostatic disturbances characteristic for the disease.

Parkinsons disease microglia induce endogenous alpha-Synuclein pathology in patient-specific midbrain organoids.

Elisa Zuccoli, Henry Kurniawan, Isabel Rosety, Alise Zagare, Sonia Sabate-Soler, Anna-Sophie Zimmermann, Jens C. Schwamborn#

Developmental and Cellular Biology, Luxembourg Centre for Systems Biomedicine (LCSB), University of Luxembourg, 6, Avenue du Swing, L-4367 Belval, Luxembourg.

#Corresponding author: Jens C. Schwamborn, jens.schwamborn@uni.lu

Keywords

α-synuclein, pathology, assembloids, microglia, Parkinson's disease

Abstract

The accumulation of misfolded alpha-synuclein and the loss of dopaminergic neurons are hallmarks of Parkinsons disease (PD), contributing to the development of synucleinopathies. Although considerable progress has been made in understanding α-synuclein's role in PD pathology, the precise mechanisms involved remain unclear. Human midbrain organoids (hMOs) have emerged as valuable models for studying PD, yet the lack of microglia limits the ability to investigate neuroimmune interactions. Recent studies show that integrating microglia into hMOs enhances neuronal maturation and functionality. Here, we generated a human midbrain assembloid model by incorporating iPSC-derived microglia into midbrain organoids from healthy control individuals and a PD patient carrying the SNCA triplication (3xSNCA) mutation. Our results show that 3xSNCA microglia alone are sufficient to induce early, endogenous formation of phosphorylated alpha-synuclein (pS129) pathology in the absence of exogenous fibril seeding. This PD-pathology emerged as early as day 50 of culture and was not observed in models lacking microglia. These findings highlight a critical role for patient-derived microglia in driving α-synuclein pathology and provide a physiologically relevant platform for studying early neuroimmune mechanisms in PD and testing potential therapeutic strategies.

Introduction

Parkinsons disease (PD) is a progressive neurodegenerative disorder characterized by the selective loss of dopaminergic neurons in the substantia nigra *pars compacta* of the midbrain and the pathological accumulation of the misfolded α-synuclein protein (Kalia and Lang, 2015; Poewe et al., 2017). A defining hallmark of PD is the formation of intracellular inclusions known as Lewy bodies and Lewy neurites, which are primarily composed of aggregated and phosphorylated α-synuclein (Spillantini et al., 1998; Goedert, 2015). These inclusions are central to the diagnosis and classification of PD and related synucleinopathies (Lashuel et al., 2013; Fujiwara et al., 2022). While the precise physiological function of α-synuclein remains under investigation, its pathological forms disrupt synaptic vesicle trafficking (Bernal-Conde et al., 2020), impair mitochondrial function (Plotegher and Duchen, 2017), and contribute to neuroinflammation and lysosomal dysfunction (Calabresi, Mechelli, et al., 2023), ultimately driving neuronal death (Stefanis, 2012; Calabresi, Di Lazzaro, et al., 2023). Furthermore, the prion-like propagation of misfolded α-synuclein between cells is thought to underlie the stereotypical progression of pathology observed in PD (Lashuel et al., 2013), with phosphorylation at Ser129 exacerbating mitochondrial dysfunction and oxidative stress (Kawahata et al., 2022).

Genetic alterations in the *SNCA* gene, including point mutations, duplications, and triplications, cause autosomal dominant forms of PD and are strongly associated with increased α-synuclein expression and the development of Lewy pathology (Polymeropoulos et al., 1997; Krüger et al., 1998; Zarranz et al., 2004; Ibáñez et al., 2004; Singleton et al., 2003). Despite major progress in understanding α-synuclein's role in disease, the mechanisms underlying its pathological accumulation and downstream effects remain unclear (Sulzer & Edwards, 2019; Burré, 2015).

Human midbrain organoids (hMOs), derived from induced pluripotent stem cells (iPSCs) (Takahashi & Yamanaka, 2006), have emerged as powerful *in vitro* systems for modelling PD. These self-organizing, three-dimensional cultures recapitulate essential features of the human midbrain, including the presence of mature dopaminergic neurons, astrocytes, and oligodendrocytes, along with dopamine release and electrophysiological activity (Monzel et al., 2017). hMOs have been successfully used to model several genetic forms of PD, including mutations in LRRK2, GBA, or PINK1, as well as the triplication in the *SNCA* gene (Smits et al., 2019; Kim et al., 2019; Rosety et al., 2023; Jarazo et al., 2022; Muwanigwa et al., 2024). However, a key limitation of standard hMO systems is the absence of microglia - the brain's resident immune cells - due to their mesodermal origin.

Microglia, which represent 5% to 15% of the brain cells in adults, are tissue-resident macrophages derived from yolk sac progenitors during early embryogenesis (Thion et al., 2018; Ginhoux et al., 2010; Li & Barres, 2018; Schulz et al., 2012). Their omission from hMOs restricts the ability to model critical immune-mediated mechanisms of neurodegeneration, such as synaptic pruning, phagocytosis of apoptotic neurons, and neuroinflammatory responses, all of which are central to Parkinson's disease (Tremblay et al., 2011; Wake et al., 2009; Ormel et al., 2018). Microglia play a key role in maintaining brain homeostasis and immune defence, interacting with neurons, astrocytes, and oligodendrocytes, and their dysfunction in PD is closely associated with chronic neuroinflammation (Shabab et al., 2017). Sabate-Soler et al. (2022) demonstrated that incorporating microglia into hMO systems leads to enhanced neuronal maturation and functionality, providing a more comprehensive model of the human midbrain and its cellular interactions. Given the critical role of microglia in neurodegenerative diseases, integrating them into midbrain organoids offers a physiologically relevant platform for studying early neuroimmune contributions to Parkinson's disease and testing potential therapeutic strategies (Cakir et al., 2022; Toh et al., 2023; Sabate-Soler et al., 2024).

In this study, we generated human midbrain assembloid models by integrating iPSC-derived microglia into midbrain organoids from both healthy individuals and PD patients with the *SNCA* triplication (3xSNCA). Upon integration into midbrain organoids, these microglia induced early and endogenous formation of phosphorylated α-synuclein (pS129) aggregates and PD-like pathology in the absence of exogenous fibril seeding. Notably, this pathology emerged by day 50 of culture, which is considerably earlier than previously observed in long-term models. Remarkably, this pathological process was observed not only in 3xSNCA assembloids but also in chimeric assembloids consisting of healthy midbrain organoids and PD specific microglia. This finding indicates that 3xSNCA microglia alone were sufficient to induce endogenous phospho-α-synuclein (pS129) pathology. These findings further highlight the crucial role of microglia in driving early-stage α-synuclein pathology and demonstrate the utility of midbrain assembloids as an advanced model for investigating the early neuroimmune contributions to Parkinson's disease.

Results

3xSNCA microglia express α-synuclein, exhibit reduced phagocytosis and show altered inflammatory activity.

In this study, we used three different iPSC lines from healthy individuals and the 3xSNCA cell line derived from a PD patient with a *SNCA* triplication (Supplementary Table 1). A *SNCA* knockout cell line (KO) was also included for validation of α-synuclein antibody specificity. To investigate the mature microglia, we derived macrophage precursors from human iPSCs that were differentiated into microglia for 14 days as previously described by Haenseler, Sansom, et al. (2017) (Figure 1a). Immunofluorescence staining confirmed expression of macrophage-specific markers, such as CD45, PU.1, and IBA1, and microglia markers, including TMEM119 and P2RY12 (Figure 1b, Supplementary Figure 1a-c, Supplementary Figure 2a). After confirming the microglial cell identity, we stained the mature microglia with an anti-α-synuclein antibody and showed that the protein is expressed in both WT and 3xSNCA microglia, but not visible in the KO microglia (Figure 1b, Supplementary Figure 2a). We could also determine a nuclear localization of the α-synuclein protein in both the WT and 3xSNCA microglia (Figure 1b, Supplementary Figure 2a). Additionally, extracellular α-synuclein release was measured by dot blot and shows a significant increase in the 3xSNCA microglial medium (Figure 1c).

Next, we assessed the phagocytic capacity of the mature microglia. Incubation with Zymosan particles showed a significant decrease in Zymosan particle uptake (Figure 1d, left panel) along with a reduced pHRodo fluorescence rate (Figure 1d, right panel) in the 3xSNCA microglia, indicating an impairment in both the internalization and phagosomal acidification process, suggesting a deficiency in effective phagocytosis. Haenseler, Zambon et al. (2017) similarly reported accumulation of α-synuclein along with impaired phagocytic function in iPSC-derived 3xSNCA macrophages, supporting our findings.

Chronic activation of microglia leads to excessive release of cytokines such as IL-1, TNF-α, IL-6, and IFN-γ, creating a toxic environment for neurons (Tansey et al., 2022). Previous studies have shown that elevated α-synuclein levels induce a pro-inflammatory response in microglia (Zhang et al., 2005; Klegeris et al., 2008; Ferreira & Romero-Ramos, 2018). Notably, we wanted to determine the impact of the SNCA triplication on microglial cytokine production in our WT and 3xSNCA microglia. Flow cytometry analysis showed that IL-1β, a key mediator of the inflammatory response, was significantly upregulated in the 3xSNCA microglia compared to the healthy controls (Figure 1e, upper left panel). Interestingly, both TNF-α and IL-6 were significantly downregulated, and no change was seen in IFN-γ (Figure 1e). Together these results indicate that 3xSNCA microglia exhibit increased α-synuclein expression,

impaired phagocytosis, and altered inflammatory activity, highlighting their potential role in neuroinflammation and Parkinson's disease pathology.

Transcriptomic data analysis reveals lysosomal dysfunction in 3xSNCA microglia.

To further elucidate the molecular mechanisms underlying these phenotypic alterations, we employed RNA sequencing to comprehensively analyse transcriptomic differences between WT and 3xSNCA microglia. By analysing transcriptomic data, we aimed to identify key dysregulated pathways and genes that may contribute to the observed cellular dysfunctions, providing further insights into the role of α-synuclein in microglial pathology. We identified 149 differentially expressed genes (DEGs) in 3xSNCA microglia compared to the three WT cell lines, using a threshold of adjusted p-value (FDR) <0.01 (Supplementary Figure 2b). Unsupervised hierarchical clustering based on normalised gene counts of top significant DEGs involved in the inflammasome pathway further highlighted clear separation between the two groups and confirms our findings on altered inflammatory activity (Supplementary Figure 2c). Gene Ontology pathway enrichment analysis of the p-value <0.01 significant DEGs between 3xSNCA and WT samples revealed that the lysosomal pathway is dysregulated, including protein localization to lysosome, lysosomal transport, and protein-targeting to lysosome, as the top enriched pathways (Figure 1f). Additionally, KEGG (Kyoto Encyclopedia of Genes and Genomes) enrichment analysis supported these results and identified "Lysosome" as the most enriched pathway, followed by metabolic pathways such as the lipid metabolism and carbohydrate metabolism (Figure 1g). The enrichment analysis suggests that lysosomal dysfunction and metabolic dysregulation are key processes affected at the transcriptomic level. Looking at the expression of individual genes of the phagocytic and lysosomal pathway, we could confirm that the key genes of these pathways are downregulated in the 3xSNCA microglia (Figure 1h). Our findings highlight disruptions in cellular clearance mechanisms and metabolic balance, emphasizing the critical role of lysosomal and phagocytic pathways in neurodegeneration.

3xSNCA microglia integrated into midbrain organoids display morphological differences.

After describing the phenotypic and transcriptomic changes in 3xSNCA microglia, we sought to investigate these cells in a physiologically relevant context. To achieve this, we integrated the microglia into midbrain organoids following the protocol described by Sabate-Soler et al. (2022) (Figure 2a). This approach allowed us to study microglial behaviour and interactions within a three-dimensional cellular environment that closely mimics the complexity of the human brain. Previous studies have shown that changes in microglial function, such as increased reactivity, enhanced pro-inflammatory response, impaired phagocytosis, altered

gene expression, and exacerbation of α-synuclein pathology, contribute to the chronic neuroinflammation and neurodegeneration observed in PD (Thi et al., 2024; Zhu et al., 2022).

First, we characterized 50-day-old assembloids (ASBs) to ensure that they expressed the relevant cell types of the midbrain, showing the presence of mature neurons (MAP2 – microtubule associated protein 2), dopaminergic neurons (TH – Tyrosine Hydroxylase) and astrocytes (S100β – S100 calcium binding protein B) (Figure 2b). Staining with the microglial marker IBA1 (Ionized calcium binding adaptor molecule 1) and the astrocyte marker GFAP (glial fibrillary acidic protein) completed the characterization of the assembloids (Figure 2c). Interestingly, when examining the morphology of the integrated microglia, we observed striking differences between WT and 3xSNCA conditions. WT microglia in WT midbrain organoids displayed a more typical ramified morphology, characteristic of resting or surveillant microglia in a healthy state (Figure 2d, left panel, and 2e). In contrast, 3xSNCA microglia in 3xSNCA midbrain organoids exhibited an ameboid morphology, indicative of an activated state (Figure 2d, right panel, and 2e). These morphological distinctions, suggest that the 3xSNCA mutation leads to a more activated microglial phenotype, within the complex 3D organoid environment.

3xSNCA assembloids exhibit elevated α-synuclein and phospho-α-synuclein (pS129) levels.

Given that the SNCA triplication leads to increased expression of α-synuclein and is associated with early-onset Parkinson's disease (Singleton et al., 2003), we investigated both total α-synuclein and its phosphorylated form (pS129) to assess disease-relevant phenotypes in 3xSNCA assembloids. α-synuclein protein levels were evaluated by Western Blot, showing an expected significant increase in the 3xSNCA assembloids (Figure 3a and 3b, left panel). The specificity of the α-synuclein antibody has been previously confirmed by the lack of signal in SNCA KO midbrain organoids (Muwanigwa et al., 2024). Consistent with its role as a hallmark of pathology, pS129 was also significantly elevated in 3xSNCA assembloids (Figure 3a and 3b, right panel), in agreement with previous findings. α-synuclein and pS129 staining of assembloids validated these findings by showing significantly increased intensities in the 3xSNCA assembloids (Figure 3c and 3d). Additionally, dot blot analysis revealed enhanced extracellular α-synuclein release (Figure 3e).

3xSNCA microglia promote endogenous formation of phospho-α-synuclein (pS129) pathology in assembloids.

To evaluate whether the PD patient-specific model recapitulates key pathological features, we examined α-synuclein aggregation. We particularly focused on phosphorylation at serine 129 (pS129). This post-translational modification is a well-established marker of Lewy-body

pathology and neuronal dysfunction (Spillantini et al., 1997; Gallegos et al., 2015; Samuel et al., 2016; Calabresi, Mechelli, et al., 2023). Notably, pS129 accounts for around 90% of α-synuclein within Lewy bodies, compared to only around 4% in healthy brains (Xu et al., 2015), and is associated with fibril formation, toxicity, and disease progression (Henderson et al., 2019).

Previous studies demonstrated that pS129 antibodies can detect diverse α-synuclein aggregate structures *in vitro*, specifically in neurons treated with preformed fibrils (PFFs) (Lashuel et al., 2022). Building on this, we assessed pS129-positive aggregates in 3xSNCA assembloids and were able to recapitulate these findings in the *in vitro* assembloid model without the addition of exogenous PFFs. Consistent with Lashuel's observations, we identified distinct pS129-positive α-synuclein structures in our 3xSNCA assembloids, including Ring-like (Figure 4a, upper panel), Filamentous-like (middle panel), and Dense-like (lower panel) formations. To confirm the specificity of the observed pS129 pathology, we tested several anti-pS129 antibodies, including D1R1R (Figure 4a), MJF-R13 (8-8) (Supplementary Figure 3a), MJFR-14-6-4-2 (Supplementary Figures 3b and 3c). All consistently labelled pathological α-synuclein structures, supporting the reliability of our findings. Together, these results demonstrate that the 3xSNCA assembloid model spontaneously develops diverse α-synuclein pathological structures, further validating its relevance for studying synucleinopathies.

Moreover, we used a comprehensive panel of markers to further validate the presence of pathological forms of α-synuclein in 3xSNCA assembloids originally detected with anti-pS129 antibodies (Canerina-Amaro et al., 2019). We observed a significant increase in the co-localization of α-synuclein with p62 (SQSTM1) and Proteostat in 3xSNCA assembloids (Figure 4b-d), indicating a substantial burden of α-synuclein–specific pathological aggregates. p62 is an autophagy adaptor protein frequently found in Lewy bodies, while Proteostat binds β-sheet–rich misfolded proteins, serving as a general marker of proteostasis disruption (Kuusisto et al., 2003; Rocha et al., 2018). Although p62 and Proteostat signals are also present in WT assembloids (Supplementary Figure 3d and 3e), the extent of their co-localisation with α-synuclein is substantially higher in the 3xSNCA assembloids (Figure 4d). To further support this finding, we confirmed additional markers through co-localization of pS129 with ubiquitin, a key component of the protein degradation machinery that accumulates at sites of misfolded protein aggregation (Figures 4e and 4f). These results suggest that elevated α-synuclein expression in the mutant assembloids drives the formation of misfolded protein aggregates.

Additionally, staining with Thioflavin S, which specifically labels β-sheet-rich amyloid structures, revealed co-localization with both α-synuclein and pS129 (Supplementary Figure

3b and 3c), indicating that these aggregates acquire amyloid-like conformations characteristic of mature pathogenic inclusions (Lee et al., 2002). In addition, co-localization of α-synuclein with the mitochondrial outer membrane marker TOM20 (Supplementary Figure 3f and 3g) suggests a potential interaction of aggregates with mitochondria, consistent with previous findings that link α-synuclein pathology to mitochondrial dysfunction (Di Maio et al., 2016). This enhanced co-localization provides strong evidence for the formation of α-synuclein aggregates in the 3xSNCA assembloid model, supporting the presence of pathological α-synuclein species and potentially indicating impaired protein degradation pathways.

3xSNCA microglia are sufficient to induce pS129 pathology in WT midbrain organoids.

To investigate whether 3xSNCA microglia are sufficient to induce α-synuclein pathology in an otherwise healthy environment, we generated chimeric assembloids by integrating 3xSNCA mutant microglia into WT midbrain organoids (WT-3xSNCA ASB) (Figure 5a). Immunofluorescence analysis revealed a significant increase in both total α-synuclein and pS129 signal intensity in WT-3xSNCA assembloids compared to WT assembloids (Figure 5b), indicating that PD microglia alone are sufficient to induce pathology. Nevertheless, while the induction of pathology is clear, it is lower than what we saw before in organoids carrying the 3xSNCA mutation themselves (Figure 3d). We further visualized disease-relevant α-synuclein pathology in WT–3xSNCA assembloids, including compact and filamentous-like formations (Figure 5c), similar to those described in Lashuel et al (2020). Notably, these structures were detectable upon integration of 3xSNCA microglia into all three WT midbrain organoid lines. Aggregation was validated through co-localization of α-synuclein with p62, whose accumulation indicates impaired autophagic clearance, and Proteostat, a marker of misfolded protein aggregates (Figure 5d–e, Supplementary Figure 4a and 4b). To strengthen this finding, we confirmed additional markers by co-localization of pS129 with ubiquitin (Supplementary Figures 4c and 4d), and α-synuclein with the mitochondrial marker TOM20 (Supplementary Figures 4e and 4f), supporting the presence of Lewy body–like structures and mitochondrial involvement. Together, these results demonstrate that 3xSNCA microglia are sufficient to initiate α-synuclein pathology in an otherwise WT environment and highlight their emerging role as drivers of Parkinson's disease pathogenesis.

Discussion

The endogenous formation of phosphorylated α-synuclein (pS129) remains a major challenge in PD modelling. Most *in vitro* systems and *in vivo* mouse models require the addition of preformed α-synuclein fibrils (PFFs) to induce Lewy body–like pathology (Luk et al., 2009; Volpicelli-Daley et al., 2011; Osterberg et al., 2015; Mahul-Mellier et al., 2020; Awa et al., 2022). In this study, we present a robust and reproducible patient-specific human midbrain

assembloid model that recapitulates hallmark features of α-synuclein pathology, including the spontaneous formation of pS129-positive aggregates in the absence of exogenous fibrils. Our system integrates 3xSNCA iPSC-derived microglia into midbrain organoids, providing a physiologically relevant, tissue-like environment for studying early PD pathology.

Already, the 3xSNCA microglia alone exhibited impaired phagocytic function, altered inflammatory signalling, and revealed significant alterations in lysosomal pathway and metabolic processes consistent with previous work on iPSC-derived macrophage precursors from SNCA triplication patients (Haenseler, Zambon et al., 2017). Upon integration into midbrain organoids, these microglia showed an ameboid, activated morphology, consistent with their pro-inflammatory profile and loss of homeostatic surveillance. These phenotypes were retained in 3D assembloids and are likely contributors to α-synuclein accumulation and impaired clearance (Choi et al., 2020; Bido et al., 2021; Eo et al., 2024).

Previous studies have consistently reported increased α-synuclein and progressive accumulation of pS129 in various SNCA triplication models. Oliveira et al. (2015) observed elevated α-synuclein in dopaminergic neurons derived from 3xSNCA iPSCs, while Jo et al. (2021) identified Lewy body–like inclusions in 3xSNCA midbrain organoids at day 90 following treatment with the lysosomal inhibitor conduritol B epoxide (CBE). Mohamed et al. (2021) reported increased aggregation of oligomeric and phosphorylated α-synuclein in 3xSNCA midbrain organoids by day 100, with pathological progression through day 170. Becerra-Calixto et al. (2023) showed progressive pS129 accumulation in 3xSNCA midbrain organoids from days 120 to 180, while Muwanigwa et al. (2024) detected pS129-rich aggregates in 3xSNCA human midbrain organoids by day 70.

While these studies describe accumulation and progressive pathology markers, our 3xSNCA assembloid model demonstrates robust pS129-positive aggregate formation with pathological morphology, as defined by Lashuel et al. (2022), by day 50. This significantly accelerated aggregation highlights the critical role of 3xSNCA microglia in promoting pathological α-synuclein accumulation. This early pathology is likely driven by an overproduction of α-synuclein that overwhelms cellular clearance systems such as chaperone-mediated autophagy, the ubiquitin–proteasome system, and macroautophagy (Cuervo et al., 2004; Martinez-Vicente et al., 2008; Snyder et al., 2003; Winslow et al., 2010), resulting in accumulation of misfolded α-synuclein and aggregate formation.

Importantly, 3xSNCA microglia induced pS129 pathology even when integrated into wild-type midbrain organoids (chimeric assembloids), demonstrating that microglial dysfunction alone can initiate α-synuclein pathology independent of neuronal SNCA overexpression. These finding positions microglia as active drivers of disease initiation and progression, rather than

passive responders (Zhang et al., 2005; Hickman et al., 2018; Ferreira & Romero-Ramos, 2018; Bido et al., 2021).

Given the prominent α-synuclein pathology observed in the here described model, these findings offer a valuable platform to explore therapeutic strategies that directly target α-synuclein aggregation or modulate downstream disruptions in proteostasis. Several small molecules have shown promising results in this context. Squalamine and Trodusquemine displace α-synuclein from lipid membranes, effectively blocking both the initiation and propagation of aggregation in preclinical models (Perni et al., 2017; Rao et al., 2000; Yang et al., 2024). Minzasolmin (UCB0599) prevents α-synuclein misfolding, while Emrusolmin (Anle138b) binds to oligomeric forms to inhibit the formation of toxic aggregates. Both compounds have demonstrated efficacy in preclinical studies and are undergoing clinical evaluation (Price et al., 2023; Heras-Garvin et al., 2019; Wegrzynowicz, et al., 2019; Levin et al., 2022). In parallel, strategies that enhance lysosomal degradation of α-synuclein may offer complementary benefits. Ambroxol, for example, boosts glucocerebrosidase activity and lysosomal function, promoting clearance of misfolded protein and reducing oxidative stress (Colucci et al, 2023). Understanding how pathological processes are shaped by microglia is particularly important, as these cells can act as both contributors to and modulators of neurodegeneration. To unravel their complex role, there is a critical need for physiologically relevant *in vitro* models that capture the most essential functional properties of microglia. These therapeutic candidates, with their distinct mechanisms of action, offer promising avenues to intervene in disease-relevant pathways.

Taken together, our findings highlight that the 3xSNCA assembloid model recapitulates key features of Parkinson’s disease, including spontaneous pS129 accumulation and microglia-driven α-synuclein pathology. By modelling microglia–neuron interactions without exogenous fibrils, the assembloid and chimeric systems offer physiologically relevant platforms to investigate early drivers of synucleinopathies and evaluate therapeutic strategies.

Materials and methods

Ethical approval

All work involving iPSCs was approved by the Ethics Review Panel (ERP) of the University of Luxembourg and the national Luxembourgish Research Ethics Committee (CNER, Comité National d'Ethique de Recherche) under CNER No. 201901/01 (ivPD) and No. 202406/03 (AdvanceOrg).

iPSCs and NESCs

In this study, three human wildtype and one human *SNCA* triplication induced pluripotent stem cell (iPSC) lines were used, which are described in Supplementary Table 1. hiPSC were maintained in Essential E8 medium (Thermo Fisher Scientific, cat.no. A1517001) supplemented with 1% Penicillin-Streptomycin (Invitrogen, cat. no. 15140122) on Geltrex-coated plates (Corning, cat. no. 354277). They were passaged with Accutase (Sigma-Aldrich, cat. no. A6964) and cultured in E8 medium supplemented with 10 µM ROCK inhibitor Y-27632 (Merck Millipore, cat. no. 688000) for 24h after seeding (Gomez-Giro et al., 2019). Afterwards, the cells were cultured in E8 medium, with daily media exchanges.

Neuroepithelial stem cells (NESCs) were derived from iPSCs following to the protocol established by Reinhardt et al. (2013). Cells were cultured on Geltrex-coated plates in freshly prepared maintenance medium. The N2B27 base medium consisted of a 1:1 ratio of DMEM-F12 (Thermo Fisher Scientific, cat. no. 21331046) and Neurobasal (Thermo Fisher Scientific, cat. no. 10888022), supplemented with 1% GlutaMAX (Thermo Fisher Scientific, cat. no. 35050061), 1% penicillin/streptomycin (Thermo Fisher Scientific, cat. no. 15140122), 1% B27 supplement without Vitamin A (Life Technologies, cat. no. 12587001) and 2% N2 supplement (Thermo Fisher Scientific, cat. no. 17502001). For maintenance, the base medium was further supplemented with 150 µM ascorbic acid (Sigma-Aldrich, cat. no. A4544), 3 µM CHIR-99021 (Axon Medchem, cat. no. CT 99021), and 0.75 µM purmorphamine (Enzo Life Science, cat. no. ALX-420-045). NESC maintenance medium was replaced every other day.

Microglia

Macrophage precursors were generated from iPSCs (van Wilgenburg et al., 2013) and subsequentially differentiated into microglia as previously described previously (Haenseler, Sansom, et al., 2017). For immunofluorescence staining, 150000 macrophage precursors were seeded onto a glass coverslip placed in 24-well plates (Thermo Fisher Scientific, cat. no. 142475). For flow cytometry and phagocytosis assays, 50000 macrophage precursors were plated in 96-well plates (Thermo Fisher Scientific, cat. no. 167008). Cells were cultured in microglia base medium composed of Advanced DMEM/F12 (Thermo Fisher Scientific, cat. no.

12634010), 1% Penicillin/Streptomycin (Invitrogen, cat. no. 15140122), 1% GlutaMAX™ (Thermo Fisher Scientific, cat. no. 35050061), 1% N2 (Thermo Fisher Scientific, cat. no. 17502001) and 50 µM 2-mercaptoethanol (Thermo Fisher Scientific, cat. no. 31350-010). The medium was further supplemented with 100 ng/ml GM-CSF (PeproTech, cat. no. 300-03) and 10 ng/ml IL-34 (PeproTech, cat. no. 200-34).

Midbrain organoids

Midbrain organoids were generated from NESCs according to the protocol previously published by Monzel et al. (2017) and Zagare et al (2020) and cultured until day 50. NESCs were detached at 80% confluence with Accutase (Sigma-Aldrich, cat. no. A6964). Viable cells were counted with trypan blue, and to initiate sphere formation, 9000 live cells were seeded per well of a 96-well ultra-low attachment plate (faCellitate, cat. no. F202003) in 150 µl of NESC maintenance media. On day 2 of culture, the maintenance media was replaced with patterning media which consists of supplemented N2B27 base medium with 200 µM ascorbic acid (Sigma-Aldric, cat. no. A4544-100G), 500 µM dibutyryl-cAMP (STEMCELL Technologies, cat. no. 100-0244), 10 ng/ml hBDNF (PeproTech, cat. no. 450-02-1mg), 10 ng/ml hGDNF (PeproTech, cat. no. 450-10-1mg), 1 ng/ml TGF-β3 (PeproTech, cat. no. 100-36E) and 1 µM purmorphamine (Enzo Life Science, cat. no. ALX-420-045). The next pattering media exchange was done on day 5 of organoid culture.

Assembloids

Assembloids (ASBs) were cultured as described by Sabate-Soler et al (2022) with minor changes. On day 8 of culture midbrain organoid each midbrain organoid was co-cultured with 50000 freshly harvested macrophage precursor cells. The culture medium was changed to the co-culture medium containing the microglia base medium supplemented with 100 ng/ml GM-CSF (PeproTech, cat. no. 300-03), 10 ng/ml IL-34 (PeproTech, cat. no. 200-34), 10 ng/ml BDNF (PeproTech, cat. no. 450-02) and 10 ng/ml GDNF (PeproTech, cat. no. 450-10). The medium was changed every 3-4 days, and the assembloids was kept for 50 days in culture. After the collection, the assembloids were either snap-frozen and stored at -80°C, or fixed with 4% formaldehyde (Millipore, cat. no. 1.00496.5000) for immunofluorescence staining.
iPSC, NESC and assembloids were regularly (once per month) tested for mycoplasma contamination using LookOut® Mycoplasma PCR Detection Kit (Sigma-Aldrich, cat. no. MP0035-1KT).

Phagocytosis assay

For the phagocytosis assay, Zymosan A (S. cerevisiae) BioParticles™ (Thermo Fisher Scientific, cat. no. Z23373) or pHRodo™-Zymosan BioParticles™ Conjugate (Thermo Fisher

Scientific, cat. no. P35364) were used. 10 µg/ml of particles were prepared in HBSS medium supplemented with 20 mM HEPES and 10% FCS. 50 µl of the microglial cell culture media was removed, and 50 µl of HBSS containing Zymosan A particles was added to the microglia. The cells were then incubated at 37°C for at least 30 minutes, washed twice with PBS, and analyzed via flow cytometry with the BD LSRFortessa (BD Biosciences, RRID:SCR_018655).

Cytokine measurement

For intracellular cytokine measurement, microglia were stimulated for 24 hours with 100 ng/ml lipopolysaccharide (LPS) on day 14 of differentiation. During the final 6 hours of stimulation, BD GolgiPlug™ (BD Biosciences, cat. no. 555029) was added to the cell culture medium at a 1:1000 dilution. Microglia were then fixed and permeabilized using the BD Pharmingen™ Transcription Buffer Set (BD Biosciences, cat. no. 562574) following the manufacturer's instructions. The microglia were washed twice in PBS and immediately analysed in flow cytometer.

Western Blot

For Western blot, 10 assembloids from three batches were pooled and lysed using RIPA buffer (Abcam, cat. no. ab156034) supplemented with cOmplete™ Protease Inhibitor Cocktail (Sigma-Aldrich, cat. no. 116974980010) and Phosphatase Inhibitor Cocktail Set (Merck Millipore, cat. no. 524629). 100 µl of lysis buffer was added to the samples, disrupted by pipetting, and incubated on ice for 20 min. Lysates were sonicated for 10 cycles (30 sec on/30 sec off) using the Bioruptor Pico (Diagenode, RRID:SCR_023470). Samples were then centrifuged at 4°C for 30 min at 15,000 x *g*. The protein concentration was determined using the Pierce™ BCA Protein Assay Kit (Thermo Fisher Scientific, cat. no. 56257423225) and samples were adjusted to the same concentration and boiled at 95°C for 5 min in denaturating loading buffer. Protein separation was achieved using SDS polyacrylamide gel electrophoresis (Bolt™ 4–12% Bis-Tris Plus Gel, Thermo Fisher Scientific, cat. no. 562574NW04120BOX) and transferred onto PVDF membrane using iBlot™ 2 Gel Transfer Device (Thermo Fisher Scientific, cat. no. IB21001). Membranes were fixed with 0.4% formaldehyde for 30 min at room temperature (RT), washed with PBS containing 0.02% Tween (PBST) and blocked for 1 h at RT in 5% BSA in PBS before incubating overnight (ON) at 4°C with the primary antibodies prepared in 5% BSA in PBS-T (Supplementary Table 2). The next day, membranes were washed three times for 5 min with PBST and incubated with DyLight™ secondary antibodies at a dilution of 1:10,000 (anti-rabbit IgG (H+L) (DyLight 800 Conjugate, Cell Signaling, cat. no. 5151; RRID:AB_10697505) or anti-mouse IgG (H+L) (DyLight 680, Cell Signaling, cat. no. 5470, RRID:AB_10696895)) for 1 h at RT. Membranes were revealed in the Odyssey® Fc

2800 Imaging (LI-COR Biosciences, RRID:SCR_023227). Western blots were analysed using Image Studio Lite (LI-COR Biosciences, RRID:SCR_013715) software.

Dot Blot for α-synuclein

150 µl assembloid media was collected from three batches, snap frozen and stored at -80°C. The supernatant was thawed on ice and centrifuged at 300 x *g* to sediment any cell debris remaining in the media. A Dot Blot Minifold I (Whatman, cat. no. 10447900) was used according to manufacturer guidelines. A nitro-cellulose membrane (Sigma-Aldrich, cat. no. GE10600001) was hydrated twice with 200 µl sterile PBS per well before sample loading. After sample run with the vacuum on, the membrane was washed with 200 µl sterile PBS per well. The membrane was retrieved and fixed for 10 min at 37°C, followed by a 1 min wash with PBS to hydrate the membrane. The membrane was incubated for 5 min with Revert 700 Total Protein Stain (LI-COR Biosciences, cat. no. 926-11016), followed by two quick washed with Milli-Q water, before revealing the membrane using the Odyssey® Fc 2800 Imaging System. The membrane was then destained for 5 min with the Revert destaining Solution (LI-COR Biosciences, cat. no. 926-11016) and washed once with PBS-T. Blocking and antibody incubation were done as previously described in the Western blotting section. Images were acquired with the Odyssey® Fc 2800 Imaging System. Images were analysed with Image Studio Lite and the relative α-synuclein amount was normalized to the total protein.

Immunofluorescence staining of microglia

Macrophage precursors were plated on glass coverslips (150K/well) and cultured for 14 days. Then, mature microglia were fixed for 15 min with 4% formaldehyde (Sigma-Aldrich, cat. no. 100496) at RT and washed three times with PBS. The glass coverslips were permeabilized with 0.3% Triton X-100 in PBS for 15 min at RT. The cells were washed again three times with PBS, followed by blocking with 3% BSA (Carl Roth, cat. no. 80764) in PBS for 1h at RT. The microglia were then incubated with the primary antibodies (Supplementary Table 3) in 3% BSA, 0.3% Triton X-100 in PBS in a wet chamber ON at 4°C. Afterwards, the cells were washed three times with PBS before incubation with secondary antibody (Supplementary Table 3) in 3% BSA, 0.3% Triton X-100 in PBS in a wet chamber for 1h at RT. After three more PBS washed, the coverslips were mounted on a glass slide with Fluorormount-G® (Southern Biotech, cat. no. 0100-01).

Immunofluorescence staining of assembloid sections

Assembloids were fixed ON at 4°C with 4% formaldehyde and then washed three times with PBS for 10 min at RT. For each condition, at least three to four assembloids were embedded in 3% low-melting point agarose (Biozym, cat. no. 840100). The solidified agarose blocks with

the assembloid were sectioned using the vibrating blade microtome (Leica VT1000s, RRID:SCR_016495) at 60 µm. Sections were permeabilised with 0.5% Triton X-100 for 30 min at RT, followed by a short wash with 0.01% Triton X-100 in PBS. They were then blocked for 2h at RT with blocking buffer containing 2.5% BSA, 2.5% donkey serum, 0.01% Triton X-100 and 0.1% sodium azide in PBS. Primary antibodies (Supplementary Table 3) were diluted in blocking buffer and sections were incubated for 48-72h at 4°C on an orbital shaker. After incubation, the sections were washed with wash buffer (0.01% Triton X-100 in PBS) and incubated with secondary antibodies (Supplementary Table 3) in blocking buffer for 2h at RT and protected from light. The sections were then washed three times for 10 min at RT, rinsed with Milli-Q water and mounted as described by Nickels et al (2020).

Proteostat® Aggresome Staining of assembloid sections

After fixation and sectioning, assembloid sections were permeabilized with 0.5% Triton X-100 and 3 mM EDTA (pH 8.0) in 1x Assay Buffer for 30 min at RT on an orbital shaker. After a wash with 0.01% Triton X-100 in PBS for 5 min at RT, they were blocked in blocking buffer as described in the immunofluorescence staining method. Primary antibodies (Supplementary Table 3) were diluted in blocking solution and incubated for 48-72h at 4°C on an orbital shaker, which was followed by one wash with 0.01% Triton-X 100 in PBS for 10 min at RT. The other two washes were done with PBS for 10 min at RT each. The secondary antibodies and the Proteostat® Aggresome Detection Reagent (Enzo, cat. no. ENZ-51035) were diluted (1:1000) in 1x Assay Buffer and incubated for 1h at RT on an orbital shaker. Sections were then washed three times with PBS for 10 min at RT each. They were once washed with Milli-Q water before mounting.

Thioflavin S staining of assembloid sections

Thioflavin S staining was performed based on the method described by Stojkovska and Mazzulli (2021). Assembloid sections were fixed and sectioned as previously described and permeabilized with 0.3% Triton X-100 in PBS for 30 min at 4°C on an orbital shaker. They were then blocked for 30 min at RT on an orbital shaker with 2.5% BSA, 2.5% normal goat serum and 0.3% Triton X-100 in PBS. Assembloid sections were then incubated with the primary antibodies (Supplementary Table 3) in blocking solution and incubated ON at 4°C on an orbital shaker. Afterwards three washes with 0.01% Triton X-100 in PBS for 10 min each at RT were performed followed by incubation of secondary antibody in 0.01% Triton X-100 in PBS (Supplementary Table 3) for 2h at RT and protected from light. It is important to note that the Hoechst 33342 dye is not added in this staining protocol. Sections were then washed again three times for 10 min at RT with the washing buffer before incubation with the fresh Thioflavin S solution which consists of 0.05% Thio S (Sigma-Aldrich, cat. no. T1892) w/v in 50%

EtOH/Milli-Q water. Afterwards the assembloid sections were washed two times with 50% EtOH for 20 min at RT, before a consecutive wash with 80% EtOH for 20 min at RT. Finally, a last wash was performed with the washing buffer before rinsing the sections with Milli-Q water and mounting.

Image acquisition

For high-content imaging, mounted assembloids were imaged with the Yokogawa CellVoyager CV8000 microscope (Yokogawa, RRID:SCR_023270). A 4x pre-scan identified the wells containing assembloid sections, which enabled the creation of masks to outline the assembloids. These masks guided the selection of the field for imaging at different wavelengths with a 20x objective.

Qualitative images were acquired with the Zeiss LSM 710 confocal laser scanning microscope (Zeiss, RRID:SCR_018063) equipped with 20x or 63x objectives. Three-dimensional reconstructions of confocal Z-stacks were created using Imaris software (Bitplane, RRID:SCR_007370). Representative images were cropped, rotated, or rescaled for visualisation using Adobe Photoshop (version 26.6.1, Adobe, RRID:SCR_014199) and Illustrator (version 29.5.1, Adobe, RRID_SCR_010279). All original, unedited images are available at https://doi.org/10.17881/syhp-k282.

Image processing, and analysis

For quantitative image analysis, at least two sections from three assembloids, each derived from three independent batch generations, were analysed in MATLAB (2021a, Mathworks, RRID:SCR_001622). A custom image-analysis algorithm, as previously described by Bolognin et al. and Monzel et al. (2018, 2020), was used. This algorithm merges overlapping sections into mosaic images, performs smoothing, combines colour channels and filters out small objects. Marker-specific masks were created based on pixel intensity thresholds and refined to quantify marker intensities in 3D space (voxels).

RNA extraction, library preparation and sequencing

Total RNA of microglia was extracted from microglia using RNeasy Mini Kit (Qiagen, cat. no. 74104) according to the manufacturer's protocol. For each cell line, RNA was isolated from three pooled wells of a 6-well plate, with each well containing $1x10^6$ macrophage precursors. Messenger RNA (mRNA) was purified from total RNA with the poly-T-oligo-attached magnetic beads. Following RNA fragmentation, first-strand cDNA was synthesized using random hexamer primers. Second-strand cDNA synthesis was performed using either dUTP (for directional library) or dTTP (for non-directional library). Libraries were sequenced on an Illumina platform by Novogene's sequencing service.

Transcriptomic analysis

RNA sequencing data from microglia were pre-processed with the Galaxy server (version 23.2.rc1, RRID:SCR_006281), following established Galaxy training tutorials (Hiltemann et al., 2023, Doyle et al., 2024). Sequencing reads were aligned to the human reference genome (hg38) using HISAT2 (RRID:SCR_015530), and read counts were generated from the resulting BAM files using the *featureCounts* function. Differential gene expression analysis was conducted in R (version 4.4.2., RRID:SCR_001905) using the "DESeq2" software package (version 1.42.1, RRID:SCR_000154) (Love et al., 2014). P-values were corrected for multiple hypothesis testing according to the Benjamini-Hochberg method (Benjamini & Hochberg, 2005). Pathway enrichment analysis was performed using the EnrichR tool (RRID:SCR_001575) (Kuleshov et al., 2016), based on the expressed genes identified by DESeq2. Two gene set libraries were used for enrichment analysis: “Gene Ontology (GO) Biological Process 2023” (Ashburner et al., 2000, Aleksander et al., 2023) and “Kyoto Encyclopedia of Genes and Genomes (KEGG) Human 2021” (Kaneshisa et al., 2000, 2019, 2025).

Statistical analysis

The data in this manuscript was processed, analysed and visualised in both GraphPad Prism (GraphPad version 10.2.3, RRID:SCR_002798) or the R software (R version 4.4.2, RRID:SCR_001905). Statistical significance of non-normally distributed data was tested with a non-parametric Mann-Whitney *U* rank sum test for comparison between the two conditions (WT microglia and 3xSNCA microglia; WT ASB and 3xSNCA ASB; WT ASB and WT-3xSNCA ASB). Each data point in the graphs corresponds to the data from one cell line for one individual differentiation experiment. Significance asterisks in the figure legends represent *$p < 0.05$, **$p < 0.01$, ***$p < 0.001$, ****$p < 0.0001$. When data was found not significant, it is not specifically stated in the figures and is expressed as ns, not significant. Error bars represent mean + standard deviation (SD). Detailed information on the number (n) of samples, replicates and batches is added to the individual Figure legends.

Data availability

All original and processed data, along with the scripts supporting the findings of this study, are publicly available at this https://doi.org/10.17881/syhp-k282. Gene expression datasets have been deposited in the Gene Expression Omnibus (GEO) under the accession number GSE299260.

Code availability

All scripts used to obtain, analyse and plot the data are available at https://gitlab.com/uniluxembourg/lcsb/developmental-and-cellular-biology/zuccoli_2025.

Acknowledgments

Image and flow cytometry data acquisition were supported by the LCSB Bioimaging Platform (BIP, RRID:SCR_026352), including its flow cytometry core, at LCSB (RRID:SCR_026168) of the University of Luxembourg (RRID:SCR_011632). We acknowledge Novogene for their RNA sequencing service and we would also like to thank Daniela Frangenberg-Hoff, Raquel Forte Marques and Mona Tuzza for excellent technical assistance.

This project has received funding from the i2TRON Doctoral Training Unit (PRIDE19/14254520) which is funded by the Luxembourg National Research Fund (FNR).

Rights retention statement: This research was funded in whole by the FNR-Luxembourg. For the purpose of Open Access, the author has applied a CC BY public copyright license to any Author Accepted Manuscript (AAM) version arising from this submission.

Author Contributions

E.Z. conceived, designed, collected data, performed data analysis, and interpretation of results. S.S.S., A.Z. and I.R. performed data analysis. H.K., A.S.Z. contributed with experiments. The work was supervised by J.C.S., E.Z. wrote the original manuscript. E.Z., H.K., S.S.S., A.Z., I.R., A.S.Z and J.C.S. revised and edited the manuscript.

Competing interests

J.C.S. declare no competing non-financial interests but declare competing financial interests as cofounders and shareholders of OrganoTherapeutics société à responsabilité limitée (SARL). The remaining authors declare no competing interests.

References

Kalia, L. V., & Lang, A. E. (2015). Parkinson's disease. *The Lancet*, *386*(9996), 896-912.

Poewe, W., Seppi, K., Tanner, C. M., Halliday, G. M., Brundin, P., Volkmann, J., ... & Lang, A. E. (2017). Parkinson disease. *Nature reviews Disease Primers, 3*(1), 1-21.

Spillantini, M. G., Crowther, R. A., Jakes, R., Hasegawa, M., & Goedert, M. (1998). α-Synuclein in filamentous inclusions of Lewy bodies from Parkinson's disease and dementia with Lewy bodies. *Proceedings of the National Academy of Sciences*, *95*(11), 6469-6473.

Goedert, M. (2015). Alzheimer's and Parkinson's diseases: The prion concept in relation to assembled Aβ, tau, and α-synuclein. *Science*, *349*(6248), 1255555.

Lashuel, H. A., Overk, C. R., Oueslati, A., & Masliah, E. (2013). The many faces of α-synuclein: from structure and toxicity to therapeutic target. *Nature Reviews Neuroscience*, *14*(1), 38-48.

Fujiwara, H., Hasegawa, M., Dohmae, N., Kawashima, A., Masliah, E., Goldberg, M. S., ... & Iwatsubo, T. (2002). α-Synuclein is phosphorylated in synucleinopathy lesions. *Nature Cell Biology*, *4*(2), 160-164.

Bernal-Conde, L. D., Ramos-Acevedo, R., Reyes-Hernández, M. A., Balbuena-Olvera, A. J., Morales-Moreno, I. D., Argüero-Sánchez, R., ... & Guerra-Crespo, M. (2020). Alpha-synuclein physiology and pathology: a perspective on cellular structures and organelles. *Frontiers in Neuroscience*, *13*, 1399.

Plotegher, N., & Duchen, M. R. (2017). Crosstalk between lysosomes and mitochondria in Parkinson's disease. *Frontiers in Cell and Developmental Biology*, *5*, 110.

Calabresi, P., Mechelli, A., Natale, G., Volpicelli-Daley, L., Di Lazzaro, G., & Ghiglieri, V. (2023). Alpha-synuclein in Parkinson's disease and other synucleinopathies: from overt neurodegeneration back to early synaptic dysfunction. *Cell Death & Disease*, *14*(3), 176.

Stefanis, L. (2012). α-Synuclein in Parkinson's disease. *Cold Spring Harbor Perspectives in Medicine*, *2*(2), a009399.

Calabresi, P., Di Lazzaro, G., Marino, G., Campanelli, F., & Ghiglieri, V. (2023). Advances in understanding the function of alpha-synuclein: Implications for Parkinson's disease. *Brain*, *146*(9), 3587-3597.

Kawahata, I., Finkelstein, D. I., & Fukunaga, K. (2022). Pathogenic impact of α-synuclein phosphorylation and its kinases in α-synucleinopathies. *International Journal of Molecular Sciences*, *23*(11), 6216.

Polymeropoulos, M. H., Lavedan, C., Leroy, E., Ide, S. E., Dehejia, A., Dutra, A., ... & Nussbaum, R. L. (1997). Mutation in the α-synuclein gene identified in families with Parkinson's disease. *Science*, *276*(5321), 2045-2047.

Krüger, R., Kuhn, W., Müller, T., Woitalla, D., Graeber, M., Kösel, S., ... & Riess, O. (1998). AlaSOPro mutation in the gene encoding α-synuclein in Parkinson's disease. *Nature Genetics*, *18*(2), 106-108.

Zarranz, J. J., Alegre, J., Gómez-Esteban, J. C., Lezcano, E., Ros, R., Ampuero, I., ... & de Yebenes, J. G. (2004). The new mutation, E46K, of α-synuclein causes parkinson and Lewy body dementia. *Annals of Neurology: Official Journal of the American Neurological Association and the Child Neurology Society*, *55*(2), 164-173.

Ibáñez, P., Bonnet, A. M., Debarges, B., Lohmann, E., Tison, F., Agid, Y., ... & Pollak, P. (2004). Causal relation between α-synuclein locus duplication as a cause of familial Parkinson's disease. *The Lancet*, 364(9440), 1169-1171.

Singleton, A., Farrer, M., Johnson, J., Singleton, A., Hague, S., Kachergus, J., ... & Gwinn-Hardy, K. (2003). α-Synuclein locus triplication causes Parkinson's disease. *Science*, *302*(5646), 841-841.

Sulzer, D., & Edwards, R. H. (2019). The physiological role of α-synuclein and its relationship to Parkinson’s Disease. *Journal of Neurochemistry*, *150*(5), 475-486.

Burré, J. (2015). The synaptic function of α-synuclein. *Journal of Parkinson’s Disease*, *5*(4), 699-713.

Takahashi, K., & Yamanaka, S. (2006). Induction of pluripotent stem cells from mouse embryonic and adult fibroblast cultures by defined factors. *Cell*, *126*(4), 663-676.

Monzel, A. S., Smits, L. M., Hemmer, K., Hachi, S., Moreno, E. L., van Wuellen, T., ... & Schwamborn, J. C. (2017). Derivation of human midbrain-specific organoids from neuroepithelial stem cells. *Stem Cell Reports*, *8*(5), 1144-1154.

Smits, L. M., Reinhardt, L., Reinhardt, P., Glatza, M., Monzel, A. S., Stanslowsky, N., ... & Schwamborn, J. C. (2019). Modeling Parkinson’s disease in midbrain-like organoids. *npj Parkinson's Disease*, *5*(1), 5.

Rosety, I., Zagare, A., Saraiva, C., Nickels, S., Antony, P., Almeida, C., ... & Schwamborn, J. C. (2023). Impaired neuron differentiation in GBA-associated Parkinson's disease is linked to cell cycle defects in organoids. *npj Parkinson's Disease*, *9*(1), 166.

Kim, H., Park, H. J., Choi, H., Chang, Y., Park, H., Shin, J., ... & Kim, J. (2019). Modeling G2019S-LRRK2 sporadic Parkinson's disease in 3D midbrain organoids. *Stem Cell Reports*, *12*(3), 518-531.

Jarazo, J., Barmpa, K., Modamio, J., Saraiva, C., Sabaté-Soler, S., Rosety, I., ... & Schwamborn, J. C. (2022). Parkinson's disease phenotypes in patient neuronal cultures and brain organoids improved by 2-hydroxypropyl-β-cyclodextrin treatment. *Movement Disorders*, *37*(1), 80-94.

Muwanigwa, M. N., Modamio-Chamarro, J., Antony, P. M., Gomez-Giro, G., Krüger, R., Bolognin, S., & Schwamborn, J. C. (2024). Alpha-synuclein pathology is associated with astrocyte senescence in a midbrain organoid model of familial Parkinson's disease. *Molecular and Cellular Neuroscience*, *128*, 103919.

Thion, M. S., Ginhoux, F., & Garel, S. (2018). Microglia and early brain development: An intimate journey. *Science*, *362*(6411), 185-189.

Ginhoux, F., Greter, M., Leboeuf, M., Nandi, S., See, P., Gokhan, S., ... & Merad, M. (2010). Fate mapping analysis reveals that adult microglia derive from primitive macrophages. *Science*, *330*(6005), 841-845.

Li, Q., & Barres, B. A. (2018). Microglia and macrophages in brain homeostasis and disease. *Nature Reviews Immunology*, *18*(4), 225-242.

Schulz, C., Perdiguero, E. G., Chorro, L., Szabo-Rogers, H., Cagnard, N., Kierdorf, K., ... & Geissmann, F. (2012). A lineage of myeloid cells independent of Myb and hematopoietic stem cells. *Science*, *336*(6077), 86-90.

Tremblay, M. È., Stevens, B., Sierra, A., Wake, H., Bessis, A., & Nimmerjahn, A. (2011). The role of microglia in the healthy brain. *Journal of Neuroscience*, *31*(45), 16064-16069.

Wake, H., Moorhouse, A. J., Jinno, S., Kohsaka, S., & Nabekura, J. (2009). Resting microglia directly monitor the functional state of synapses in vivo and determine the fate of ischemic terminals. *Journal of Neuroscience*, *29*(13), 3974-3980.

Ormel, P. R., Vieira de Sá, R., Van Bodegraven, E. J., Karst, H., Harschnitz, O., Sneeboer, M. A., ... & Pasterkamp, R. J. (2018). Microglia innately develop within cerebral organoids. *Nature Communications*, *9*(1), 4167.

Shabab, T., Khanabdali, R., Moghadamtousi, S. Z., Kadir, H. A., & Mohan, G. (2017). Neuroinflammation pathways: a general review. *International Journal of Neuroscience*, *127*(7), 624-633.

Sabate-Soler, S., Nickels, S. L., Saraiva, C., Berger, E., Dubonyte, U., Barmpa, K., ... & Schwamborn, J. C. (2022). Microglia integration into human midbrain organoids leads to increased neuronal maturation and functionality. *Glia*, *70*(7), 1267-1288.

Cakir, B., Kiral, F. R., & Park, I. H. (2022). Advanced in vitro models: microglia in action. *Neuron*, *110*(21), 3444-3457.

Toh, H. S., Choo, X. Y., & Sun, A. X. (2023). Midbrain organoids—development and applications in Parkinson's disease. *Oxford Open Neuroscience*, *2*, kvad009.

Sabate-Soler, S., Kurniawan, H., & Schwamborn, J. C. (2024). Advanced brain organoids for neuroinflammation disease modeling. *Neural Regeneration Research*, *19*(1), 154-155.

Haenseler, W., Zambon, F., Lee, H., Vowles, J., Rinaldi, F., Duggal, G., ... & Cowley, S. A. (2017). Excess α-synuclein compromises phagocytosis in iPSC-derived macrophages. *Scientific Reports*, *7*(1), 9003.

Gomez-Giro, G., Arias-Fuenzalida, J., Jarazo, J., Zeuschner, D., Ali, M., Possemis, N., ... & Schwamborn, J. C. (2019). Synapse alterations precede neuronal damage and storage pathology in a human cerebral organoid model of CLN3-juvenile neuronal ceroid lipofuscinosis. *Acta Neuropathologica Communications*, *7*, 1-19.

Reinhardt, P., Glatza, M., Hemmer, K., Tsytsyura, Y., Thiel, C. S., Höing, S., ... & Sterneckert, J. (2013). Derivation and expansion using only small molecules of human neural progenitors for neurodegenerative disease modeling. *PloS one*, *8*(3), e59252.

Wilgenburg, B. V., Browne, C., Vowles, J., & Cowley, S. A. (2013). Efficient, long term production of monocyte-derived macrophages from human pluripotent stem cells under partly-defined and fully-defined conditions. *PloS one*, *8*(8), e71098.

Haenseler, W., Sansom, S. N., Buchrieser, J., Newey, S. E., Moore, C. S., Nicholls, F. J., ... & Cowley, S. A. (2017). A highly efficient human pluripotent stem cell microglia model displays a neuronal-co-culture-specific expression profile and inflammatory response. *Stem Cell Reports*, *8*(6), 1727-1742.

Zagare, A., Gobin, M., Monzel, A. S., & Schwamborn, J. C. (2021). A robust protocol for the generation of human midbrain organoids. *STAR protocols*, *2*(2), 100524.

Nickels, S. L., Modamio, J., Mendes-Pinheiro, B., Monzel, A. S., Betsou, F., & Schwamborn, J. C. (2020). Reproducible generation of human midbrain organoids for in vitro modeling of Parkinson's disease. *Stem Cell Research*, *46*, 101870.

Stojkovska, I., & Mazzulli, J. R. (2021). Detection of pathological alpha-synuclein aggregates in human iPSC-derived neurons and tissue. *STAR protocols*, *2*(1), 100372.

Bolognin, S., Fossépré, M., Qing, X., Jarazo, J., Ščančar, J., Moreno, E. L., ... & Schwamborn, J. C. (2019). 3D cultures of Parkinson's disease-specific dopaminergic neurons for high content phenotyping and drug testing. *Advanced Science*, *6*(1), 1800927.

Monzel, A. S., Hemmer, K., Kaoma, T., Smits, L. M., Bolognin, S., Lucarelli, P., ... & Schwamborn, J. C. (2020). Machine learning-assisted neurotoxicity prediction in human midbrain organoids. *Parkinsonism & Related Disorders*, *75*, 105-109.

Hiltemann, S., Rasche, H., Gladman, S., Hotz, H. R., Larivière, D., Blankenberg, D., ... & Batut, B. (2023). Galaxy Training: A powerful framework for teaching!. *PLoS computational biology*, *19*(1), e1010752.

Doyle, M., Phipson, B., & Dashnow, H. (2024). 1: RNA-Seq reads to counts.

Love, M. I., Huber, W., & Anders, S. (2014). Moderated estimation of fold change and dispersion for RNA-seq data with DESeq2. *Genome Biology*, *15*, 1-21.

Benjamini, Y., & Hochberg, Y. (1995). Controlling the false discovery rate: a practical and powerful approach to multiple testing. *Journal of the Royal statistical society: series B (Methodological)*, *57*(1), 289-300.

Kuleshov, M. V., Jones, M. R., Rouillard, A. D., Fernandez, N. F., Duan, Q., Wang, Z., ... & Ma'ayan, A. (2016). Enrichr: a comprehensive gene set enrichment analysis web server 2016 update. *Nucleic acids research*, *44*(W1), W90-W97.

Kanehisa, M., Furumichi, M., Sato, Y., Matsuura, Y., & Ishiguro-Watanabe, M. (2025). KEGG: biological systems database as a model of the real world. *Nucleic Acids Research*, *53*(D1), D672-D677.

Kanehisa, M. (2019). Toward understanding the origin and evolution of cellular organisms. *Protein Science*, *28*(11), 1947-1951.

Kanehisa, M., & Goto, S. (2000). KEGG: kyoto encyclopedia of genes and genomes. *Nucleic acids research*, *28*(1), 27-30.

Ashburner, M., Ball, C. A., Blake, J. A., Botstein, D., Butler, H., Cherry, J. M., ... & Sherlock, G. (2000). Gene ontology: tool for the unification of biology. *Nature Genetics*, *25*(1), 25-29.

Aleksander, S. A., Balhoff, J., Carbon, S., Cherry, J. M., Drabkin, H. J., Ebert, D., ... & Zarowiecki, M. (2023). The gene ontology knowledgebase in 2023. *Genetics*, *224*(1), iyad031.

Tansey, M. G., Wallings, R. L., Houser, M. C., Herrick, M. K., Keating, C. E., & Joers, V. (2022). Inflammation and immune dysfunction in Parkinson disease. *Nature Reviews Immunology*, *22*(11), 657-673.

Lieberman, R., Elnaggar, K., Jesseman, K., DeFrancisco, S., Degouveia, K., Suneby, E., ... & Graef, J. D. (2022). Elevated α-synuclein attenuates phagocytosis in SNCA triplication human iPSC-derived neuron: microglia co-cultures. *bioRxiv*, 2022-11.

Zhang, W., Wang, T., Pei, Z., Miller, D. S., Wu, X., Block, M. L., ... & Zhang, J. (2005). Aggregated α-synuclein activates microglia: a process leading to disease progression in Parkinson's disease. *The FASEB Journal*, *19*(6), 533-542.

Klegeris, A., Pelech, S., Giasson, B. I., Maguire, J., Zhang, H., McGeer, E. G., & McGeer, P. L. (2008). α-Synuclein activates stress signaling protein kinases in THP-1 cells and microglia. *Neurobiology of Aging*, *29*(5), 739-752.

Ferreira, S. A., & Romero-Ramos, M. (2018). Microglia response during Parkinson's disease: alpha-synuclein intervention. *Frontiers in cellular neuroscience, 12*, 247.

Thi Lai, T., Kim, Y. E., Nguyen, L. T. N., Thi Nguyen, T., Kwak, I. H., Richter, F., ... & Ma, H. I. (2024). Microglial inhibition alleviates alpha-synuclein propagation and neurodegeneration in Parkinson's disease mouse model. *npj Parkinson's Disease*, *10*(1), 32.

Zhu, R., Luo, Y., Li, S., & Wang, Z. (2022). The role of microglial autophagy in Parkinson's disease. *Frontiers in Aging Neuroscience*, *14*, 1039780.

Spillantini, M. G., Schmidt, M. L., Lee, V. M. Y., Trojanowski, J. Q., Jakes, R., & Goedert, M. (1997). α-Synuclein in Lewy bodies. *Nature*, *388*(6645), 839-840.

Samuel, F., Flavin, W. P., Iqbal, S., Pacelli, C., Renganathan, S. D. S., Trudeau, L. E., ... & Tandon, A. (2016). Effects of serine 129 phosphorylation on α-synuclein aggregation, membrane association, and internalization. *Journal of Biological Chemistry*, *291*(9), 4374-4385.

Gallegos, S., Pacheco, C., Peters, C., Opazo, C. M., & Aguayo, L. G. (2015). Features of alpha-synuclein that could explain the progression and irreversibility of Parkinson's disease. *Frontiers in Neuroscience*, *9*, 59.

Xu, Y., Deng, Y., & Qing, H. (2015). The phosphorylation of α-synuclein: development and implication for the mechanism and therapy of the Parkinson's disease. *Journal of Neurochemistry*, *135*(1), 4-18.

Henderson, M. X., Trojanowski, J. Q., & Lee, V. M. Y. (2019). α-Synuclein pathology in Parkinson's disease and related α-synucleinopathies. *Neuroscience letters*, *709*, 134316.

Becerra-Calixto, A., Mukherjee, A., Ramirez, S., Sepulveda, S., Sinha, T., Al-Lahham, R., ... & Soto, C. (2023). Lewy body-like pathology and loss of dopaminergic neurons in midbrain organoids derived from familial Parkinson's disease patient. *Cells*, *12*(4), 625.

Mohamed, N. V., Sirois, J., Ramamurthy, J., Mathur, M., Lépine, P., Deneault, E., ... & Durcan, T. M. (2021). Midbrain organoids with an SNCA gene triplication model key features of synucleinopathy. *Brain Communications*, *3*(4), fcab223.

Jo, J., Yang, L., Tran, H. D., Yu, W., Sun, A. X., Chang, Y. Y., ... & Je, H. S. (2021). Lewy Body–like Inclusions in Human Midbrain Organoids Carrying Glucocerebrosidase and α-Synuclein Mutations. *Annals of Neurology*, *90*(3), 490-505.

Oliveira, L. M. A., Falomir-Lockhart, L. J., Botelho, M. G., Lin, K. H., Wales, P., Koch, J. C., ... & Jovin, T. M. (2015). Elevated α-synuclein caused by SNCA gene triplication impairs neuronal differentiation and maturation in Parkinson's patient-derived induced pluripotent stem cells. *Cell death & disease*, *6*(11), e1994-e1994.

Canerina-Amaro, A., Pereda, D., Diaz, M., Rodriguez-Barreto, D., Casañas-Sánchez, V., Heffer, M., ... & Marin, R. (2019). Differential aggregation and phosphorylation of alpha synuclein in membrane compartments associated with Parkinson disease. *Frontiers in Neuroscience*, *13*, 382.

Kuusisto, E., Parkkinen, L., & Alafuzoff, I. (2003). Morphogenesis of Lewy bodies: dissimilar incorporation of α-synuclein, ubiquitin, and p62. *Journal of Neuropathology & Experimental Neurology*, *62*(12), 1241-1253.

Rocha, E. M., De Miranda, B., & Sanders, L. H. (2018). Alpha-synuclein: Pathology, mitochondrial dysfunction and neuroinflammation in Parkinson's disease. *Neurobiology of disease*, *109*, 249-257.

Lee, H. J., Shin, S. Y., Choi, C., Lee, Y. H., & Lee, S. J. (2002). Formation and removal of α-synuclein aggregates in cells exposed to mitochondrial inhibitors. *Journal of Biological Chemistry*, *277*(7), 5411-5417.

Di Maio, R., Barrett, P. J., Hoffman, E. K., Barrett, C. W., Zharikov, A., Borah, A., ... & Greenamyre, J. T. (2016). α-Synuclein binds to TOM20 and inhibits mitochondrial protein import in Parkinson's disease. *Science Translational Medicine*, *8*(342), 342ra78-342ra78.

Luk, K. C., Song, C., O'Brien, P., Stieber, A., Branch, J. R., Brunden, K. R., ... & Lee, V. M. Y. (2009). Exogenous α-synuclein fibrils seed the formation of Lewy body-like intracellular inclusions in cultured cells. *Proceedings of the National Academy of Sciences*, *106*(47), 20051-20056.

Volpicelli-Daley, L. A., Luk, K. C., Patel, T. P., Tanik, S. A., Riddle, D. M., Stieber, A., ... & Lee, V. M. Y. (2011). Exogenous α-synuclein fibrils induce Lewy body pathology leading to synaptic dysfunction and neuron death. *Neuron*, *72*(1), 57-71.

Osterberg, V. R., Spinelli, K. J., Weston, L. J., Luk, K. C., Woltjer, R. L., & Unni, V. K. (2015). Progressive aggregation of alpha-synuclein and selective degeneration of lewy inclusion-bearing neurons in a mouse model of parkinsonism. *Cell Reports*, *10*(8), 1252-1260.

Mahul-Mellier, A. L., Burtscher, J., Maharjan, N., Weerens, L., Croisier, M., Kuttler, F., ... & Lashuel, H. A. (2020). The process of Lewy body formation, rather than simply α-synuclein fibrillization, is one of the major drivers of neurodegeneration. *Proceedings of the National Academy of Sciences*, *117*(9), 4971-4982.

Awa, S., Suzuki, G., Masuda-Suzukake, M., Nonaka, T., Saito, M., & Hasegawa, M. (2022). Phosphorylation of endogenous α-synuclein induced by extracellular seeds initiates at the pre-synaptic region and spreads to the cell body. *Scientific Reports*, *12*(1), 1163.

Cuervo, A. M., Stefanis, L., Fredenburg, R., Lansbury, P. T., & Sulzer, D. (2004). Impaired degradation of mutant α-synuclein by chaperone-mediated autophagy. *Science*, *305*(5688), 1292-1295.

Martinez-Vicente, M., Talloczy, Z., Kaushik, S., Massey, A. C., Mazzulli, J., Mosharov, E. V., ... & Cuervo, A. M. (2008). Dopamine-modified α-synuclein blocks chaperone-mediated autophagy. *The Journal of Clinical Investigation*, *118*(2), 777-788.

Snyder, H., Mensah, K., Theisler, C., Lee, J., Matouschek, A., & Wolozin, B. (2003). Aggregated and monomeric α-synuclein bind to the S6′ proteasomal protein and inhibit proteasomal function. *Journal of Biological Chemistry*, *278*(14), 11753-11759.

Winslow, A. R., Chen, C. W., Corrochano, S., Acevedo-Arozena, A., Gordon, D. E., Peden, A. A., ... & Rubinsztein, D. C. (2010). α-Synuclein impairs macroautophagy: implications for Parkinson's disease. *Journal of Cell Biology*, *190*(6), 1023-1037.

Zhang, W., Wang, T., Pei, Z., Miller, D. S., Wu, X., Block, M. L., ... & Zhang, J. (2005). Aggregated α-synuclein activates microglia: a process leading to disease progression in Parkinson's disease. *The FASEB Journal*, *19*(6), 533-542.

Hickman, S., Izzy, S., Sen, P., Morsett, L., & El Khoury, J. (2018). Microglia in neurodegeneration. *Nature Neuroscience*, *21*(10), 1359-1369.

Bido, S., Muggeo, S., Massimino, L., Marzi, M. J., Giannelli, S. G., Melacini, E., ... & Broccoli, V. (2021). Microglia-specific overexpression of α-synuclein leads to severe dopaminergic neurodegeneration by phagocytic exhaustion and oxidative toxicity. *Nature Communications*, *12*(1), 6237.

Perni, M., Galvagnion, C., Maltsev, A., Meisl, G., Müller, M. B., Challa, P. K., ... & Dobson, C. M. (2017). A natural product inhibits the initiation of α-synuclein aggregation and suppresses its toxicity. *Proceedings of the National Academy of Sciences*, *114*(6), E1009-E1017.

Yang, K., Lv, Z., Zhao, W., Lai, G., Zheng, C., Qi, F., ... & Zheng, W. (2024). The potential of natural products to inhibit abnormal aggregation of α-Synuclein in the treatment of Parkinson's disease. *Frontiers in Pharmacology*, *15*, 1468850.

Rao, M. N., Shinnar, A. E., Noecker, L. A., Chao, T. L., Feibush, B., Snyder, B., ... & Zasloff, M. (2000). Aminosterols from the dogfish shark Squalus acanthias. *Journal of natural products*, *63*(5), 631-635.

Price, D. L., Khan, A., Angers, R., Cardenas, A., Prato, M. K., Bani, M., ... & Biere, A. L. (2023). In vivo effects of the alpha-synuclein misfolding inhibitor minzasolmin supports clinical development in Parkinson's disease. *npj Parkinson's Disease*, *9*(1), 114.

Heras-Garvin, A., Weckbecker, D., Ryazanov, S., Leonov, A., Griesinger, C., Giese, A., ... & Stefanova, N. (2019). Anle138b modulates α-synuclein oligomerization and prevents motor decline and neurodegeneration in a mouse model of multiple system atrophy. *Movement Disorders*, *34*(2), 255-263.

Wegrzynowicz, M., Bar-On, D., Calo', L., Anichtchik, O., Iovino, M., Xia, J., ... & Spillantini, M. G. (2019). Depopulation of dense α-synuclein aggregates is associated with rescue of dopamine neuron dysfunction and death in a new Parkinson's disease model. *Acta Neuropathologica*, *138*, 575-595.

Levin, J., Sing, N., Melbourne, S., Morgan, A., Mariner, C., Spillantini, M. G., ... & Giese, A. (2022). Safety, tolerability and pharmacokinetics of the oligomer modulator anle138b with exposure levels sufficient for therapeutic efficacy in a murine Parkinson model: A randomised, double-blind, placebo-controlled phase 1a trial. *EBioMedicine*, *80*.

Colucci, F., Avenali, M., De Micco, R., Poli, M. F., Cerri, S., Stanziano, M., ... & Cilia, R. (2023). Ambroxol as a disease-modifying treatment to reduce the risk of cognitive impairment in GBA-associated Parkinson's disease: a multicentre, randomised, double-blind, placebo-controlled, phase II trial. The AMBITIOUS study protocol. *BMJ Neurology Open*, *5*(2), e000535.

Figure Legends

Figure 1: 3xSNCA iPSC-derived microglia express α-synuclein and functional deficits. (a) Schematic representation of iPSC-derived microglia via macrophage precursors (pMacPre). (b) Representative immunofluorescence staining of mature (day 14) WT, 3xSNCA and KO microglia for the microglial marker P2RY12 (Purinergic Receptor P2Y12), total α-synuclein and a DNA marker (Hoechst 33342) (scale bar 20 µm, 63x). (c) Representative dot blot (right panel) of total protein (Revert700) and anti-α-synuclein antibody showing higher levels of extracellular α-synuclein released by 3xSNCA microglia compared to WT microglia (left panel) at day 14. Data is represented as boxplots and shows the mean of two technical replicates normalized to the total protein (Revert700) of three independent microglia batches (n=3). Mann-Whitney *U* test; **p < 0. 01. Dot blots are cropped from original images found in Supplementary original blots. (d) Flow cytometry analysis of microglial phagocytosis in WT and 3xSNCA microglia using fluorescently labelled Zymosan beads (left panel) and pH sensitive fluorescent Zymosan beads (pHRodo) (right panel). Data is represented as bar plots and shows three independent batches (n=3) normalized to the mean of the controls per batch. Mann-Whitney *U* test; ****p < 0.0001. (e) Flow cytometry analysis of intracellular IL-1β (upper left panel), TNF-α (upper right panel), IL-6 (lower left panel) and IFN-γ (lower right panel) in WT and 3xSNCA microglia after 24h stimulation with LPS. Data is represented as bar plots and shows three independent batches (n=3) normalized to the mean of the controls per batch. Mann-Whitney *U* test; *p<0.05, ***p<0.001, ****p < 0.0001. (f) GO pathway enrichment analysis of the DEGs (p.adjusted <0.01) between 3xSNCA and WT samples, showing the top 10 significantly enriched pathways based on EnrichR results. (g) KEGG pathway enrichment analysis of the DEGs (p.adjusted <0.01) between 3xSNCA and WT samples, showing the top 10 significantly enriched pathways based on EnrichR results. (h) Log_2 fold changes (FC) of predefined genes associated with phagocytosis (blue), the lysosomal pathway (orange), or both pathways (phagolysosomal, magenta).

Figure 2: 3xSNCA microglia integrated into midbrain organoids display morphological differences. (a) Schematic representation of microglia integration into the midbrain organoid. At day 8 of culture, macrophage precursor cells are added to the midbrain organoid and the assembloids are culture until 50 days of culture. WT microglia are integrated into the WT midbrain organoid, and 3xSNCA patient-derived microglia into the 3xSNCA midbrain organoid. (b) Representative immunofluorescence staining of WT assembloids (WT ASB) and 3xSNCA assembloids (3xSNCA ASB) with the dopaminergic neuron marker TH (tyrosine hydroxylase), the neuronal marker MAP2 (Microtubule-associated protein 2), the astrocyte marker S100β (S100 calcium-binding protein B) and Hoechst 33342. (c) Representative immunofluorescence staining of WT ASBs and 3xSNCA ASBs with the microglial marker IBA1

(Ionized calcium-binding adaptor molecule 1), the astrocyte marker GFAP (Glial fibrillary acidic protein) and Hoechst 33342 (scale bar 100 µm, 20x; 20 µm, 63x). (d) Representative immunofluorescence staining of WT and 3xSNCA microglia integrated into midbrain organoids stained with the microglial marker IBA1 and Hoechst 33342 (scale bar 100 µm, 20x; 20 µm, 63x). 3D reconstruction with IMARIS software showing the microglial morphology of the WT and 3xSNCA microglia in the midbrain organoid. (e) High-content automated image analysis of immunofluorescence stainings showing the foldchange of IBA1 skeleton in microglia. Data is represented as boxplots and show three to four independent batches (n=3-4) normalized to the mean IBA1 skeleton value within each batch. Mann-Whitney *U* test; **p < 0.01.

Figure 3: 3xSNCA assembloids exhibit elevated total α-synuclein and phospho-α-synuclein (pS129) levels. (a) Representative immunoblots of α-synuclein, phospho-α-synuclein (pS129) and β-actin of day 50 WT and 3xSNCA ASBs. Western blots are cropped from original images found in Supplementary original blots. (b) Quantification of α-synuclein and phospho-α-synuclein (pS129) protein levels. Data is shown as boxplots and represents a summary of three to four independent batches (n=3-4) per cell line. Values are normalized to β-actin levels. Mann-Whitney *U* test; *p < 0.05, **p < 0.01. (c) Representative immunofluorescence staining of WT and 3xSNCA ASBs with total α-synuclein, pS129 and Hoechst 33342 (scale bar 100 µm, 20x; 20 µm, 63x). (d) High-content automated image analysis of immunofluorescence stainings showing the foldchange of α-synuclein (left panel) and pS129 (right panel) normalized by total nuclei. Data is shown as boxplots and represents three to four independent batches (n=3-4) normalized to the mean of the controls per batch. Mann-Whitney *U* test; ***p < 0.001. (e) Representative dot blot (left panel) of total protein (Revert700) and anti-a-synuclein antibody showing higher levels of extracellular α-synuclein released by 3xSNCA ASBs (right panel) at 50 days. The Boxplots represents three to four independent batches (n=3-4) normalized to the total protein (Revert700). Mann-Whitney *U* test; ****p < 0.0001. Rep = replicate. Dot blots are cropped from original image found in Supplementary original blots.

Figure 4: 3xSNCA microglia promote endogenous formation of phospho-α-synuclein (pS129) pathology in assembloids. (a) Representative image of the morphological diversity of pS129 in 3xSNCA ASBs. The ring-like (upper panel), the filamentous-like (middle panel) and the dense-like (lower panel) can be distinguished with the pS129 marker (scale bar 20 µm, 63x). Zoom in of inset shows the pS129 structures (scale bar 5 µm). 3D reconstruction with IMARIS software shows the pS129 structural morphology. (b) Representative immunofluorescence staining of WT and 3xSNCA ASBs with total α-synuclein, Proteostat, p62 (SQSTM1) and Hoechst 33342 (scale bar 20 µm, 63x; 5 µm, zoom in of inset). (c) *Top panel:* The same representative image of 3xSNCA ASB as shown in (b), displayed here with total α-

synuclein, Proteostat, and p62 (SQSTM1) markers (Hoechst omitted). *Lower panel:* 3D reconstruction of this image using IMARIS software (scale bar, 5 µm; zoom-in of inset). (d) High-content automated image analysis of immunofluorescence stainings showing the foldchange of α-synuclein+, p62+, Proteostat+ normalized by total nuclei. Data is shown as boxplots and represents three independent batches (n=3) normalized to the mean of the controls per batch. Mann-Whitney *U* test; ****p < 0.0001. (e) Representative immunofluorescence staining of WT and 3xSNCA ASBs with pS129, Ubiquitin and Hoechst 33342 (scale bar 20 µm, 63x; 5 µm, zoom in of inset). (f) *Left panel:* The same representative image of 3xSNCA ASB as shown in (e) displayed here with pS129 and Ubiquitin markers (Hoechst omitted). *Right panel:* 3D reconstruction of this image using IMARIS software (right panel) of 3xSNCA with (scale bar 5 µm, zoom in of inset).

Figure 5: 3xSNCA microglia are sufficient to form pS129 pathology in WT midbrain organoids. (a) Schematic representation of the chimeric assembloid model. WT microglia are integrated into the WT midbrain organoid (WT ASB), and 3xSNCA microglia into the WT midbrain organoid (WT-3xSNCA ASB). (b) High-content automated image analysis of immunofluorescence stainings showing the foldchange of α-synuclein (left panel) and pS129 (right panel) normalized by total nuclei. Data is shown as boxplots and represents three to four independent batches (n=3-4) normalized to the mean of the controls per batch. Mann-Whitney *U* test; *p < 0.05, ***p < 0.001. (c) Representative image of pS129 structures in 3xSNCA-WT ASBs. Sections were stained with pS129 marker and Hoechst 33342 (scale bar 100 µm, 20x; 20 µm, 63x; 5 µm, zoom in of inset). 3D reconstruction with IMARIS software shows the pS129 structural morphology. (d) Representative immunofluorescence staining of WT and WT-3xSNCA ASBs with total α-synuclein, Proteostat, p62 (SQSTM1) and Hoechst 33342 (scale bar 20 µm, 63x; 5 µm, zoom in of inset) and 3D reconstruction with IMARIS software (scale bar 5 µm, zoom in of inset). (e) High-content automated image analysis of immunofluorescence stainings showing the foldchange of α-synuclein+, p62+, Proteostat+ normalized by total nuclei. Data is shown as boxplots and represents three independent batches (n=3) normalized to the mean of the controls per batch. Mann-Whitney *U* test; ****p < 0.0001.

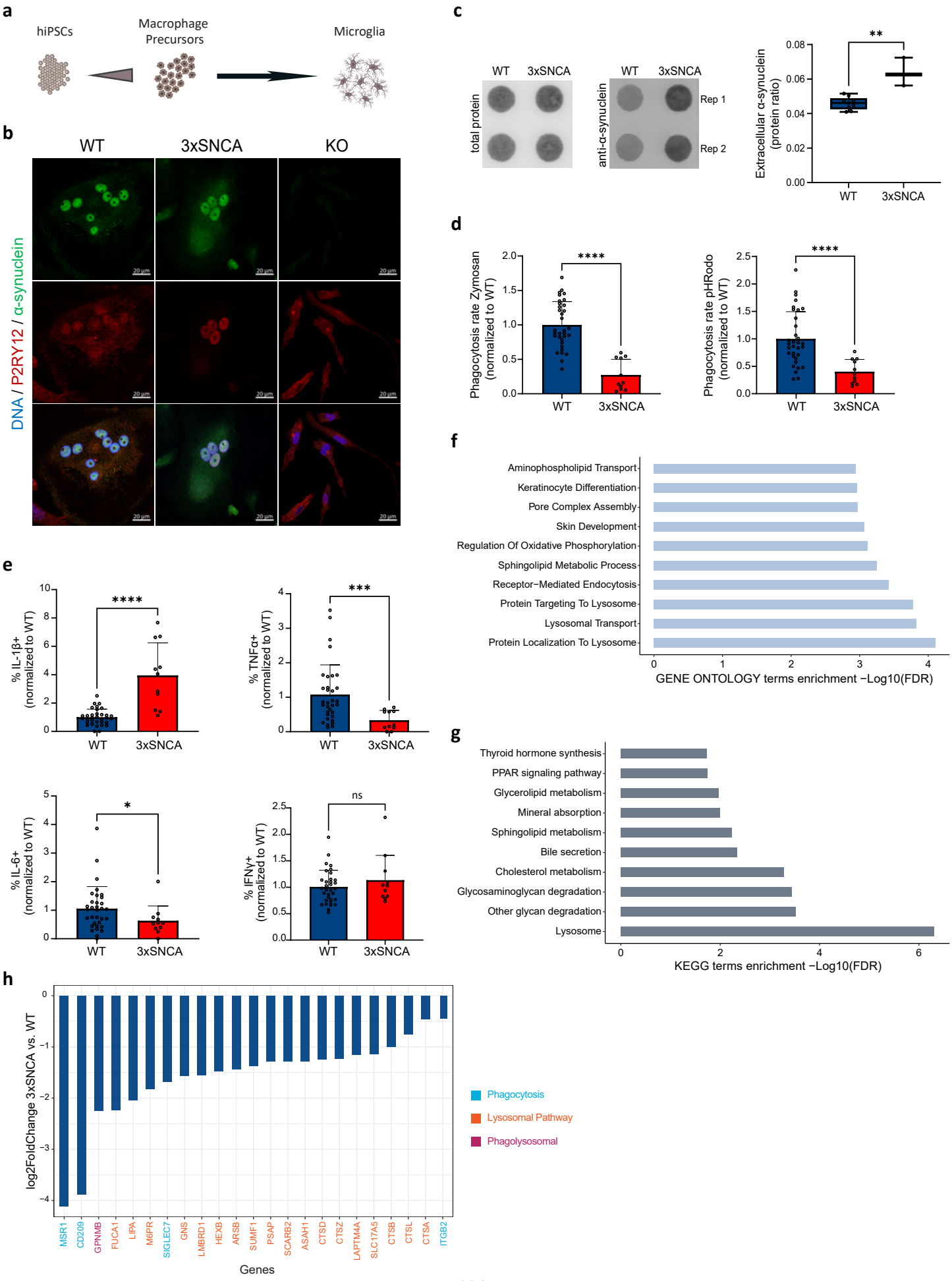
a
hiPSCs
Macrophage Precursors
Microglia
b
WT
3xSNCA
KO
DNA / P2RY12 / α-synuclein
c
WT
3xSNCA
total protein
anti-α-synuclein
Rep 1
Rep 2
Extracellular α-synuclein (protein ratio)
**
d
Phagocytosis rate Zymosan (normalized to WT)
Phagocytosis rate pHRodo (normalized to WT)
****
e
% IL-1β+ (normalized to WT)
% TNFα+ (normalized to WT)
% IL-6+ (normalized to WT)
% IFNγ+ (normalized to WT)
***
*
ns
f
Aminophospholipid Transport
Keratinocyte Differentiation
Pore Complex Assembly
Skin Development
Regulation Of Oxidative Phosphorylation
Sphingolipid Metabolic Process
Receptor−Mediated Endocytosis
Protein Targeting To Lysosome
Lysosomal Transport
Protein Localization To Lysosome
GENE ONTOLOGY terms enrichment −Log10(FDR)
g
Thyroid hormone synthesis
PPAR signaling pathway
Glycerolipid metabolism
Mineral absorption
Sphingolipid metabolism
Bile secretion
Cholesterol metabolism
Glycosaminoglycan degradation
Other glycan degradation
Lysosome
KEGG terms enrichment −Log10(FDR)
h
log2FoldChange 3xSNCA vs. WT
MSR1
CD209
GPNMB
FUCA1
LIPA
M6PR
SIGLEC7
GNS
LMBRD1
HEXB
ARSB
SUMF1
PSAP
SCARB2
ASAH1
CTSD
CTSZ
LAPTM4A
SLC17A5
CTSB
CTSL
CTSA
ITGB2
Genes
Phagocytosis
Lysosomal Pathway
Phagolysosomal

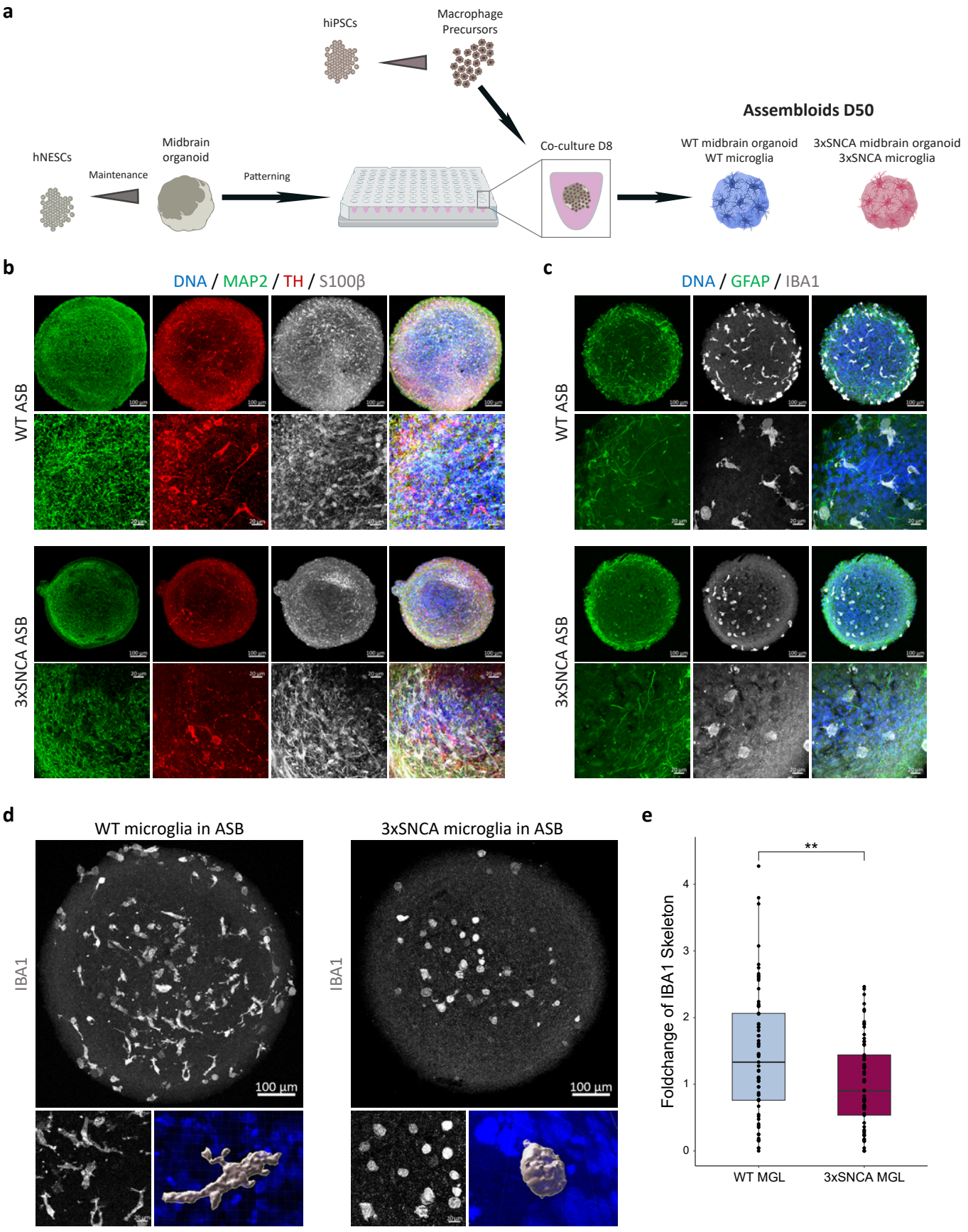
a
hiPSCs
Macrophage Precursors
Assembloids D50
hNESCs
Maintenance
Midbrain organoid
Patterning
Co-culture D8
WT midbrain organoid WT microglia
3xSNCA midbrain organoid 3xSNCA microglia
b
DNA / MAP2 / TH / S100β
WT ASB
3xSNCA ASB
c
DNA / GFAP / IBA1
WT ASB
3xSNCA ASB
d
WT microglia in ASB
3xSNCA microglia in ASB
IBA1
IBA1
100 µm
100 µm
e
Foldchange of IBA1 Skeleton
**
0
1
2
3
4
WT MGL
3xSNCA MGL

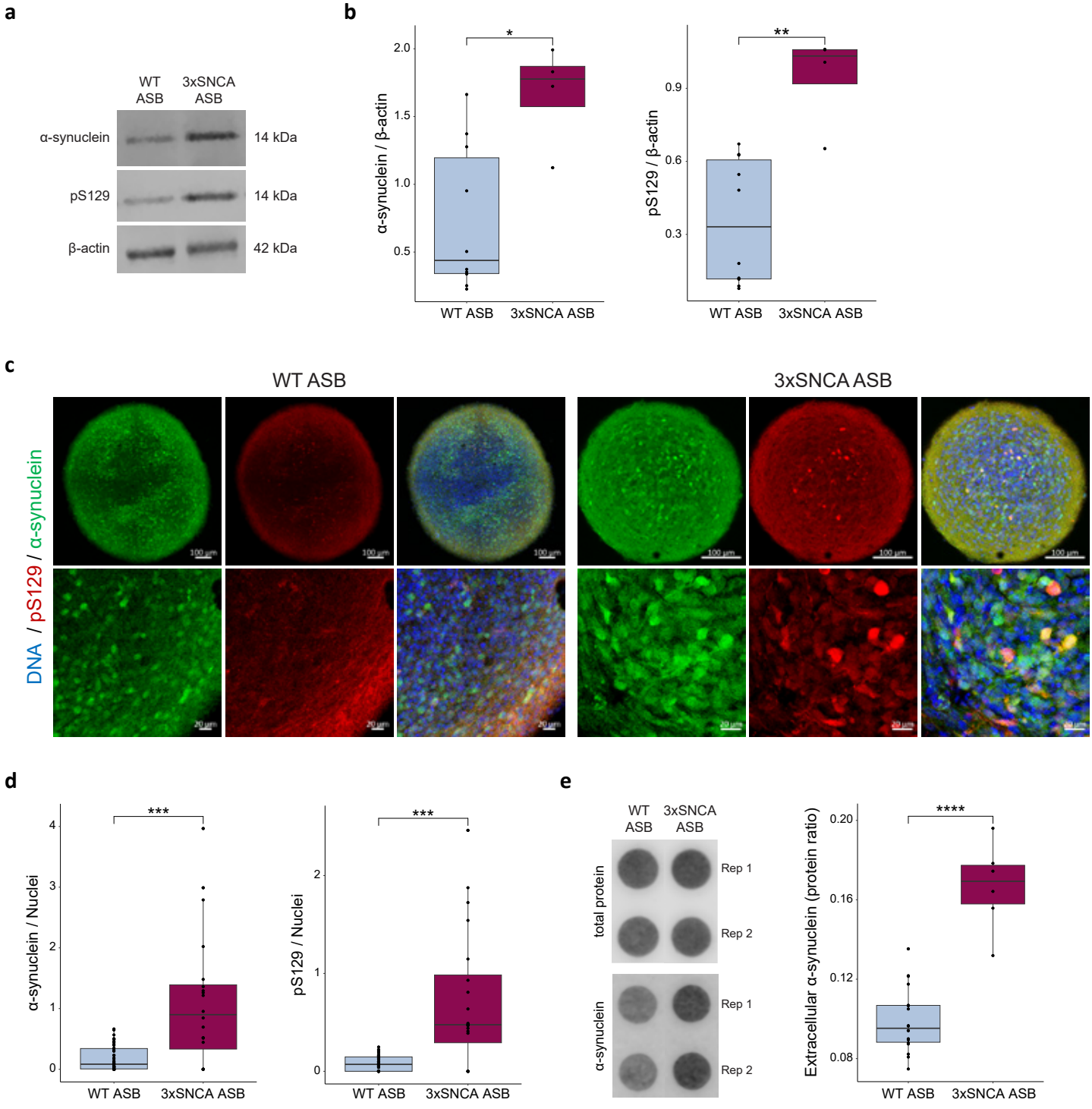
a
WT ASB
3xSNCA ASB
α-synuclein
14 kDa
pS129
14 kDa
β-actin
42 kDa
b
α-synuclein / β-actin
pS129 / β-actin
WT ASB
3xSNCA ASB
c
WT ASB
3xSNCA ASB
DNA / pS129 / α-synuclein
d
α-synuclein / Nuclei
pS129 / Nuclei
e
total protein
α-synuclein
Rep 1
Rep 2
Extracellular α-synuclein (protein ratio)

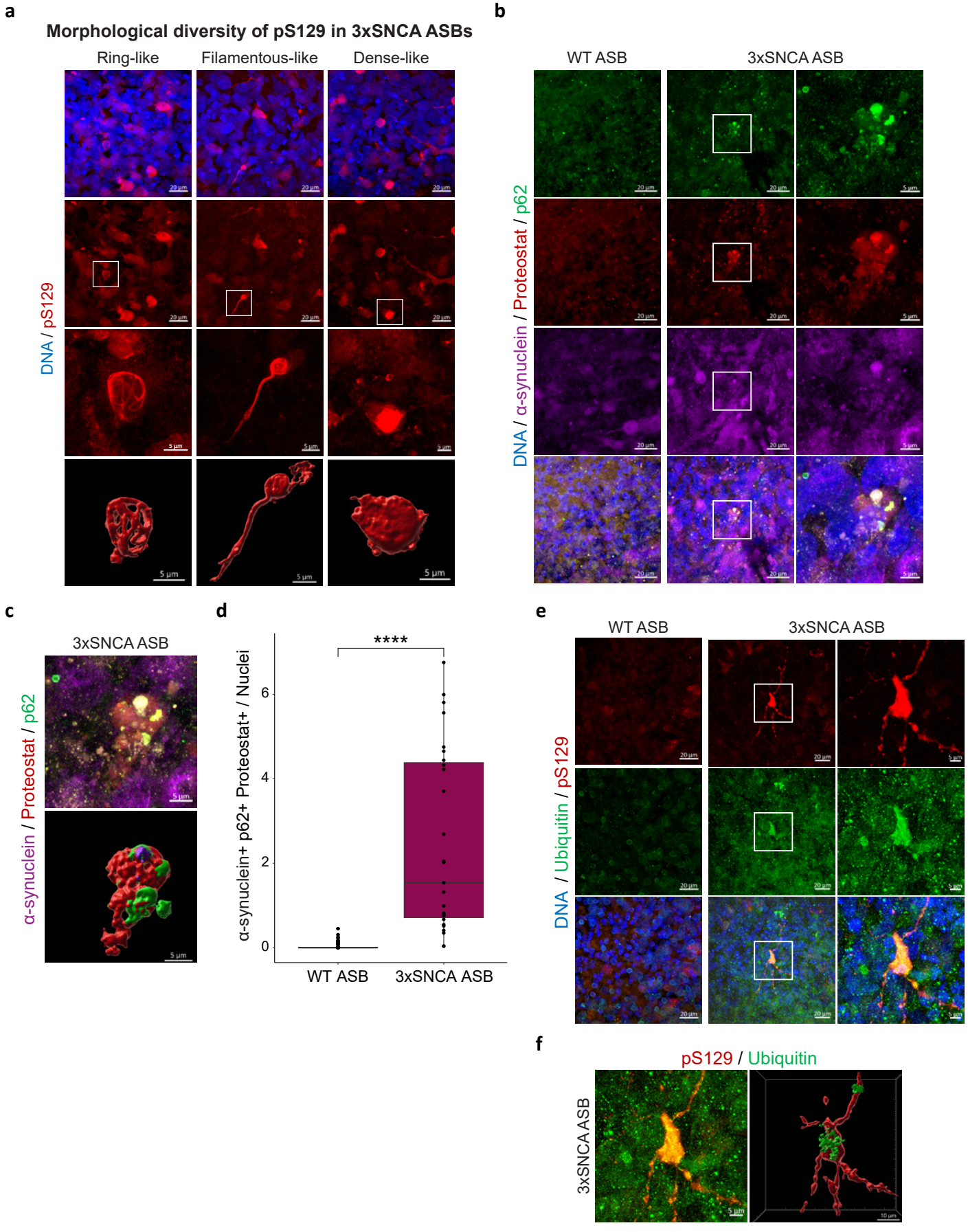
a
Morphological diversity of pS129 in 3xSNCA ASBs
Ring-like
Filamentous-like
Dense-like
DNA / pS129
b
WT ASB
3xSNCA ASB
DNA / α-synuclein / Proteostat / p62
c
3xSNCA ASB
α-synuclein / Proteostat / p62
d
****
α-synuclein+ p62+ Proteostat+ / Nuclei
0
2
4
6
WT ASB
3xSNCA ASB
e
WT ASB
3xSNCA ASB
DNA / Ubiquitin / pS129
f
pS129 / Ubiquitin
3xSNCA ASB

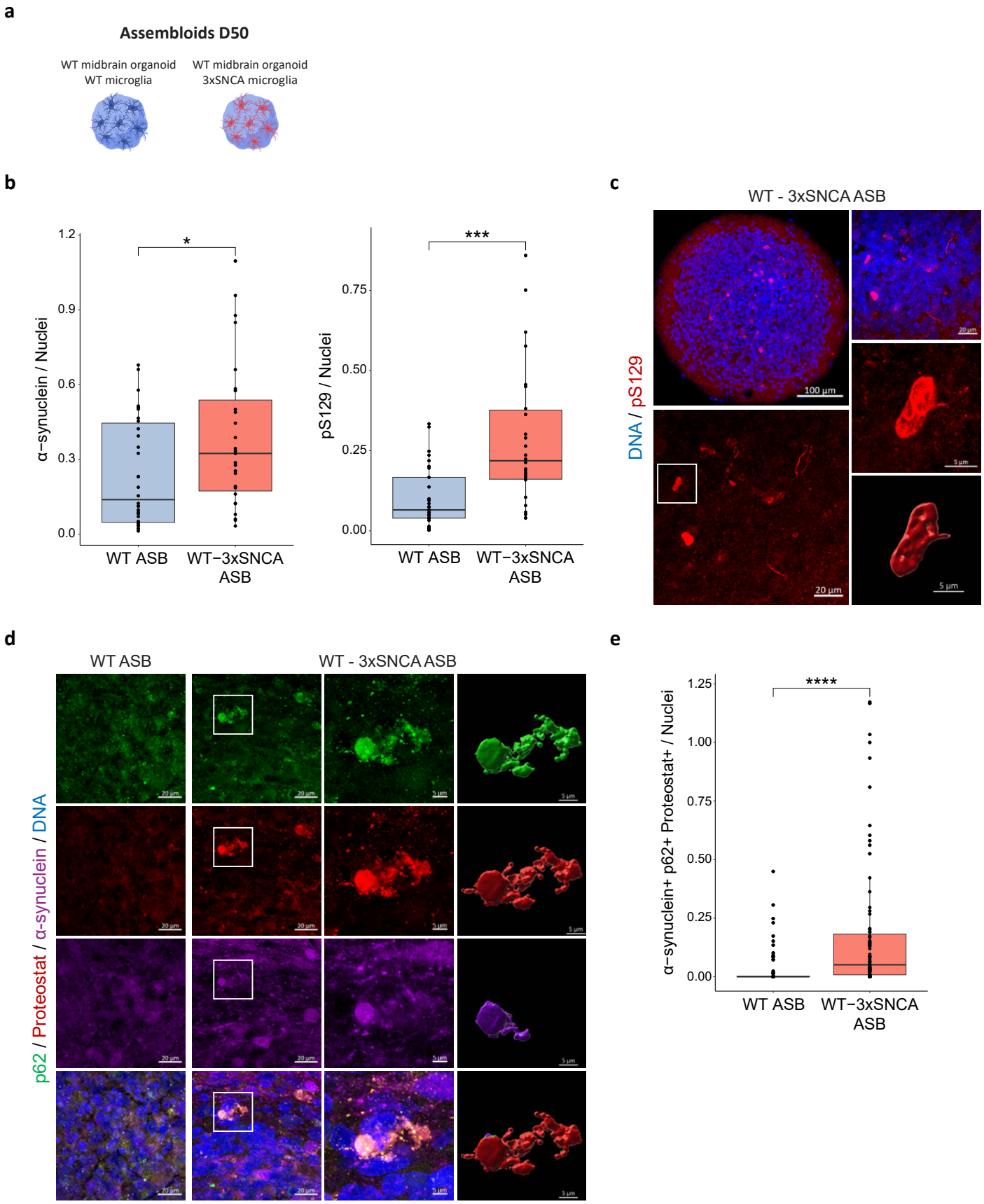
a
Assembloids D50
WT midbrain organoid
WT microglia
WT midbrain organoid
3xSNCA microglia
b
α−synuclein / Nuclei
1.2
0.9
0.6
0.3
0.0
*
WT ASB
WT−3xSNCA ASB
pS129 / Nuclei
0.75
0.50
0.25
0.00
***
WT ASB
WT−3xSNCA ASB
c
WT - 3xSNCA ASB
DNA / pS129
100 µm
20 µm
5 µm
d
WT ASB
WT - 3xSNCA ASB
p62 / Proteostat / α-synuclein / DNA
e
α−synuclein+ p62+ Proteostat+ / Nuclei
1.25
1.00
0.75
0.50
0.25
0.00
****
WT ASB
WT−3xSNCA ASB

Supplementary Information

Parkinson's disease microglia induce endogenous alpha-Synuclein pathology in patient-specific midbrain organoids.

Elisa Zuccoli, Henry Kurniawan, Isabel Rosety, Alise Zagare, Sonia Sabate-Soler, Anna-Sophie Zimmermann, Jens C. Schwamborn

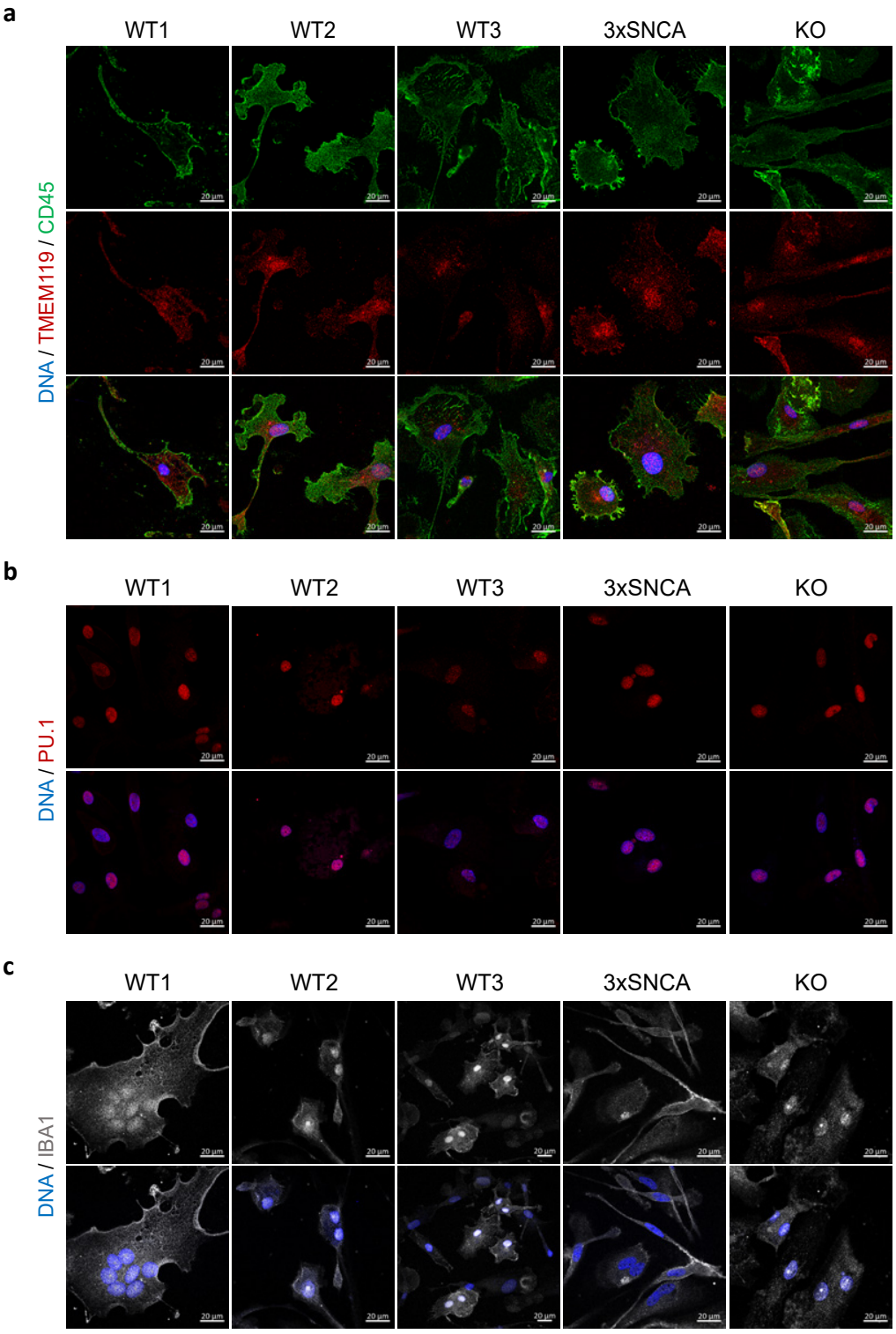
a
WT1
WT2
WT3
3xSNCA
KO
DNA / TMEM119 / CD45
b
WT1
WT2
WT3
3xSNCA
KO
DNA / PU.1
c
WT1
WT2
WT3
3xSNCA
KO
DNA / IBA1

Supplementary Figure 1: iPSC-derived microglia express specific microglial markers. (a) Representative immunofluorescence staining of mature (day 14) WT cell lines (WT1, WT2 and WT3), 3xSNCA and KO microglia for macrophage markers TMEM119 (Transmembrane Protein 119) and CD45, (b) the macrophage marker PU.1, (c) the microglial marker IBA1 as well as Hoechst 33342 (scale bar 20 µm, 63x).

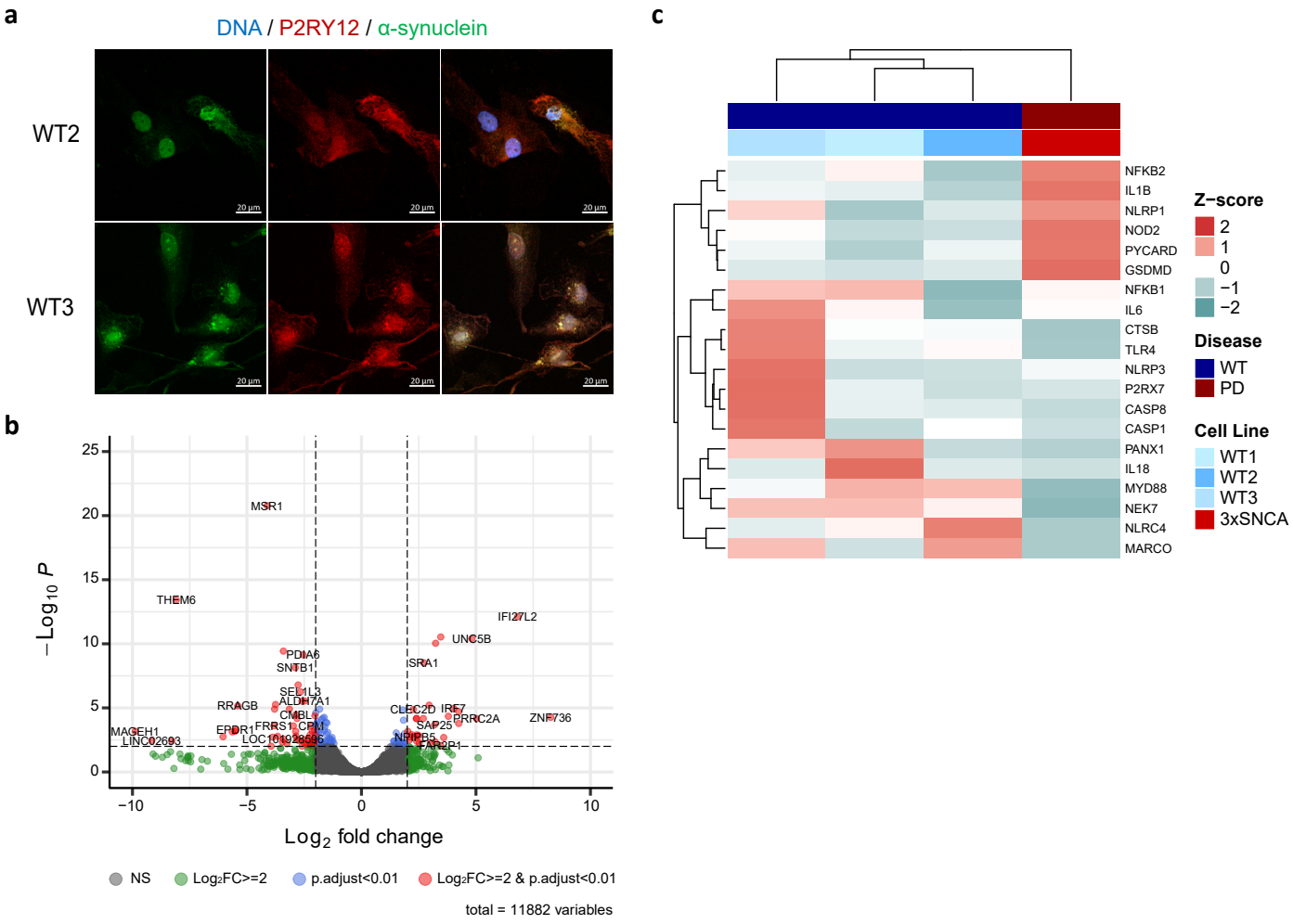
a
DNA / P2RY12 / α-synuclein
WT2
WT3
20 µm
b
−Log10 P
Log2 fold change
MSR1
THEM6
IFI27L2
UNC5B
PDIA6
SNTB1
SRA1
SEL1L3
ALDH7A1
RRAGB
CMBL
CLEC2D
IRF7
PRRC2A
ZNF736
MAGEH1
LINC02693
EPDR1
FRRS1
CPM
SAP25
NPHP3
FAR2P1
NS
Log2FC>=2
p.adjust<0.01
Log2FC>=2 & p.adjust<0.01
total = 11882 variables
c
NFKB2
IL1B
NLRP1
NOD2
PYCARD
GSDMD
NFKB1
IL6
CTSB
TLR4
NLRP3
P2RX7
CASP8
CASP1
PANX1
IL18
MYD88
NEK7
NLRC4
MARCO
Z−score
2
1
0
−1
−2
Disease
WT
PD
Cell Line
WT1
WT2
WT3
3xSNCA

Supplementary Figure 2: α-synuclein expression in WT lines and transcriptomic alterations in 3xSNCA microglia. (a) Representative immunofluorescence staining of additional WT cell lines showing the microglial marker P2RY12 (Purinergic Receptor P2Y12), total α-synuclein and nuclei (Hoechst 33342) (scale bar 20 µm, 63x). (b) Volcano plot showing differential gene expression (DEGs) between 3xSNCA and WT microglia. Genes with $log_2FC>2$ and p.adjust <0.01 are highlighted. (c) Unsupervised hierarchical clustering of 3xSNCA and WT samples based on normalised gene counts of top significant DEGs involved in the inflammasome pathway.

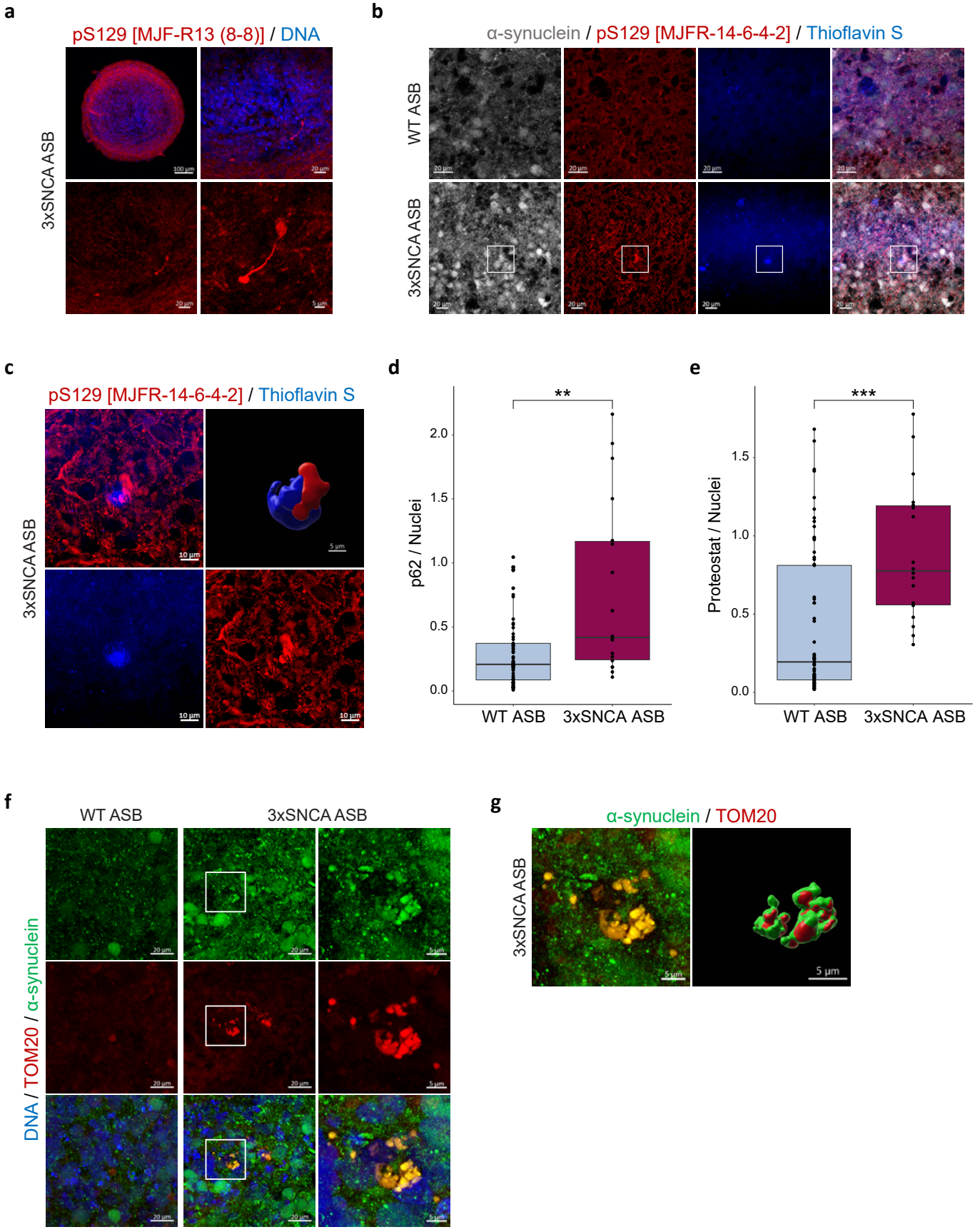
a
pS129 [MJF-R13 (8-8)] / DNA
3xSNCA ASB
b
α-synuclein / pS129 [MJFR-14-6-4-2] / Thioflavin S
WT ASB
3xSNCA ASB
c
pS129 [MJFR-14-6-4-2] / Thioflavin S
3xSNCA ASB
d
p62 / Nuclei
**
WT ASB
3xSNCA ASB
e
Proteostat / Nuclei
***
WT ASB
3xSNCA ASB
f
WT ASB
3xSNCA ASB
DNA / TOM20 / α-synuclein
g
α-synuclein / TOM20
3xSNCA ASB
5 µm

Supplementary Figure 3: Co-localization of aggregation markers with α-synuclein and pS129 in 3xSNCA ASBs. (a) Representative image of 3xSNCA ASBs to show pS129 antibody specificity. Sections were stained with pS129 [MJF-R13 (8-8)] and Hoechst 33342 (scale bar 100 µm, 20x; 20 µm, 63x; 5 µm, zoom in of inset). (b) Representative image of WT and 3xSNCA ASBs stained with total α-synuclein, pS129 [MJFR-14-6-4-2)] and the aggregation marker Thioflavin S (scale bar 100 µm, 20x; 20 µm, 63x). (c) Zoom in of inset of representative image and 3D reconstruction of 3xSNCA ASBs stained with pS129 [MJFR-14-6-4-2)] and the aggregation marker Thioflavin S (5 µm, zoom in of inset). (d) High-content automated image analysis of immunofluorescence stainings showing the foldchange of p62+ cells and (e) Proteostat+ cells normalized by total nuclei in WT and 3xSNCA ASBs. Data represents three independent batches (n=3) normalized to the mean of the controls per batch. Mann-Whitney *U* test; **p < 0.01, ***p < 0.001. (f) Representative image of WT and 3xSNCA ASBs stained with total α-synuclein, the mitochondrial marker TOM20 and Hoechst 33342 (scale bar 100 µm, 20x; 20 µm, 63x). (g) *Left panel:* The same representative image of 3xSNCA ASB as shown in (f), displayed here with total α-synuclein and TOM20 markers (Hoechst omitted). *Right panel:* 3D reconstruction of this image using IMARIS software (scale bar, 5 µm; zoom-in of inset).

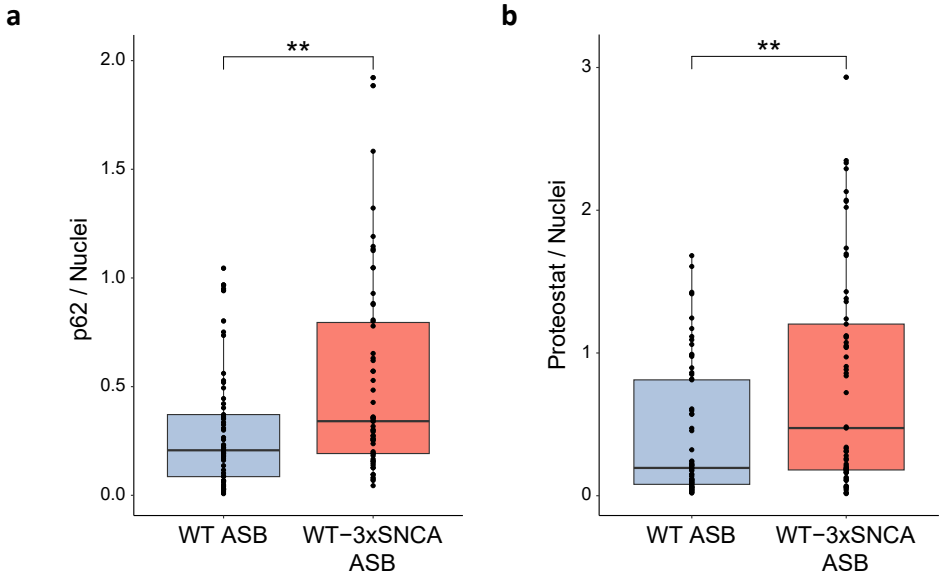
a
**
p62 / Nuclei
2.0
1.5
1.0
0.5
0.0
WT ASB
WT−3xSNCA ASB
b
**
Proteostat / Nuclei
3
2
1
0
WT ASB
WT−3xSNCA ASB

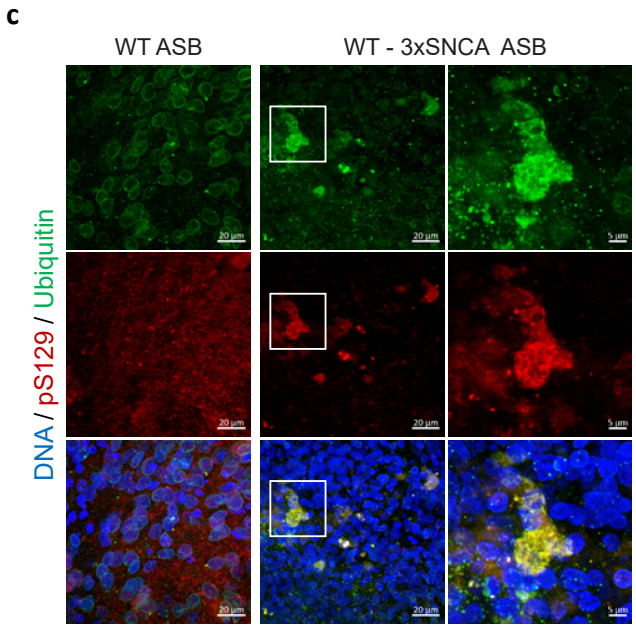
c
WT ASB
WT - 3xSNCA ASB
DNA / pS129 / Ubiquitin

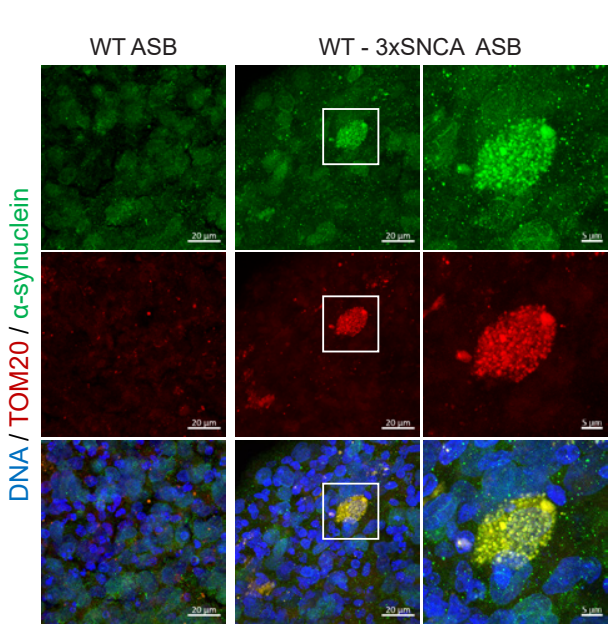
e
WT ASB
WT - 3xSNCA ASB
DNA / TOM20 / α-synuclein

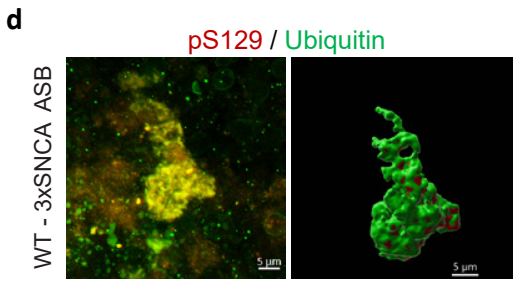
d
pS129 / Ubiquitin
WT - 3xSNCA ASB

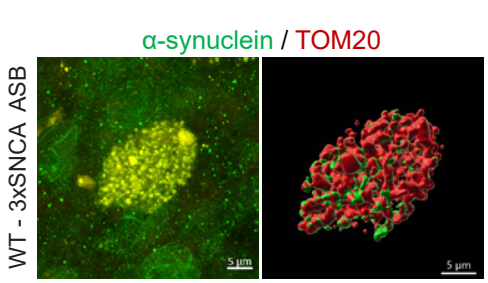
f
α-synuclein / TOM20
WT - 3xSNCA ASB

Supplementary Figure 4: WT-3xSNCA ASBs show co-localization of aggregation markers with α-synuclein and pS129 antibodies. (a) High-content automated image analysis of immunofluorescence stainings showing the foldchange of p62+ cells and (b) Proteostat+ cells normalized by total nuclei in WT and WT-3xSNCA ASBs. Data represents three independent batches (n=3) normalized to the mean of the controls per batch. Mann-Whitney *U* test; **p < 0.01. (c) Representative image of WT and WT-3xSNCA ASBs stained with pS129, Ubiquitin and Hoechst 33342 (scale bar 100 µm, 20x; 20 µm, 63x). (d) *Left panel:* The same representative image of WT-3xSNCA ASB as shown in (c), displayed here with pS129 and Ubiquitin markers (Hoechst omitted). *Right panel:* 3D reconstruction of this image using IMARIS software (scale bar, 5 µm; zoom-in of inset). (e) Representative image of WT and WT-3xSNCA ASBs stained with total α-synuclein, the mitochondrial marker TOM20 and Hoechst 33342 (scale bar 100 µm, 20x; 20 µm, 63x). (f) *Left panel:* The same representative image of WT-3xSNCA ASB as shown in (e), displayed here with total α-synuclein and TOM20 markers (Hoechst omitted). *Right panel:* 3D reconstruction of this image using IMARIS software (scale bar, 5 µm; zoom-in of inset).

Supplementary Table 1. Cell lines used in this study

Lab Identifier	Sample ID	Diagnosis	Patient	Sex	Age of sampling	Source of iPSC
201	WT1	Healthy	A13777	F	-	Gibco
232	WT2	Healthy	T12.9/C1-2	F	53	Reinhardt et al. 2013
277	WT3	Healthy	2716623-MDPD1-CHL	F	65	IBBL / Muenster
336	3xSNCA	PD	ND27760	F	55	European Bank for induced pluripotent stem cells - EDi001-A
374	KO	PD	ND27760	F	55	Chen et al. 2019

Supplementary Table 2: Primary and secondary antibodies used in western blot and dot blot.

Antibody	Source	Cat. no.	RRID	Species	Dilution	Method
β-Actin	Cell Signaling Technology	3700S	*AB_2242334*	mouse	1:20000	WB
α-synuclein (2A7)	Novus Biologicals	NBP1-05194	*AB_1555287*	mouse	1:1000	WB
α-synuclein [MJFR1]	Abcam	ab138501	*AB_2537217*	rabbit	1:1000	Dot Blot
pS129 (D1R1R)	Cell Signaling Technology	23706S	*AB_2798868*	rabbit	1:1000	WB

Supplementary Table 3: Primary and secondary antibodies used in immunofluorescence stainings.

Antibody	Source	Cat. no.	RRID	Species	Dilution
TMEM119	Sigma-Aldrich	HPA051870	*AB_2681645*	rabbit	1:250
CD45	BioLegend	304002	*AB_314390*	mouse	1:1000
PU.1 (9G7)	Cell Signaling Technology	2258	*AB_2186909*	rabbit	1:250
IBA1	Abcam	ab5076	*AB_2224402*	goat	1:250
P2RY12	Sigma-Aldrich	HPA014518	*AB_2669027*	rabbit	1:250
MAP2	Abcam	ab92434	*AB_2138147*	chicken	1:1000
TH	Abcam	ab112	*AB_297840*	rabbit	1:1000
S100β	Sigma-Aldrich	S2532	*AB_477499*	mouse	1:600
GFAP	Millipore	MAB3402	*AB_94844*	mouse	1:1000
α-synuclein (2A7)	Novus Biologicals	NBP1-05194	*AB_1555287*	mouse	1:1000
α-synuclein [MJFR1]	Abcam	ab138501	*AB_2537217*	rabbit	1:1000
pS129 (D1R1R)	Cell Signaling Technology	23706S	*AB_2798868*	rabbit	1:1000
pS129 [MJF-R13 (8-8)]	Abcam	ab168381	*AB_2728613*	rabbit	1:500
pS129 [MJFR-14-6-4-2]	Abcam	ab209538	*AB_2714215*	rabbit	1:500
SQSTM1 / p62	Abcam	ab155686	*AB_2847961*	rabbit	1:500
Ubiquitin (P4D1)	Santa Cruz Biotechnology	sc-8017	*AB_628423*	mouse	1:500
Tom20 (D8T4N)	Cell Signaling Technology	42406	*AB_2687663*	rabbit	1:300
Anti-mouse 488	Invitrogen	A32766	*AB_2762823*	Donkey	1:1000
Anti-mouse 647	Invitrogen	A-31571	*AB_162542*	Donkey	1:1000
Anti-rabbit 488	Invitrogen	A21206	*AB_2535792*	Donkey	1:1000
Anti-rabbit 568	Invitrogen	A-10042	*AB_2534017*	Donkey	1:1000
Anti-chicken 488	Jackson Immunoresearch	703-545-155	*AB_2340375*	Donkey	1:1000
Anti-goat 647	Invitrogen	A32849	*AB_2762840*	Donkey	1:1000

Chapter 4: Conclusions and Perspectives

The research presented in this thesis explores the contribution of genetic risk factors and neuroimmune mechanisms to Parkinson's disease using advanced human stem-cell derived models. Across the three manuscripts, we dissect how distinct PD-associated mutations, GBA-N370S, LRRK2-G2019S, and SNCA triplication, converge on shared pathophysiological features, particularly those affecting dopaminergic neurons.

We established a robust and reproducible midbrain organoid model using iPSCs from patients carrying the GBA-N370S mutation in Manuscript I. This study confirms the consistent emergence of disease-relevant features, such as dopaminergic neuron loss and senescence-associated phenotype, as previously described in other studies. Importantly, we demonstrate that these phenotypes occur reliably across independent midbrain organoid batches, directly addressing the well-recognized challenges of reproducibility and experimental variability in the stem cell and organoid field (Ludwig et al., 2023; Sandoval et al., 2024). Our findings position this midbrain organoid platform as a scalable, disease-relevant system for modelling PD with high biological accuracy. At the same time, the work offers opportunities to extend its scope and applicability. Our analyses focused solely on GBA-N370S organoids, and power analysis confirmed that the number of donor lines and samples used was sufficient to capture robust transcriptomic and phenotypic differences. However, these lines still represent only a fraction of the genetic diversity and patient heterogeneity in PD, which may limit the generalizability of our results to other genetic backgrounds of PD. Expanding this approach to include other PD-associated mutations such as LRRK2, SNCA, and DJ-1 would help to determine whether the reproducibility observed in this study also applies to other disease backgrounds. This broader genetic coverage could also clarify whether the passage-dependent changes we observed, such as the clustering of late-passage D30 samples closer to D60 samples using Euclidean distance (Manuscript I, Figure 3), are a general feature across PD background or specific to the GBA mutation. While aged midbrain organoids and assembloids can now be generated through progerin induction (Barmpa et al., 2024), our findings suggest that passage number may serve as an additional, experimentally accessible variable for modelling aging. Since NESCs are lineage-committed progenitors, they are more vulnerable to replicative stress and aging-like changes than iPSCs. Prolonged passaging may accelerate the onset of cellular aging features such as reduced proliferative potential and neurogenic capacity (Wright et al., 2006; Cantor et al., 2022), mitochondrial dysfunction and oxidative stress

(Stoll et al., 2011; Dong et al., 2014), and epigenetic drift and altered transcriptional programs (Negredo et al., 2020). These hallmarks of stem cell aging could explain why late-passage NESC-derived midbrain organoids display a more age-like molecular signature, resembling later developmental or even early degenerative states. This creates new possibilities for investigating age-related mechanisms in neurodegenerative diseases using established culture systems, while positioning passage number as an experimentally accessible variable to mimic aspects of cellular aging *in vitro*, complementing genetic or progerin-based approaches and expanding strategies for modelling neurodegeneration. In addition, a more comprehensive representation of patient diversity by including rarer mutations, a larger number of donor lines, and a balanced distribution of female and male genetic backgrounds, would strengthen the translational relevance of the model and allow the exploration of sex-specific transcriptomic effects. Considering these aspects will be crucial for fully exploiting the potential of this reproducible model in PD research.

While this work has provided a robust and reproducible platform for modelling PD-related phenotypes, midbrain organoids lack mesoderm-derived microglia, key mediators of neuroinflammation and disease progression (Molnár et al., 2019; Badanjak et al., 2021). To address this, microglia have been successfully integrated into midbrain organoids, enabling the study of neuroimmune interactions in a more physiologically relevant context (Sabate-Soler et al., 2022).

In Manuscript II, we show the successful integration of LRRK2-G2019S mutant microglia into the midbrain organoid. These microglia exhibit a metabolically reprogrammed, pro-inflammatory state that promotes dopaminergic neuron degeneration. Importantly, we demonstrate that oxamic acid effectively rescues dopaminergic neuron loss induced by LRRK2-G2019S microglia, highlighting the role of microglial metabolic reprogramming as a driver of neurotoxicity. Oxamic acid selectively dampens inflammatory TNF-α signalling while preserving beneficial microglial functions, underscoring the therapeutic potential of targeting metabolic pathways in disease-associated microglia. Other glycolysis-targeting compounds such as 2-deoxy-D-glucose (2-DG) or 3-bromopyruvate (3-BP) could achieve similar protective effects by normalizing microglial metabolism and reducing pro-inflammatory signalling (Cheng et al., 2021; Shoshan, 2012), although their efficacy in human PD-relevant iPSC-derived or assembloid models has not yet been tested. In addition, metabolic interventions such as metformin have already been shown to rescue dopaminergic neuron loss in GBA patient-derived midbrain organoids (Zagare et al., 2025), supporting the concept that modulation of metabolism can confer neuroprotection in PD models.

Building on these findings, the next step is the development of fully patient-specific assembloids, in which both midbrain organoids and microglia carry the LRRK2-G2019S mutation. This approach would allow us to investigate whether the combined presence of neuron- and microglia-intrinsic pathology modifies the response to glycolysis-targeting therapies. Such a model also enables a precise distinction between cell-autonomous and non-cell-autonomous contributions to neurodegeneration and allows testing the robustness of metabolic interventions across different genetic backgrounds. Our oxamic acid results provide proof that correcting microglial metabolic dysfunction can rescue dopaminergic neuron loss, offering a strong rational for testing other glycolysis-modulating compounds such as 2-DG, 3-BP, or metformin in both chimeric and fully patient-specific assembloids.

In parallel, improving the physiological relevance of the assembloid model by integrating vasculature is another promising direction. The recent successful incorporation of vascular networks into assembloids (Zimmermann et al., 2025), presents new opportunities for the study of neurovascular interactions, blood-brain barrier integrity, and cytokine diffusion in a more realistic tissue environment. These advances would support longer-term cultures, improve drug-delivery strategies, and provide a more comprehensive platform for modelling PD and evaluating therapeutic interventions.

LRRK2-G2019S and GBA-N370S are uncommon genetic risk variants that exert an intermediate risk for developing PD. In contrast, SNCA triplication is a rare but fully penetrant mutation in which increased gene dosage alone is sufficient to cause disease. This monogenic form of PD is typically identified through linkage analysis in affected families (Day & Mullin, 2021) and offers a unique opportunity to investigate whether microglial dysfunction alone can initiate core pathological features of the disease.

Manuscript III applies the assembloid approach to integrate microglia derived from a patient with the SNCA genomic triplication (3xSNCA) into midbrain organoids. This individual carries a genetic predisposition for elevated α-synuclein expression and early-onset PD. Our findings show that 3xSNCA microglia adopt a pro-inflammatory profile and accelerate the formation of Lewy body-like α-synuclein aggregates in co-cultured midbrain organoids. Remarkably, this pathology emerges in the absence of external stressors or seeded α-synuclein fibrils, suggesting that intrinsic microglial dysfunction is sufficient to initiate hallmark PD pathology. This provides direct evidence that patient-specific microglia can actively trigger protein aggregation and neuroinflammation. Our results lay the foundation for multiple follow-up studies.

Mechanistically, expanding the study to include additional patient-derived cell lines will be essential for assessing generalizability of our findings. In this study, we used the SNCA

triplication line derived from the Iowa kindred, a unique and valuable cell line for modelling α-synuclein overexpression, though it only reflects one individual's genetic background (Zafar et al., 2018). Including other patient-derived variants, such as SNCA duplication or the pathogenic A53T mutation, would allow us to determine whether the observed pathology is driven by overexpression alone, specific sequence alterations, or shared downstream mechanisms (Magistrelli et al., 2021; Bayati & McPherson; 2024; Li et al., 2025). Such comparative studies would enhance the robustness of our findings and clarify universal and mutation-specific disease pathways. Notably, integrating 3xSNCA microglia into three independent WT midbrain organoid lines consistently recapitulated the α-synuclein aggregation in each line, highlighting the robustness and the reproducibility of the model.

Further investigation into the mechanisms driving pathogenic α-synuclein aggregation in the assembloid model system is warranted. Our microglia exhibit lysosomal and metabolic impairment alongside reduced phagocytic capacity. A multi-omics approach, integrating transcriptomics, proteomics, and metabolomics, could comprehensively map the inflammatory landscape of the assembloids and reveal how microglia dysfunction intersects with neuronal α-synuclein dysregulation (Irwin et al., 2013; Booms & Coetzee, 2021). This would allow a detailed analysis of bidirectional interactions and investigate not only how dysfunctional microglia exacerbate neuronal pathology, but also how α-synuclein pathology within the midbrain organoid affects microglial state and function (Yi et al., 2022). An important next step is to understand the temporal dynamics of these processes in assembloids. Specifically, it is crucial to identify which cellular or molecular changes occur first, which act as secondary amplifiers, and how these events interact (Lopes da Fonseca et al., 2015; Arias-Carrión et al., 2025). This could be approached by combining longitudinal multi-omics, live-cell imaging, and targeted functional assays to build a mechanistic timeline, a pathology progression map, that links microglial dysfunction to α-synuclein pathology in a cause-and-effect framework. This approach would help clarify the sequence of disease-related events and highlight the most promising stages for therapeutic targeting.

From a translational perspective, our model offers a unique opportunity to test whether clearing α-synuclein aggregates from assembloids can halt or reverse pathology. This could involve direct microglia-targeted interventions, such as depletion with PLX5622 (Spangenberg et al., 2019; Guenoun et al., 2025), applied either during early co-culture to prevent pathology emergence, or at later stages to assess the stability of established pathology. Complementary experiments could explore whether modulating inflammatory signalling, for instance with IL-1β, recapitulates or mitigates disease features. Finally, given that some early microglial responses might initially be protective, determining whether they shift later toward driving dopaminergic neuron degeneration will be important for

understanding the dual nature of neuroimmune interactions in PD. As described in Chapter 1.2: Summary and Discussion of the results, this model also provides a clinically relevant platform to evaluate pharmacological strategies targeting lysosomal function and α-synuclein clearance, offering a path toward translating mechanistic insights into therapeutic advances (Dehay et al., 2015; Wong & Krainc, 2017; Dai et al., 2024; Arias-Carrión et al., 2025; Yang et al., 2024).

Beyond the mechanistic insights gained from Manuscript II and III, these patient-derived assembloids offer a clinically relevant platform for translational research. They enable testing of genotype-targeted interventions, evaluation of drug efficacy and safety, and identification of early molecular or cellular biomarkers predictive of disease progression. Multi-omics readouts, including transcriptomics, proteomics, and metabolomics, can reveal signatures of microglial dysfunction, α-synuclein aggregation, or dopaminergic neuron vulnerability, supporting patient stratification and personalized therapeutic strategies.

Moreover, the assembloid model provides opportunities to explore complex brain processes and disease propagation in patient-specific context. The incorporation of vascular networks could improve tissue physiology and drug delivery, while combining midbrain and striatum organoids would allow investigation of α-synuclein propagation across interconnected regions. These capabilities make the model a valuable tool for identifying novel therapeutic targets and testing compounds with potential efficacy not only in Parkinson’s disease but also in other neurodegenerative disorders, including Alzheimer’s disease and related proteinopathies. By leveraging functional and regional readouts, this approach supports the development of interventions that may be broadly applicable across multiple neurodegenerative diseases.

Despite the advances presented here, some limitations of our models should be acknowledged. The current models remain constrained by culture maturity, as even passage-dependent aging or progerin induction only partially recapitulate the temporal complexity of human brain aging. Generalizability is further limited by the number and diversity of patient-derived lines, including incomplete representation of sex balance. Finally, midbrain organoids and assembloids lack vasculature and peripheral immune trafficking, which restricts the physiological relevance of neuroimmune and neurovascular interactions.

Collectively, these studies present a multidimensional view of Parkinson’s disease characterised by developmental vulnerability, cell-type specific dysfunction, and intercellular interactions. Our results reveal that PD-associated mutations disrupt not only neuronal processes but also immune pathways, with microglial dysfunction affecting susceptible

dopaminergic neurons. Although each genetic background (GBA, LRRK2, SNCA) contributes via distinct molecular mechanisms, the resulting phenotypes, including neuroinflammation, protein aggregation, and dopaminergic neuron loss, converge to common pathological outcomes. Using reproducible, human-relevant, disease-specific models such as iPSC-derived midbrain organoids and assembloids, with structural tissue organization, developmental trajectories, and neuroimmune complexity, we gain mechanistic insights into PD progression. These insights deepen our understanding of gene-environment interactions and provide a foundation for developing targeted therapeutic strategies for the diverse pathways underlying Parkinson's disease.

References

Abud, E. M., Ramirez, R. N., Martinez, E. S., Healy, L. M., Nguyen, C. H., Newman, S. A., ... & Blurton-Jones, M. (2017). iPSC-derived human microglia-like cells to study neurological diseases. *Neuron*, *94*(2), 278-293.

Aguilar, C., Alves da Silva, M., Saraiva, M., Neyazi, M., Olsson, I. A. S., & Bartfeld, S. (2021). Organoids as host models for infection biology–a review of methods. *Experimental & Molecular Medicine*, *53*(10), 1471-1482.

Antón-Bolaños, N., Faravelli, I., Faits, T., Andreadis, S., Kastli, R., Trattaro, S., ... & Arlotta, P. (2024). Brain Chimeroids reveal individual susceptibility to neurotoxic triggers. *Nature*, *631*(8019), 142-149.

Arenas, E. (2014). Wnt signaling in midbrain dopaminergic neuron development and regenerative medicine for Parkinson's disease. *Journal of molecular cell biology*, *6*(1), 42-53.

Arenas, E., Denham, M., & Villaescusa, J. C. (2015). How to make a midbrain dopaminergic neuron. *Development*, *142*(11), 1918-1936.

Arias-Carrión, O., Guerra-Crespo, M., Padilla-Godínez, F. J., Soto-Rojas, L. O., & Manjarrez, E. (2025). α-Synuclein Pathology in Synucleinopathies: Mechanisms, Biomarkers, and Therapeutic Challenges. *International Journal of Molecular Sciences*, *26*(11), 5405.

Athauda, D., Evans, J., Wernick, A., Virdi, G., Choi, M. L., Lawton, M., ... & Gandhi, S. (2022). The impact of type 2 diabetes in Parkinson's disease. *Movement Disorders*, *37*(8), 1612-1623.

Auburger, G., Klinkenberg, M., Drost, J., Marcus, K., Morales-Gordo, B., Kunz, W. S., ... & Jendrach, M. (2012). Primary skin fibroblasts as a model of Parkinson's disease. *Molecular neurobiology*, *46*(1), 20-27.

Avazzadeh, S., Baena, J. M., Keighron, C., Feller-Sanchez, Y., & Quinlan, L. R. (2021). Modelling Parkinson’s disease: iPSCs towards better understanding of human pathology. *Brain Sciences*, *11*(3), 373.

Babu, H. W. S., Kumar, S. M., Kaur, H., Iyer, M., & Vellingiri, B. (2024). Midbrain organoids for Parkinson's disease (PD)-A powerful tool to understand the disease pathogenesis. *Life Sciences*, *345*, 122610.

Badanjak, K., Fixemer, S., Smajić, S., Skupin, A., & Grünewald, A. (2021). The contribution of microglia to neuroinflammation in Parkinson’s disease. *International Journal of Molecular Sciences*, *22*(9), 4676.

Baldi, I., Lebailly, P., Mohammed-Brahim, B., Letenneur, L., Dartigues, J. F., & Brochard, P. (2003). Neurodegenerative diseases and exposure to pesticides in the elderly. *American journal of epidemiology*, *157*(5), 409-414.

Barmpa, K., Saraiva, C., Lopez-Pigozzi, D., Gomez-Giro, G., Gabassi, E., Spitz, S., ... & Schwamborn, J. C. (2024). Modeling early phenotypes of Parkinson’s disease by age-induced midbrain-striatum assembloids. *Communications biology*, *7*(1), 1561.

Bayati, A., & McPherson, P. S. (2024). Alpha-synuclein, autophagy-lysosomal pathway, and Lewy bodies: Mutations, propagation, aggregation, and the formation of inclusions. *Journal of Biological Chemistry*, *300*(10), 107742.

Becerra-Calixto, A., Mukherjee, A., Ramirez, S., Sepulveda, S., Sinha, T., Al-Lahham, R., ... & Soto, C. (2023). Lewy body-like pathology and loss of dopaminergic neurons in midbrain organoids derived from familial Parkinson's disease patient. *Cells*, *12*(4), 625.

Bentley-DeSousa, A., Clegg, D., & Ferguson, S. M. (2025). LRRK2, lysosome damage, and Parkinson's disease. *Current Opinion in Cell Biology*, *93*, 102482.

Biedler, J. L., Roffler-Tarlov, S., Schachner, M., & Freedman, L. S. (1978). Multiple neurotransmitter synthesis by human neuroblastoma cell lines and clones. *Cancer research*, *38*(11_Part_1), 3751-3757.

Birtele, M., Lancaster, M., & Quadrato, G. (2025). Modelling human brain development and disease with organoids. *Nature Reviews Molecular Cell Biology*, *26*(5), 389-412.

Bisaglia, M., Trolio, A., Bellanda, M., Bergantino, E., Bubacco, L., & Mammi, S. (2006). Structure and topology of the non-amyloid-β component fragment of human α-synuclein bound to micelles: Implications for the aggregation process. *Protein science*, *15*(6), 1408-1416.

Blasco-Agell, L., Pons-Espinal, M., Testa, V., Roch, G., Montero-Muñoz, J., Fernandez-Carasa, I., ... & Consiglio, A. (2025). LRRK2-mutant microglia and neuromelanin synergize to drive dopaminergic neurodegeneration in an iPSC-based Parkinson's disease model. *Communications Biology*, *8*(1), 1203.

Bloem, B. R., Okun, M. S., & Klein, C. (2021). Parkinson's disease. The Lancet, 397(10291), 2284-2303.

Bolam, J. P., & Pissadaki, E. K. (2012). Living on the edge with too many mouths to feed: why dopamine neurons die. *Movement Disorders*, *27*(12), 1478-1483.

Bonet-Ponce, L., & Cookson, M. R. (2022). LRRK2 recruitment, activity, and function in organelles. *The FEBS journal*, *289*(22), 6871-6890.

Booms, A., & Coetzee, G. A. (2021). Functions of intracellular alpha-synuclein in microglia: Implications for Parkinson's disease risk. *Frontiers in Cellular Neuroscience*, *15*, 759571.

Booth, H. D., Hirst, W. D., & Wade-Martins, R. (2017). The role of astrocyte dysfunction in Parkinson's disease pathogenesis. *Trends in neurosciences*, *40*(6), 358-370.

Braak, H., Del Tredici, K., Rüb, U., De Vos, R. A., Steur, E. N. J., & Braak, E. (2003). Staging of brain pathology related to sporadic Parkinson's disease. *Neurobiology of aging*, *24*(2), 197-211.

Braak, H., Ghebremedhin, E., Rüb, U., Bratzke, H., & Del Tredici, K. (2004). Stages in the development of Parkinson's disease-related pathology. *Cell and tissue research*, *318*(1), 121-134.

Braak, H., Sandmann-Keil, D., Gai, W., & Braak, E. (1999). Extensive axonal Lewy neurites in Parkinson's disease: a novel pathological feature revealed by α-synuclein immunocytochemistry. *Neuroscience letters*, *265*(1), 67-69.

Brenner, D., Blaser, H., & Mak, T. W. (2015). Regulation of tumour necrosis factor signalling: live or let die. *Nature Reviews Immunology*, *15*(6), 362-374.

Brockmann, K., Quadalti, C., Lerche, S., Rossi, M., Wurster, I., Baiardi, S., ... & Parchi, P. (2021). Association between CSF alpha-synuclein seeding activity and genetic status in Parkinson's disease and dementia with Lewy bodies. *Acta neuropathologica communications*, *9*(1), 175.

Butler, C. A., Popescu, A. S., Kitchener, E. J., Allendorf, D. H., Puigdellívol, M., & Brown, G. C. (2021). Microglial phagocytosis of neurons in neurodegeneration, and its regulation. *Journal of neurochemistry*, *158*(3), 621-639.

Cakir, B., Xiang, Y., Tanaka, Y., Kural, M. H., Parent, M., Kang, Y. J., ... & Park, I. H. (2019). Engineering of human brain organoids with a functional vascular-like system. *Nature methods*, *16*(11), 1169-1175.

Campbell, M. C., Jackson, J. J., Koller, J. M., Snyder, A. Z., Kotzbauer, P. T., & Perlmutter, J. S. (2020). Proteinopathy and longitudinal changes in functional connectivity networks in Parkinson disease. *Neurology*, *94*(7), e718-e728.

Cantor, E. L., Shen, F., Jiang, G., Tan, Z., Cunningham, G. M., Wu, X., ... & Schneider, B. P. (2022). Passage number affects differentiation of sensory neurons from human induced pluripotent stem cells. *Scientific Reports*, *12*(1), 15869.

Cattaneo, C., & Pagonabarraga, J. (2025). Sex differences in Parkinson's disease: a narrative review. *Neurology and Therapy*, *14*(1), 57-70.

Caudle, W. M., Guillot, T. S., Lazo, C. R., & Miller, G. W. (2012). Industrial toxicants and Parkinson's disease. *Neurotoxicology*, *33*(2), 178-188.

Cenci, M. A., & Björklund, A. (2020). Animal models for preclinical Parkinson's research: an update and critical appraisal. *Progress in brain research*, *252*, 27-59.

Cerneckis, J., Cai, H., & Shi, Y. (2024). Induced pluripotent stem cells (iPSCs): molecular mechanisms of induction and applications. *Signal Transduction and Targeted Therapy*, *9*(1), 112.

Chambers, S. M., Fasano, C. A., Papapetrou, E. P., Tomishima, M., Sadelain, M., & Studer, L. (2009). Highly efficient neural conversion of human ES and iPS cells by dual inhibition of SMAD signaling. *Nature biotechnology*, *27*(3), 275-280.

Chandler, R. J., Cogo, S., Lewis, P. A., & Kevei, E. (2021). Modelling the functional genomics of Parkinson's disease in Caenorhabditis elegans: LRRK2 and beyond. *Bioscience Reports*, *41*(9), BSR20203672.

Chaudhuri, K. R., Healy, D. G., & Schapira, A. H. (2006). Non-motor symptoms of Parkinson's disease: diagnosis and management. *The Lancet Neurology*, *5*(3), 235-245.

Chen, H., Zhang, S. M., Schwarzschild, M. A., Hernan, M. A., & Ascherio, A. (2005). Physical activity and the risk of Parkinson disease. *Neurology*, *64*(4), 664-669.

Chen, H., Zhang, S. M., Schwarzschild, M. A., Hernán, M. A., Willett, W. C., & Ascherio, A. (2004). Obesity and the risk of Parkinson's disease. *American journal of epidemiology*, *159*(6), 547-555.

Cheng, J., Zhang, R., Xu, Z., Ke, Y., Sun, R., Yang, H., ... & Zheng, L. T. (2021). Early glycolytic reprogramming controls microglial inflammatory activation. *Journal of neuroinflammation*, *18*(1), 129.

Choi, I., Zhang, Y., Seegobin, S. P., Pruvost, M., Wang, Q., Purtell, K., ... & Yue, Z. (2020). Microglia clear neuron-released α-synuclein via selective autophagy and prevent neurodegeneration. *Nature communications*, *11*(1), 1386.

Colucci, F., Avenali, M., De Micco, R., Poli, M. F., Cerri, S., Stanziano, M., ... & Cilia, R. (2023). Ambroxol as a disease-modifying treatment to reduce the risk of cognitive impairment in GBA-associated Parkinson's disease: a multicentre, randomised, double-blind, placebo-controlled, phase II trial. The AMBITIOUS study protocol. *BMJ Neurology Open*, *5*(2), e000535.

Cox, D., Carver, J. A., & Ecroyd, H. (2014). Preventing α-synuclein aggregation: the role of the small heat-shock molecular chaperone proteins. *Biochimica et biophysica acta*, *1842*(9), 1830–1843.

Cui, X., Li, X., Zheng, H., Su, Y., Zhang, S., Li, M., Hao, X., Zhang, S., Hu, Z., Xia, Z., Shi, C., Xu, Y., & Mao, C. (2024). Human midbrain organoids: a powerful tool for advanced Parkinson's disease modeling and therapy exploration. *NPJ Parkinson's disease*, *10*(1), 189.

Dai, L., Liu, M., Ke, W., Chen, L., Fang, X., & Zhang, Z. (2024). Lysosomal dysfunction in α-synuclein pathology: Molecular mechanisms and therapeutic strategies. *Cellular and Molecular Life Sciences*, *81*(1), 382.

Damier, P., Hirsch, E. C., Agid, Y., & Graybiel, A. (1999). The substantia nigra of the human brain: II. Patterns of loss of dopamine-containing neurons in Parkinson's disease. *Brain*, *122*(8), 1437-1448.

Day, J. O., & Mullin, S. (2021). The genetics of Parkinson’s disease and implications for clinical practice. *Genes*, *12*(7), 1006.

Dehay, B., Bourdenx, M., Gorry, P., Przedborski, S., Vila, M., Hunot, S., ... & Meissner, W. G. (2015). Targeting α-synuclein for treatment of Parkinson's disease: mechanistic and therapeutic considerations. *The Lancet Neurology*, *14*(8), 855-866.

Delic, V., Beck, K. D., Pang, K. C., & Citron, B. A. (2020). Biological links between traumatic brain injury and Parkinson’s disease. *Acta neuropathologica communications*, *8*(1), 45.

DeMaagd, G., & Philip, A. (2015). Parkinson’s disease and its management: part 1: disease entity, risk factors, pathophysiology, clinical presentation, and diagnosis. *Pharmacy and therapeutics*, *40*(8), 504.

Devine, M. J., Gwinn, K., Singleton, A., & Hardy, J. (2011). Parkinson's disease and α-synuclein expression. *Movement disorders : official journal of the Movement Disorder Society*, *26*(12), 2160–2168.

Di Domenico, A., Carola, G., Calatayud, C., Pons-Espinal, M., Muñoz, J. P., Richaud-Patin, Y., ... & Consiglio, A. (2019). Patient-specific iPSC-derived astrocytes contribute to non-cell-autonomous neurodegeneration in Parkinson's disease. *Stem cell reports*, *12*(2), 213-229.

Dong, C. M., Wang, X. L., Wang, G. M., Zhang, W. J., Zhu, L., Gao, S., ... & Xu, J. (2014). A stress-induced cellular aging model with postnatal neural stem cells. *Cell death & disease*, *5*(3), e1116-e1116.

Dong-Chen, X., Yong, C., Yang, X., Chen-Yu, S., & Li-Hua, P. (2023). Signaling pathways in Parkinson’s disease: molecular mechanisms and therapeutic interventions. *Signal transduction and targeted therapy*, *8*(1), 73.

Dorsey, E. A., Constantinescu, R., Thompson, J. P., Biglan, K. M., Holloway, R. G., Kieburtz, K., ... & Tanner, C. M. (2007). Projected number of people with Parkinson disease in the most populous nations, 2005 through 2030. *Neurology*, *68*(5), 384-386.

Dorsey, E. R., Sherer, T., Okun, M. S., & Bloem, B. R. (2018). The emerging evidence of the Parkinson pandemic. *Journal of Parkinson’s disease*, *8*(s1), S3-S8.

Du, X. Y., Xie, X. X., & Liu, R. T. (2020). The role of α-synuclein oligomers in Parkinson’s disease. *International journal of molecular sciences*, *21*(22), 8645.

Eo, H., Kim, S., Jung, U. J., & Kim, S. R. (2024). Alpha-synuclein and microglia in parkinson’s disease: From pathogenesis to therapeutic prospects. Journal of Clinical Medicine, 13(23), 7243.

Falkenburger, B. H., Saridaki, T., & Dinter, E. (2016). Cellular models for Parkinson's disease. *Journal of neurochemistry*, *139*, 121-130.

Fearnley, J. M., & Lees, A. J. (1991). Ageing and Parkinson's disease: substantia nigra regional selectivity. *Brain*, *114*(5), 2283-2301.

Ferrari, E., Cardinale, A., Picconi, B., & Gardoni, F. (2020). From cell lines to pluripotent stem cells for modelling Parkinson's disease. *Journal of Neuroscience Methods*, *340*, 108741.

Fiorenzano, A., Sozzi, E., Kastli, R., Iazzetta, M. R., Bruzelius, A., Arlotta, P., & Parmar, M. (2025). Advances, challenges, and opportunities of human midbrain organoids for modelling of the dopaminergic system. *The EMBO Journal*, 1-15.

Fiume, L., Vettraino, M., Manerba, M., & Di Stefano, G. (2011). Inhibition of lactic dehydrogenase as a way to increase the anti-proliferative effect of multi-targeted kinase inhibitors. *Pharmacological Research*, *63*(4), 328-334.

Fu, R., Shen, Q., Xu, P., Luo, J. J., & Tang, Y. (2014). Phagocytosis of microglia in the central nervous system diseases. *Molecular neurobiology*, *49*(3), 1422-1434.

Gadhave, D. G., Sugandhi, V. V., Jha, S. K., Nangare, S. N., Gupta, G., Singh, S. K., ... & Paudel, K. R. (2024). Neurodegenerative disorders: Mechanisms of degeneration and therapeutic approaches with their clinical relevance. *Ageing research reviews*, *99*, 102357.

Gai, W. P., Yuan, H. X., Li, X. Q., Power, J. T. H., Blumbergs, P. C., & Jensen, P. H. (2000). In situ and in vitro study of colocalization and segregation of α-synuclein, ubiquitin, and lipids in Lewy bodies. *Experimental neurology*, *166*(2), 324-333.

Galet, B., Cheval, H., & Ravassard, P. (2020). Patient-derived midbrain organoids to explore the molecular basis of Parkinson's disease. *Frontiers in Neurology*, *11*, 1005.

Gao, C., Jiang, J., Tan, Y., & Chen, S. (2023). Microglia in neurodegenerative diseases: mechanism and potential therapeutic targets. Signal transduction and targeted therapy, 8(1), 359.

Geirsdottir, L., David, E., Keren-Shaul, H., Weiner, A., Bohlen, S. C., Neuber, J., ... & Prinz, M. (2019). Cross-species single-cell analysis reveals divergence of the primate microglia program. *Cell*, *179*(7), 1609-1622.

Ginhoux, F., Lim, S., Hoeffel, G., Low, D., & Huber, T. (2013). Origin and differentiation of microglia. *Frontiers in cellular neuroscience*, *7*, 45.

Guenoun, D., Blaise, N., Sellam, A., Roupret-Serzec, J., Jacquens, A., Steenwinckel, J. V., ... & Bokobza, C. (2025). Microglial Depletion, a New Tool in Neuroinflammatory Disorders: Comparison of Pharmacological Inhibitors of the CSF-1R. *Glia*, *73*(4), 686-700.

Haenseler, W., Sansom, S. N., Buchrieser, J., Newey, S. E., Moore, C. S., Nicholls, F. J., ... & Cowley, S. A. (2017). A highly efficient human pluripotent stem cell microglia model displays a neuronal-co-culture-specific expression profile and inflammatory response. *Stem cell reports*, *8*(6), 1727-1742.

Hartmann, A. (2004). Postmortem studies in Parkinson's disease. *Dialogues in clinical neuroscience*, *6*(3), 281-293.

Hatcher, J. M., Pennell, K. D., & Miller, G. W. (2008). Parkinson's disease and pesticides: a toxicological perspective. *Trends in pharmacological sciences*, *29*(6), 322-329.

Healy, D. G., Falchi, M., O'Sullivan, S. S., Bonifati, V., Durr, A., Bressman, S., ... & Wood, N. W. (2008). Phenotype, genotype, and worldwide genetic penetrance of LRRK2-associated Parkinson's disease: a case-control study. *The Lancet Neurology*, *7*(7), 583-590.

Hegarty, S. V., Sullivan, A. M., & O'keeffe, G. W. (2013). Midbrain dopaminergic neurons: a review of the molecular circuitry that regulates their development. *Developmental biology*, *379*(2), 123-138.

Heras-Garvin, A., Weckbecker, D., Ryazanov, S., Leonov, A., Griesinger, C., Giese, A., ... & Stefanova, N. (2019). Anle138b modulates α-synuclein oligomerization and prevents motor decline and neurodegeneration in a mouse model of multiple system atrophy. *Movement Disorders*, *34*(2), 255-263.

Hickman, S., Izzy, S., Sen, P., Morsett, L., & El Khoury, J. (2018). Microglia in neurodegeneration. *Nature neuroscience*, *21*(10), 1359-1369.

Ho, D. H., Lee, H., Son, I., & Seol, W. (2019). G2019s LRRK2 promotes mitochondrial fission and increases TNFα-mediated neuroinflammation responses. *Animal Cells and Systems*, *23*(2), 106-111.

Hong, Y., Dong, X., Chang, L., Xie, C., Chang, M., Aguilar, J. S., ... & Li, Q. Q. (2023). Microglia-containing cerebral organoids derived from induced pluripotent stem cells for the study of neurological diseases. *Iscience*, *26*(3).

Irwin, D. J., Lee, V. M. Y., & Trojanowski, J. Q. (2013). Parkinson's disease dementia: convergence of α-synuclein, tau and amyloid-β pathologies. *Nature Reviews Neuroscience*, *14*(9), 626-636.

Isik, S., Yeman Kiyak, B., Akbayir, R., Seyhali, R., & Arpaci, T. (2023). Microglia mediated neuroinflammation in Parkinson’s disease. *Cells*, *12*(7), 1012.

Jackson-Lewis, V., Blesa, J., & Przedborski, S. (2012). Animal models of Parkinson's disease. *Parkinsonism & related disorders*, *18*, S183-S185.

Jankovic J. (2008). Parkinson's disease: clinical features and diagnosis. *Journal of neurology, neurosurgery, and psychiatry*, *79*(4), 368–376.

Jankovic, J., & Tan, E. K. (2020). Parkinson’s disease: etiopathogenesis and treatment. *Journal of Neurology, Neurosurgery & Psychiatry*, *91*(8), 795-808.

Jarazo, J., Barmpa, K., Modamio, J., Saraiva, C., Sabaté-Soler, S., Rosety, I., ... & Schwamborn, J. C. (2022). Parkinson's disease phenotypes in patient neuronal cultures and brain organoids improved by 2-hydroxypropyl-β-cyclodextrin treatment. *Movement Disorders*, *37*(1), 80-94.

Jo, J., Xiao, Y., Sun, A. X., Cukuroglu, E., Tran, H. D., Göke, J., ... & Ng, H. H. (2016). Midbrain-like organoids from human pluripotent stem cells contain functional dopaminergic and neuromelanin-producing neurons. *Cell stem cell*, *19*(2), 248-257.

Jo, J., Yang, L., Tran, H. D., Yu, W., Sun, A. X., Chang, Y. Y., ... & Je, H. S. (2021). Lewy Body–like Inclusions in Human Midbrain Organoids Carrying Glucocerebrosidase and α-Synuclein Mutations. *Annals of Neurology*, *90*(3), 490-505.

Kalia, L. V., & Lang, A. E. (2015). Parkinson's disease. The lancet, 386(9996), 896-912.

Kim, Y. S., & Joh, T. H. (2006). Microglia, major player in the brain inflammation: their roles in the pathogenesis of Parkinson's disease. *Experimental & molecular medicine*, *38*(4), 333-347.

Klein, C., & Westenberger, A. (2012). Genetics of Parkinson’s disease. *Cold Spring Harbor perspectives in medicine*, *2*(1), a008888.

Koga, S., Sekiya, H., Kondru, N., Ross, O. A., & Dickson, D. W. (2021). Neuropathology and molecular diagnosis of Synucleinopathies. *Molecular neurodegeneration*, *16*(1), 83.

Konnova, E. A., & Swanberg, M. (2018). Animal models of Parkinson's disease. *Exon Publications*, 83-106.

Kouli, A., Torsney, K. M., & Kuan, W. L. (2018). Parkinson's disease: etiology, neuropathology, and pathogenesis. *Exon Publications*, 3-26.

Kwon, H. S., & Koh, S. H. (2020). Neuroinflammation in neurodegenerative disorders: the roles of microglia and astrocytes. *Translational neurodegeneration*, *9*(1), 42.

Lacaud, G., & Kouskoff, V. (2017). Hemangioblast, hemogenic endothelium, and primitive versus definitive hematopoiesis. *Experimental hematology*, *49*, 19-24.

Lancaster, M. A., Corsini, N. S., Wolfinger, S., Gustafson, E. H., Phillips, A. W., Burkard, T. R., ... & Knoblich, J. A. (2017). Guided self-organization and cortical plate formation in human brain organoids. *Nature biotechnology*, *35*(7), 659-666.

Lancaster, M. A., Renner, M., Martin, C. A., Wenzel, D., Bicknell, L. S., Hurles, M. E., ... & Knoblich, J. A. (2013). Cerebral organoids model human brain development and microcephaly. *Nature*, *501*(7467), 373-379.

Langston, J. W., Ballard, P., Tetrud, J. W., & Irwin, I. (1983). Chronic Parkinsonism in humans due to a product of meperidine-analog synthesis. *Science*, *219*(4587), 979-980.

Langston, R. G., Beilina, A., Reed, X., Kaganovich, A., Singleton, A. B., Blauwendraat, C., ... & Cookson, M. R. (2022). Association of a common genetic variant with Parkinson's disease is mediated by microglia. *Science Translational Medicine*, *14*(655), eabp8869.

Lashuel, H. A., Mahul-Mellier, A. L., Novello, S., Hegde, R. N., Jasiqi, Y., Altay, M. F., ... & Guex, N. (2022). Revisiting the specificity and ability of phospho-S129 antibodies to capture alpha-synuclein biochemical and pathological diversity. *npj Parkinson's Disease*, *8*(1), 136.

Lee, C. T., Bendriem, R. M., Wu, W. W., & Shen, R. F. (2017). 3D brain Organoids derived from pluripotent stem cells: promising experimental models for brain development and neurodegenerative disorders. *Journal of biomedical science*, *24*(1), 59.

Li, D., Yau, W. Y., Chen, S., Wilton, S., & Mastaglia, F. (2025). A personalised and comprehensive approach is required to suppress or replenish SNCA for Parkinson's disease. *npj Parkinson's Disease*, *11*(1), 42.

Li, P., Zhu, X., Liu, M., Wang, Y., Huang, C., Sun, J., Tian, S., Li, Y., Qiao, Y., Yang, J., Cao, S., Cong, C., Zhao, L., Su, J., & Tian, D. (2025). Joint effect of modifiable risk factors on Parkinson's disease: a large-scale longitudinal study. *Frontiers in human neuroscience*, *19*, 1525248.

Lind-Holm Mogensen, F., Seibler, P., Grünewald, A., & Michelucci, A. (2025). Microglial dynamics and neuroinflammation in prodromal and early Parkinson's disease. *Journal of neuroinflammation*, *22*(1), 136.

Lopes da Fonseca, T., Villar-Piqué, A., & Outeiro, T. F. (2015). The interplay between alpha-synuclein clearance and spreading. *Biomolecules*, *5*(2), 435-471.

López-Otín, C., Blasco, M. A., Partridge, L., Serrano, M., & Kroemer, G. (2023). Hallmarks of aging: An expanding universe. *Cell*, *186*(2), 243-278.

Ludwig, T. E., Andrews, P. W., Barbaric, I., Benvenisty, N., Bhattacharyya, A., Crook, J. M., ... & Mosher, J. T. (2023). ISSCR standards for the use of human stem cells in basic research. *Stem cell reports*, *18*(9), 1744-1752.

Lv, Q. K., Tao, K. X., Wang, X. B., Yao, X. Y., Pang, M. Z., Liu, J. Y., ... & Liu, C. F. (2023). Role of α-synuclein in microglia: autophagy and phagocytosis balance neuroinflammation in Parkinson's disease. Inflammation Research, 72(3), 443-462.

Ma, Y., Erb, M. L., & Moore, D. J. (2025). Aging, cellular senescence and Parkinson's disease. *Journal of Parkinson's Disease*, *15*(2), 239-254.

Madureira, M., Connor-Robson, N., & Wade-Martins, R. (2020). LRRK2: autophagy and lysosomal activity. *Frontiers in neuroscience*, *14*, 498.

Magistrelli, L., Contaldi, E., & Comi, C. (2021). The impact of SNCA variations and its product alpha-synuclein on non-motor features of Parkinson's disease. *Life*, *11*(8), 804.

Mahul-Mellier, A. L., Burtscher, J., Maharjan, N., Weerens, L., Croisier, M., Kuttler, F., ... & Lashuel, H. A. (2020). The process of Lewy body formation, rather than simply α-synuclein fibrillization, is one of the major drivers of neurodegeneration. *Proceedings of the National Academy of Sciences*, *117*(9), 4971-4982.

Majbour, N. K., Vaikath, N. N., Eusebi, P., Chiasserini, D., Ardah, M., Varghese, S., ... & El-Agnaf, O. M. (2016). Longitudinal changes in CSF alpha-synuclein species reflect Parkinson's disease progression. *Movement Disorders*, *31*(10), 1535-1542.

Makrygianni, E. A., & Chrousos, G. P. (2021). From brain organoids to networking assembloids: implications for neuroendocrinology and stress medicine. *Frontiers in physiology*, *12*, 621970.

Mark, J. R., & Tansey, M. G. (2025). Immune cell metabolic dysfunction in Parkinson's disease. *Molecular Neurodegeneration*, *20*(1), 36.

Marsden, C. D. (1961). Pigmentation in the nucleus substantiae nigrae of mammals. *Journal of anatomy*, *95*(Pt 2), 256.

McCormack, A. L., Thiruchelvam, M., Manning-Bog, A. B., Thiffault, C., Langston, J. W., Cory-Slechta, D. A., & Di Monte, D. A. (2002). Environmental risk factors and Parkinson's disease: selective degeneration of nigral dopaminergic neurons caused by the herbicide paraquat. *Neurobiology of disease*, *10*(2), 119-127.

McGeer, P. L., Itagaki, S., Boyes, B. E., & McGeer, E. G. (1988). Reactive microglia are positive for HLA-DR in the substantia nigra of Parkinson's and Alzheimer's disease brains. *Neurology*, *38*(8), 1285-1285.

Menegas, W., Bergan, J. F., Ogawa, S. K., Isogai, Y., Venkataraju, K. U., Osten, P., ... & Watabe-Uchida, M. (2015). Dopamine neurons projecting to the posterior striatum form an anatomically distinct subclass. *elife*, *4*, e10032.

Milosevic, J., Schwarz, S. C., Ogunlade, V., Meyer, A. K., Storch, A., & Schwarz, J. (2009). Emerging role of LRRK2 in human neural progenitor cell cycle progression, survival and differentiation. *Molecular Neurodegeneration*, *4*(1), 25.

Miura, Y., Li, M. Y., Birey, F., Ikeda, K., Revah, O., Thete, M. V., ... & Pașca, S. P. (2020). Generation of human striatal organoids and cortico-striatal assembloids from human pluripotent stem cells. *Nature Biotechnology*, *38*(12), 1421-1430.

Moehle, M. S., Webber, P. J., Tse, T., Sukar, N., Standaert, D. G., DeSilva, T. M., ... & West, A. B. (2012). LRRK2 inhibition attenuates microglial inflammatory responses. *Journal of Neuroscience*, *32*(5), 1602-1611.

Mohamed, N. V., Sirois, J., Ramamurthy, J., Mathur, M., Lépine, P., Deneault, E., ... & Durcan, T. M. (2021). Midbrain organoids with an SNCA gene triplication model key features of synucleinopathy. *Brain Communications*, *3*(4), fcab223

Molnár, Z., Clowry, G. J., Šestan, N., Alzu'bi, A., Bakken, T., Hevner, R. F., ... & Kriegstein, A. (2019). New insights into the development of the human cerebral cortex. *Journal of anatomy*, *235*(3), 432-451.

Monzel, A. S., Smits, L. M., Hemmer, K., Hachi, S., Moreno, E. L., van Wuellen, T., ... & Schwamborn, J. C. (2017). Derivation of human midbrain-specific organoids from neuroepithelial stem cells. *Stem cell reports*, *8*(5), 1144-1154.

Morris, H. R., Spillantini, M. G., Sue, C. M., & Williams-Gray, C. H. (2024). The pathogenesis of Parkinson's disease. *Lancet (London, England)*, *403*(10423), 293–304.

Muguruma, K., Nishiyama, A., Kawakami, H., Hashimoto, K., & Sasai, Y. (2015). Self-organization of polarized cerebellar tissue in 3D culture of human pluripotent stem cells. *Cell reports*, *10*(4), 537-550.

Muwanigwa, M. N., Modamio-Chamarro, J., Antony, P. M., Gomez-Giro, G., Krüger, R., Bolognin, S., & Schwamborn, J. C. (2024). Alpha-synuclein pathology is associated with astrocyte senescence in a midbrain organoid model of familial Parkinson's disease. *Mol Cell Neurosci*, *128*(103919), 10-1016.

Nalls, M. A., Blauwendraat, C., Vallerga, C. L., Heilbron, K., Bandres-Ciga, S., Chang, D., ... & Rizig, M. (2019). Identification of novel risk loci, causal insights, and heritable risk for Parkinson's disease: a meta-analysis of genome-wide association studies. *The Lancet Neurology*, *18*(12), 1091-1102.

Negredo, P. N., Yeo, R. W., & Brunet, A. (2020). Aging and rejuvenation of neural stem cells and their niches. *Cell stem cell*, *27*(2), 202-223.

Negrini, M., Tomasello, G., Davidsson, M., Fenyi, A., Adant, C., Hauser, S., ... & Heuer, A. (2022). Sequential or simultaneous injection of preformed fibrils and AAV overexpression of alpha-synuclein are equipotent in producing relevant pathology and behavioral deficits. Journal of Parkinson's Disease, 12(4), 1133-1153.

Ni, A., & Ernst, C. (2022). Evidence that substantia nigra pars compacta dopaminergic neurons are selectively vulnerable to oxidative stress because they are highly metabolically active. *Frontiers in cellular neuroscience*, *16*, 826193.

Nickels, S. L., Modamio, J., Mendes-Pinheiro, B., Monzel, A. S., Betsou, F., & Schwamborn, J. C. (2020). Reproducible generation of human midbrain organoids for in vitro modeling of Parkinson's disease. *Stem Cell Research*, *46*, 101870.

Nimmerjahn, A., Kirchhoff, F., & Helmchen, F. (2005). Resting microglial cells are highly dynamic surveillants of brain parenchyma in vivo. *Science*, *308*(5726), 1314-1318.

Nuytemans, K., Theuns, J., Cruts, M., & Van Broeckhoven, C. (2010). Genetic etiology of Parkinson disease associated with mutations in the SNCA, PARK2, PINK1, PARK7, and LRRK2 genes: a mutation update. *Human mutation*, *31*(7), 763-780.

Ohtonen, S., Giudice, L., Jäntti, H., Fazaludeen, M. F., Shakirzyanova, A., Gómez-Budia, M., ... & Malm, T. (2023). Human iPSC-derived microglia carrying the LRRK2-G2019S mutation show a Parkinson's disease related transcriptional profile and function. *Scientific Reports*, *13*(1), 22118.

Oliveira, L. M. A., Falomir-Lockhart, L. J., Botelho, M. G., Lin, K. H., Wales, P., Koch, J. C., ... & Jovin, T. M. (2015). Elevated α-synuclein caused by SNCA gene triplication impairs neuronal

differentiation and maturation in Parkinson's patient-derived induced pluripotent stem cells. *Cell death & disease*, *6*(11), e1994-e1994.

Oltra, J., Uribe, C., Segura, B., Campabadal, A., Inguanzo, A., Monté-Rubio, G. C., ... & Iranzo, A. (2022). Brain atrophy pattern in de novo Parkinson's disease with probable RBD associated with cognitive impairment. *npj Parkinson's Disease*, *8*(1), 60.

Ormel, P. R., Vieira de Sá, R., Van Bodegraven, E. J., Karst, H., Harschnitz, O., Sneeboer, M. A., ... & Pasterkamp, R. J. (2018). Microglia innately develop within cerebral organoids. *Nature communications*, *9*(1), 4167.

Ou, Z., Pan, J., Tang, S., Duan, D., Yu, D., Nong, H., & Wang, Z. (2021). Global trends in the incidence, prevalence, and years lived with disability of Parkinson's disease in 204 countries/territories from 1990 to 2019. *Frontiers in public health*, *9*, 776847.

Pajares, M., I. Rojo, A., Manda, G., Boscá, L., & Cuadrado, A. (2020). Inflammation in Parkinson's disease: mechanisms and therapeutic implications. *Cells*, *9*(7), 1687.

Pang, S. Y. Y., Ho, P. W. L., Liu, H. F., Leung, C. T., Li, L., Chang, E. E. S., ... & Ho, S. L. (2019). The interplay of aging, genetics and environmental factors in the pathogenesis of Parkinson's disease. *Translational Neurodegeneration*, *8*(1), 23.

Paolicelli, R. C., Bolasco, G., Pagani, F., Maggi, L., Scianni, M., Panzanelli, P., ... & Gross, C. T. (2011). Synaptic pruning by microglia is necessary for normal brain development. *science*, *333*(6048), 1456-1458.

Paolicelli, R. C., Sierra, A., Stevens, B., Tremblay, M. E., Aguzzi, A., Ajami, B., ... & Wyss-Coray, T. (2022). Microglia states and nomenclature: A field at its crossroads. *Neuron*, *110*(21), 3458-3483.

Parkinson, J. (2002). An essay on the shaking palsy. The Journal of neuropsychiatry and clinical neurosciences, 14(2), 223-236.

Pașca, S. P. (2018). The rise of three-dimensional human brain cultures. *Nature*, *553*(7689), 437-445.

Pașca, S. P., Arlotta, P., Bateup, H. S., Camp, J. G., Cappello, S., Gage, F. H., ... & Vaccarino, F. M. (2022). A nomenclature consensus for nervous system organoids and assembloids. *Nature*, *609*(7929), 907-910.

Pembroke, W. G., Hartl, C. L., & Geschwind, D. H. (2021). Evolutionary conservation and divergence of the human brain transcriptome. *Genome biology*, *22*(1), 52.

Peña-Zelayeta, L., Delgado-Minjares, K. M., Villegas-Rojas, M. M., León-Arcia, K., Santiago-Balmaseda, A., Andrade-Guerrero, J., ... & Arias-Carrión, O. (2025). Redefining non-motor symptoms in Parkinson's disease. *Journal of Personalized Medicine*, *15*(5), 172.

Perni, M., Galvagnion, C., Maltsev, A., Meisl, G., Müller, M. B., Challa, P. K., ... & Dobson, C. M. (2017). A natural product inhibits the initiation of α-synuclein aggregation and suppresses its toxicity. *Proceedings of the National Academy of Sciences*, *114*(6), E1009-E1017.

Pickrell, A. M., & Youle, R. J. (2015). The roles of PINK1, parkin, and mitochondrial fidelity in Parkinson's disease. *Neuron*, *85*(2), 257-273.

Pissadaki, E. K., & Bolam, J. P. (2013). The energy cost of action potential propagation in dopamine neurons: clues to susceptibility in Parkinson's disease. *Frontiers in computational neuroscience*, *7*, 13.

Plaza-Zabala, A., Sierra-Torre, V., & Sierra, A. (2017). Autophagy and microglia: novel partners in neurodegeneration and aging. International journal of molecular sciences, 18(3), 598.Eo et al., 2024

Poewe, W., Seppi, K., Tanner, C. M., Halliday, G. M., Brundin, P., Volkmann, J., Schrag, A. E., & Lang, A. E. (2017). Parkinson disease. *Nature reviews. Disease primers*, *3*, 17013.

Polinski, N. K., Volpicelli-Daley, L. A., Sortwell, C. E., Luk, K. C., Cremades, N., Gottler, L. M., ... & Dave, K. D. (2018). Best practices for generating and using alpha-synuclein pre-formed fibrils to model Parkinson's disease in rodents. *Journal of Parkinson's disease*, *8*(2), 303-322.

Potashkin, J. A., Blume, S. R., & Runkle, N. K. (2011). Limitations of animal models of Parkinson′ s disease. *Parkinson's disease*, *2011*(1), 658083.

Price, D. L., Khan, A., Angers, R., Cardenas, A., Prato, M. K., Bani, M., ... & Biere, A. L. (2023). In vivo effects of the alpha-synuclein misfolding inhibitor minzasolmin supports clinical development in Parkinson's disease. *npj Parkinson's Disease*, *9*(1), 114.

Qian, X., Song, H., & Ming, G. L. (2019). Brain organoids: advances, applications and challenges. *Development*, *146*(8).

Qian, X., Su, Y., Adam, C. D., Deutschmann, A. U., Pather, S. R., Goldberg, E. M., ... & Ming, G. L. (2020). Sliced human cortical organoids for modeling distinct cortical layer formation. *Cell stem cell*, *26*(5), 766-781.

Quick, J. D., Silva, C., Wong, J. H., Lim, K. L., Reynolds, R., Barron, A. M., ... & Lo, C. H. (2023). Lysosomal acidification dysfunction in microglia: an emerging pathogenic mechanism of neuroinflammation and neurodegeneration. *Journal of neuroinflammation*, *20*(1), 185.

Rao, M. N., Shinnar, A. E., Noecker, L. A., Chao, T. L., Feibush, B., Snyder, B., ... & Zasloff, M. (2000). Aminosterols from the dogfish shark Squalus acanthias. *Journal of natural products*, *63*(5), 631-635.

Reinhardt, P., Glatza, M., Hemmer, K., Tsytsyura, Y., Thiel, C. S., Höing, S., ... & Sterneckert, J. (2013). Derivation and expansion using only small molecules of human neural progenitors for neurodegenerative disease modeling. *PloS one*, *8*(3), e59252.

Richardson, J. R., Quan, Y. U., Sherer, T. B., Greenamyre, J. T., & Miller, G. W. (2005). Paraquat neurotoxicity is distinct from that of MPTP and rotenone. *Toxicological sciences*, *88*(1), 193-201.

Rosborough, K., Patel, N., & Kalia, L. V. (2017). α-Synuclein and parkinsonism: updates and future perspectives. *Current neurology and neuroscience reports*, *17*(4), 31.

Rosety, I., Zagare, A., Saraiva, C., Nickels, S., Antony, P., Almeida, C., ... & Schwamborn, J. C. (2023). Impaired neuron differentiation in GBA-associated Parkinson's disease is linked to cell cycle defects in organoids. *npj Parkinson's Disease*, *9*(1), 166.

Russillo, M. C., Andreozzi, V., Erro, R., Picillo, M., Amboni, M., Cuoco, S., ... & Pellecchia, M. T. (2022). Sex differences in Parkinson's disease: from bench to bedside. *Brain sciences*, *12*(7), 917.

Russo, I., Bubacco, L., & Greggio, E. (2014). LRRK2 and neuroinflammation: partners in crime in Parkinson's disease?. *Journal of neuroinflammation*, *11*(1), 52.

Ryan, S. K., Jordan-Sciutto, K. L., & Anderson, S. A. (2020). Protocol for tri-culture of hiPSC-derived neurons, astrocytes, and microglia. *STAR protocols*, *1*(3), 100190.

Sabate-Soler, S., Bernini, M., & Schwamborn, J. C. (2022). Immunocompetent brain organoids—microglia enter the stage. Progress in Biomedical Engineering, 4(4), 042002.

Sabate-Soler, S., Kurniawan, H., & Schwamborn, J. C. (2024). Advanced brain organoids for neuroinflammation disease modeling. *Neural Regeneration Research*, *19*(1), 154-155.

Sabate-Soler, S., Nickels, S. L., Saraiva, C., Berger, E., Dubonyte, U., Barmpa, K., ... & Schwamborn, J. C. (2022). Microglia integration into human midbrain organoids leads to increased neuronal maturation and functionality. *Glia*, *70*(7), 1267-1288.

Sakaguchi, H., Kadoshima, T., Soen, M., Narii, N., Ishida, Y., Ohgushi, M., ... & Sasai, Y. (2015). Generation of functional hippocampal neurons from self-organizing human embryonic stem cell-derived dorsomedial telencephalic tissue. *Nature communications*, *6*(1), 8896.

Samuel, F., Flavin, W. P., Iqbal, S., Pacelli, C., Renganathan, S. D. S., Trudeau, L. E., ... & Tandon, A. (2016). Effects of serine 129 phosphorylation on α-synuclein aggregation, membrane association, and internalization. *Journal of Biological Chemistry*, *291*(9), 4374-4385.

Sandoval, S. O., Cappuccio, G., Kruth, K., Osenberg, S., Khalil, S. M., Méndez-Albelo, N. M., ... & Zhao, X. (2024). Rigor and reproducibility in human brain organoid research: Where we are and where we need to go. *Stem Cell Reports*, *19*(6), 796-816.

Schapira, A. H., & Gegg, M. E. (2013). Glucocerebrosidase in the pathogenesis and treatment of Parkinson disease. *Proceedings of the National Academy of Sciences*, *110*(9), 3214-3215.

Schmidt, S. I., Bogetofte, H., Ritter, L., Agergaard, J. B., Hammerich, D., Kabiljagic, A. A., ... & Meyer, M. (2021). Microglia-secreted factors enhance dopaminergic differentiation of tissue-and iPSC-derived human neural stem cells. *Stem cell reports*, *16*(2), 281-294.

Schober, A. (2004). Classic toxin-induced animal models of Parkinson's disease: 6-OHDA and MPTP. *Cell and tissue research*, *318*(1), 215-224.

Setia, H., & Muotri, A. R. (2019, November). Brain organoids as a model system for human neurodevelopment and disease. In *Seminars in cell & developmental biology* (Vol. 95, pp. 93-97). Academic Press

Shahmoradian, S. H., Lewis, A. J., Genoud, C., Hench, J., Moors, T. E., Navarro, P. P., ... & Lauer, M. E. (2019). Lewy pathology in Parkinson's disease consists of crowded organelles and lipid membranes. *Nature neuroscience*, *22*(7), 1099-1109.

Shepherd, C. E., Alvendia, H., & Halliday, G. M. (2019). Brain banking for research into neurodegenerative disorders and ageing. *Neuroscience bulletin*, *35*(2), 283-288.

Shoshan, M. C. (2012). 3-Bromopyruvate: targets and outcomes. *Journal of bioenergetics and biomembranes*, *44*(1), 7-15.

Sidransky, E., Nalls, M. A., Aasly, J. O., Aharon-Peretz, J., Annesi, G., Barbosa, E. R., ... & Ziegler, S. G. (2009). Multicenter analysis of glucocerebrosidase mutations in Parkinson's disease. *New England Journal of Medicine*, *361*(17), 1651-1661.

Signaevsky, M., Marami, B., Prastawa, M., Tabish, N., Iida, M. A., Zhang, X. F., ... & Crary, J. F. (2022). Antemortem detection of Parkinson's disease pathology in peripheral biopsies using artificial intelligence. *Acta Neuropathologica Communications*, *10*(1), 21.

Singleton, A. B., Farrer, M., Johnson, J., Singleton, A., Hague, S., Kachergus, J., Hulihan, M., Peuralinna, T., Dutra, A., Nussbaum, R., Lincoln, S., Crawley, A., Hanson, M., Maraganore, D., Adler, C., Cookson, M. R., Muenter, M., Baptista, M., Miller, D., Blancato, J., … Gwinn-Hardy, K. (2003). alpha-Synuclein locus triplication causes Parkinson's disease. *Science (New York, N.Y.)*, *302*(5646), 841.

Smith, L., & Schapira, A. H. (2022). GBA variants and Parkinson disease: mechanisms and treatments. *Cells*, *11*(8), 1261.

Smits, L. M., Magni, S., Kinugawa, K., Grzyb, K., Luginbühl, J., Sabate-Soler, S., ... & Schwamborn, J. C. (2020). Single-cell transcriptomics reveals multiple neuronal cell types in human midbrain-specific organoids. *Cell and tissue research*, *382*(3), 463-476.

Smits, L. M., Reinhardt, L., Reinhardt, P., Glatza, M., Monzel, A. S., Stanslowsky, N., ... & Schwamborn, J. C. (2019). Modeling Parkinson's disease in midbrain-like organoids. *NPJ Parkinson's disease*, *5*(1), 5.

Song, L., Yuan, X., Jones, Z., Vied, C., Miao, Y., Marzano, M., ... & Li, Y. (2019). Functionalization of brain region-specific spheroids with isogenic microglia-like cells. *Scientific reports*, *9*(1), 11055.

Sonninen, T. M., Goldsteins, G., Laham-Karam, N., Koistinaho, J., & Lehtonen, Š. (2020). Proteostasis disturbances and inflammation in neurodegenerative diseases. *Cells*, *9*(10), 2183.

Spangenberg, E., Severson, P. L., Hohsfield, L. A., Crapser, J., Zhang, J., Burton, E. A., ... & Green, K. N. (2019). Sustained microglial depletion with CSF1R inhibitor impairs parenchymal plaque development in an Alzheimer's disease model. *Nature communications*, *10*(1), 3758.

Spillantini, M. G., Crowther, R. A., Jakes, R., Hasegawa, M., & Goedert, M. (1998). α-Synuclein in filamentous inclusions of Lewy bodies from Parkinson's disease and dementia with Lewy bodies. *Proceedings of the National Academy of Sciences*, *95*(11), 6469-6473.

Spillantini, M. G., Schmidt, M. L., Lee, V. M. Y., Trojanowski, J. Q., Jakes, R., & Goedert, M. (1997). α-Synuclein in Lewy bodies. *Nature*, *388*(6645), 839-840.

Srivastava, R., Dilnashin, H., Kapoor, D., Aparna, S., Heidarli, E., Singh, S. P., & Jain, V. (2024). Role of animal models in Parkinson's disease (PD): what role they play in preclinical translational research. *CNS & Neurological Disorders-Drug Targets-CNS & Neurological Disorders)*, *23*(2), 181-202.

Sterneckert, J. L., Reinhardt, P., & Schöler, H. R. (2014). Investigating human disease using stem cell models. *Nature Reviews Genetics*, *15*(9), 625-639.

Stoll, E. A., Cheung, W., Mikheev, A. M., Sweet, I. R., Bielas, J. H., Zhang, J., ... & Horner, P. J. (2011). Aging neural progenitor cells have decreased mitochondrial content and lower oxidative metabolism. *Journal of Biological Chemistry*, *286*(44), 38592-38601.

Streubel-Gallasch, L., Giusti, V., Sandre, M., Tessari, I., Plotegher, N., Giusto, E., ... & Civiero, L. (2021). Parkinson's disease–associated LRRK2 interferes with astrocyte-mediated alpha-synuclein clearance. Molecular Neurobiology, 58(7), 3119-3140.

Takahashi, K., & Yamanaka, S. (2006). Induction of pluripotent stem cells from mouse embryonic and adult fibroblast cultures by defined factors. *cell*, *126*(4), 663-676.

Tansey, M. G., Wallings, R. L., Houser, M. C., Herrick, M. K., Keating, C. E., & Joers, V. (2022). Inflammation and immune dysfunction in Parkinson disease. *Nature reviews. Immunology*, *22*(11), 657–673.

Taylor, K. S. M., Cook, J. A., & Counsell, C. E. (2007). Heterogeneity in male to female risk for Parkinson's disease. *Journal of Neurology, Neurosurgery & Psychiatry*, *78*(8), 905-906.

Tenchov, R., Sasso, J. M., & Zhou, Q. A. (2025). Evolving Landscape of Parkinson's Disease Research: challenges and perspectives. *ACS omega*, *10*(2), 1864-1892.

Thakur, P., Breger, L. S., Lundblad, M., Wan, O. W., Mattsson, B., Luk, K. C., ... & Björklund, A. (2017). Modeling Parkinson's disease pathology by combination of fibril seeds and α-synuclein overexpression in the rat brain. *Proceedings of the National Academy of Sciences*, *114*(39), E8284-E8293.

Toh, H. S., Choo, X. Y., & Sun, A. X. (2023). Midbrain organoids—development and applications in Parkinson's disease. *Oxford Open Neuroscience*, *2*, kvad009.

Tolosa, E., Garrido, A., Scholz, S. W., & Poewe, W. (2021). Challenges in the diagnosis of Parkinson's disease. *The Lancet. Neurology*, *20*(5), 385–397.

Trainor, A. R., MacDonald, D. S., & Penney, J. (2024). Microglia: roles and genetic risk in Parkinson's disease. Frontiers in Neuroscience, 18, 1506358.

Tremblay, C., Rahayel, S., Vo, A., Morys, F., Shafiei, G., Abbasi, N., ... & Dagher, A. (2021). Brain atrophy progression in Parkinson's disease is shaped by connectivity and local vulnerability. *Brain Communications*, *3*(4), fcab269.

Tsalenchuk, M., Gentleman, S. M., & Marzi, S. J. (2023). Linking environmental risk factors with epigenetic mechanisms in Parkinson's disease. *npj Parkinson's Disease*, *9*(1), 123.

Ungerstedt, U. (1968). 6-Hydroxy-dopamine induced degeneration of central monoamine neurons. *European journal of pharmacology*, *5*(1), 107-110.

Urrestizala-Arenaza, N., Cerchio, S., Cavaliere, F., & Magliaro, C. (2024). Limitations of human brain organoids to study neurodegenerative diseases: a manual to survive. *Frontiers in Cellular Neuroscience*, *18*, 1419526.

Vaccari, C., El Dib, R., Gomaa, H., Lopes, L. C., & De Camargo, J. L. (2019). Paraquat and Parkinson's disease: a systematic review and meta-analysis of observational studies. *Journal of Toxicology and Environmental Health, Part B*, *22*(5-6), 172-202.

Vila, M. (2019). Neuromelanin, aging, and neuronal vulnerability in Parkinson's disease. *Movement Disorders*, *34*(10), 1440-1451.

Wegrzynowicz, M., Bar-On, D., Calo', L., Anichtchik, O., Iovino, M., Xia, J., ... & Spillantini, M. G. (2019). Depopulation of dense α-synuclein aggregates is associated with rescue of dopamine neuron dysfunction and death in a new Parkinson's disease model. *Acta Neuropathologica*, *138*, 575-595.

Westenberger, A., Brüggemann, N., & Klein, C. (2025). Genetics of Parkinson's disease: from causes to treatment. *Cold Spring Harbor perspectives in medicine*, *15*(7), a041774.

Wong, Y. C., & Krainc, D. (2017). α-synuclein toxicity in neurodegeneration: mechanism and therapeutic strategies. *Nature medicine*, *23*(2), 1-13.

Wright, L. S., Prowse, K. R., Wallace, K., Linskens, M. H., & Svendsen, C. N. (2006). Human progenitor cells isolated from the developing cortex undergo decreased neurogenesis and eventual senescence following expansion in vitro. *Experimental cell research*, *312*(11), 2107-2120.

Xicoy, H., Wieringa, B., & Martens, G. J. (2017). The SH-SY5Y cell line in Parkinson's disease research: a systematic review. *Molecular neurodegeneration*, *12*(1), 10.

Xu, R., Boreland, A. J., Li, X., Erickson, C., Jin, M., Atkins, C., ... & Jiang, P. (2021). Developing human pluripotent stem cell-based cerebral organoids with a controllable microglia ratio for modeling brain development and pathology. *Stem cell reports*, *16*(8), 1923-1937.

Yang, K., Lv, Z., Zhao, W., Lai, G., Zheng, C., Qi, F., ... & Zheng, W. (2024). The potential of natural products to inhibit abnormal aggregation of α-Synuclein in the treatment of Parkinson's disease. *Frontiers in Pharmacology*, *15*, 1468850.

Yi, S., Wang, L., Wang, H., Ho, M. S., & Zhang, S. (2022). Pathogenesis of α-synuclein in Parkinson's disease: from a neuron-glia crosstalk perspective. *International journal of molecular sciences*, *23*(23), 14753.

Yin, X., Mead, B. E., Safaee, H., Langer, R., Karp, J. M., & Levy, O. (2016). Stem cell organoid engineering. *Cell stem cell*, *18*(1), 25.

Youle, R. J., & Narendra, D. P. (2011). Mechanisms of mitophagy. *Nature reviews Molecular cell biology*, *12*(1), 9-14.

Zafar, F., Valappil, R. A., Kim, S., Johansen, K. K., Chang, A. L. S., Tetrud, J. W., ... & Schüle, B. (2018). Genetic fine-mapping of the Iowan SNCA gene triplication in a patient with Parkinson's disease. *npj Parkinson's Disease*, *4*(1), 18.

Zagare, A., Barmpa, K., Smajic, S., Smits, L. M., Grzyb, K., Grünewald, A., ... & Schwamborn, J. C. (2022). Midbrain organoids mimic early embryonic neurodevelopment and recapitulate LRRK2-p. Gly2019Ser-associated gene expression. *The American Journal of Human Genetics*, *109*(2), 311-327.

Zagare, A., Gobin, M., Monzel, A. S., & Schwamborn, J. C. (2021). A robust protocol for the generation of human midbrain organoids. *STAR protocols*, *2*(2), 100524.

Zagare, A., Hemedan, A., Almeida, C., Frangenberg, D., Gomez-Giro, G., Antony, P., ... & Schwamborn, J. C. (2025). Insulin resistance is a modifying factor for Parkinson's disease. *Movement Disorders*, *40*(1), 67-76.

Zechel, S., Meinhardt, A., Unsicker, K., & und Halbach, O. V. B. (2010). Expression of leucine-rich-repeat-kinase 2 (LRRK2) during embryonic development. *International Journal of Developmental Neuroscience*, *28*(5), 391-399.

Zeighami, Y., Ulla, M., Iturria-Medina, Y., Dadar, M., Zhang, Y., Larcher, K. M. H., ... & Dagher, A. (2015). Network structure of brain atrophy in de novo Parkinson's disease. *elife*, *4*, e08440.

Zhang, J., Shen, Q., Ma, Y., Liu, L., Jia, W., Chen, L., & Xie, J. (2022). Calcium homeostasis in Parkinson's disease: from pathology to treatment. *Neuroscience Bulletin*, *38*(10), 1267-1270.

Zhang, W., Jiang, J., Xu, Z., Yan, H., Tang, B., Liu, C., ... & Meng, Q. (2023). Microglia-containing human brain organoids for the study of brain development and pathology. *Molecular Psychiatry*, *28*(1), 96-107.

Zhang, W., Wang, T., Pei, Z., Miller, D. S., Wu, X., Block, M. L., ... & Zhang, J. (2005). Aggregated α-synuclein activates microglia: a process leading to disease progression in Parkinson's disease. *The FASEB Journal*, *19*(6), 533-542.

Zhang, W., Xiao, D., Mao, Q., & Xia, H. (2023). Role of neuroinflammation in neurodegeneration development. *Signal transduction and targeted therapy*, *8*(1), 267.

Zhao, Y., Ray, A., Portengen, L., Vermeulen, R., & Peters, S. (2023). Metal exposure and risk of Parkinson disease: a systematic review and meta-analysis. *American Journal of Epidemiology*, *192*(7), 1207-1223.

Zhao, Z., Han, F., Yang, S., Wu, J., & Zhan, W. (2015). Oxamate-mediated inhibition of lactate dehydrogenase induces protective autophagy in gastric cancer cells: Involvement of the Akt–mTOR signaling pathway. *Cancer letters*, *358*(1), 17-26.

Zimmermann, A. S., Sabate-Soler, S., Zagare, A., Barmpa, K., Haendler, K., Rosa, S., ... & Schwamborn, J. C. (2025). Vascularized midbrain assembloids show neuroinflammation and dopaminergic neuron vulnerability in Parkinsons Disease. *bioRxiv*, 2025-08.